

Accelerator-driven Systems: Safety and Kinetics

Marcus Eriksson

Doctoral Thesis
Department of Nuclear and Reactor Physics
Royal Institute of Technology
Stockholm 2005

Akademisk avhandling som med tillstånd av Kungliga Tekniska Högskolan framlägges till offentlig granskning för avläggande av teknologie doktorsexamen fredagen den 18 mars 2004 kl. 10.00 i sal FA32, Albanova universitetscentrum, Roslagstullsbacken 21, Stockholm.

ISBN 91-7283-988-0

TRITA-FYS 2005:13

ISSN 0280-316X

ISRN KTH/FYS/--05:13—SE

Copyright Marcus Eriksson

Tryckeri: Universitetservice US-AB, Stockholm 2005

Corrections to thesis Accelerator-driven Systems: Safety and Kinetics

Page	Correction
ii	Typo. Replace "fredagen den 18 mars 2004" with "fredagen den 18 mars 2005"
Page 1	Typo. First paragraph, "λ-emitters" should be "γ-emitters"
Page 10	<p>Inconsistency in Fig. 1. The horizontal reference line referred to as "7.8 g natural uranium" corresponds to the amount of natural uranium that must be recovered from the ore to produce 1 g uranium fuel with ²³⁵U enrichment of 4.2% and tails enrichment of 0.2%, whereas the figure displays the radiotoxic inventory for uranium fuel with initial enrichment of 3.7%.</p> <p><i>Comment:</i> To produce 1 g of fuel with initial enrichment of 3.7% and equivalent tails assay would require $(3.7-0.2)/(0.71-0.2)=6.9$ g of natural uranium. Alternatively, we could say that the 7.8 g line corresponds to the amount required to produce fuel with enrichment of 3.7%, but with tails assay of 0.27%, which is a reasonable number (the tails from the enrichment plant is typically in the range 0.2-0.3 %). This would then leave the figure intact.</p>
Page 13	At the end of the first paragraph, ¹³⁵ C should be ¹³⁵ Cs.
Page 21	Missing reference. In figures 7, 8, 11, 13, and 14, the nuclides represented by the squares containing the radioactive decay data were taken from the Karlsruher Nuklidkarte, November 1995.
Page 36	<p>Typo. Near end of page. The weighted mean lifetime of all neutrons, considering both prompt and delayed is 0.07 seconds (for thermal fission in ²³⁵U). Not ~10 sec, as quoted.</p> <p><i>Comment:</i> The average mean life of the delayed neutron precursors is ~10 seconds (similar for all isotopes).</p>
Page 52-53	Typo. The Doppler constants referred to in the text on pages 52-53 and as shown in Fig. 22 should be negative! It is assured that the corresponding negative values were used in the related calculation. These values were calculated in Paper II .

Abstract

The accelerator-driven system (ADS) is recognized as a promising system for the purpose of nuclear waste transmutation and minimization of spent fuel radiotoxicity. The primary cause for this derives from its accelerator-driven, sub-critical operating state, which introduces beneficial safety-related features allowing for application of cores employing fuel systems containing pure transuranics or minor actinides, thereby offering increased incineration rate of waste products and minimal deployment of advanced (and expensive) partitioning and transmutation technologies. The main theme of the thesis is safety and kinetics performance of accelerator-driven nuclear reactors. The studies are confined to the examination of ADS design proposals employing fast neutron spectrum, uranium-free lattice fuels, and liquid-metal cooling, with emphasis on lead-bismuth coolant. The thesis consists of computational studies under normal operation and hypothetical accidents, and of evaluation and identification of safety design features.

By itself, subcritical operation provides a distinct safety advantage over critical reactor operation, distinguished by high operational stability and additional margins for positive reactivity insertion. For a uranium-free minor actinide based fuel important safety parameters deteriorate. Specific analyses suggest that operation of such cores in a critical state would be very difficult. The studies of unprotected transients indicate that lead-bismuth cooled accelerator-driven reactors can be effective in addressing the low effective delayed neutron fraction and the high coolant void reactivity that comes with the minor actinide fuel, but some supportive prompt negative feedback mechanism might be considered necessary to compensate for a weak Doppler effect in case of a prompt critical transient. Although lead-bismuth features a high boiling point, the work underlines the importance of maintaining a low coolant void reactivity value. The transient design studies identified a molybdenum-based Ceramic-Metal (CerMet) fuel with favourable inherent safety features. A higher lattice pitch is suggested to avoid mechanical failure during unprotected loss-of-flow. Detailed coupled neutron kinetics and thermal hydraulic analyses demonstrated that the point kinetics approximation is capable of providing highly accurate transient calculations of subcritical systems. The results suggest better precision at lower k_{eff} levels, which is an effect of the reduced sensitivity to system reactivity perturbations in a subcritical state resulting in small spatial distortions. In the course of a beam reliability study, the accelerator was identified as responsible for frequent beam interruptions. It is clear that extensive improvement in the mean-time between beam failures is required.

List of Papers

The thesis is based on Papers I through VI. These papers are appended in the thesis and are referred to in the text by their Roman numerals.

- I. M. Eriksson, J. Wallenius, M. Jolkkonen, and J. E. Cahalan
Inherent Safety of Fuels for Accelerator-driven Systems
Accepted Nuclear Technology (January 2005).
- II. J. Wallenius and M. Eriksson
Neutronics of Minor Actinide Burning Accelerator Driven Systems with Ceramic Fuel
Accepted Nuclear Technology (January 2005).
- III. M. Eriksson, J. E. Cahalan, and W. S. Yang
On the Performance of Point Kinetics for the Analysis Accelerator-driven Systems
Nuclear Science and Engineering, 149, 298-311 (2005)
- IV. M. Eriksson, J. Wallenius, J. E. Cahalan, K. Tucek, and W. Gudowski
Safety Analysis of Na and Pb-Bi Coolants in Response to Beam Instabilities
Proc. 3rd International Workshop on Utilisation and Reliability of High Power Proton Accelerators, Santa Fe, May 12-16, NEA/OECD (2002).
- V. M. Eriksson and J. E. Cahalan
Inherent Shutdown Capabilities in Accelerator-driven Systems
Annals of Nuclear Energy, vol. 29/14 pp 1689-1706, (2002).
- VI. M. Eriksson and C. Piaszczyk
Reliability Assessment of the LANSCE Accelerator System
Proc. Workshop on Utilisation and Reliability of High Power Proton Accelerators, Mito, Japan, 13-15 October (1998)

Author's contribution

With the exception for **paper II**, the author is the principal writer and bears the main responsibility for the papers included in the thesis. The author took active part in the discussions and preparation of **paper II**, but his contribution is primarily related to the subject reported in **Paper I**. **Paper III** consists mainly of computational studies and data interpretation, which were performed by the author, with important comments and suggestions by the co-authors. The author performed the main parts of **Papers IV** and **V** including the transient and thermal hydraulics calculations, data analysis and the writing of the manuscripts, supported with neutron transport data for **Paper IV**. **Paper VI** is the result of Diploma work performed by the author at the department.

Acknowledgements

I owe thanks to many people who supported me in various different ways during the completion of this thesis. I wish to express my appreciation to friends and colleagues (past and present) of the reactor physics department (Royal Institute of Technology) for, among many other things, their helpful interactions and advice, and for providing a rich social life at the department as well as many memorable events outside work, including stimulating discussions on various topics covered, conference trips, unforgettable “fikas”, and so on. My sincere appreciation goes to W. Gudowski, who originally stimulated my interest in reactor physics and accepted me as graduate student, and to J. Wallenius, from whom I received much guidance and inspiration over the years and also for his efforts in reading the manuscript. It is also a pleasure to acknowledge the continued guidance of J. Cahalan of Argonne National Laboratory, for devoting so much time to me and for his untiring assistance on the topics of reactor safety analysis, whose thinking on the subject in many ways influenced my own. Also, thanks are due to numerous people working at Argonne National Laboratory at the former Reactor Analysis Division who provided considerable assistance and hospitality during my stay as visiting graduate student, in the year 2000-2001, and for their courtesy in allowing me to use their computing facilities. Sincere thanks are due to Svensk Kärnbränslehantering AB for supporting my research in transmutation systems for more than half a decade. I gratefully acknowledge The Swedish Centre for Nuclear Technology, for generously providing the extra resources to carry out part of my studies in the U.S., which I had the fortune to experience. Thanks are also due to the students and staff of the nuclear physics department not mentioned thus far for providing an enjoyable, friendly, and inspiring working environment.

Further, I wish to express my deep appreciation and love to my wife, Ellinor, for her continued support, encouragement, patience, and extraordinary understanding for my countless late returns and absent weekends throughout the many years of research, and for providing tasteful lunches (although I must confess I lost 9% of my initial body weight during the writing of this text!) and for her tending of the family during the trying period of writing. Without her support this task would have been impossible. I also extend my affectionate to my two daughters, Elvira and Lovisa, who truly provided the greatest inspiration of all, for their cheerful smile and loving company (understandably with varying degree of patience). Last but not least, special thanks must be given to my parents, Thomas and Elsy, who always followed my work with genuine interest, no matter what, and for their early stimulation on matters that finally brought me into academia.

Marcus Eriksson

Stockholm 2005

Content

Chapter 1: Nuclear Waste	1
Introduction	1
Classification of radioactive wastes	1
Spent nuclear fuel	3
Options for spent fuel management	11
Chapter 2: Partitioning & Transmutation	15
Partitioning	15
Transmutation	20
Chapter 3: Transmutation Strategies	24
Introduction	24
Transmutation of plutonium	25
Transmutation of minor actinides	27
Transmutation of fission products	31
Chapter 4: Accelerator-driven Systems	33
General principles	33
Safety features of uranium-free cores	36
Motivation for subcritical operation	42
Responsiveness of the ADS	44
Accident performance	45
Safety performance in super-prompt critical transients	52
Computational performance of the point kinetics method	55
Accelerator reliability	60
Conclusions	62
Appendix A: Reactor Kinetics Equations	64
Appendix B: Short Summary of the SAS4A Code	67
Bibliography	68
Papers	

“A grad student in procrastination tends to stay in procrastination unless an external force is applied to it”

Also known as Newton's first law of graduation or the “Law of Inertia” originally discovered experimentally by Galileo when he threatened to cut his grad student's funding!
(From <http://www.phdcomics.com>, originally published 2001)

Chapter 1:

Nuclear Waste

Introduction

Nuclear energy is used throughout the world and radioactive waste is an unavoidable by-product of its utilization. It is generated in every stage of the nuclear fuel cycle, but by far the largest amount of radioactivity is contained in the spent nuclear fuel produced in connection with nuclear power operation. Although the radioactive wastes arising from other steps of the nuclear fuel cycle are not to be neglected quantitatively, these wastes play only a minor role because of their low activity levels. The radioactivity contained in the spent fuel is typically several orders of magnitude higher than in wastes from other steps of the fuel cycle [1]. The radioactivity of the spent fuel after reactor service is due primarily to the radioisotopes generated by fission; however, because of the relatively short half-lives of many fission products, the activity levels of the fission products rapidly decrease with time. In comparison, a small amount of transuranic waste (~1 % of initial actinide loading) is generated by successive neutron capture in uranium. While the fission products are β - and λ -emitters, the transuranic elements are mainly α -emitters. The transuranic waste raises special problems because of the high radiotoxicity and long half-life in comparison with the fission products. From a global radiotoxicity point of view, the transuranic waste presents the greatest obstacle, an aspect that suggests special waste management treatment. This chapter discusses the types, composition, and hazards involved in the spent nuclear fuel produced by light-water reactors, which serves as the reference case.

Classification of radioactive wastes

A reasonable starting point for discussions on nuclear waste management might be to try to define the term “radioactive waste”. The Swedish Radiation Protection Authority (SSI) [2] has a definition according to “a material which contains or is contaminated with radionuclides and for which there is no use”, which traces back to the definition considered in EU Directive 92/3/Euratom [3]. The Department of Energy [4] in the U.S. has a definition of radioactive waste as “Solid, liquid, or gaseous material that contains radionuclides regulated under the Atomic Energy Act of 1954, as amended, and of negligible economic value considering costs of recovery.” These definitions are quite ambiguous and subjective in nature, which open for different interpretations of the meaning of radioactive waste. What is considered as waste under one set of assumptions and in one place may be of use or value under another set of assumptions or in another place. For example, what is the appropriate declaration of spent nuclear fuel? If the fuel is disposed directly without reprocessing, spent nuclear fuel is considered to be radioactive waste. With reprocessing, spent nuclear fuel is considered to be a resource. With the latter definition the spent nuclear fuel is not ‘spent’ in a true sense. Dictionary meanings offer little further clarification on the interpretation of radioactive waste. While the Swedish Environmental Act [5], also known as “Miljöbalken”, defines “waste” as a material “that the owner disposes of or intends to, or is bound to dispose of” and this is regardless of whether the material has an economic value or can be reused, it does not clearly

specify the meaning of the term “radioactive waste”. So far the usefulness or the economic value of the waste material remain as our only definitions, yet the SSI has given consideration [6] to adopt a similar definition of radioactive waste as defined for general wastes under the Environmental Act. Nevertheless, from a radiation protection viewpoint, radioactive waste products are all products whose radioactivity exceeds certain levels, and which, for this reason must be managed in order to protect humans and the environment.

Radioactive waste may be classified in a variety of ways according to the specific radioactivity, half-life of the radionuclides, type of ionizing radiation emitted, physical state of the waste, i.e., whether it is in a gaseous, liquid, or solid form. With respect to the activity concentration, radioactive wastes are commonly classified as high-, intermediate-, and low-level wastes, but no strict distinction between these categories exists that is accepted worldwide. Low level waste (LLW) is generally characterized by low radioactivity levels that can be handled without shielding. It includes both short-lived and long-lived radionuclides. Intermediate level waste (ILW), however, requires special shielding measures but no cooling during handling, transportation, and storage. High-level waste (HLW), finally, generates a considerable amount of heat and requires cooling, as well as shielding because of its high intensity of ionizing radiation. Based on the decay heat emitted, a lower value of 2 kW/m^3 is used to distinguish between high level radioactive wastes from other radioactive waste classes. Handling this waste requires special procedures to manage both the heat and the radioactivity. Based on the time required for the nuclei of the radioactive material to decay, the waste is often described as short-lived or long-lived. Short-lived radioactive waste usually includes radionuclides that have a half-life of less than thirty years. As noted in TABLE 1, the International Atomic Energy Agency (IAEA) suggests a set of 4 classes based on a combination of the activity concentration and the half-life [7]. Practically, HLW is produced only in connection with the operation of nuclear reactors and therefore it is often synonymous with the spent nuclear fuel. HLW also arises in the reprocessing of spent nuclear fuel in the form of concentrated liquid solutions containing fission products. In the process, transuranic radionuclides (also called the alpha-bearing waste) are extracted, which represents special problems because of its long half-life and high radiotoxicity, aspects that are very important with regard to waste management. These implications will be discussed furthermore in the following sections. Most nations apply a similar classification system as indicated by the IAEA, however, variations occur. In the U.S. [8], radioactive waste classes are source-defined (as in spent nuclear fuel, uranium mill tailings, transuranic waste, etc.) rather than defined by some measurable quality of the waste. In that classification, high-level waste is per definition the highly radioactive material created from the reprocessing of the spent fuel that contains the fission products. Irradiated reactor fuel is, however, for the purpose of the repository also regulated as high-level waste.

TABLE 1
Classification of radioactive waste according to IAEA [7]

Waste class	Definition
Low level	Contains enough radioactive material to require action for the protection of people, but not so much that it requires shielding during handling, storage or transportation. The activity clearance level is based on an annual dose to members of the public of less than 0.01 mSv.
Intermediate, short lived	Waste which requires shielding, but needs little or no provision for heat dissipation and contains low concentrations of long-lived radionuclides (less than 4000 Bq/g of alpha-emitters). The radionuclides generally have a half-life of less than 30 years.
Intermediate, long lived	Waste that requires shielding, but needs little or no provision for heat dissipation. The radionuclides generally have a half life of more than 30 years.
High level	Waste which contains large concentrations of both short- and long-lived radionuclides and is sufficiently radioactive to require both shielding and cooling. The waste generates more than 2 kilowatts of heat per cubic metre.

Spent nuclear fuel

The bulk of all spent fuel results from the operation of light water reactors (LWR). The fuel material of LWRs consists of ceramic uranium dioxide (UO₂) in the form of compacted (and sintered) pellets. The pellets are stacked inside metallic tubes, which are then bundled and collected in a metal case, referred to as an assembly or subassembly. The subassemblies are loaded into the reactor core and irradiated for a period of several years. During this period energy is released as the heavy atoms undergo fission and the fuel is said to be burned. After irradiation the spent fuel is removed from the core and stored in water pools for several months to allow the short-lived fission products to decay. Depending on national policy, the spent fuel is sent directly to storage facilities without reprocessing or shipped to reprocessing facilities in order to recycle plutonium and unused uranium. Today, a smaller fraction (20-30%) of the spent fuel is reprocessed while the majority is sent to direct disposal.

Production facts

As of October 2004, there were 440 nuclear reactors (commercial power producing) in operation worldwide with a total net installed capacity of 366 GWe [9]. Of these 207 are located in Europe (173 GWe), including Russia and Ukraine, and 104 (76 GWe) reactors in the Far East (mainly in Japan, South Korea, and China). The United States has 104 operating nuclear reactors that produce 98 GWe and 17 reactors (12 GWe) are in operation in Canada, the remaining 8 (6 GWe) reactors are located in South America (Brazil, Argentina, and Mexico) and South Africa. They provide about 2800 TWh of electricity in total, which correspond to approximately 16% of the global electricity supply [10]. TABLE 2 shows the operational reactors by type. Over 87% of the electricity production is produced by reactors of the light water reactor (LWR) type, i.e., PWR, BWR, ABWR, and VVER. It may be noted

that three fast breeder reactors (FBR) are in operation worldwide (BN-600 in Russia, Phenix in France, and Monju^a in Japan) with a total electrical output of 1 GW.

A standard light water reactor generates 1 GW of electric power and produces some 23 tons HM (oxygen not accounted for) of spent nuclear fuel annually [11], assuming an average burnup of 40 MWdays/ton U. Based on this figure, together with electricity production data, a rough estimate of the annual production of spent fuel can be made. TABLE 3 gives an idea of the regional quantities involved. The estimated global spent nuclear fuel production is approximately 8,400 tons per year. This number does not include spent fuel of military origin (e.g. spent naval fuel, weapons production) or from research establishments. It should be kept in mind that the actual discharge rate of spent fuel (tons/year) depends on the burnup, which varies between reactors. Higher burnup essentially increases fuel utilization and generates less waste per unit electric capacity. According to a recent report by the IAEA [10], the global spent fuel generation is around 10,500 tons HM/year, which should then include spent fuel of all origins. According to the same report, the total amount of spent fuel cumulatively generated worldwide by the beginning of 2003 was close to 255,000 tons HM. The projected quantity for the year 2010 is close to 340,000 tons HM. By the year 2020, the time when most of the presently operated nuclear power reactors approach the end of their current licensed operational life time, the total amount of spent nuclear fuel will be around 445,000 tons HM. These figures are given in TABLE 4.

TABLE 2
Operational reactors by type, according to the IAEA [9]

Reactor type (abbreviation)	No. of units	Electric capacity (GWe)	%-electric capacity
PWR	214	204	55.9%
BWR	90	78	21.3%
VVER	52	35	9.6%
PHWR	39	20	5.5%
LWGR	17	13	3.4%
AGR	14	8	2.3%
GCR	8	2	0.6%
ABWR	3	4	1.1%
FBR	3	1	0.3%
Total:	440	366	100.0%

TABLE 3
Estimated annual production (tons/year) of spent nuclear fuel. Based on production rate of 23 tons HM/GWe [10]

Region	Generating capacity (GWe)	Estimated production of spent fuel from nuclear power plants (tons HM)
Europe (including Russia and Ukraine)	173	3990
North America (U.S. and Canda)	110	2540
Far East (mainly Japan, S. Korea, China)	76	1740
Others (South America, South Africa)	6	140
Worldwide	366	8410

^aAlthough Monju has been shutdown since an accident in 1995, it is categorized as ‘operational’ according to the IAEA since no permanent decision has been taken for its closure.

TABLE 4

Present and projected inventory (tons HM) of spent nuclear fuel accumulated worldwide [10].

Year	Worldwide inventory (ktons HM)
2003	255
2010 projected	340
2020 projected	445

Composition

The spent fuel is a multi-component system consisting of radionuclides with very different half-lives and toxicities. Besides the original components, i.e., uranium and oxygen, the spent fuel contains highly radioactive fission products, and transuranic elements. Fission products are created from the fission of heavy atoms (U,Pu) and transuranic elements (Pu, Am, Cm, etc.) are formed by capture reactions in heavy atoms. In addition, activation products are created by neutron capture in metal parts of the fuel element. There are many possible fission reactions, all producing different fission products. The amount of radioactivity and composition of the spent fuel is largely determined by the burnup and to limited degree on the burnup history, i.e., neutron spectrum, flux level, irradiation time, and cooling time after removal from the reactor. The term ‘burnup’ is a measure of the energy produced in the fuel (MWd per kg heavy atoms) or the fraction of heavy atoms that has fissioned. Increased burnup increases the concentration of fission products and transuranic elements. The local burnup depends on the position of the fuel rod in the core and varies also for each pin along its length. For this reason, burnup is usually reported as an average over local burnup levels. As a rule of thumb, 1% fission fraction corresponds to an energy production of 10 MWd per kg heavy atoms. Spectrum hardening in a LWR increases the formation of plutonium as it leads to more resonance capture. Although a higher neutron flux permits more secondary neutron capture reactions, the build-up of heavy actinides is less efficient. Since most actinides formed are fissile or fissionable but have a short lifetime relatively more will disappear by decay than will fission in a low flux. Long irradiation time tend to increase the proportion of long-lived products, while increased cooling time reduces the fraction of short-lived products. Because of these effects, the spent fuel varies in composition between reactor types but also between different fuel batches from the same reactor. TABLE 5 gives the composition of PWR fuel with an average burnup of 35 MWd/kg and 60 MWd/kg, three years after unloading [12]. The composition is normalized to the amount of initially present heavy atoms.

TABLE 5

Composition of spent PWR fuel in %-weight of initial heavy atoms (3 y of cooling) [12]

Family	Average burnup	
	35 MWd/kg U 3.25% initial ²³⁵ U	60 MWd/kg U 4.95% initial ²³⁵ U
Uranium	95.3%	92.4%
Plutonium	1.0%	1.3%
Minor actinides	0.08%	0.16%
Fission products	3.6%	6.1%

One can see that the fission product content increases from 3.6% for 35 MWd/kg to 6.1% for 60 MWd/kg. The plutonium (TRU) content increases slightly with burnup, from 1.0% for 35 MWd/kg to 1.3% for 60 MWd/kg. In addition, the minor actinide (Np, Am, Cm) content increases with burnup, where the production of ²⁴⁴Cm is problematic because of its neutron

emitting properties and its relatively short half-life of 18 years. The isotopic composition for plutonium changes with burnup [12], as shown in TABLE 6. The increase in burnup is accompanied by a decrease in fissile isotopes (^{239}Pu and ^{241}Pu) and build-up of even neutron numbered plutonium isotopes (which is well known from weapons plutonium production). ^{240}Pu and ^{242}Pu act as neutron absorbers. ^{238}Pu is produced through neutron capture in ^{237}Np and subsequent beta decay of ^{238}Np . It is a neutron emitter (from spontaneous fission) and strong heat source because of alpha emission. ^{240}Pu is also a neutron source because of its spontaneous fission. This has an adverse effect in handling high-burnup or multi-recycled spent fuel and also, reduces the fissile potential of the recycled fuel.

TABLE 6

Isotopic composition of plutonium in spent PWR fuel (in %-weight) 3 years of cooling [12].

Burnup	^{238}Pu	^{239}Pu	^{240}Pu	^{241}Pu	^{242}Pu
33 MWd/kg 3.25% initial ^{235}U	1.7%	57.2%	22.8%	12.2%	6.0%
60 MWd/kg 4.95% initial ^{235}U	3.9%	49.5%	24.8%	12.9%	8.9%

In high burnup fuel, the irradiation time is usually limited by material stability, e.g., due to fuel swelling, embrittlement of cladding or structural materials, rather than by reactivity limitations. A typical LWR fuel reaches an average burnup level in the range 40-50 MWd per kg U., which implies that 4-5% of the heavy atoms, undergoes fission in standard LWR fuel. TABLE 7 lists the composition of the transuranic elements contained in spent fuel with an average burnup of 40 MWd/kg U after 15 years of decay [11]. The cooling time has an immediate effect on the content of the shorter lived isotopes, primarily ^{241}Pu , ^{238}Pu , and ^{244}Cm , and on the concentration of ^{241}Am . The amount of ^{241}Am increases with burnup because it is the daughter of ^{241}Pu with a half-life of 14.4 years. Reduction of the inventory of ^{238}Pu and ^{244}Cm simplifies reprocessing and waste handling. Small amounts of elements heavier than curium are formed.

TABLE 7

TRU composition in LWR spent fuel (40 MWd/kg) 15 years after unloading [11]

Nuclide	%-weight	Half-life (y)
^{237}Np	5.60%	$2.1 \cdot 10^6$
^{238}Pu	1.98%	$8.8 \cdot 10^1$
^{239}Pu	50.8%	$2.4 \cdot 10^4$
^{240}Pu	22.4%	$6.6 \cdot 10^3$
^{241}Pu	5.86%	$1.4 \cdot 10^1$
^{242}Pu	5.17%	$3.8 \cdot 10^5$
^{241}Am	6.63%	$4.3 \cdot 10^2$
$^{242\text{m}}\text{Am}$	0.02%	$1.4 \cdot 10^2$
^{243}Am	1.21%	$7.4 \cdot 10^3$
^{244}Cm	0.27%	$1.8 \cdot 10^1$
^{245}Cm	0.02%	$8.5 \cdot 10^3$

Radiotoxicity

The activity of a radioactive substance is expressed in Bequerels (Bq) or Curies (1 Ci=3.7·10¹⁰ Bq). It is simply the number of disintegrations in a sample per unit time without regard to the properties of the radiation or the induced biological effects. Although comparisons involving radioactivity sometimes appear in the literature, it is generally recognized as a poor measure of the hazard. The most common way of measuring the risk associated with a radioactive substance, that gives a better measure of the biological harm to the body, is through the concept of “radiotoxicity”. It takes into account the sensitivity of the human body to a particular radioisotope after intake. The radiotoxicity is determined by the product of the activity (Bq) and an effective dose coefficient, *e*, for a given isotope:

$$\text{Radiotoxicity} = e \cdot \text{Activity}$$

While the activity is given by the number of atoms present in the sample multiplied with the decay constant of the radioactive nuclei, the effective dose coefficient depends on the type and energy of emitted particle, mode of intake (inhalation or ingestion), metabolism of the substance in the body, and sensitivity of the exposed organs. The effective dose coefficient corresponds to the committed dose (integrated over the life expectancy) resulting from the intake of 1 Bq of the specific radionuclide. Relevant data are regularly published by the International Commission on Radiological Protection (ICRP) [13]. The dose coefficients depend on the mode of intake. Plutonium, for example, is far more hazardous if inhaled than if ingested, because it is more readily absorbed into the blood stream via the lungs than via the stomach and intestines [14]. Before being transported to other organs, inhaled plutonium will deliver a radiation dose to the lungs, increasing the risk for lung cancer; ingested plutonium will deliver a radiation dose to the walls of the intestines. The uptake fraction in the gut is low because plutonium is not very soluble in the body fluids. To evaluate the hazard risk of a radioactive substance it must also be taken into account the particular pathway by which the substance reaches man. The transportation of radionuclides in the environment is not explicitly considered in the concept of the effective dose coefficients. But, in comparing the radiotoxicity of buried wastes in a repository, the inhalation pathway is less likely. The principal route of intake for members of the public is through water or food. Thus, in most hazard comparisons ingestion toxicity is in favour for inhalation [15]. Effective Dose Coefficients for ingestion of radionuclides are listed in TABLE 8. The effective dose coefficient is age dependent as it corresponds to the committed dose per unit intake (Bq). The integration time depends on the time from intake to age 70 y; for an adult it is taken to be 50 years. Depending on the absorption fraction of radionuclides in the adult, the uptake fraction may be 2-10 times higher in the infant. This is reflected in the effective dose coefficients, as shown in TABLE 8.

TABLE 8

Effective dose coefficients, e (Sv/Bq), for ingestion of radionuclides and their associated half-life [13].

Isotope	Half-life (years)	Uptake fraction (adults)	Uptake fraction (infant)	e , adults (Sv/Bq)	e , infants (Sv/Bq)	Minimum amount for acquiring fatal cancer* (g)
Actinides:						
²³⁵ U	$7.0 \cdot 10^8$	0.02	0.04	$4.7 \cdot 10^{-8}$	$3.5 \cdot 10^{-7}$	$5.3 \cdot 10^3$
²³⁸ U	$4.5 \cdot 10^9$	0.02	0.04	$4.5 \cdot 10^{-8}$	$3.4 \cdot 10^{-7}$	$3.6 \cdot 10^4$
²³⁷ Np	$2.1 \cdot 10^6$	$5.0 \cdot 10^{-4}$	$5.0 \cdot 10^{-3}$	$1.1 \cdot 10^{-7}$	$2.0 \cdot 10^{-6}$	$6.8 \cdot 10^0$
²³⁸ Pu	$8.8 \cdot 10^1$	$5.0 \cdot 10^{-4}$	$5.0 \cdot 10^{-3}$	$2.3 \cdot 10^{-7}$	$4.0 \cdot 10^{-6}$	$1.4 \cdot 10^{-4}$
²³⁹ Pu	$2.4 \cdot 10^4$	$5.0 \cdot 10^{-4}$	$5.0 \cdot 10^{-3}$	$2.5 \cdot 10^{-7}$	$4.2 \cdot 10^{-6}$	$3.5 \cdot 10^{-2}$
²⁴⁰ Pu	$6.6 \cdot 10^3$	$5.0 \cdot 10^{-4}$	$5.0 \cdot 10^{-3}$	$2.5 \cdot 10^{-7}$	$4.2 \cdot 10^{-6}$	$9.6 \cdot 10^{-3}$
²⁴¹ Pu	$1.4 \cdot 10^1$	$5.0 \cdot 10^{-4}$	$5.0 \cdot 10^{-3}$	$4.8 \cdot 10^{-9}$	$5.6 \cdot 10^{-8}$	$1.1 \cdot 10^{-3}$
²⁴² Pu	$3.8 \cdot 10^5$	$5.0 \cdot 10^{-4}$	$5.0 \cdot 10^{-3}$	$2.4 \cdot 10^{-7}$	$4.0 \cdot 10^{-6}$	$5.8 \cdot 10^{-1}$
²⁴¹ Am	$4.3 \cdot 10^2$	$5.0 \cdot 10^{-4}$	$5.0 \cdot 10^{-3}$	$2.0 \cdot 10^{-7}$	$3.7 \cdot 10^{-6}$	$7.8 \cdot 10^{-4}$
²⁴³ Am	$7.4 \cdot 10^3$	$5.0 \cdot 10^{-4}$	$5.0 \cdot 10^{-3}$	$2.0 \cdot 10^{-7}$	$3.6 \cdot 10^{-6}$	$1.4 \cdot 10^{-2}$
²⁴⁴ Cm	$1.8 \cdot 10^1$	$5.0 \cdot 10^{-4}$	$5.0 \cdot 10^{-3}$	$1.2 \cdot 10^{-7}$	$2.9 \cdot 10^{-6}$	$5.5 \cdot 10^{-5}$
²⁴⁵ Cm	$8.5 \cdot 10^3$	$5.0 \cdot 10^{-4}$	$5.0 \cdot 10^{-3}$	$2.1 \cdot 10^{-7}$	$3.7 \cdot 10^{-6}$	$1.5 \cdot 10^{-2}$
Fission products:						
⁹⁰ Sr	$2.9 \cdot 10^1$	0.3	0.6	$2.8 \cdot 10^{-8}$	$2.3 \cdot 10^{-7}$	$1.4 \cdot 10^{-4}$
⁹⁹ Tc	$2.1 \cdot 10^5$	0.5	1.0	$6.4 \cdot 10^{-10}$	$1.0 \cdot 10^{-8}$	$4.9 \cdot 10^1$
¹²⁹ I	$1.6 \cdot 10^7$	1.0	1.0	$1.1 \cdot 10^{-7}$	$1.8 \cdot 10^{-7}$	$2.8 \cdot 10^1$
¹³⁵ Cs	$2.0 \cdot 10^6$	1.0	1.0	$2.0 \cdot 10^{-9}$	$4.1 \cdot 10^{-9}$	$2.0 \cdot 10^2$
¹³⁷ Cs	$3.0 \cdot 10^1$	1.0	1.0	$1.3 \cdot 10^{-8}$	$2.1 \cdot 10^{-8}$	$4.8 \cdot 10^{-4}$

*Based on a dose of 20 Sv to acquire mortal cancer with 100% certainty (chemical toxicity not accounted for).

In terms of the level radiotoxicity per Bq, the plutonium isotopes belong to the most hazardous elements, despite that these are not easily absorbed from gastrointestinal tract. One may note that the effective dose coefficients are generally many times higher for the transuranic elements than for the fission products, which is principally due to their high alpha activity. One exception is ²⁴¹Pu, which is a β -emitter. Once transferred into the blood stream, the heavy elements are often concentrated in the bone, liver, and kidneys, where their α -emissions provide essentially lifetime irradiation since the biological exchange-rate in these organs is low [15]. Once inside the body, α -emitters are far more hazardous than β - and λ -emitters. The energy of the α -particle is dissipated in a small volume where the radionuclide is located and considerably increases the local biological damage. Beta particles are generally much less energetic and dissipate their energy over a larger volume than that of the alpha-particles. Elements such as strontium, iodine and cesium are hazardous because they are readily absorbed and their body chemistry tends to localize them and retain them in a particular critical organ (strontium is incorporated in the bone and iodine is enriched in the thyroid gland).

An illustrative example can be made, which gives a relative measure of the intrinsic radiotoxic properties of a particular nuclide. According to the ICRP, the risk of fatal cancer induction is 5% per Sv (committed effective dose) [16]. This risk is on top of the natural lifetime risk of fatal cancer, which is around 24% for males and 20% for females in the U.S [17]. The usual assumption is that the risk of getting cancer is linearly related to the exposure [15]. Thus, based on this rule, there is a 100% chance for an individual to acquire (and die) of cancer if exposed to a dose of 20 Sv. For perspective, the average background dose is typically in the range 1-2 mSv per year, depending on the geographical location and ground properties (the largest contribution to the background radiation comes from the daughters of

radon). With this information it is possible to calculate the minimum ingested mass of a particular radionuclide to acquire fatal cancer with 100% probability. Results are shown in the last column in TABLE 8. It is seen that, among the listed elements, the most radiotoxic isotopes are ^{244}Cm followed by ^{238}Pu , ^{90}Sr , and ^{137}Cs . The common property of these nuclides is that they are rather short-lived and hence, deliver the greatest activity per unit mass, in combination with a high effective dose coefficient. ^{239}Pu is hazardous, but it is not immediately as hazardous as many other transuranic isotopes because of its long half-life. As outlined in TABLE 8, ingestion of about 35 mg of ^{239}Pu would be necessary to result in the expectation of 100% risk of cancer mortality. The calculated amounts should not be regarded as a sharp line between death and survival as the actual lethal amount would depend on a variety of circumstances, e.g., the uptake fraction varies strongly with chemical form of the radionuclide. It is noted that ingestion of a radionuclide induces a long-term health-effect primarily, as cancer may take several years or decades to appear. Relatively high doses are required to deliver an acutely lethal dose. According to one report [18], ingestion of about 500 mg of plutonium would be necessary to produce acute sickness. (For comparison, the acute lethal dose of arsenic is around 100 mg). There are obviously all sorts of alternatives to this calculation; the values presented in TABLE 8 are intended to provide a frame of comparison about the hazard for a particular radionuclide as given by its radiotoxicity value. It is stressed that the ICRP dose limit apply to softly-ionizing radiation, i.e., primarily β - and γ -rays, administered to a person over a long time-period. In fact, there are several arguments for the assumption that the response to low dose-rates and softly-ionizing radiation may not be extrapolated to a high dose-rate and highly-ionizing radiation. For example, the value 20 Sv is twice as large as the lethal dose for instantaneous exposure [15], i.e., acute radiation sickness, which is a result of the fact that the biological harm is related to the dose-rate.

From the activity concentration and the effective dose coefficients, each radionuclide in the spent fuel can be assigned a radiotoxicity value. Fig. 1 shows the evolution of the ingestion radiotoxicity of spent uranium at a burnup of 40 MWd/kg as function of cooling time, where the results are grouped according to fission products and transuranic elements. The values are normalized to 1 g of initially present heavy metal (IHM). It is emphasized that the radiotoxicity corresponds to the committed dose that would be received over a time period of 50 years. This dose decreases over time as the radioactivity of the fission products and actinides decreases by time.

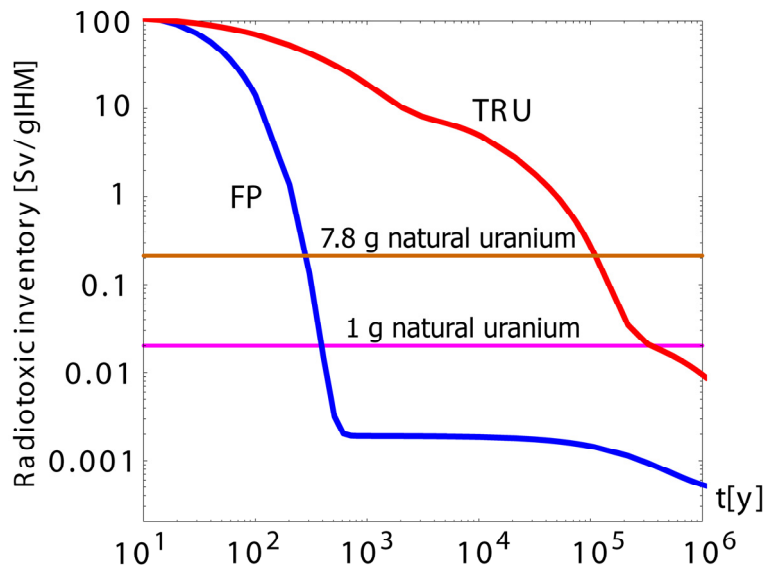


Fig. 1 Radiotoxic inventory of the fission products and transuranic elements in spent nuclear fuel (3.7% ^{235}U , 42 MWd/kgIHM).

In the diagram, the horizontal lines refer to the total ingestion radiotoxicity for 7.8 g and 1 g of natural uranium, respectively. The 7.8 g of natural uranium correspond to the amount that must be recovered from the ore to produce 1 g of uranium fuel enriched to 4.2% in ^{235}U (0.2% tails assay). Notice that these figures include not only the uranium isotopes but the uranium daughters that are in natural mixture with the uranium recovered from the mine. The use of the radiotoxicity value for an equal amount of natural uranium is easy to relate to in terms of the risk associated with the storage of spent fuel in an underground facility. It may be argued that when the radiotoxicity value for the spent fuel products crosses this reference level, it does not constitute a greater risk than natural uranium contained in the ore^a (provided that the waste product is as equally fixed as the original ore). An alternative approach is to compare with the amount of uranium that must be recovered from the ore to produce the nuclear fuel. This way of comparison is often used by waste management people to provide a comparison with the risk if the wastes not been produced at all. The idea here is that disposal need not to provide any greater safety than if the uranium had never been mined in the first place.

Fig. 1 indicates the extreme difference in the long-term radiotoxicity associated with the fission products and the transuranic elements. During the first 20-30 years after discharge the fission products (primarily ^{90}Sr and ^{137}Cs) determine the total radiotoxicity of the spent nuclear fuel. At later time the transuranic elements dominate the hazard. According to Fig. 1, it would take approximately 300,000 years before the radiotoxicity of the transuranic elements reaches natural levels. The cross over point for the fission products radiotoxicity curve is around 300 years. Obviously, if the transuranic elements could be eliminated, the long-term hazard would be considerably reduced. This is the basic motivation for partitioning and transmutation strategies, and for the deployment of dedicated reactor systems, which will be discussed in the following chapter.

^aAs Koplik [19] has pointed out, this analogy is not entirely satisfactory since the release probability for buried waste may be quite different to that of average material of the uranium-ore. Firstly, the nuclear waste form differ both chemically and physically from the ores and thus their mobility in the ground may be different. Secondly, it overlooks the fact that the nuclear wastes will be buried at great depths in a well-chosen location surrounded by engineered barriers, which suggests lower release probability than average material in an ore. The latter may be located at or near the surface with flowing ground water present.

prior to disposal. The most commonly suggested solidification scheme is to vitrify the waste into an insoluble glass material. If the spent fuel is not reprocessed, the material to be disposed of is contained within the spent fuel itself (UO₂). Before final deposition, the waste matrix (either the spent unprocessed fuel or the vitrified high-level waste) is encapsulated in a metal canister. The spent fuel elements may be placed as intact assemblies or the fuel rods may be removed from the assembly and framed inside the canister. The objective for rearranging the rods is to reduce the volume to be stored and improve heat removal characteristics. There is no essential difference between the repositories for vitrified high-level waste or spent fuel. Only the canisters differ somewhat between the two concepts.

Waste treatment by partitioning followed by transmutation is also being seriously considered. This is the subject of the remaining chapters. It may be added that partitioning and transmutation does not completely eliminate the need for a storage facility, but it may significantly reduce the risk of storing the remaining waste and also simplify the conditions for the final storage. Over the years, several other disposal methods have been suggested. These are mentioned here for completeness, but it should be noted that these are not being seriously considered at present. In theory, all radionuclides could be dispersed into the global air and sea volumes to reach acceptable concentrations, but the limitations are practical (no process for uniform dispersal exist), together with the social/moral and political difficulties involved. Another proposal is to launch the high-level waste into outer space, either by sending waste packages in an orbit around the earth or transportation to the sun or solar escape. The argument against this method is the obvious risk for an accident during launch (considering the large number of launches necessary) and the high cost. Other methods include: burial of waste containers under the ocean floor between tectonic plates, or placing them in deep bore holes in the ground, or even lowered into holes in the polar ice-sheet where they would begin propelling downwards through the melting ice. The problems shared by these proposals are the highly uncertain disposal processes (e.g. uncertain movement of canisters) and difficulty of inspection and retrievability/reversibility, which forecloses the possibility of future adjustments. It is possible that the environmental conditions changes which could motivate relocating the waste at a later stage or it could be decided to recover its resource value as a result of scientific progress.

Safety performance of a geologic repository

The principal safety issue of a repository is the risk of spread of radionuclides to the biosphere, where they can cause harm to humans. In the typical case in which the post-closure safety performance of the waste repository is analyzed [20], two distinct release scenarios can be identified (it should be noted that other definitions of “scenario” from that adopted here are in use, but essentially these can be grouped into the following two categories):

- Indirect release scenarios, via groundwater transport.
- Direct release to surface (by some natural event or human intrusion)

It is generally agreed, among waste management experts, that by a combination of physical barriers and environmental conditions, a carefully chosen repository can guarantee isolation for at least one thousand years and probably much longer. This conclusion is supported partly by the results of radioactive materials behaviour in natural analogues (e.g. Oklo) and findings of man-made objects which have withstood degradation since ancient times (e.g. The Egyptian pyramids and the bronze cannons of the Swedish warship Kronan which were found buried in seabed after the ship had been sunk in 1676). Beyond 10,000 years, however, it is recognized that the impact of major climate changes (e.g., glaciations) could affect the evolution of the repository system and canister containment cannot be guaranteed in general (although the SKB concludes that it is realistic to expect canister lifetime of 100,000 years or

even a million-year in the Swedish repository system [20]). For hazard assessment related to the natural break down of a canister, it is important to consider the processes involved in the pathway of the radioactive substance from the repository to man. Once the released from the repository, the waste products can only be carried to the surface via the groundwater. Under these circumstances, the solubility of the radionuclides in the groundwater, and their adhesion in the ground, and dispersion or buildup in the biosphere (food, water, background radiation) are the major factors determining the potential exposure to man. The actual transport rate of nuclides depend on many factors (geologic media, water composition, ground water velocity, etc.) and are site specific, but in general the actinide species move much slower in the ground water system compared with certain fission products (mainly technetium, iodine, cesium, and tin), and thus are not easily transported to the surface. Therefore, from the viewpoint of release scenarios associated with leakage through defective canisters, the risk is dominated by the long-lived fission products. The dominant contribution would then come from fission products such as ^{99}Tc , ^{129}I , ^{135}C , ^{126}Sn , and ^{79}Se .

As was shown in Fig. 1, some fission products (^{90}Sr and ^{137}Cs) dominate the radiotoxic inventory in the spent fuel during the first 30 years or so after discharge. However, after a few hundreds of years, the fission products are small contributors to the radiotoxicity being many orders of magnitude below that of the actinides (^{239}Pu , ^{240}Pu , and ^{241}Am). Thus, from the standpoint of the radiotoxicity contained in a repository, the risk is dominated by the transuranic elements. Considering their much lower mobility, release of actinides to the biosphere involves events that can bring some of the waste directly to the surface. Direct release to the surface, whether by natural phenomena or human activity, circumvents the pathway between the waste and the biosphere. Natural phenomena, such as earthquakes, volcanic eruptions, or impact of a giant meteorite, could lead to direct release of buried waste, but repeated studies have shown that the probability of these events (with the potential of lifting up the waste to the surface) is sufficiently low to be neglected [19, 21]. In the Swedish study of a granite repository [20], it was concluded that canister damage by seismic activity can be avoided in connection with the siting of the repository. Thus, causes for direct release of buried waste have focused on human intrusion scenarios.

Fig. 3 presents the calculated annual dose following the release from defective waste canisters for four repository cases of interest: 63,000 tons of spent fuel in oxidizing environment (volcanic rock in Yucca Mountain, U.S.), 2,600 tons of spent fuel in reducing environment (deep bedrock in Finland), 3,600 tons of vitrified high-level waste in granite (Switzerland), and 4,200 tons of vitrified high-level waste in clay (Belgium). The figure illustrates schematically the fact that the long-term risk is dominated by those nuclides that have high mobility in the ground (^{129}I , ^{99}Tc , ^{79}Se , and ^{135}Cs). The quality of the groundwater greatly influences the migration properties from the repository. An oxidizing environment increases the solubility of many radioactive substances (and promotes early deterioration of the canister). For example, Tc-99 is a major contributor to dose in the Yucca Mountain within the first 10,000 yr after closure. This is due in large part to its high mobility under the prevailing conditions. In a reducing environment, technetium is remarkably stable. With regards to the Swedish repository concept (granite repository containing spent fuel elements), the dominant isotopes for the release to the biosphere are ^{129}I and ^{79}Se and some activation products: ^{36}Cl , and ^{59}Ni [20]. The iodine, for example, has very high solubility and is not adhered in the granite. During reprocessing it is released to the off-gases and discharged into the sea and for that reason it is not present in any significant quantities in vitrified high-level waste. In general, the actinides have a negligible influence to the release to the biosphere for a canister break down scenario. An important exception is the mobility of ^{237}Np in oxidising groundwater conditions, which makes it an important isotope for the long-term performance of Yucca Mountain. Groundwater release scenarios similar to the ones presented in Fig. 3 are

often used in repository safety analysis. In these scenarios the long-term risk is mainly associated with long-lived fission products not with the actinides. As a result, it has been reasoned [22, 23] that there is no real strong incentive for reducing the actinide inventory from the point of view repository performance. Yet, one should bear in mind that such account disregards human intrusion into the repository (malicious or accidental) and also overlooks the possibility for unanticipated natural events. These events are by their very nature extremely difficult to predict. A striking feature in the groundwater transportation scenarios is the complete absence of the most radiotoxic materials – plutonium, americium, and curium – since the retarding capacity of the repository is very good for these nuclides. Beyond 300 years the radiotoxicity of the transuranic elements is significantly higher than of the fission products. In a human intrusion scenario these elements are a major concern. We believe it is fair to consider the radiotoxicity of the spent fuel waste also from global point of view.

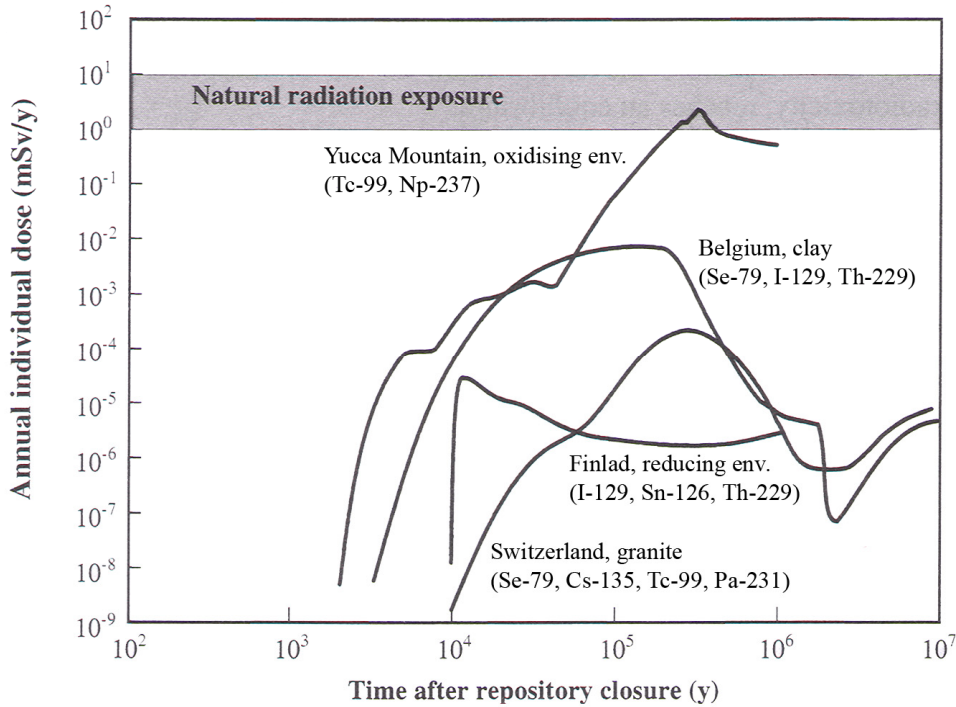


Fig. 3 Predicted annual individual dose from indirect release of defective waste canisters (adapted from OECD/NEA report [24]).

Chapter 2:

Partitioning & Transmutation

Partitioning and transmutation (P&T) is the general term for the techniques involved in the conversion process of long-lived radiotoxic isotopes into shorter-lived nuclides. In the following Chapter we will briefly describe the partitioning and transmutation operations considered with comments on their merits and limitations. The aqueous separation techniques, corresponding to the PUREX process, are briefly described together with the possible and desirable extensions to recover the minor actinides. Pyro-processing is another technique being investigated. The remainder of the chapter is devoted to describing the basic transmutation processes involved.

Partitioning

Partitioning refers to the chemical operations applied for the separation and extraction of selected elements from the spent nuclear fuel. It is closely related to the conventional reprocessing techniques of spent fuel, but embraces further separation operations to extract the minor actinides (MA) and the fission products (FP). Partitioning is a prerequisite for preparation of the spent nuclear fuel to realize further transmutation steps.

Plutonium separation technologies were developed in the United States during the Manhattan Project. Most plutonium reprocessing methods make use of the ‘oxidation-reduction principle’ in which plutonium is placed in different oxidation states whose chemical properties differ. The earliest attempts were based on “carrier” techniques, which were later replaced by the solvent extraction process that also forms the basis for the REDOX process and the PUREX process. The carrier technique was used to isolate the first amounts of plutonium to power the Fat Man bomb [25]. Today, all commercial reprocessing plants make use of the PUREX process, which is short for Plutonium Uranium Redox EXtraction. Major PUREX plants exist at La Hague, France, with a total capacity around 1600 tons IHM/y (two 800 t/yr units), the Magnox plant and the THORP reprocessing plant at Sellafield, United Kingdom, with capacities of 1500 and 850 tons IHM/y, respectively. At Marcoule in France one 400 t/yr reprocessing plant is operating for metal fuels from gas-cooled reactors. India has a 100 t/yr oxide fuel plant operating at Tarapur, and Japan is constructing a 800 t/y PUREX reprocessing plant at Rokkasho. Russia has a 400 t/yr oxide fuel reprocessing plant at Ozersk, Chelyabinsk. The worldwide annual capacity for civilian spent fuel reprocessing is around 5000 tons.

PUREX

According to a DOE historical overview [26], the solvent extraction processes (first the REDOX followed by the PUREX process) replaced the bismuth phosphate (carrier) method for plutonium production at the Hanford Site in the 1950s. The solvent extractions method is a wet (aqueous) process involving the dissolving of the fuel in nitric acid (nitric acid diluted with water). As it includes using a liquid-mixture of aqueous and organic solvents the

separations process is also known as liquid-liquid extraction. The solvent extraction process is adaptable to continuous operation, whereas the carrier technique operates in separate stages, meaning that only a limited amount of material can be treated in every stage. From an industrial production standpoint, processing a continuous stream of materials is generally preferred over batch processing. The solvent extraction processes make use of an alteration between the oxidation states of plutonium (IV, VI and III) whose chemical properties differ. Advantage is taken by the relative stability of the oxidation state of uranium and most fission products, while plutonium is easily reduced. Successive solvent extraction cycles are carried out until the desired decontamination and purification is achieved. The PUREX process was developed by Knolls Atomic Power Laboratory [26] in the United States and it is presented schematically in Fig. 4.

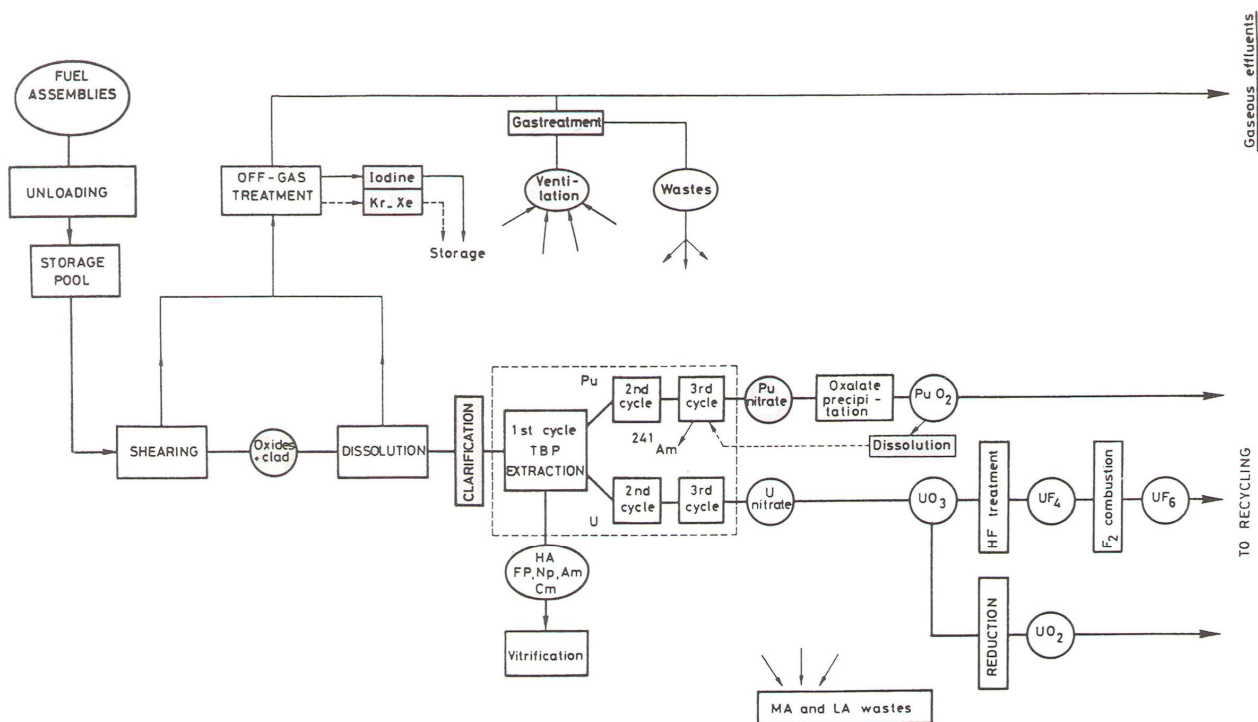


Fig. 4 Schematic flowsheet of the PUREX process. Adopted from textbook by G. Choppin, J. O. Liljenzin, and J. Rydberg [15].

As shown in Fig. 4, the first step of the PUREX process is to cut or saw the fuel pins into pieces, 3-5 cm long. This is usually done under water or inert gas. Gaseous fission products are collected and taken off in a separate stream. The chopped fuel pieces (oxide + cladding) are then dissolved in hot nitric acid. Remaining fission gas is released and transferred to the off-gas treatment. The cladding material is not dissolved in the nitric acid. The product solution is cooled and transferred to the separation section (the section enclosed in the dotted box in Fig. 4). At this point the uranium is in the hexavalent state, and plutonium in the tetravalent. Three purification cycles are conducted for both U and Pu. The first cycle consists of three solvent extraction stages (extraction stage, U-Pu partitioning stage, U stripping stage). In the first extraction stage, the aqueous fuel solution is contacted with an organic solution in special extraction columns. Presently, tributyl phosphate (TBP) is the chemical extractant used in all PUREX plants. It is normally used as a 30% solution in kerosene. The aqueous and the organic liquids will form separate layers in the extraction column with the aqueous flowing downward, while the organic flows up. This is the solvent extraction process and is the chemical basis for the PUREX method. The organic compound carries along the 4- and 6-

valent actinides (U, Np, Pu), leaving most fission products (I, II, III, V, and VII-valent species) and the trivalent actinides (Am and Cm) in the aqueous nitric acid solution. Thus, the uranium and plutonium are stripped out of the solution. More than 99.8% of the U and Pu are extracted into organic phase, leaving >99% of the fission products including most of the Am and Cm in the aqueous. Np exist in nitric medium in oxidation states V and VI, of which only the higher oxidation state (~60%) is extracted. The FP and MAs are transferred to the high-level waste residue. The HNO₃ concentration influences the extraction performance. In a second stage, plutonium is separated from the uranium by reducing it to its trivalent state which is insoluble in TBP. By adding fresh kerosene-TBP solvent, the plutonium is then stripped to a new aqueous phase and sent to the plutonium purification line. The uranium, which is in the tetravalent state, stays in the organic phase. In the third stage, the uranium is washed out of the TBP with dilute HNO₃. The uranium and plutonium products are then subject to further purification cycles to reach higher purity. The 2nd and 3rd separation cycles are essentially based upon the same chemical reactions as in the first cycle. The separations process end with purified and separated plutonium and uranium in the form of nitrate paste, which is further refined into plutonium- and uranium-oxides or uranium hexafluorides. The high-level liquid waste contains the fission products including the Am, Cm, and some Np in nitric acid solution.

Partitioning of Np, Am, and Cm

As mentioned in Chapter 1, after plutonium, the minor actinides (Np, Am, and Cm) are the next most radiotoxic elements in the spent fuel. If they could be transmuted, the radiotoxic inventory would be considerably reduced. Transmutation of Am and Cm is a prerequisite for a significant reduction of the long-term radiotoxic inventory. The purpose for transmutation of Np is mainly to reduce the radiotoxic risk (mobility in the certain geological repository conditions) associated with the spent fuel repository in the very long term.

Before the minor actinides could be subject to transmutation operations, they must first be partitioned. In the conventional PUREX cycle, the minor actinides are left together with the fission products in the high-level waste. Neptunium is distributed between the oxidation states V and VI and is therefore partly discharged with the fission products and partly transferred with U and Pu. Recovery of separated neptunium is technically possible in a slightly modified version of the PUREX process. New processes are however necessary to separate Am and Cm. It is difficult to separate these from the lanthanides (Ln) as they have similar chemical properties (both are present in trivalent oxidation state). Depending on the burnup, the concentration of the lanthanides may be 30 times higher than Am and Cm in the high-level waste. A high purity of minor actinides is required in order to avoid neutron capture processes by the lanthanides in later reactor operations. The general scheme for separation of Am and Cm from the spent nuclear fuel is shown in Fig. 5. Firstly, the PUREX process is applied to recover U and Pu. Secondly, a process (e.g. TRUEX, DIAMEX, TALSPEAK/DIDPA) is used to co-extract the minor actinides and the lanthanides from the rest of the fission products. The processes require additional steps to extract the minor actinides from the Ln. A two step partitioning process is suggested, as described below. The techniques are not yet operational on an industrial scale.

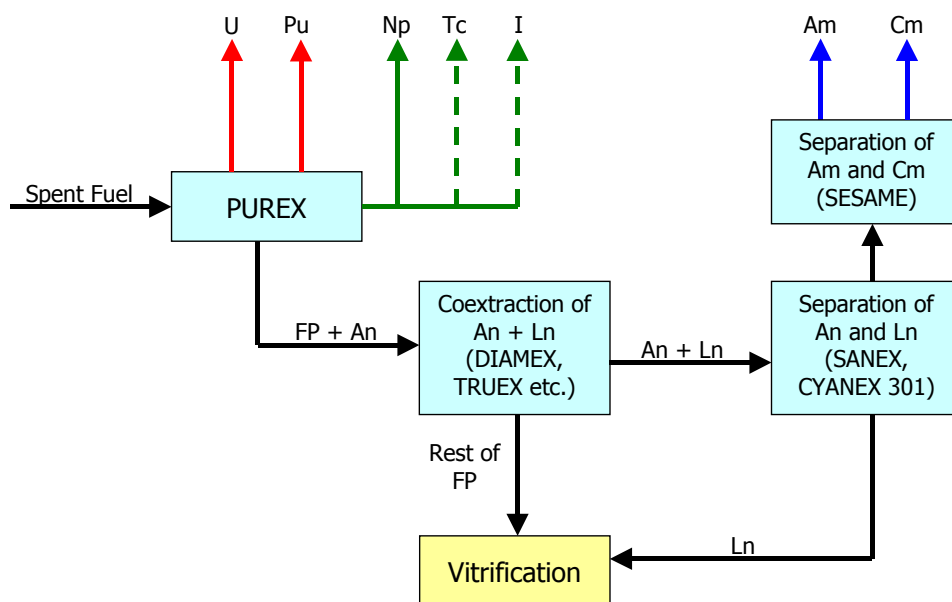


Fig. 5 General flow sheet for partitioning of Am and Cm from the spent nuclear fuel. (with permission by P. Seltborg [27])

The TRUEX (TransUranic Extraction) [28] process was developed by the U.S. Department of Energy (DOE) in the 1980s for separating actinides (and the lanthanides) from the high-level wastes generated by defence related reprocessing plant operations or during plutonium production and purification operations (at the Hanford, INEEL, Oak Ridge, and Savannah River Site sites). Complemented with the SREX (Strontium Extraction) process it can be used to remove strontium and cesium. An overall removal efficiency of 99.79% has been obtained for the actinides using TRUEX [29]. The CEA in France is developing the DIAMEX process (DIAMide EXtraction) as a method for combined extraction of actinides and lanthanides. It has been demonstrated on actual waste. In contrast to the TRUEX process, no secondary solid wastes are expected. The DIAMEX process has demonstrated recovery efficiencies of more than 99.9% of the Am and Cm, and very high decontamination factors were achieved for both Ln and An [30]. Difficulties are related to the partial co-extraction of palladium and ruthenium with the MAs. Subsequent separation of Am and Cm from lanthanides can be carried out in various versions of the SANEX processes (CYANEX 301, ALINA, BTP). Reasonably good separation efficiency of americium has been achieved (>99%), but further improvement is required for the recovery of curium (97.6% at present). Methods for selective separation of Am and Cm are under investigation. The current reference process is the SESAME process based on oxidation of Am(III) to Am(VI) and selective extraction of Am(VI) from Cm(III) by solvent extraction. In principle, a high extraction efficiency of Am is possible. But, it appears to be difficult to realize on a larger scale because of the instability of the higher oxidation states of Am in aqueous medium [31]. The use of stabilising agent increases the waste volume.

Dry techniques

The challenges anticipated by the aqueous partitioning processes with regards to MA-fuels include: 1) degradation of organic solvents at high radiation doses restricting the recycle potential, 2) Possibility of criticality which limits the concentrations which can be handled, and 3) Low solubility in nitric acid of many of the fuel forms considered.

As alternative to aqueous separation, dry fuel cycle processes have been investigated. These generally aim at pyroprocess methods. Opposite to conventional aqueous processing,

pyroprocessing does not involve dissolving the spent fuel in nitric acid. Refining is carried out in molten salt (fluorides, chlorides) and at high temperatures, around 500°C. As a result, these processes are often called “dry” processes. Instead of a solvent extraction principle, the recovery of individual actinides from the liquid mixture is achieved by electrorefining operation. The major advantages of pyrochemical techniques, in comparison to aqueous techniques, are that the materials used in the pyrochemical process are much more radiation resistant compared to the organic solutions used in the aqueous processes. Thus, pyrochemical techniques offer potential for the treatment of highly active spent fuel. This is a significant advantage when dealing with multi-recycled and high-burnup minor actinide fuels. In combination with the high solubility of most fuel forms in molten salts and less strict criticality constraints due to the absence of water, pyrochemical reprocessing can handle higher concentrations than aqueous solutions, and thus reduce the process volumes and also the size of the plant. Several process steps can be performed in a single vessel both reducing the size of equipments and the need for transportation of nuclear materials. It is often advocated that pyrochemistry is more economical than hydrochemical processes and that waste treatment is easier (small waste volumes and solid waste forms). Presently, actinide recovery in pyrochemical processing is limited to about 99% and thus multi-stage operation will be necessary.

Although several pyrochemical separations processes are known, two methods have been investigated extensively and developed up to industrial scale. One is the molten salt electrorefining method of metallic fuel developed by Argonne National Laboratory (ANL) for the treatment of spent EBR-II fuel and in connection with the Integral Fast Reactor (IFR) project [32]. The other route developed is the pyroelectrochemical method for oxide fuels (UOX and MOX) developed by the Research Institute for Atomic Reactors (RIAR), Russia [33].

The basic ANL method [34] was developed for the treatment of the sodium bonded U-Pu-Zr fuel. The first step is the dismantling of the fuel assemblies and removal of the cladding. The second step is dissolution of the fuel in a molten salt (LiCl-KCl) and molten metal (Cd) bath and the third step is the electrorefining of this liquid mixture. A schematic diagram of the electrorefining of U-Pu-Zr based minor actinide fuel involved using a molten eutectic of LiCl+KCl as electrolyte is shown in Fig. 6 [35]. The fuel is placed inside a basket where it is dissolved in the electrolyte. The uranium and transuranic elements are deposited on different cathodes. The fission products are not dissolved and remain in the basket or sink down to the bottom (although some remain dissolved in the molten salt). Uranium is partially deposited on a solid cathode (metal) and the transuranic elements together with the remaining uranium and a small amount of lanthanides are recovered into a liquid cadmium cathode. Whereas metallic alloy type fuel can be treated directly, oxide cycle must be first reduced to the metallic state before it can serve as feed material for the metal cycle. So far the oxide reduction technology has been experimentally demonstrated, but only at the laboratory level. Selective recovery of actinides beyond uranium and plutonium still needs to be demonstrated.

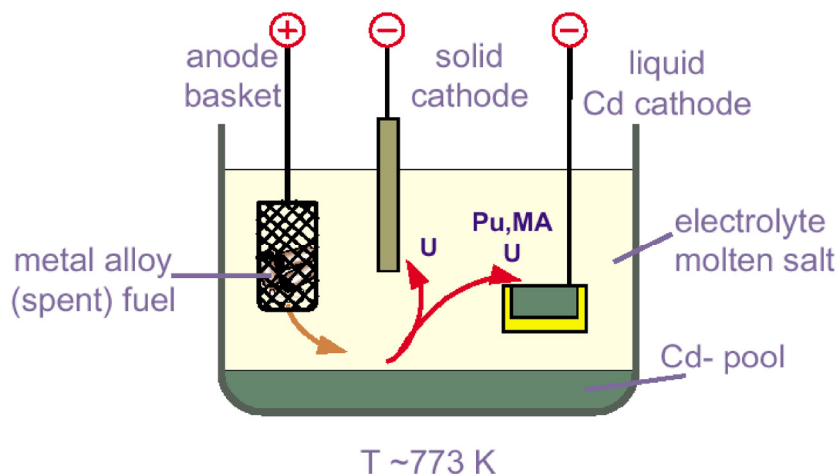


Fig. 6 Schematic picture of the pyroprocess treatment of U-Pu-Zr based minor actinide fuel [35]

Transmutation

Physics of transmutation

The term “transmutation” is used in reference to nuclear transformation processes in which one nuclide is converted into another. Transmutation of atomic nuclei can be artificially induced by collisions with neutrons, protons, alpha particles, and gamma quantum, or by natural disintegration processes such as α - and β -decay, and spontaneous fission decay resulting in changes in the nuclear composition. In all cases, transmutation involves a change in the constitution of the atomic nuclei, i.e., change to the number of protons and/or neutrons, and is accompanied with a change to its properties.

In order to induce a nuclear reaction between charged particles, the incoming particle must possess sufficient kinetic energy to overcome the Coulomb barrier (there is a chance of tunnelling but the probability is very small unless the kinetic energy is close to the threshold energy). If the energy of the incoming nuclei is small, nuclear reaction is limited to elements of low atomic number. Nuclear reaction with heavy nuclei requires the largest kinetic energy. Nuclear interactions involving neutrons and photons are not subject to the coulomb repulsion, and hence may occur at any energy. In principle, a photon can transfer sufficient energy to a nucleus for a transmutation reaction to occur, but the energy required is still quite high and the probability for reaction is low in comparison with neutron-induced reactions. For example, the photofission threshold in uranium (around 6 MeV) is much higher than the neutron induced fission threshold (0-1 MeV), which is a consequence of the binding energy of the neutron added to the target nucleus. Such energetic gamma rays are rarely emitted in radioactive decay and even if they are the potential intensities are limited. As a result, large-scale transmutation by photonuclear reactions or bombardment by charged-particles can be dismissed on practical and economical grounds. Neutron induced transmutation is yet the only feasible means for transmutation at industrial scale. There are many ways of producing neutron sources of moderate intensity, but high neutron fluxes are most conveniently produced in a nuclear reactor.

Neutron induced transmutation encompasses two principle nuclear transformation processes^a: fission and neutron capture. Besides the fission fragments, the reaction products of fission are several neutrons (between zero and five) as well as gamma radiation, beta particles, neutrinos, and of course energy. The exact identities of the two lighter nuclei vary from fission to fission, but a typical reaction can look like:

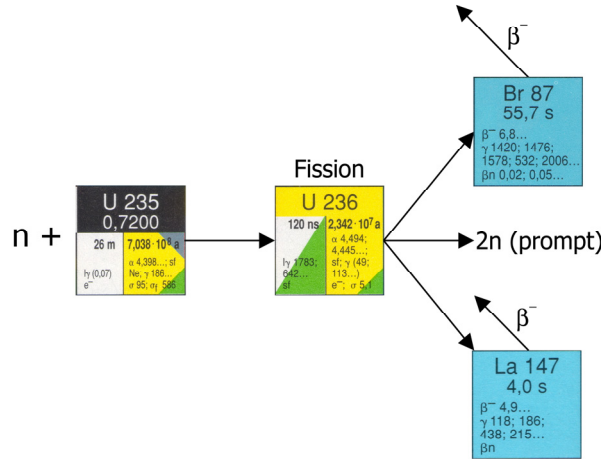


Fig. 7 Example of neutron-induced fission reaction in ²³⁵U

The fission products are neutron-rich and will therefore decay mainly by beta particle emission. The half lives of the fission products are usually much shorter than the half life of the initial heavy nuclei. The second transmutation reaction is neutron capture, or “radiative capture” since the neutron is trapped inside the nucleus and only a gamma ray comes out (n,γ). Neutron capture increases the mass number by one and the reaction is often accompanied by beta-decay. Neutron capture is the cause for build-up of transuranic elements from natural uranium. This is shown in Fig. 8.

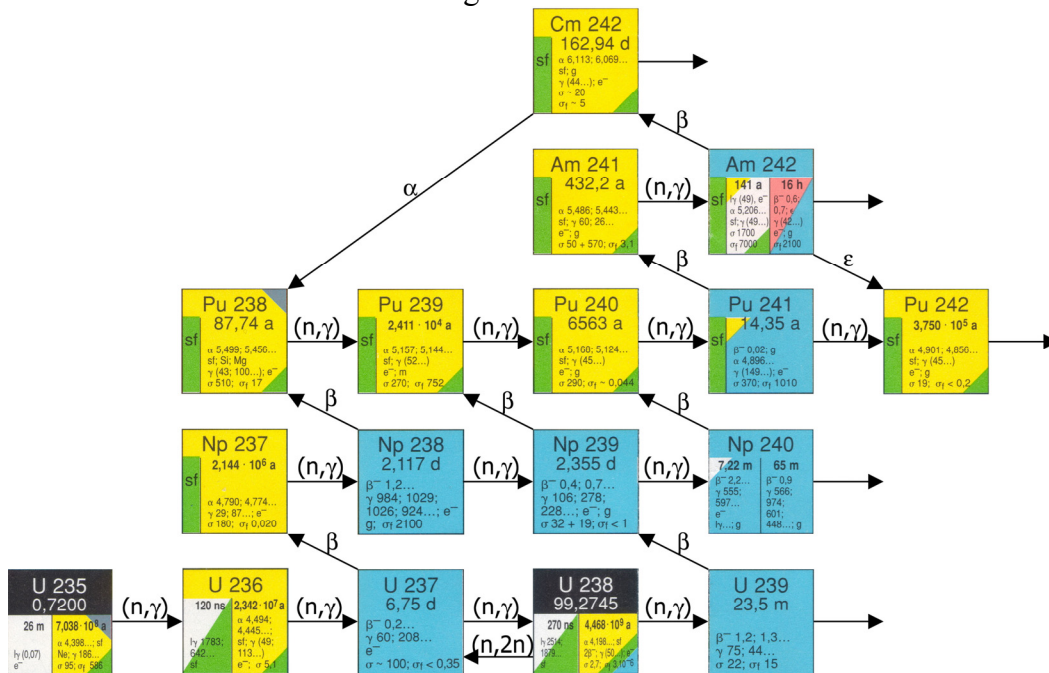


Fig. 8 Heavy-isotope build-up by neutron capture in natural uranium

^aAlthough other transmutation reactions also occur, e.g., (n,p), (n,2n), and (n,α), these are of secondary importance for P&T purposes.

From the viewpoint of reducing the long-term radiotoxicity of the actinides, the most efficient reaction is fission since capture merely builds-up other heavier long-lived elements. It may be noted that fission results in higher radiotoxicity in the very short term (<100 years) because of the generation of the highly active fission products, but the resulting material will be much less radiotoxic in the long-term. In addition, a significant amount of energy is generated. However there is no guarantee that a neutron absorbed in a heavy nucleus causes fission. Both fission and capture take place simultaneously during irradiation. The probability of occurrence depends on the nucleus and on the energy of the incident neutron. The principal isotopes that are responsible for fission in a nuclear reactor are the heavy elements with odd number of neutrons, such as ^{233}U , ^{235}U , ^{239}Pu , ^{241}Pu , and $^{242\text{m}}\text{Am}$. In these nuclides fission can be induced by neutrons of any energy. Such nuclides are referred to as fissile. Yet, it is still possible that the nuclei formed in the neutron absorption process in fissile isotopes will decay to its ground state by the emission of gamma, but it is less likely. For most heavy nuclides, however, absorption of low-energy neutrons is not likely to cause fission. Examples are the even-neutron numbered actinides (^{238}U , ^{237}Np , ^{238}Pu , ^{240}Pu , ^{242}Pu , ^{241}Am , etc.). These nuclides can only be fissioned by neutrons above a certain threshold (roughly 1 MeV). Such isotopes are referred to as fissionable. The fission probability upon neutron absorption is the ratio between the fission cross section and absorption cross section (fission + capture). It is of great importance in the discussion on transmutation. Its value depends on the properties of the reacting nucleus as well as on the energy of the incoming neutron. TABLE 9 compares this ratio for some actinides of particular interest, together with spectrum averaged cross-sections for fission and capture in a thermal spectrum and in a typical fast reactor spectrum. It can be seen that, for all nuclides the fission probability is higher in a fast spectrum than in a thermal spectrum, but the largest relative increase occurs for the even neutron numbered nuclei. It is further seen (Fig. 9) that the fission probability increases markedly for the even neutron numbered isotopes at energies above 0.1 MeV, which is a result of a significant energy variation of the fission cross section in this range. The conclusion to be drawn is that the spectrum should be as hard as possible to realize a high probability for direct fission. It ought to be mentioned that, in principle, transmutation of the minor actinides is possible in a thermal spectrum through breeding into fissile nuclides and successive build-up of heavier short-lived isotopes (Cm, Bk, Cf). However, limitations are set by the low burnup potential and insufficient neutron economy in a thermal spectrum, which require long irradiations, multiple-recycling, and high fissile loading. In practice, recycling is made difficult because of high neutron dose rates and the residence time is limited by helium generation in the fuel. This will later impact our choice for reactor system for transmutation purposes.

TABLE 9

Effective cross-sections of actinides for thermal systems and fast systems [31]

Nuclide	Thermal spectrum (PWR)			Fast spectrum (FBR)		
	σ_f	σ_c	$\sigma_f/(\sigma_f+\sigma_c)$	σ_f	σ_c	$\sigma_f/(\sigma_f+\sigma_c)$
^{238}U	0.10	0.94	0.10	0.04	0.30	0.12
^{237}Np	0.52	33	0.02	0.32	1.70	0.16
^{238}Pu	2.4	27.7	0.08	1.10	0.58	0.65
^{239}Pu	102	58.7	0.63	1.86	0.56	0.77
^{240}Pu	0.50	110.6	0.00	0.36	0.57	0.39
^{241}Pu	95	36.7	0.72	2.49	0.47	0.84
^{242}Pu	0.43	29.0	0.01	0.23	0.44	0.34
^{241}Am	1.10	110	0.01	0.27	2.00	0.12
$^{242\text{m}}\text{Am}$	595	137	0.81	3.30	0.60	0.85
^{243}Am	0.44	49.0	0.01	0.21	1.80	0.10
^{244}Cm	1.0	16.0	0.06	0.42	0.60	0.41

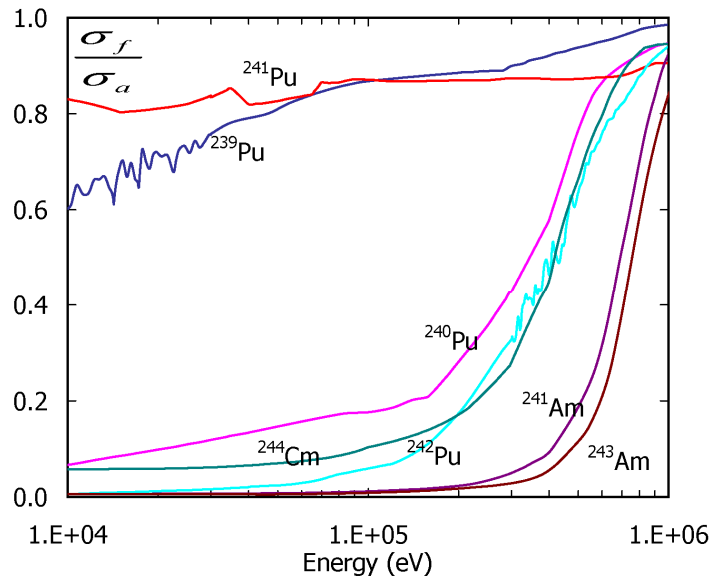


Fig. 9 Variation of fission probability (σ_f/σ_a) with energy of some transuranic isotopes (ENDF/B-VI).

Chapter 3:

Transmutation Strategies

In this section we shall review the different P&T strategies and discuss their essential differences, mainly with respect to the achievable global waste radiotoxicity reduction. Numerous evaluations of transmutation scenarios have been performed. Much use has been made of available material on the subject with appropriate attribution. A comprehensive evaluation of P&T strategies was performed in a recent OECD/NEA study [24].

Introduction

The goal of P&T is to achieve a hundredfold reduction of the radiotoxicity in the medium- and long-term (beyond a few hundreds of years), which would considerably ease the performance requirements for an underground repository. Most likely an underground storage can provide confinement for at least 1000 years, during which the most radiotoxic fission products have decayed. The conditions for a hundredfold reduction require management of both plutonium and minor actinides. In addition a few long-lived fission products (mainly ^{99}Tc and ^{129}I) are being considered for transmutation. Although their contribution to the global radiotoxicity is small some of them are mobile in the geosphere and may pose a radiological hazard under certain repository conditions. Various reactor concepts and fuel cycle strategies could be envisaged for transmutation purposes, incorporating both conventional light water reactors and fast fission reactors with conventional MOX-recycling and dedicated critical or sub-critical reactors with advanced reprocessing schemes. Fig. 10 provides an overview of the transmutation scenarios most commonly considered.

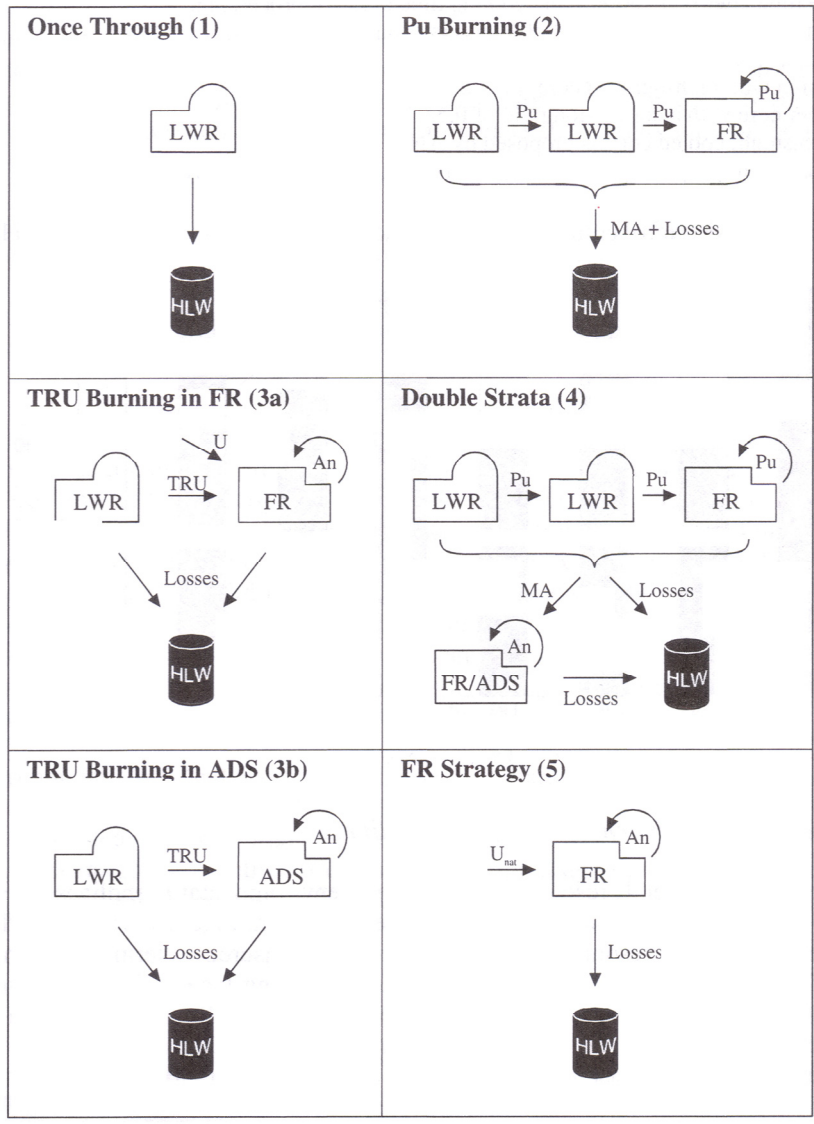


Fig. 10 Overview of principle fuel cycle scenarios (adapted from OECD/NEA report [24]).

Transmutation of plutonium

In the once-through cycle (scenario 1 in Fig. 10) the spent fuel is sent directly to long-term storage with no recycling (the once-through cycle is in fact not a cycle at all but an open-ended process). The fissile material content (approx. 1% Pu and 0.8% ²³⁵U) and the remaining fertile material (²³⁸U) are considered as waste and excluded for further use. At present time, the once-through cycle is the main alternative for countries in which reprocessing is not practiced (for different reasons) such as Sweden, United States, Spain, and Canada. In the once-through cycle a geologic waste repository must be provided including demonstration of its long-term safety. In this scenario, the transuranic elements dominate the long-term radiotoxicity and it takes about 100,000-300,000 years (depending on the level of reference) before the radiotoxicity decays to natural levels.

In a LWR(MOX) recycling scenario, the spent fuel is reprocessed and the uranium and plutonium is recovered. In principle, both the uranium and plutonium could be recycled in LWRs but in practice, this is done only for plutonium. Nearly all of the uranium recovered

from reprocessing is sent into storage because fresh uranium is comparatively cheap and depleted uranium (from enrichment processes) is available in large quantities. Besides, the uranium recovered from reprocessing is less desirable for reactor use (higher neutron absorption and radiation levels) than fresh uranium because of the presence of troublesome isotopes like ^{232}U , ^{234}U , and ^{236}U , which necessitates re-enrichment and makes the reprocessed uranium more difficult to manage (due to radiotoxic daughter nuclides). Thus, nearly all of the uranium recovered from reprocessing remains in storage. After successive reactor cycles, the plutonium involved will become depleted in fissile isotopes (^{239}Pu and ^{241}Pu). Furthermore, the fuel will build-up minor actinides, especially ^{244}Cm , as the irradiation increases because of the very low fission probability of fertile isotopes in a thermal spectrum. Obviously, this increases neutron emission rates and heat generation levels, which makes the fuel more difficult to reprocess with the PUREX method. The reduction of fissile plutonium also requires successively increased plutonium concentrations (or alternatively increased ^{235}U enrichment) for reactivity compensation in subsequent cycles. But the amount of plutonium in the core is limited by reactor safety concerns (e.g., deterioration of moderator coefficient and lower delayed neutron fraction). According to one report [36], the plutonium content in a standard PWR core must not exceed 12 wt% on similar grounds. While the technical issues are important factors, they are not the only ones affecting decisions on plutonium recycling. Other subjects which have a critical impact include: environmental concerns, resource utilization, waste issues, cost, and proliferation aspects, and these are debated with considerable controversy. As of today, plutonium reprocessing operations has not kept pace with its use in reactors and this has led to a growing amount of separated civilian reactor-grade plutonium in storage around the world. According to the Washington based Institute for Science and International Security (ISIS) [37], roughly 235 tonnes of separated reactor-grade plutonium were available world-wide at the end of 2003, which may be compared with 155 tonnes of weapon-grade plutonium in military stocks. In the U.S., reprocessing of civilian nuclear fuel is not permitted because of proliferation concerns. It is advocated that as long as the plutonium remains in the spent fuel, it remains inaccessible and the risk of being used for weapons is reduced. On the other hand, this non-separated plutonium, while more proliferation resistant than separated, is not permanently inaccessible in the spent fuel. After a few hundreds of years, when the fission products have decayed, extraction processes are much easier to perform. In terms of cost, the advantages of reprocessing uranium and plutonium are reduced need for mining new uranium and decrease in enrichment works. However, there is the added cost for reprocessing and also increased cost for fabrication and transportation of MOX fuel compared to freshly mined uranium. According to a recent comparative study [38], reprocessing and recycling of plutonium in LWRs will be more expensive than direct disposal of spent fuel until the uranium price reaches over \$360 per kilogram of uranium (kgU), which is significantly higher than the current uranium price of \$40/kgU. From a waste management point of view, the volume of the residual high-level waste aimed for disposal is reduced since the uranium and plutonium are separated from the spent fuel, but the effect on the long-term radiotoxicity is marginal [35]. For reasons mentioned above, the number of cycles is limited to one or maybe two. In the first cycle around 25% of the recycled plutonium may be consumed and 10% is transformed into heavier nuclei (Am, Cm, and higher actinides) [24].

The use of fast reactors was discussed in the early days of nuclear energy. It deserves to be mentioned that the first fast reactor was Clementine, built at Los Alamos in 1946, and the first reactor to produce usable quantities of electricity from nuclear energy was the Experimental Breeder Reactor I (December 20, 1951). As early as 1944, the plan was to build reactors “to breed fissile materials from natural uranium or thorium”, according to minutes from the meetings of the “New Piles Committee”, which was formed to explore the peaceful uses of nuclear energy in the United States after the second-world war [39]. At that time the main

motivation was the limited supply of uranium. It was projected that the number of reactors would grow rapidly, and as a result the price of uranium would increase quickly. Since fast breeder reactors (FBR) could offer superior usage of uranium resources, representing a hundred-fold increase in utilization factor than that of thermal reactors, these were considered necessary not to run out of resources very soon. Undoubtedly, the early considerations lay the foundation for the nuclear energy research in the United States for many decades ahead and influenced the development in many other countries as well. However, uranium turned out to be abundant and inexpensive and mastering the fast reactor technology was more problematic than expected [40]. In the nineteen-sixties the FBRs were challenged by the cheap and technically attractive light-water reactors. Although much research work continued to be invested into the breeder technology, the expected transition to FBRs slowed considerably and in some cases even halted. In the 1990s, large-scale development programmes on FBRs essentially terminated in the United States, France, Britain, and Germany, though some longer-term research work continued. Plutonium recovered in reprocessing operations, which were initially intended for FBR use, became redundant and was reused in LWRs. More recently, as part of the transmutation strategies and the “Generation IV” initiative, and quite opposite to the initial purpose of breeding, it is the burning characteristic of fast neutron spectrum in which fast reactors see a possible future redeployment. In these new reactor strategies, the fast reactor can demonstrate a distinct advantage over the light water reactor. In contrast to plutonium recycling in LWRs, which is limited by safety concerns, complete plutonium burning is possible by integration of fast reactors. This option could be envisaged in special fast burner reactors (FBuR) operated in symbiosis with a park of LWRs. For example, in the French CAPRA project, MOX fuel with very high concentrations of plutonium oxide (up to 45%) and core designs without blanket region are investigated to achieve as high plutonium consumption as possible. However, aqueous reprocessing is valid only for MOX fuel with Pu-enrichment below 25%. Any higher Pu-concentrations would require the dissolution yield of the PUREX process to be improved or some other reprocessing scheme or alternative fuel material is required, e.g. nitride. Although recycling of plutonium in LWRs and FRs (with limited plutonium concentrations) is conceptually possible with current technology, rapid expansion of a large park of fast reactors is not a realistic scenario. It is estimated that 36% of the park power must be produced by fast reactors in order to achieve zero plutonium build-up at equilibrium conditions [41]. Capital costs are not in favor of FBRs. Traditionally, the estimated FBR/LWR plant capital cost ratio has been in the range 1.25-1.50 [42]. Theoretically, if all plutonium would be eliminated (without losses) from the spent fuel, the long-term radiotoxicity would decrease by a factor of ten relative to the once-through cycle. But in practice, due to the continuous build-up of Am and Cm, multi-recycling of plutonium in LWR/FR facilities only reduces the radiotoxicity by a factor of five (see Fig. 12) in the time frame >1000 years. Thus, from a radiotoxic point of view, multiple recycling of plutonium alone does not qualify as a transmutation strategy. In order to reduce further the radiotoxic inventory, it is necessary to recycle also the remaining TRU content, i.e. the minor actinides, which is the purpose of the advanced fuel cycle.

Transmutation of minor actinides

Recycling of the plutonium is a first, but not sufficient step in a transmutation strategy. Only by a fully closed fuel cycle, i.e., close the stream of all transuranic materials (plutonium + minor actinides) to the waste, is it possible to achieve a significant reduction (by a factor of one hundred or more) of the long-term radiotoxicity (>300 years), which is the main goal of a transmutation strategy. The minor actinides considered for transmutation are americium, curium, and neptunium. Americium is responsible for the second highest contribution to the

radiotoxicity in the spent fuel after plutonium, see Fig. 2. It dominates the radiotoxicity during the first 2000 years after discharge and it is produced in large amounts during multi-recycling of plutonium. Various types of reactors could be considered for transmutation of minor actinides, such as light-water reactors (LWR), fast reactors (FR), and dedicated critical or sub-critical reactors (ADS), either in homogeneous or heterogeneous mode. In the heterogeneous mode the minor actinides are diluted at low concentration in the standard fuel material. In the heterogeneous mode the MAs are separated from the conventional fuel and concentrated in special fuel elements known as “targets”.

Generally speaking, addition of minor actinides to the fuel leads to deterioration of the reactor safety parameters (less negative reactivity coefficients, lower delayed neutron fraction) and degradation of physical characteristics of the fuel (thermal properties, helium generation). The addition of americium also decreases the reactivity of the fuel due to higher capture losses and hence higher fissile enrichment is required. In a thermal system the introduction of minor actinides leads to a less negative moderator coefficient. In homogeneous mode, the MA content is restricted to 1% in a MOX-fuelled PWR [31]. Studies have shown that a somewhat higher MA content (2%) is possible in high moderation reactors (in which the ratio of moderator volume to fuel volume is greater than 3, compared to standard PWR with a ratio of 2). Heterogeneous recycling avoids dilution of nuclides with high alpha activity in the larger volume of spent LWR-MOX fuel, which later complicates chemical reprocessing and fuel fabrication operations. From fuel cycle point of view, it is advantageous to confine the treatment of the minor actinides to a separate side-stream. Moreover, in heterogeneous recycling, the negative effects on the reactor are somewhat reduced, if the targets are placed at the core periphery. However, transmutation of americium targets in a thermal spectrum leads to formation of ^{242}Cm and ^{244}Cm through neutron capture in ^{241}Am and ^{243}Am , see Fig. 11. Since ^{242}Cm decays rapidly (162 days) into ^{238}Pu , the proportion of ^{238}Pu and ^{244}Cm increases during successive recycles. Reprocessing and recycling of fuels containing high quantities of ^{238}Pu and ^{244}Cm is problematic because of their strong alpha activity and neutron emission rates. Multi-recycling is not possible with aqueous techniques because of the high density of radiation and fuel fabrication operations are made difficult by the need for remote control and cooling in shielded compartments. Because of these difficulties the so-called “once-through” recycling of americium targets in thermal systems has been suggested. Instead of multi-recycling, the targets would be subject to a single extended irradiation cycle and then sent for disposal. In this case, the incineration rate is limited by the residence time as the fertile actinides gradually convert into fissile nuclides. It has been shown that very long residence periods are required to achieve a significant americium destruction rate. Since the residence time is limited by fuel swelling and cladding irradiation damage, a high incineration fraction is not possible with once-through recycling. In principle a high incineration rate is achievable in a thermal system through secondary fission reactions [43,44], but in practice the transmutation capability is constrained by the performance and safety parameters, such as the reactivity swing during burn-up which require very high initial ^{235}U enrichment. Transmutation in a thermal spectrum is generally not attractive from neutron-economics point of view (since most thermal neutrons are spent on conversion into higher TRU isotopes) and due to the much lower fluxes. In a recent IAEA report [35] it was concluded that neither conventional nor dedicated transmutation LWRs qualify for transmutation of minor actinides on the basis of the reasons mentioned above and other practical considerations. It should be noted that even a small amount (1%) of americium in the fuel produces sufficient curium in a thermal spectrum to cause serious transportation problems. Preferably, americium transmutation should be completed in a fast spectrum with its higher fission-to-capture probability, either in a dedicated fast burner or in symbioses with LWRs. It has also been suggested that transmutation in a thermal system could serve as an intermediate irradiation

In order to overcome the safety issues associated with highly enriched MA cores (or MA and Pu), accelerator-driven systems (ADS) with a fast spectrum have been proposed. Since these systems would operate in a *sub-critical mode* they could more easily address the adverse safety characteristics of MA-based fuels. While a critical system requires a substantial fraction of fertile materials in the fuel to ensure acceptable core safety characteristics, accelerator-driven systems offer higher flexibility in fuel composition. In the extreme case an ADS could permit pure minor actinide fuels (or MA mixed with some Pu). The great advantage is that the MA transmutation rate per unit of power is maximised and so the fraction of specialised burners can be kept to a minimum. It would also confine the treatment of the MA to a small side-stream of the nuclear power park. Hence, the safety performance of the conventional reactors need not be affected and the effect on the fuel fabrication and reprocessing steps in the main cycle would be minimal. The cost analysis indicates that the ADS-based strategies can be made very competitive through minimal usage of innovative technology.

Various fuel cycle strategies could be foreseen involving ADS, FRs, and LWRs. ADSs could be used to burn transuranics in a two component strategy (3b in Fig. 10), “TRU burning in ADS” or as pure minor actinide burner in the so-called “double-strata scheme” (4 in Fig. 10). In the two-component strategy, the FR is replaced by an ADS and the transuranics are recycled in a sub-critical burner with a closed fuel cycle using pyrochemical reprocessing without MA-Pu separation. This approach was adopted in the USA [46], since it reduces the proliferation risk as the plutonium is always together with the minor actinides. Alternatively the ADS could operate in symbiosis with LWRs for Pu recycling (not shown specifically in Fig. 10). The capability of the latter to burn Pu reduces the LWR-to-ADS support ratio from 21% (no MOX recycling in LWRs) to 15%. In the double-strata cycle, first suggested in Japan in 1984 [47], the ADS would operate together with both LWRs and FRs. In the first stratum, plutonium is recycled in commercial LWRs and FRs using conventional reprocessing and MOX fuel technology. The MAs (mixture from LWRs and FRs) and some Pu (for reactivity management) are later transferred to the second stratum for final destruction. The double-strata scheme is sometimes considered to be an evolutionary approach as the fuel cycle is basically closed in successive steps, first Pu in LWRs and then in FRs, and last MA+Pu in ADS. Economically, it is more competitive since it reduces the number of ADSs by a factor of four relative to the TRU burning strategy (without MOX-recycling). The ADS support ratio in the double-strata scheme is around 5-10%. It is worth noticing that recycling of americium and curium alone could reduce the ADS support ratio even further, as we show in **Paper II**.

At first sight, the hazard of neptunium evaluated from its radiotoxicity value seems to be of little concern. However, the long half life ($2.1 \cdot 10^6$ yr) and the build-up with time due to decay of ^{241}Am and potential mobility of ^{237}Np in groundwater is of concern for the long-term disposal of spent nuclear fuel under certain geological disposal conditions. This can to some extent counteract its far lower radiotoxicity and make it a greater risk in the overall risk assessment. For that reason many P&T strategies includes Np in the recycling scheme. From the global radiotoxicity point of view, however, Np is of little concern.

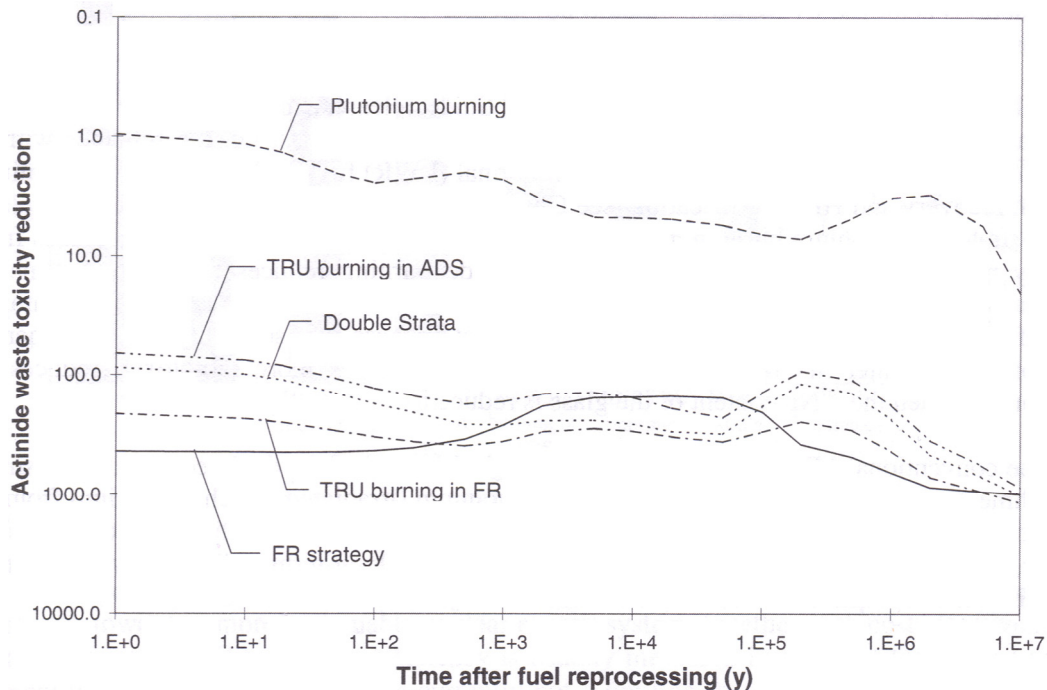


Fig. 12 Actinide waste radiotoxicity reduction relative to the once-through fuel cycle (adapted from OECD/NEA report [24]).

Transmutation of fission products

The fission products are small contributors to the radiotoxicity contained in the spent fuel, being many orders of magnitude below that of the transuranic elements after a few hundreds of years. Thus, from the viewpoint of reducing radiotoxicity, transmuting fission products would appear to be of little interest. However, as mentioned before, some fission products are mobile in groundwater and therefore can contribute significantly to the surface dose rate under certain repository leakage conditions, i.e. groundwater release scenarios. The fission products that are relevant in this respect are primarily ^{99}Tc , ^{129}I , ^{135}Cs , ^{79}Se , and possibly ^{126}Sn , depending on the type of repository considered. It is theoretically possible to transmute fission products to shorter-lived or stable nuclides by means of neutron capture^a. But, taking into account the small neutron capture cross sections for many of the long-lived fission products rather long irradiation times are required. Transmutation of fission products is only reasonable if the neutron capture cross-section of the targeted isotope is sufficiently high to allow transmutation rates which are high in relation to the natural decay [24]. This immediately excludes ^{90}Sr and ^{137}Cs for potential transmutation purposes because of their short half-life (~30 years) and limited transmutability. The only reasonable route for these nuclides appears to be disposal, special separation could be employed to reduce the heat load in the repository.

^aIt may be added that, in a quite opposite way to neutron capture, laser-driven gamma generation for photo-transmutation [49], through (γ, n) reactions, has been demonstrated for transmutation of ^{129}I into ^{128}I (with a half-life of 25 min). However, the technology is still at the fundamental level and considering the low transmutation rate achievable with present-day lasers it is not a realistic alternative for transmutation of industrial quantities.

^{79}Se ($T_{1/2}=6.5\cdot 10^4$ years) and ^{126}Sn ($T_{1/2}\sim 1\cdot 10^5$ years) are rather long-lived but their capture cross sections are very small, and thus the potential transmutation rate is limited. ^{135}Cs is long-lived ($T_{1/2}\sim 2.3\cdot 10^6$ years) and has moderate thermal capture cross-section, but Cs occurs in many isotopic forms in the high-level waste and would require isotopic separation to isolate ^{135}Cs in order prevent neutron capture in ^{133}Cs and ^{134}Cs [35]. This is an unrealistic undertaking from an economical and technical point of view. So far, the isotopes that have received the highest transmutation priorities, considering both their practical ability to transmute and in terms of their potential impact on the long-term radiological risk, are ^{99}Tc ($T_{1/2}\sim 2.1\cdot 10^5$ years) and ^{129}I ($T_{1/2}\sim 1.6\cdot 10^7$ years). ^{99}Tc is present as single isotopic species and can be transmuted into ^{100}Tc , which beta-decays rapidly ($T_{1/2}\sim 16$ seconds) into stable ^{100}Ru . Iodine separated from spent fuel is a mixture of ^{127}I and ^{129}I , but the former is present to an extent of 16%, which is tolerable [31]. Hence, ^{129}I can be transformed to ^{130}I , which decays with a half-life of 12 h to stable ^{130}Xe . It is noteworthy that reactions involving successive neutron capture in ^{99}Tc and ^{129}I will still yield stable nuclides after beta-decay. Although the lower flux level in a thermal system is partly compensated by high capture cross sections, neutron economy requirements favor the use of fast systems. One must consider that fission products act as poisons without compensating neutron production. Fast systems offer better neutron economy which can be utilized for transmutation while a LWR system would require higher enrichment [31]. An optimal strategy, for transmutation of ^{99}Tc and ^{129}I , is to use moderated target assemblies of fast reactors, which could then combine the high flux of a fast system with the high cross-sections in a thermal system [48].

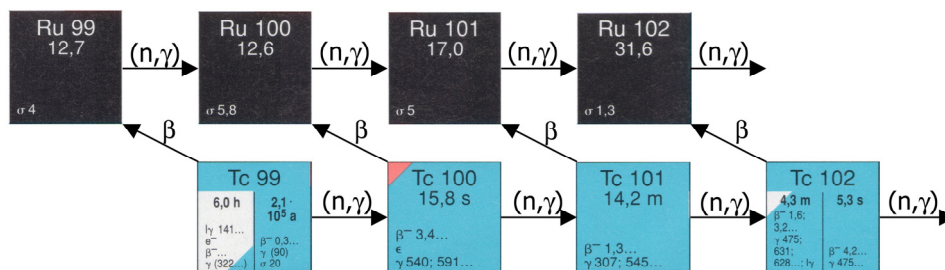


Fig. 13 Transmutation path of ^{99}Tc

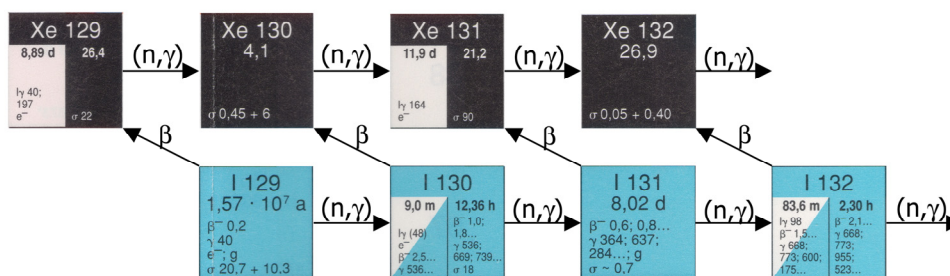


Fig. 14 Transmutation path of ^{129}I

Chapter 4:

Accelerator-driven Systems

In the previous chapters we have given brief accounts of the spent fuel composition, waste management strategies, chemical separation operations, and an overview of various transmutation strategies. The purpose was to provide background information on the general problems of spent fuel management and to explore possible means for reducing the radiotoxic inventory. It was found that the actinides, mainly plutonium, americium, and curium, are responsible for the majority of the radiotoxicity and the most efficient way to reduce the radiotoxic inventory is to fission them. Of the many transmutation schemes suggested, one is recognized as being the most promising: the accelerator-driven system. We shall now present the design principles upon which this system is based. The first part provides a brief description of the general principles, the remaining of the chapter deals with the safety and kinetics performance of ADS. A brief description will also be given of the reliability of the accelerator built to provide high-energy protons for the system.

General principles

A vital feature of the fission reaction is that it generates neutrons that can cause further fission. If the fission reaction repeats itself the process that occurs is called a “chain reaction”. The fission chain-reaction is common to all nuclear reactors. If the neutrons from one fission cause on the average one more fission a “self-sustained chain reaction” is accomplished and the reactor is said to be “critical”. The neutrons in the first fission are said to belong to the first generation and the neutrons from the second fission which they caused belong to the next generation and so on. The effective multiplication factor^a, k_{eff} , gives the ratio of the number of neutrons of one generation to the preceding generation (taking all losses into account):

$$k_{eff} = \frac{\text{number of neutrons in one generation}}{\text{number of neutrons in the previous generation}}$$

It is obvious that a self-sustained reactor will continue to operate at a constant fission rate as long as the effective multiplication factor remains unity. If k_{eff} is smaller than one, there are fewer neutrons produced in each generation than in the previous generation and the reactor is said to be subcritical. Without any help from an outside source of neutrons the chain-reaction will eventually die. In contrast, if k_{eff} is greater than 1, the neutron population will increase with or without the presence of an external source, and the reactor is supercritical. It should be realized that the value of k_{eff} depends solely upon the properties of the reactor core (size, shape, material composition, and temperature) not on the characteristics of the source. The material composition consists of a mixture of nuclear fuel, coolant, structural, and control material. To establish a self-sustained chain-reaction the material must be arranged in a suitable configuration of sufficient size and right shape.

^aStatic multiplication factor for a reactor in the eigenstate. The index “*eff*” refers to the multiplicative properties of a reactor of finite size as opposed to the infinite multiplication factor, k_{∞} , assuming an infinite system. The latter neglects neutron leakage effects.

Source multiplication in a subcritical reactor

In operator formulation, the steady-state Boltzmann neutron balance equation for a subcritical reactor including a neutron source reads:

$$(\mathbf{M} - \mathbf{F})\Phi_s = S \quad (1)$$

Where \mathbf{F} is the fission operator, \mathbf{M} is the migration and loss operator, $\Phi_s(\mathbf{r}, E, \Omega)$ is the angle-dependent inhomogeneous neutron flux, and $S(\mathbf{r}, E, \Omega)$ is the independent neutron source. From the above neutron balance formulation, it is seen that in a subcritical reactor, fewer neutrons are produced through fission ($\mathbf{F}\Phi$) than lost ($\mathbf{M}\Phi$), and the difference is compensated by neutrons from the outside source, S . The fundamental mode flux is defined as:

$$\left(\mathbf{M} - \frac{1}{k_{eff}} \mathbf{F} \right) \Phi = 0 \quad (1)$$

The subcritical multiplication factor, k_s , is defined as the ratio of the fission neutrons to the total neutron source as:

$$k_s = \frac{\langle \mathbf{F}\Phi_s \rangle}{\langle \mathbf{M}\Phi_s \rangle} = \frac{\langle \mathbf{F}\Phi_s \rangle}{\langle \mathbf{M}\Phi_s \rangle + \langle S \rangle} \quad (2)$$

where $\langle \rangle$ denotes phase-space integration. Unlike the effective multiplication factor, k_{eff} , which is a characteristic of the core, the subcritical multiplication factor depends on the characteristics of the external source neutrons (spatial position, energy, angular distribution). It is a local multiplication factor in that sense that it describes the multiplication of source neutrons from the point of where they are inserted. Using the inhomogeneous flux in Eq. (1), the fission neutrons per external source neutron can be related according to:

$$\frac{\langle \mathbf{F}\Phi_s \rangle}{\langle S \rangle} = \frac{1}{1/k_s - 1} \quad (3)$$

The fission power of the inhomogeneous system can be represented as

$$P_{fission} = E_f \langle \Sigma_f \Phi_s \rangle \quad (4)$$

Where E_f is the energy recovered per fission. If we now combine Eq. (3) and (4), the fission power can be written as:

$$P_{fission} = \frac{E_f}{\bar{\nu}} \frac{k_s}{1 - k_s} \langle S \rangle \quad (4)$$

Where the average number of neutrons per fission is defined as

$$\bar{\nu} = \frac{\langle \mathbf{F}\Phi_s \rangle}{\langle \Sigma_f \Phi_s \rangle} \quad (5)$$

Definition of an accelerator-driven system

Conventional power reactors generally do not require external neutron sources for normal operation. These reactors are based on the self-multiplication of neutrons in a critical state. In a critical reactor the fission reactions alone are able to maintain a steady-state. In contrast, the accelerator-driven system (ADS) is a subcritical reactor driven by an external neutron source. The external source is maintained by a spallation neutron target (as explained below) driven by a high power proton accelerator thereby the leading adjective ‘‘accelerator-driven’’. Taken by itself, critical or near-critical reactor operation would seem like the optimum solution, since it eliminates the need for an external source. But safety and controllability are the main

issues for the ADS. The main purpose is to minimize the risk for uncontrolled reactivity excursions. Among the advantages of subcritical operation is the stable nature of operation, increased margin to prompt criticality, and reduced influence of reactivity feedbacks.

External neutron source intensity

Spallation is a nuclear reaction that may occur when a high energy particle strikes a heavy element, in which the nucleon(s) struck by the incoming particle may collide with other nucleons inside the nucleus causing an “intra-nuclear cascade”. In the process, the incoming particle may “spall” the target nucleus, breaking it into smaller pieces, releasing protons, neutrons and other nuclear fragments. The incoming particle may be a proton, and the target material may, for example, be tungsten, lead or lead-bismuth. High-energy secondary particles (neutron, protons, or pions) may be knocked out in the initial collision. The remaining nucleus is left in an excited state. In the de-excitation process (evaporation stage) the nucleus may emit additional nucleons or it may fission. Most of the particles emitted in the de-excitation process are neutrons which are emitted isotropically. The neutron yield depends on the energy of the incident proton, as shown in Fig. 15. The yield increases almost linearly in the range 1-4 GeV.

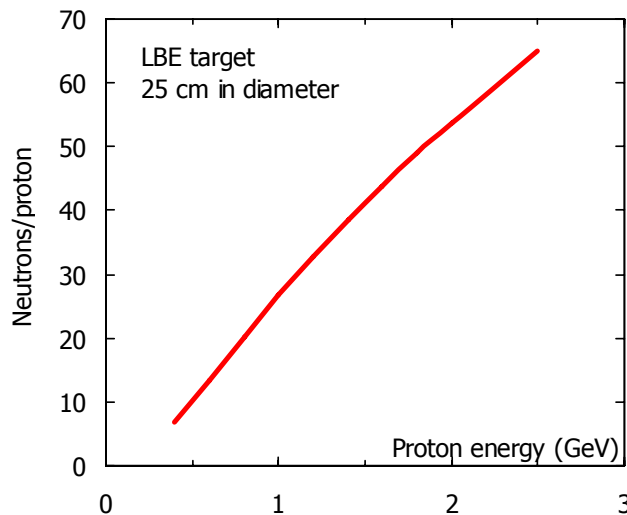


Fig. 15 Spallation neutron yield as function of incident neutron energy (by courtesy of P. Seltborg)

In order to produce a spallation neutron source of sufficient intensity the accelerator must be capable of delivering energetic protons at high current. As we saw in the previous paragraph, the total system power depends on both the source strength and the multiplication factor. Increasing the system power requires either reduced subcriticality or stronger source. To reduce the cost of the source it may seem desirable to increase the multiplication. This will, on the other hand, reduce reactivity safety margins. The degree of criticality offset is a fundamental design parameter of ADS systems. The choice of multiplication involves trade-off among various design goals such as reactor safety performance, core characteristics, and desired power rating, and at the same time remain consistent with current accelerator performance and cost goals. For typical industrial-scale ADS designs, it is envisioned that the thermal rating would be of the order of 500 MWth to 1500 MWth and employ k_{eff} values in the range 0.95-0.98. A legitimate question to ask then is what source intensity is required to drive this type of ADS? Consider a subcritical reactor operating at steady-state at 800 MWth with a k_{eff} =0.95. The required source intensity to maintain a fission power of 800 MWth is

given by the source multiplication formula (for the sake of simplicity let's assume that k_s is close k_{eff} which is almost true):

$$S = \frac{800 \cdot 10^6 [\text{W}] \cdot 2.5 [\text{neutrons/fission}]}{0.35 \cdot 10^{-10} [\text{W} \cdot \text{s/fission}]} \left(\frac{1-0.95}{0.95} \right) \approx 3 \cdot 10^{18} \text{ neutrons released per second}$$

Considering that the neutron production rate in ^{252}Cf is $2.3 \cdot 10^{12}$ n/s·gram, the required source intensity seems tremendous. The next question that comes to mind is whether an accelerator can produce a spallation neutron source of this intensity and what would the resulting beam power amount to? As we saw in Fig. 15, the spallation neutron yield depends on the incoming proton energy and the yield curve increases almost linearly in the range 1-4 GeV. However, most studies suggest optimum proton energy for an industrial ADS plant, in terms of cost and system efficiency, somewhere in the range 0.8-1 GeV. At 1 GeV each proton will on the average expel 25 neutrons, according to Fig. 15. Thus, the required proton intensity would roughly amount to $1.2 \cdot 10^{17}$ protons/sec, which equals a beam current of roughly 20 mA ($1.2 \cdot 10^{17}$ protons/sec $\cdot 1.6 \cdot 10^{-19}$ C/proton) or expressed in different units, 20 MW of beam power ($1 \cdot 10^9 \cdot 1.6 \cdot 10^{-19}$ J/proton $\cdot 1.2 \cdot 10^{17}$ protons/sec). Although a beam power of 20 MW is an ambitious goal (such powerful machines do not exist today), it is not without reach with existing accelerator technology. Recent advances in accelerator technology have confirmed that a linear accelerator capable of delivering up to 100 MW at 1 GeV is a relatively direct extension of existing technology. Well-supported designs for this class of accelerator were completed several years ago at Los Alamos National Lab [50]. So the answer to the last question is: -Yes, high power proton accelerators can be built and they can be used to produce neutron sources of very high intensities, sufficient to drive an industrial sized ADS. The beam power required will be in the range 10-30 MW.

As a comparison, around one tonne of ^{252}Cf would be necessary to deliver similar source intensities. The annual sales of ^{252}Cf is less than 100 mg with a cost around \$60/ μg (CRC Handbook, 2004-2005), and it would decay with a half-life 2.6 years. The heat generated in this source would be close to 30 MW. Thus, the neutron intensity required for an industrial ADS plant is well beyond the capabilities of any radioactive-decay type of source. It should be clear at this point that only a spallation neutron source driven by a high-power proton accelerator can produce neutron intensities of sufficient strength.

Safety features of uranium-free cores

Delayed neutron fraction

Just as most fission neutrons appear instantaneously in the fission reaction, it happens that a few neutrons are released in the subsequent radioactive decay of certain fission products. These neutrons are referred to as delayed. Although the fraction of delayed neutrons in the reactor is small in comparison with the total number of neutrons, their presence is extremely important for the control of the chain reaction. The time delay for the delayed neutron emission is essentially determined by the time it took to undergo beta decay for the specific parent nuclei (e.g. delayed neutron precursor). The precursor nuclei usually disintegrates within a minute after fission (the longest-lived delayed neutron precursor has a 54-second half-life). If the delayed neutrons are considered along with the prompt neutrons, the weighted mean lifetime of all neutrons is considerably longer (~ 10 sec) than the prompt neutron lifetime ($\sim 1 \cdot 10^{-6}$ sec in fast spectrum). Without the contribution from the delayed neutrons the reactor period following reactivity insertion (and removal) would be very small.

Since the isotopic fission yield will vary for different isotopes, the decay scheme leading to delayed neutron emission will be isotope-dependent. The two main delayed neutron

precursors are ^{87}Br and ^{137}I . One may recall that these nuclides have similar mass numbers as the two peaks in the fission-yield curve. The average number of prompt neutrons released in the fission event is denoted ν_p and the corresponding yield of delayed neutrons is ν_d . The delayed neutron fraction, β , then appears as:

$$\beta = \frac{\nu_d}{\nu_p + \nu_d}$$

In TABLE 10 we have tabulated prompt neutron yield, delayed neutron yield, and delayed neutron fraction characteristic for some principle fuel isotopes. The nuclides are listed in order of decreasing delayed neutron fraction. As noted by Keepin [51], the delayed neutron yield tends to increase with increasing number of neutrons for a given element, but decrease with increasing number of protons. This regularity is not that surprising since the fission yield of the most important delayed neutron precursor, ^{87}Br , decreases with increasing mass number. The formation of ^{137}I is roughly constant, however. Also the prompt neutron yield, ν_p , tend to increase with increasing mass number, which lowers the β value even further. The effect is particularly pronounced in ^{241}Am and ^{244}Cm . The delayed neutron yield in ^{238}U is about 7 times larger than ^{239}Pu and for that reason it may contribute significantly in an FBR although its fission rate is lower (^{238}U may contribute with around 10% of the fissions). The dependence of the delayed neutron yield on the initiating neutron energy appears to be small up to 4 MeV [52]. The variation of the number of prompt neutrons emitted in fission is also small up to a few hundred keV, but increases thereafter. Therefore the energy dependence of the delayed neutron fraction is not very pronounced up to a few hundred keV. In general the isotope dependence of the delayed neutron precursor decay constants is not strong.

TABLE 10

Comparison delayed neutron yield (ν_d), prompt neutron yield (ν_p), and delayed neutron fraction (β) for thermal induced fission (ENDF/B-VI.8).

Nuclide	ν_d^{th}	ν_p^{th}	β
^{238}U	0.0440	2.45	1.77%
^{242}Pu	0.0197	2.79	0.70%
^{235}U	0.0167	2.42	0.69%
^{241}Pu	0.0162	2.93	0.55%
^{237}Np	0.0108	2.63	0.41%
^{240}Pu	0.0090	2.79	0.32%
^{243}Am	0.0080	3.26	0.24%
^{239}Pu	0.0065	2.87	0.22%
$^{245}\text{Cm}^*$	0.0064	3.59	0.18%
^{238}Pu	0.0042	2.89	0.14%
$^{244}\text{Cm}^*$	0.0044	3.24	0.13%
^{241}Am	0.0043	3.23	0.13%

*JENDL 3.3 data

Since the difference in the excitation energy and the neutron separation energy in the delayed neutron emitter is normally much smaller than in the prompt neutron emitter (i.e. direct fission product), the delayed neutrons are generally emitted with a much smaller average energy than prompt neutrons. Whereas the average fission neutron energy is roughly 2 MeV, the delayed neutrons are born at energies around (~ 0.5 MeV). This is illustrated in Fig. 16 for the thermal fission of ^{239}Pu .

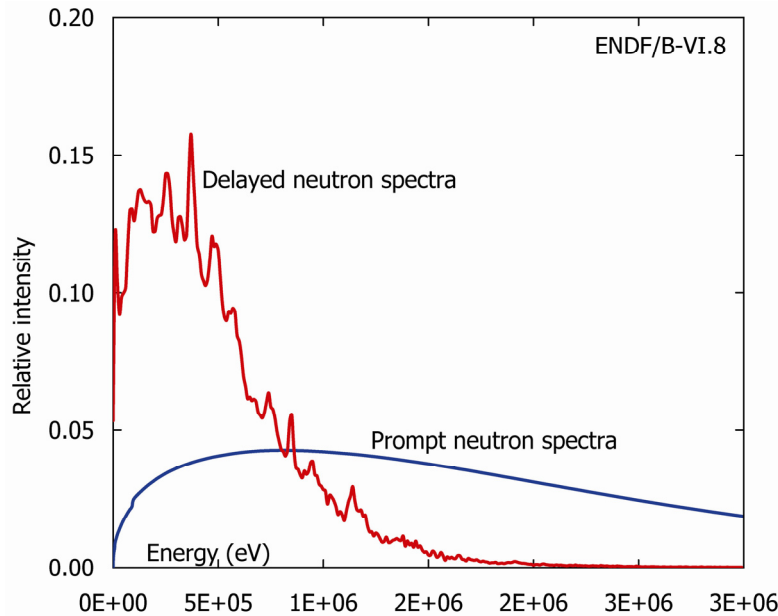


Fig. 16 Delayed neutron spectra vs. prompt neutron spectra for thermal neutron induced fission in ^{239}Pu . Delayed neutron spectra is the weighted average of all six delay groups.

As the delayed neutrons emerge at lower energies than prompt neutrons, they are subject to different absorption, leakage, and neutron production properties. A more refined representation of the delayed neutron fraction, that takes into account the emission spectra influence, is the concept of the effective delayed neutron fraction, β_{eff} . The effective delayed neutron fraction can be interpreted as the number of delayed neutrons inducing fission in the system compared to the number of all neutrons inducing fission [53]. Depending on the core characteristics this value may be smaller or larger than the actual delayed neutron fraction. TABLE 11 gives the β and β_{eff} values for some oxide fuels of principle interest in a sodium cooled fast reactor. The table is extracted from **Paper II**. As can be observed, the effective delayed neutron fraction is 14% smaller than the delayed neutron fraction for the conventional fast reactor fuel ($\text{U}_{0.8}\text{Pu}_{0.2}$). This is the usual situation in fast reactors as the delayed neutrons are emitted with average energies below the fast fission threshold in ^{238}U (~ 1 MeV). The prompt neutron yield also decreases with energy, which further reduces the efficiency of delayed neutrons and suppresses the β_{eff} . Note that the relative drop in β_{eff} strongly increases with the addition of americium. For the fuels containing 30% Am, the effective β is 30-35% lower than the physical β . This is an effect of the higher capture probability of delayed neutrons in americium, as compared to prompt fission neutrons. Although the presence of uranium may contribute to some degree to the physical β , it has a limited effect on the effective delayed neutron fraction. TABLE 11 shows that even with 50% ^{238}U in the fuel, the β_{eff} remains at 200 pcm. Not only does americium possess a low physical β , it reduces the advantage of adding uranium to the fuel. The effective delayed neutron fraction for the uranium-free zirconium-matrix fuel containing plutonium and americium is in the range 140 to 200 pcm, which is about half the value for the conventional FBR, and about a fifth the value for a LWR. Clearly, such a low beta value leaves a very small margin to prompt criticality. This feature combined with the enhanced neutron-kinetics response that follows with a small β_{eff} would make critical reactor control very difficult.

TABLE 11

The delayed neutron fraction (β) and the effective delayed neutron fraction (β_{eff}) for some oxide fuels in sodium cooled reactor. Results reproduced from **Paper II**.

U [%]	Pu [%]	Zr [%]	Am [%]	β [pcm]	β_{eff} [pcm]
80	20	-	-	399±11	342 ±10
50	20	-	30	307±10	204 ±11
-	20	80	-	221±11	206 ±13
-	20	50	30	213±11	143 ±11

Void reactivity

Considerable attention is given to the reduction of the coolant void worth in current ADS designs. Coolant voiding could introduce reactivities that may override the subcritical reactivity for certain combinations of fuel and liquid-metal coolants [54]. It was shown in **Paper II** that the void reactivity effect increases with the americium content. The use of lead-bismuth yields lower void worths than sodium for a wide range of fuel types and core sizes [55, 56]. The low void worth and high boiling point in comparison with sodium are principal advantages that favour the selection of lead-bismuth, see **Paper IV**. The higher sodium void worth is partly due to its higher moderating power, which causes a larger spectrum shift during voiding. In general, hardening of the neutron spectrum and increased neutron leakage are the two dominating physical phenomena contributing to the void reactivity effect in liquid-metal cooled reactors [57]. Hardening of the spectrum leads to a positive reactivity effect due to an increase in the fission probability and an increase in the number of neutrons released per fission (see Fig. 9) while increased leakage gives rise to a reactivity loss since more neutrons may escape the core. Lead-bismuth void worths for a molybdenum-based Ceramic-Metal (CerMet) fuel, a magnesia-based Ceramic-Ceramic (CerCer) fuel, and a zirconium-nitride based fuel are reported in **Paper II**. For convenience, these results are tabulated in TABLE 12..

TABLE 12

Lead-bismuth void reactivity worth (in pcm) computed for the examined fuels in various lattice configurations. Results adapted from **Paper II**.

Fuel	P/D=1.50, D _o =5.7 mm		P/D=1.75, D _o =5.7 mm		P/D=1.50, D _o =6.8 mm	
	Core	Core+ plenum	Core	Core+ plenum	Core	Core+ plenum
CerCer	4060	1790	5300	2300	4570	2250
CerMet	2460	220	3580	470	2990	520
Nitride	2960	680	4150	880	3610	1080

The effect of changing the core size and pin diameter is shown. The negative leakage component tends to decrease with increasing reactor size, while the spectrum hardening effect increases for higher coolant volume fractions. The net effect is that the void effect becomes more positive when the core size increases. The calculations indicate an increase in void worth for larger pin diameters. The effect of separately voiding the core region and plenum region was investigated. The spectral contribution to the void reactivity is closely related to the flux spatial distribution (and the spatial distribution of the adjoint flux) and is usually more positive near the center of the core, while the leakage component is more negative near the edges where the flux gradient is stronger. As a result, expulsion of coolant from the central region results in a positive reactivity gain. However, if the plenum region is voided simultaneously, the reactivity effect may decrease considerably. Evidently, the CerMet fuel

offers low void worths. For tight lattice configurations with this fuel, even central voiding can be accommodated. The void worth of the CerCer core is considerably higher than the CerMet and nitride. The reason is the larger core size (more fuel pins) of the CerCer core, which is an effect of the lower linear rating requirement of this fuel. It is noted, however, that all three fuels provide acceptable Lead-bismuth void values when the core and plenum is voided simultaneously.

Doppler coefficient

The presence of a strong Doppler effect produced by resonance absorption in ^{238}U greatly contributes to the stability in thermal reactors as well as fast reactors. If in a power transient the temperature should increase, the Doppler feedback provides a prompt negative reactivity reduction. The Doppler broadening of resonances follows the fuel temperature instantaneously (increases as the temperature of the fuel rises, making fewer neutrons available to continue the chain-reaction). The Doppler effect is especially valuable under super prompt critical accidents, in which it will advance the shutdown process and thus reduce the energy release and limit the destructive force on the containment [58]. Its effectiveness in terms of “turning around” prompt-critical transients in the fast reactor was experimentally demonstrated in the SEFOR reactor tests [59]. The effect of uranium and americium content on the Doppler constant was investigated in **Paper II** for oxide fuels in a sodium-cooled core. It was found that the Doppler constant decreases drastically with increasing Am-content. The relatively high capture cross section of americium in the energy range of 10-500 keV leads to a decrease in Doppler feedback. As shown in figure 1, the capture cross section of ^{241}Am is 10 times higher than that of ^{238}U in the important energy range. ^{241}Am exhibits no sharp resolved resonances above 100 eV and thus, in a fast spectrum there are few exposed resonances. Not only is ^{241}Am a poor resonance absorber in itself, it prevents absorption in other possible resonant absorber nuclides, like ^{238}U or ^{240}Pu . Even with a large fraction of ^{238}U in the fuel, most captures will take place in ^{241}Am , at energies above the resolved resonance region. It is evident that the Doppler effect will be very small in fuels containing high concentrations of ^{241}Am .

In the absence of a prompt negative reactivity feedback mechanism when passing through prompt criticality, the power will essentially continue to rise until the fuel vaporizes, which will disperse the core and eventually bring the reactor below critical. Consequent hazards are potential damage to the containment, internal structures, and heat-removal equipment. The absence of a significant negative Doppler effect requires greater care in the design to prevent accidents that might lead to prompt-critical conditions. For an ADS, the built-in subcritical margin is the first step in this direction. Other means include minimization of material reactivity potentials. To some degree thermal expansion of fuel can compensate for a small Doppler coefficient in a fast reactor, but it is not as reliable or as prompt as the Doppler effect.

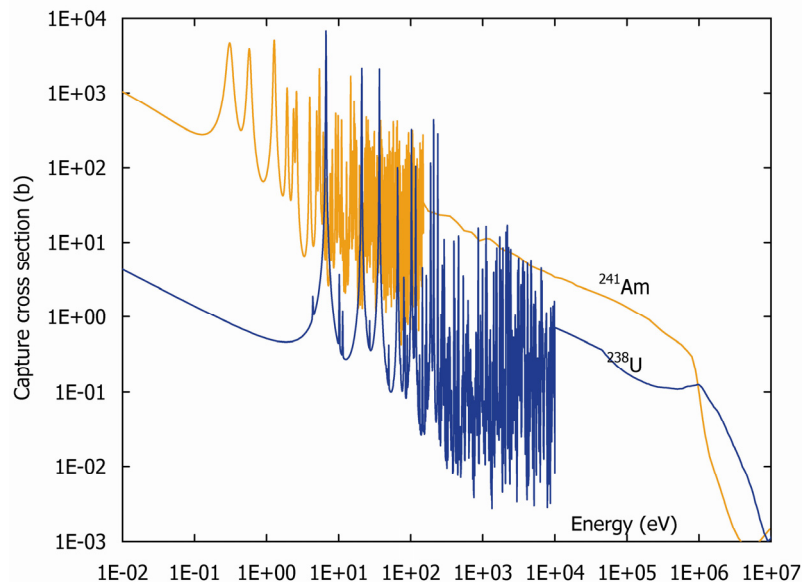


Fig. 17 Capture cross sections of ^{238}U and ^{241}Am as function of energy (ENDF/B-VI)

Clad reactivity

Significant amounts of reactivity could be inserted if molten cladding would be ejected into the coolant and swept upwards out of the core. The effect is important if the cladding leaves the core ahead of the fuel. It is most likely to be associated with undercooling events if the cladding melts. Phenomenological studies of sodium systems [60] suggested that major clad relocation was not to be expected due to sodium-vapor streaming effects (which is the result of an alternating flooding and bypass process of sodium vapor in the channel). This may not be the case for a lead/bismuth-cooled reactor since clad melting will advance lead-bismuth boiling. On a longer timescale, positive reactivity could be inserted because of dissolution of structural materials in lead-bismuth. The reactivity effect of removing the cladding from the core is presented in **Paper I**. It was found that cladding removal leads to a net positive reactivity insertion around 3000 pcm. This value was more or less the independent of the fuel type. Use of a thinner cladding could further reduce the positive reactivity effect, but it would also degrade mechanical strength.

Fuel relocation and recriticality

Reactivity might be introduced in a fast spectrum reactor if the fuel would collect in a denser configuration. Such redistribution of the fuel might result from a meltdown accident or structural collapse of the core. Fuel densification essentially allows fewer neutrons to leak out of the core. This is a fundamental distinction between reactors operating on a fast neutron spectrum and thermal systems. The latter is arranged in nearly an optimum configuration to maximize neutron multiplication and any change to the configuration will shut down the chain reaction. By comparison, if the core of an ADS melts the issue of recriticality must be addressed. The recriticality problem is aggravated by the lack of a negative Doppler effect. Neutronic calculations were performed in **Paper I** to determine critical fuel geometries. These results are shown TABLE 13. The critical mass is sensitive to the material composition (additions of steel, neutron absorbing materials, reflective conditions, etc.) and the fuel geometry. Calculations for standard fast reactor fuel ($\text{U}_{0.8}\text{Pu}_{0.2}\text{O}_2$ surrounded by Na) were also performed to enable comparison. It is seen that the critical mass of the minor actinide fuels is quite small in comparison with standard fast reactor fuel, however, variations occur. The nitride fuel has the smallest critical mass (70 kg), which is approximately 20 times

smaller than classical MOX-fuel surrounded by sodium. This corresponds to the fuel mass contained in three subassemblies (127-pin bundles). The critical mass of the CerMet fuel is 340 kg, which is a factor of 5 larger than the nitride fuel. The critical mass of the CerCer fuel is somewhat smaller than for the CerMet. Clearly, an ADS core contains sufficient fuel to assemble several critical masses. About 69 critical masses were calculated for the nitride core while the oxide cores contain 18 critical masses each. By comparison, Super-Phénix held about 17 critical masses. Given that the total fuel mass in the French reactor is about 4 times larger than for the present ADS cores, a direct comparison is not appropriate. Based solely on the critical mass, it would seem desirable to use a neutron absorbing matrix material, such as molybdenum or magnesia. However, the recriticality question is complex and in comparison with fast reactors, the behavior of an ADS under these conditions is not well known. It is possible that the recriticality problem may be relaxed in lead-bismuth system where the fuel would tend to rise and possibly disperse at the surface rather than collect at the bottom. Moreover, the enhanced fission gas retention in americium based fuels may also provide a natural dispersive mechanism, although this remains to be demonstrated. The critical size of the fuel is merely one element affecting the recriticality potential.

TABLE 13

Critical mass studies for simple fuel geometry*			
Fuel	Critical mass (kg)	Critical volume (dm ³)	Reactor total (critical masses)
CerCer	290	47	18
CerMet	340	33	18
Nitride	70	9	69
Super-Phénix	1370	130	17**

*Cylindrical volume element (H/D=1) surrounded by lead-bismuth.

**Based on (U_{0.8}Pu_{0.2})O₂, 3000 MWth (23 tons of fuel).

Motivation for subcritical operation

The reactivity burnup swing influences the safety characteristics in many aspects. A low burnup reactivity swing lowers the power peaking during burnup and minimizes the built-in excess reactivity for burnup compensation. In an ADS it reduces the proton beam current capability. In a recent design study of a lead/bismuth-cooled ADS [61] it was shown that initial plutonium loading around 40% and 60% MA may provide optimum internal conversion and thus minimum reactivity swing when approaching equilibrium. It is then of interest to determine whether or not such a fuel could be operated in a critical mode. The previous analyses indicate that the addition of minor actinides to a fast spectrum reactor lowers the Doppler coefficient and reduces the effective delayed neutron fraction. Critical fast reactors rely heavily on the delayed neutrons and on the Doppler effects to achieve smooth power control during normal operation and protection against severe reactivity insertion accidents. In addition, the void reactivity effect becomes increasingly positive in uranium-free and liquid-metal cooled minor actinide cores, especially using sodium coolant.

The possibility of operating a uranium-free minor actinide oxide fuel in a sodium cooled fast reactor was investigated in **Paper II**. The analysis took advantage of a balance-of-reactivity approach^a as suggested by Wade and Fujita [62] to determine the asymptotic core outlet temperature rise following unprotected transient events (loss-of-flow, loss-of-heat-sink, transient overpower). The method is useful to extract passive safety trends for slow transients (equilibrium conditions) from a quasi-static balance of all reactivity coefficients (Doppler, axial expansion, radial expansion, and sodium density). In the case of a total loss-of-heat sink accident, it was found that the minor actinide core featured a distinct positive inlet temperature coefficient. While structural expansion feedback was similar in the conventional core and the dedicated core, the dedicated core presented a marked positive void coefficient together with a non-existing Doppler effect. A positive inlet temperature coefficient is unacceptable from a passive safety viewpoint since it will eventually drive a sodium cooled core to boiling. The calculations also indicated a low value of the maximum acceptable reactivity insertion (dictated by the resulting increase in core outlet temperature), which effectively limits the control rod worth to a small value, a complication which is of practical importance. From these survey analyses it appears that operation of a critical uranium-free minor-actinide core would be difficult. It should be recognized that the survey analysis did not consider fast reactivity insertion transients, in which a critical minor actinide core would perform poorly due to the small effective delayed neutron fraction and weak Doppler effect, as discussed in a later section.

From an inherent safety standpoint, the Nuclear Regulatory Commission (NRC) requires [63] that “The reactor core and associated coolant systems shall be designed so that in the power operating range the net effect of the prompt inherent nuclear feedback characteristics tends to compensate for a rapid increase in reactivity.” In a conventional metal or oxide sodium-cooled design (\$3 to \$5 voiding worth) with a nominal Doppler coefficient (around -0.5 pcm/K), the Doppler feedback is sufficient to retard the reactivity addition to avoid super-prompt criticality for a boiling initiator [64]. Clearly, compensating reactivity at this level will be difficult to achieve in a sodium-cooled minor actinide based core. In the preliminary safety evaluation report of the PRISM design [65], the commission issued the following statement “The existence of a positive sodium void coefficient, or any reactivity feedback effect that tends to make a postulated accident more severe, is a significant concern”, which indicates the great importance attached to this issue.

With a subcritical reactor, one can adjust the initial level of subcriticality with regards to the void value and thus prevent progression into prompt critical conditions in voiding scenarios (one may note that there are other ways of voiding the reactor besides coolant boil-out). In that case the probability for core disruptive accidents could perhaps be made sufficiently low ($<10^{-6}$ per reactor-year) to be excluded in the formal licensing process, similar to the approach adopted in the design and licensing of the FBRs [66].

^aAs cautioned by Wade and Fujita, the quasi-static reactivity balance approach is a blunt method to obtain precise safety data and cannot be used to extract transient effects. The list of design variables would also have to include power and flow distributions in the reactor, the pump flow coast-down characteristic, the reactivity feedback coefficients (Doppler, axial exp., radial exp., coolant density), the corresponding core pressure drop, and in the long term, the decay heat removal performance is important and the natural circulation capability. However, the conditions considered in the reactivity balance proved to be useful to evaluate safety trends in the frame of modular-sized liquid-metal cooled reactor concepts and the issue here is whether similar characteristics could be achieved in sodium-cooled minor actinide cores.

Responsiveness of the ADS

The kinetics behaviour of an ADS differs substantially from a conventional (critical) reactor. The critical operating state represents a sensitive balance between the production rate of neutrons through fission and the neutron loss rate (through absorption and leakage) and a relatively small off-balance in these two quantities can lead to large deviations in the fission rate. In contrast, a subcritical reactor is inherently stable to reactivity changes within the subcritical range or changes in the external neutron source. If a subcritical reactor is subject to a change in the strength of the external source, or a change in reactivity within the subcritical range, the neutron population will adjust to a new stationary level. This is quite the contrary of critical reactors. In the absence of reactivity feedbacks the response in a critical reactor will either diverge exponentially or decay to zero depending on the sign of the reactivity disturbance. In the response to a reactivity insertion accident this feature provides to a distinct safety advantage over critical reactor operation, distinguished by high operational stability and additional margins for positive reactivity insertion. An example is shown in Fig. 18a for a linear reactivity-ramp-induced transient ($\$1$ in 1 sec.) in a lead-bismuth cooled critical reactor and in similar reactors made subcritical by -1β , -5β , and -10β . The cores (800 MWth, $\beta_{\text{eff}}=0.19\%$, MA-oxide fuel) are identical except for the initial reactivity. The reactivity feedbacks consist of coolant density (+0.53 pcm/K), axial fuel expansion (-0.28 pcm/K), radial core expansion (-1.0 pcm/K), and a small Doppler effect (-0.05 pcm/K). The increase in power is significantly weaker in the subcritical systems. The closer to criticality, the larger the power increase. For the power to double in a subcritical reactor, half of the reactivity required for criticality must be added. In response to negative reactivity feedbacks, however, subcritical operation is less favourable since the power will not drop as much as in a critical reactor. In Fig. 18b, an unprotected loss-of-flow is exercised for the same cores (featuring overall negative feedbacks) as in the previous example, which shows that the influence of such feedbacks will be much smaller in an ADS compared to any critical system.

Critical systems rely on delayed neutrons and smoothly varying feedbacks to level out reactivity disturbances. Since the operating point of a subcritical reactor is largely offset from prompt criticality both the delayed neutrons as well as reactivity feedbacks have a weak influence on the kinetics behaviour. The response is dominated by the prompt neutrons which follows the external neutron source. Hence, the time constant of change is essentially determined by the prompt period. Thus source changes and reactivity changes lead to abrupt power changes in the subcritical reactor. Delayed neutrons play an increasing role when the system approaches critical conditions. It should also be recognized that, an almost critical reactor behaves, for all practical purposes, nearly like a critical reactor. The essential difference is that for $k_{\text{eff}} > 1$, power continues to rise; for a reactivity increase that leaves $k_{\text{eff}} < 1$ the power stops rising at a level that depends on reactivity.

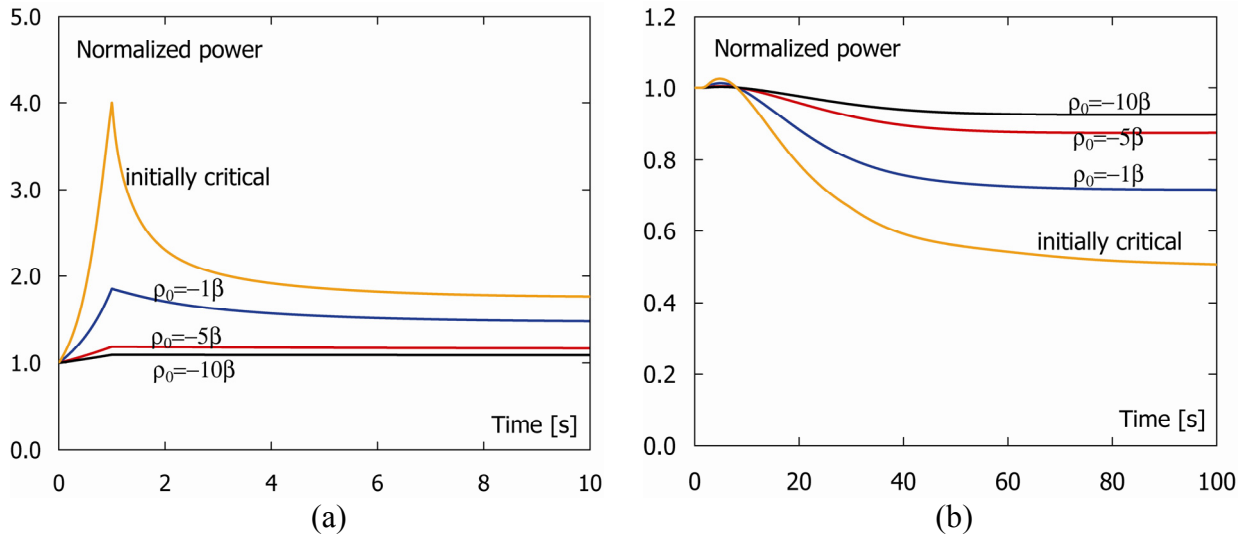


Fig. 18 Relative power vs. time following (a) linear reactivity-ramp insertion ($\$1$ in 1 sec) and (b) unprotected loss-of-flow in subcritical systems and critical system.

Accident performance

Transient computational modelling

The SAS4A/SASSYS-1 [69] computer code is applied to the analysis of accident sequences. A detailed description of the SAS code is outside the scope. However, a brief background and overview of the basic features is provided in Appendix B. The primary system includes models of the core, primary pumps, shell side of the steam generators, connecting piping, and compressible pool volumes with cover-gas surfaces. Reactivity feedbacks are calculated for coolant expansion, fuel elongation, radial core expansion, and Doppler effect. Changes in power level are computed with point kinetics theory. The performance of the point kinetics approximation for transient analysis of ADS's is discussed in **Paper III** and found adequate for similar problems.

Accelerator beam overpower

In an ADS, the traditional reactivity based shutdown system is replaced with a beam regulating system that controls the intensity of the external neutron source. The magnitude of the external neutron source is adjusted by changing the proton beam intensity. It is relevant to consider system disturbances in which the source strength suddenly changes. This could for example happen due to a control system failure, accelerator malfunction, or operator error. It may be noted that the source strength in an ADS may change abruptly while transients in a traditional reactor are limited by mechanical speeds. Since the prompt adjustment time in an ADS is very short (tens of Λ), the power will instantaneously respond to any source variation, which permits accidents with very short initial ramp times in comparison with transients in critical reactors. No safety system can act instantaneously; there are always time delays involved. For a traditional safety rod based shutdown system, there is typically a 200 ms delay from detection to control rod motion [70], and then an insertion time of the order of a second. This is fast enough to detect all accident initiators identified for fast reactors [71], which always appear as gradual changes. A beam overpower accident, however, can produce a considerable power change before the malfunction has been detected. Hence, failure prevention should be precluded by the design, and not simply rely on proper control system action.

Fig. 19 compares the response in a sodium cooled and a lead-bismuth cooled ADS when the external source strength is multiplied by a factor of 2 (see **Paper IV**). The ramp is initiated at $t=1$ second and halted at 1.001 seconds. The source is held constant thereafter. The fuel is diluted in zirconium oxide (Pu/TRU ratio is 0.4). The initial k_{eff} is 0.97 and the beta effective is 0.2%. The P/D ratio is 1.50 for the case shown. Following the initial jump the power changes as a result of reactivity feedbacks. The steam generators are assumed to remove heat at a rate of nominal power, resulting in increasing core inlet temperature as the transient proceeds. Coolant void reactivity feedbacks contribute to the course of the accident by adding reactivity. The void value for the sodium core is 6500 pcm ($\beta_{32.5}$) and in the case of Pb/Bi it is 3700 pcm ($\beta_{18.5}$). Differences in transient behaviour between lead/bismuth and sodium result primarily from the difference in boiling point and void reactivity effect. Coolant density changes provide modest changes in reactivity compared to the full void reactivity effect, which may introduce significant positive reactivity values. This causes the reactivity insertion rate to be considerable larger in the sodium-cooled core. Void generation, and thus positive reactivity insertion, is abrupt in the vicinity when boiling starts. Sodium boiling begins at the core outlet and develops axially downward. In the sodium-cooled core, the void effect adds enough reactivity to bring the reactor to a prompt critical state, with possible severe safety consequences. The small negative reactivity feedback associated with the Doppler effect does not influence the course of the accident, which is contrary to the situation in a boiling transient in a conventional FBR. Prompt critical conditions are established about 400 seconds after accident initiation. Large positive reactivity insertions are potentially possible due to lead/bismuth voiding as well. But the high boiling temperature for lead/bismuth (1943 K) compared to sodium (1154 K) makes voiding less probable even though there are other ways of voiding the coolant besides boiling, i.e. large scale steam generator failure or possibly sudden gas release from ruptured pins. The results point to a distinct advantage of using lead-bismuth as coolant.

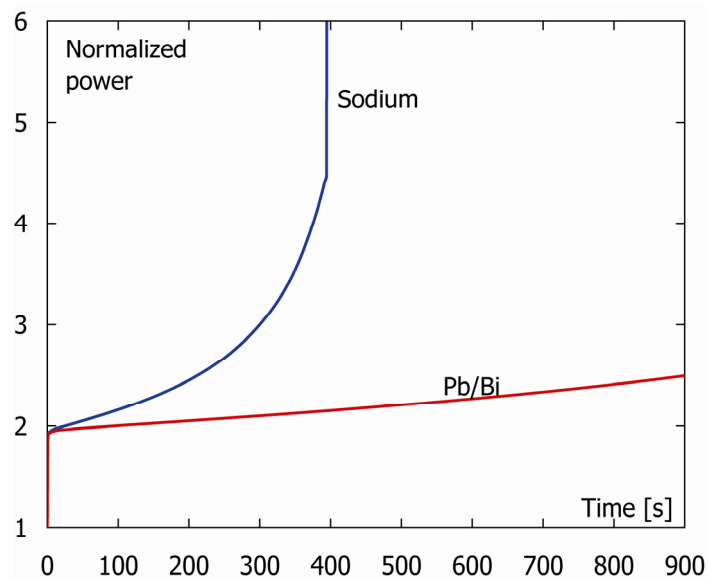


Fig. 19 Comparison of a beam overpower accident for sodium cooled and lead-bismuth cooled ADS.

Unprotected loss-of-flow

The safety performance of a lead-bismuth cooled ADS in response to unprotected loss-of-flow is investigated in **Paper I**. The results are presented here in a condensed form. The studies encompass three inert matrix fuel systems: a molybdenum-based Ceramic-Metal (CerMet) fuel, a magnesia-based Ceramic-Ceramic (CerCer) fuel, and a zirconium-nitride based fuel. Major plant specifications are presented in TABLE 14. A pool system is used to take advantage of a simple tank design and to avoid any nozzles and pipes of a loop system. Due to high corrosion activity, coolant temperatures and velocities are limited. The coolant flow velocity in the pin bundle is limited to 2.5 m/s and the reactor inlet temperature is set at 573 K. Lead-bismuth is chemically inert with water/steam. Hence, a two-circuit system is utilized, with the steam generator located in the primary system, which simplifies the overall plant design and reduces the cost. The primary system includes four centrifugal pumps (two for each loop) and four steam generators (two for each loop). Based on a seismic analysis, a vessel height of 10 m is selected. The separation distance between the core midplane and the thermal center of the steam generators is 5.5 m. The pump design includes flywheels to prolong the coast-down time in the event of a loss of pumping power accident.

TABLE 14
ADS plant specifications

ADS plant specifications	
General	
Type of plant	Pool type
Reactor power	800 MWth
Coolant	LBE (44.5%Pb+55.5%Bi)
Reactor inlet temperature	573 K
Coolant inlet velocity	2.5 m/s
Reactor vessel	
Height	10 m
Diameter	6 m
Wall thickness	13 cm
Weight (incl. coolant)	~2500 ton
Primary system	
Steam generators	4 (integrated)
No. of pumps	4
Pump mass of inertia	400 kg·m ²
Distance between thermal centers of core and SG's	5.5 m

It is assumed that all primary pumps are tripped in conjunction with failure of the shutdown system, i.e., the proton beam remains on. It is further assumed that the heat rejection system maintains core inlet temperature at the pre-transient value. During the transition to natural circulation condition, the flow rate is determined by the inertia of the pump and the thermal buoyant drive, which is counterbalanced by the system pressure losses. The pump moment of inertia has been optimized to soften the cladding-heating rate following pump trip. In principle, slower cladding heating rates and longer grace periods can be achieved with ever increasing pump inertia. There are, however, operational problems associated with high inertia pumps that impose an upper limit on the pump mass. Besides mechanical problems on the pump shaft, an adverse negative effect is sluggish speed control. In a controlled shutdown event, it is desirable to match the flow and power to avoid thermal cold shock in reactor components. This problem is of particular concern for ADS's because of the possibility for frequent beam interruptions, as discussed in **Paper VI**. Therefore, a balance must be struck in the selection of the flywheel size. The pitch-to-diameter (P/D) ratio and the pin diameter are

design parameters. The reference configuration uses a P/D equal 1.50 and a pin diameter of 5.72 mm. In a second configuration, the P/D value is increased to 1.75 by changing the pin pitch. In a third modification, the pin diameter is increased to 6.8 mm while holding the P/D ratio at 1.50. Matrix fractions are adjusted to obtain an initial k_{eff} equal 0.97 and a radial peak-to-average power ratio factor of 1.3. The β_{eff} is around 180 pcm for all three fuels. The plutonium fraction is fixed at 40% Pu and 50% MA. Because of lower thermal conductivity, the CerCer fuel is required to operate at lower linear powers; 25 kW/m compared to 35 kW/m for the CerMet and the nitride fuel. The calculational model used in this study employs two thermal-hydraulic channels. One channel represents an average pin within the core and a second channel represents the hottest pin in the core (with a power peaking factor of 1.3). The fuel-cladding gap conductance model accounts for gas conduction, radiative heat-transfer, surface roughness, and differential thermal expansion of fuel and cladding during transient conditions. Reactivity feedbacks are calculated for coolant expansion, fuel elongation, radial core expansion, and Doppler effect. Maximum temperatures during transients are determined and compared with design limits. Preliminary design limits are listed in TABLE 15, with detailed motivation given in **Paper I**. Si-modified 15-15Ti austenitic stainless steel (Phénix type) is the reference cladding material [72, 73].

TABLE 15

Summary of thermal limits for fuel and cladding.

Component	Failure temp. (K)	Failure mechanism
Fuel		
CerCer	2200-2300	Eutectic melt
CerMet	2640	Oxide melting
Nitride	2400	AmN dissociation
Cladding (type 15-15Ti)		
Surface (steady-state)	840	Corrosive thinning
Midwall (steady-state)	920	Creep rupture
Midwall (transient)	1330	Mech. burst limit

Fig. 20a shows the coolant flow rate and the power history for a core configuration with pitch-to-diameter ratio equal 1.75. It is seen that the natural circulation flow reaches a quasi-steady value of 23-27% of initial flow at 50-60 seconds after the pump trip. The power decreases steadily during the entire transition to natural circulation conditions. Reactivity feedbacks are illustrated in Fig. 20b. For simplicity only the case with CerCer fuel is shown. All three cores feature overall negative temperature-induced reactivity feedbacks. Reactivity feedback from radial expansion of the core is the dominant negative feedback mechanism – it contributes about minus one dollar at equilibrium conditions. Axial fuel expansion reactivity differs somewhat between the fuels. As the coolant temperature increases it produces a positive reactivity effect. The resulting reactivity increment due to coolant expansion amounts to +0.5\$ for the CerCer core and +0.4\$ for the nitride. The coolant reactivity is however exceeded by the reactivity losses due to radial expansion and fuel elongation. The positive coolant expansion effect is largely compensated by the negative feedback from fuel elongation. The Doppler effect is insignificant. The overall effect of the reactivity feedbacks is not great, however. The power falls to approximately 95% of the initial value of 800 MWth when equilibrium is reached. The power response behaviour is similar among the cores.

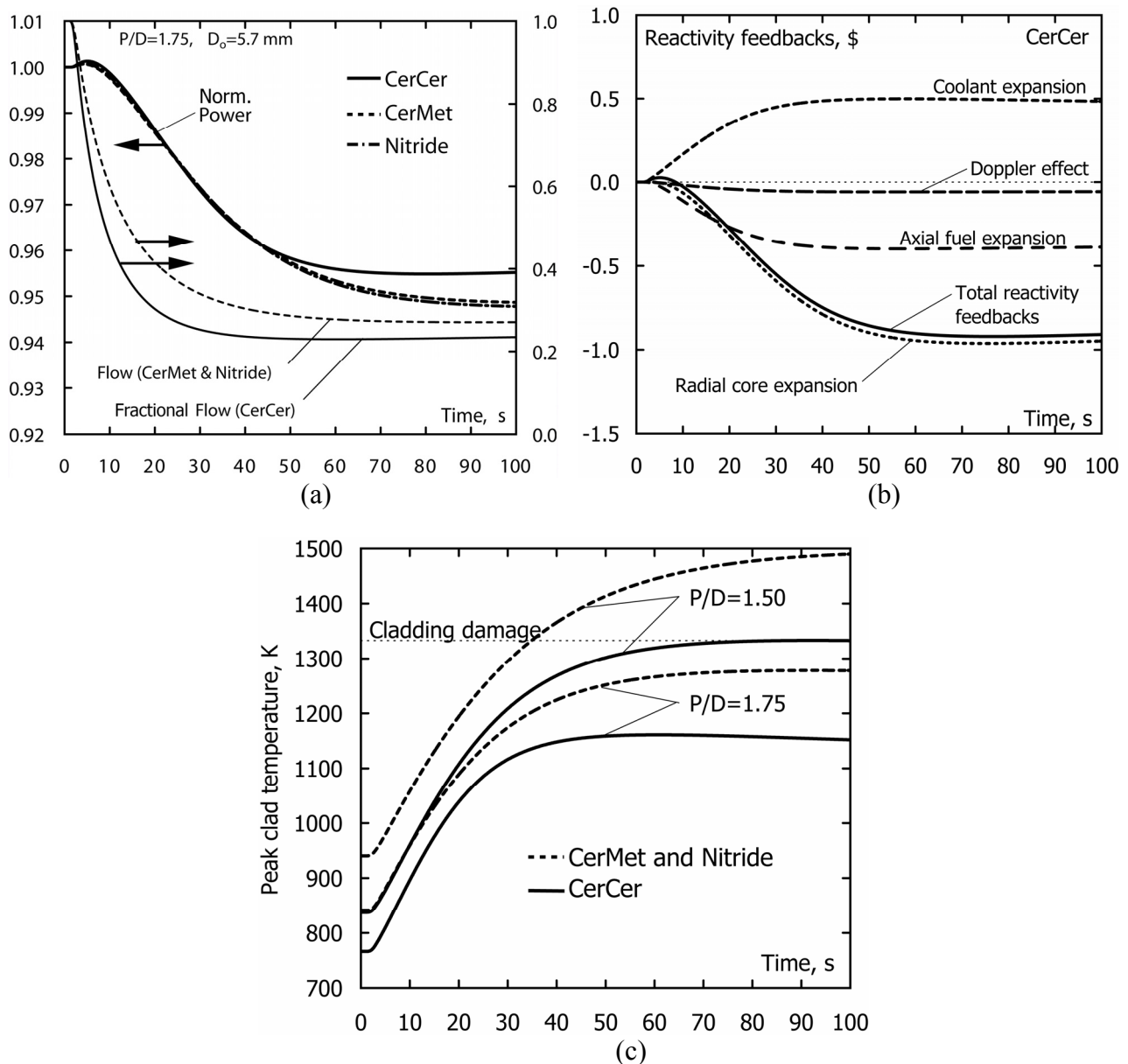


Fig. 20 Transient results for an ADS subject to unprotected loss-of-flow. (a) transient power and flow (b) associated reactivity feedbacks for the CerCer fuel (c) cladding temperatures.

The immediate effect of the flow reduction is a temperature rise in the coolant, and this in turn leads to higher cladding and fuel temperatures. Coolant boilout is not an issue with lead/bismuth. The primary concern is whether the cladding exceeds design limits. Lower cladding temperatures are promoted by higher coolant volume fractions. Larger distance between the fuel pins reduces the core pressure drop and in turn increases contribution from natural circulation. As a result, less forced flow is lost in a pump failure event. A comparison of cladding temperatures for these cores corresponding to $P/D=1.50$ and $P/D=1.75$ is shown in Fig. 20c. Cladding temperature is highest for the CerMet and nitride cores because of their higher power rating. The burst temperature for the cladding is 1330 K, as shown in TABLE 15. Thus, for the smaller pitch design, the cladding exceeds the failure point within 30-40 seconds after pump failure, which leaves small safety margins. On the other hand, increasing the P/D ratio to 1.75 reduces cladding temperatures by more than 200 degrees. In that case, early cladding failure can be avoided. It is noted however, that a safe state cannot be assured

indefinitely. The burst limit is applicable in transients in which the cladding is heated, without interruption, until failure. Thermal creep rates increase rapidly at high temperatures. Based on creep rupture data for D9 alloy [75], the lifetime at 1280 K is in the minute-scale. Thus, damage prevention will eventually require the need for shutdown and restored cooling capability. Maximum fuel and cladding temperatures as function of pitch-to-diameter ratio and pin diameter are presented in TABLE 16. Since the fuel temperature increases along with the coolant temperature, the potential for fuel damage must also be considered. The temperature of the CerMet fuel reaches 2120 K for the reference configuration (P/D=1.50 and $D_o=5.7$ mm), which corresponds to a margin to melting of 500 degrees. The nitride fuel, which has lower thermal conductivity than the CerMet fuel but smaller gap size, is slightly colder (2080 K) leaving a margin to dissociation of 320 degrees. The CerCer temperature reaches close to the damage limit for the same configuration. Increasing the pin diameter should be considered in this case.

TABLE 16

Peak fuel and cladding temperatures at a time $t=100$ seconds during unprotected loss-of-flow transient as function of P/D and pin diameter.

Fuel	P/D=1.50		P/D=1.75		P/D=1.50	
	$D_o=5.7$ mm		$D_o=5.7$ mm		$D_o=6.8$ mm	
	Fuel	Clad	Fuel	Clad	Fuel	Clad
CerCer	2160	1330	2130	1160	1970	1200
CerMet	2120	1490	2030	1280	1920	1340
Nitride	2080	1490	1980	1280	1920	1340

Coolant voiding

Extensive voiding in a liquid-metal reactor (LMR) may be caused by a leak in the primary system, sudden release of fission gases, failure in the heat-transport system that causes gas bubbles to enter the coolant, or coolant overheating and vaporization. Usually, LMR plant designs are arranged with backup protection to mitigate the impact of vessel leakage or rupture, to the degree that large-scale loss-of-coolant accidents (LOCA) are extremely unlikely. Pool systems typically have a second guard vessel, and loop systems are normally double pipe and tank designs. Since the liquid-metal coolant is not pressurized under normal operation, a leak in the primary system will not automatically result in coolant boiling, as opposed to the situation in LWR's. In a sodium-cooled reactor, voiding may arise due to boiling out of coolant. This is prevented in a lead-bismuth system. In order for the lead-bismuth to get hot enough to boil ($T_b=1940$ K), temperatures have to be above the melting point of steel ($T_m=1700$ K). In that case, much larger reactivity changes may become available due to fuel or cladding relocation. Coolant can be expelled by the rapid escape of fission gases from ruptured fuel pins. Fission gas release is of concern for unvented and high burnup ADS fuels. Another possible mechanism for coolant voiding, without the precondition of steel melting, is the possibility of entrainment of air into the core from the cover gas region or steam/water during a failure in the steam generator, i.e., a so-called steam generator tube rupture (SGTR) event. In sodium plants, intermediate sodium-loops are introduced as a second physical barrier to minimize the consequences of SGTRs and to avoid violent chemical reactions between water and sodium in the primary system. Because lead/bismuth is chemically inert with water/steam, two-circuit designs are suggested, with the steam generators located in the primary system. In such designs, there will only be one barrier to fail in order to get high-pressure steam into the primary system. It is noted that the pressure on the steam side can be as high as 100-150 bars and low pressure on the metal side, about 1 bar. Thus, a significant head is available to push steam into the primary system or cause

overpressurization in the circuit, which could open further leakage paths. Normally, steam generator tube failures have a high enough probability occurrence to be considered in the licensing procedure. It is noteworthy that a steam-generator failure was the cause of a LOCA and radioactive contamination in a Russian lead/bismuth-cooled nuclear submarine in 1982 [76].

Results for a transient test case study of a postulated steam generator tube rupture event leading to extensive cooling voiding were presented in **Paper I**. The core model and fuels are the same as the previous study of the unprotected loss-of-flow event. In the following analysis, it is assumed that the coolant is swept upwards through the core, beginning at the lower cold-leg region, and the void front moves at the average coolant velocity through the core (2.5 m/s). Since the total height of the core plus plenum regions is 2.5 m, the passage occurs in 1 second. The transient calculation uses a reactivity history based on progressive axial voiding of the core. It is assumed that the void spreads axially and simultaneously in all subassemblies. The reactivity effect, as function of axial void level, is illustrated in Fig. 21a. Note that the reactivity effect is strongest for the CerCer fuel and most positive when the core has been voided up to slightly below the top of the active fuel region. The reactivity insertion rate is highest at core midlevel. As a coincidence, the maximum reactivity insertion due to coolant void corresponded to the initial subcritical reactivity of the CerCer core.

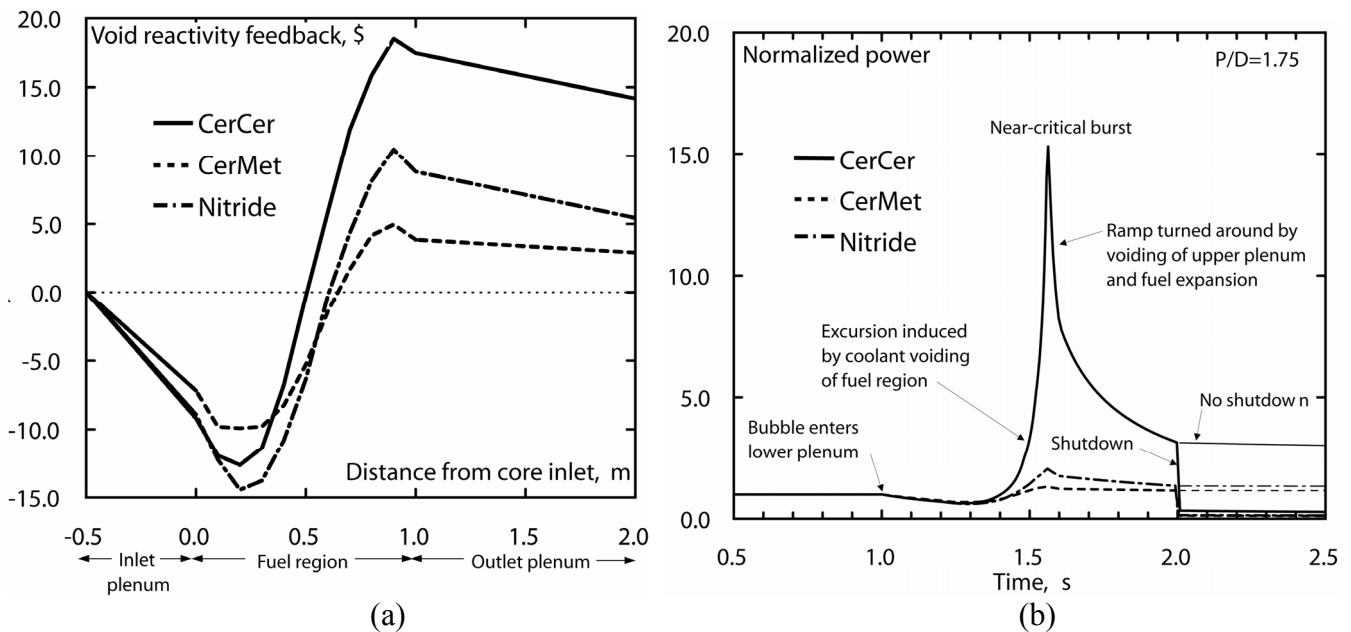


Fig. 21 Transient results for a postulated steam generator tube rupture accident. (a) shows the reactivity effect (\$) following progressive axial voiding of coolant beginning at the lower plenum. (b) Illustrates the transient power for the same accident.

The resulting power history is presented in Fig. 21b. The steam bubble reaches the lower plenum at 1 second after the steam generator failure. Initially, the bubble passage produces a negative reactivity effect due to increased neutron leakage, as the lower plenum is voided first. The power will find its peak as the reactivity reaches its maximum. The reactivity at peak power, is -0.2% , -12.3% , and -6.8% , respectively for the CerCer, CerMet, and nitride cores, the corresponding peak power is 15.3, 1.3, and 2.1, times the initial power. The power rise in the nitride and CerMet fueled cores is quite modest. The CerCer core, on the other hand, suffers from a sharp power peak. Except from coolant void, axial fuel expansion is the only feedback effect that has some impact on the transient. At peak conditions, the contribution from axial expansion provided an extra reactivity margin, which was sufficient to

maintain the reactor in the subcritical state, thereby limiting the magnitude of the peak. Radial core expansion is too slow to be of any significance. It was found that the flux shape in the voided state was similar to the initial shape, and power peaking factors were even lower. The power rise is halted when the void has extended to the top of the core and begins to void the upper plenum region. Judging from Fig. 21b, voiding of the upper plenum plays a vital role in reversing the accident. It is assumed that the beam is shutdown after 2 seconds.

Due to the strong positive reactivity effect, the CerCer system is subject to a sharp power peak, while the power rise in the nitride and CerMet fueled cores is quite modest, which simply confirms the importance of having a low coolant void reactivity value in a lead/bismuth system, despite of its high boiling temperatures.

Safety performance in super-prompt critical transients

Even if the probability for prompt critical transients can be made very low, the safety analyses usually require them to be investigated. Considering the high reactivity potentials available by core compaction (see TABLE 13) it is always possible to postulate an accident that will proceed into a prompt critical state. The resolution for the large FBR's was to demonstrate a low energetic potential (within the capabilities of the containment) of such accidents [66]. The large oxide cores relied on the presence of a strong Doppler effect to limit the energy yield (and pressure buildup) in a prompt critical reactivity transient. In such cores, the negative reactivity is provided by the Doppler broadening of resonances in primarily ^{238}U resulting in a relative increase in resonance capture over resonance fission. Since the Doppler effect is inherent in the fuel, the feedback mechanism is completely passive. The resulting reactivity effect is applied immediately since the Doppler broadening occurs simultaneously with the temperature change. As is well-known, the Doppler effect is small for fuels dominated by MA. Hence, the prompt negative effects, might be insufficient to stop an excursion before energetic disassembly occurs. Here we treat a classical problem of reactor excursions, induced by a rapid reactivity ramp in systems with different prompt negative feedbacks. It may be postulated that the accident is caused by a loss-of-coolant (e.g. as a result of a major break in the primary system) and that some fuel is melted and the core collapses by gravity forming a supercritical configuration (traditional Bethe-Tait scenario).

Fig. 22 illustrates the essential characteristics of the transient in a MA-fueled ADS. The results are compared with calculations for a conventional sodium-cooled and MOX-fueled fast reactor ($\text{U}_{0.8}\text{Pu}_{0.2}$) presented in the same graph. Consider at first the ADS with initial $k_{\text{eff}}=0.97$. The transient is driven by a linear reactivity insertion, 100 \$/s (0.167 $\Delta k/s$), a value which is frequently related to core compaction/meltdown phenomena. It is further assumed that this reactivity ramp continues uninterminated. The value for the Doppler constant ($T \cdot dk/dT$) as well as the effective delayed neutron fraction are chosen to simulate the conditions in the respective cores. The Doppler constant in the fast spectrum MA core ($\text{Pu}_{0.4}\text{Am}_{0.6}$) is taken as $2.0 \cdot 10^{-4}$ with a $\beta_{\text{eff}}=0.167\%$. The Doppler constant for the oxide fast reactor is $8.1 \cdot 10^{-3}$ (see TABLE 11), which is about 40 times larger than the MA core. The corresponding ramp rate for the fast reactor is 50 \$/s since the effective delayed neutron fraction ($\beta_{\text{eff}}=0.34\%$) is about two times larger than the MA core. The Doppler effect contribution is assumed proportional to $1/T$, as in the case of large oxide-fueled fast reactor, where T is the average fuel temperature in the core. As comparison the Doppler coefficient decreases somewhat faster with temperature ($T^{-3/2}$) in the smaller, highly enriched FR's. For the LWR's it approaches $T^{-1/2}$. The fuel heat-up is treated for the simple case of adiabatic boundary conditions for any additional heating above steady-state levels. This is a reasonable approximation considering the overall speed of the transient. The steady-state operational power density is $\sim 1.3 \text{ W/mm}^3$, which is fairly typical for the FBR as well an ADS employing

oxide fuel. During the transient, around 86% of the additionally produced fission energy is deposited in the fuel (~8% of the heat is deposited outside the fuel and 6% appears as decay heat which is not immediately affected by the transient). For simplicity, equal prompt neutron generations times ($\Lambda=0.81 \mu\text{s}$) are applied for both cores. Reactivity contributions from core disassembly are not treated. The reactor behavior is described by the standard point kinetics equations with six delayed neutron groups coupled with a temperature dependent Doppler feedback.

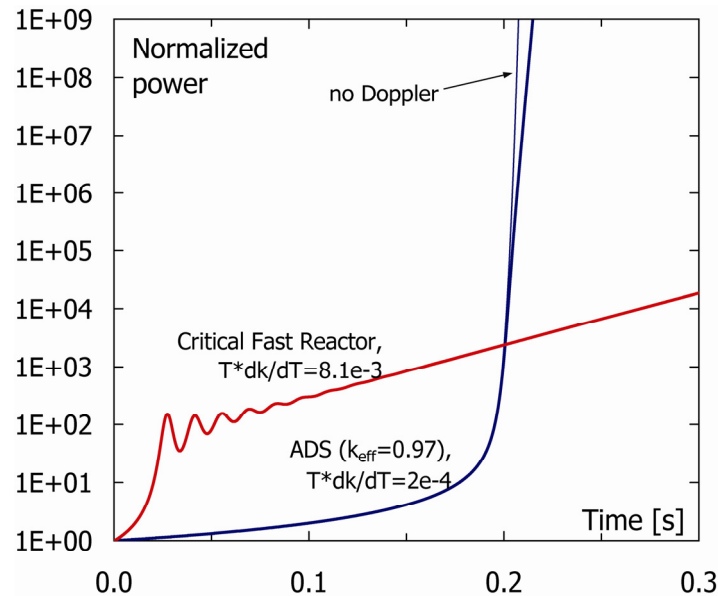


Fig. 22 Effect of Doppler feedback on prompt critical transients induced by a reactivity ramp insertion. Transients initiated from operating conditions in a conventional fast reactor with a large Doppler constant ($T^*dk/dT=8.1 \cdot 10^{-3}$) and an ADS ($k_{\text{eff}}=0.97$) with a small Doppler feedback ($T^*dk/dT=2.0 \cdot 10^{-4}$). Core disassembly is neglected.

In the fast reactor the reactivity quickly reaches a prompt critical state. Prompt criticality is established around 20 ms after the onset of the transient. It follows that the power increases rapidly at first. However, as the temperature in the fuel increases, the negative Doppler feedback compensates the ramp-induced reactivity; this causes a decrease in reactivity and a corresponding power reduction. In the example given, the fast reactor is superprompt critical for 6 ms in connection with the first pulse. After the power is reduced, the rate of reactivity reduction by Doppler feedback slows down while the ramp drives the reactor to prompt criticality again, allowing for a second power surge. This causes the familiar damped oscillation in reactor power, where the maxima and minima occur when the reactivity passes through β . As the oscillations die-away, in the given example, the reactivity finds a balance at a level slightly below β . Since the Doppler effect contribution decreases with temperature ($1/T$ dependence), the power tends to increase with time, but at a much slower rate than if the Doppler effect had not been present. It should be noted that progression with ever increasing power is physically unrealistic. At some point the ramp is terminated and the excursion is turned around by fuel displacement, possibly involving some vaporization. As first discussed by Bethe and Tait [67], rapid fuel motion is resisted by inertial effects and this may prolong the shutdown process, in which additional energy can be produced to enhance the very fast excursion. Under these conditions the Doppler effect is very effective [58], by reactivity reduction to subprompt critical values resulting in substantially lower energy releases.

The transient in the ADS is quite different according to the magnitude of the Doppler reactivity effect and the level of subcriticality. Since the reactivity in the ADS starts at a low

value (-\$18.5), the power increases slowly initially. Prompt criticality is reached at 195 ms. Because of the weak Doppler feedback the reactor settles on a fast period above prompt critical (\$1.4). As can be seen from the figure, the Doppler effect has an overall small effect on the transient. While no attempt has been made to calculate the disassembly process in this study, it is well-known [58] that a small Doppler can pose a serious threat to the containment structure in a maximum accident. At this point, it may be added that core disassembly generally starts when fuel boiling begins. The energy released during core disassembly is sensitive to the fuel boiling point [68], which may differ between the investigated fuels, but depends also on the fuel temperature at the start of the excursion. Higher starting temperature together with a low Doppler coefficient generally causes a reduction in the energy release as less reactivity is inserted [58]. One may realize that, starting from a highly subcritical state, the additionally produced heating during the subcritical reactivity insertion phase will cause higher fuel temperatures at the start of the excursion. Thus, subcriticality may in principle advance the shutdown process and limit the energy release. Nevertheless, it was found that for the rapid reactivity ramp (100 \$/s) the fuel temperature rise prior to approaching prompt criticality was rather small ($\Delta\bar{T}_f \sim 170$ K). Hence, the majority of the temperature rise occurred in the prompt critical burst which suggests that the potential benefit may be small for rapid reactivity ramps (~ 100 \$/s). The subsequent fuel displacement would then mainly occur during the excursion phase and hence differences in the Doppler feedback plays a crucial role. It was found that the subcriticality is more effective in raising the starting temperature for slower reactivity ramps. For example, a reduction of the ramp rate from 100 \$/s to 10 \$/s increases the average fuel temperature by ~ 2700 K at the onset of prompt criticality.

Longitudinal thermal expansion of the fuel column is a second feedback effect that may contribute with negative reactivity in a fast power excursion. This was not taken into account in the examples presented above. In most cases, fuel expansion may be considered as a prompt reactivity effect, although it is subject to certain time delay conceivably of some importance under disassembly conditions. It is a neutron leakage effect caused by a change in fuel density. Expansion coefficients for a standard MOX-fueled fast reactor and MA oxide-fueled ADS were calculated in **Paper II**. It was found to be similar for both cores and equal to $-0.2 \cdot 10^{-5} \Delta k/T$. This number refers to uniform temperature increase and axial expansion throughout the reactor. It is calculated for the intact core. Hence, it is well-defined during the startup period of the accident, but could be very misleading during the excursion phase involving partial melting. A partly melted core cannot be expected to possess the usual negative reactivity feedbacks from solid fuel expansion, so direct application to the meltdown problem may not be applicable. It is still of some interest to investigate the basic influence, partly due to its traditional usage in fast reactors. It may be noted that, thermal expansion effects were frequently included in the prompt excursion analyses of the early fast reactors (GODIVA, Fermi, EBR-I and EBR-II). These small and highly-enriched reactors essentially relied on this mechanism for early shutdown. Its effect on the present cores is illustrated in Fig. 23. Apparently, when axial expansion is included in the feedback description the characteristics of the transient are quite similar in the fast reactor core and the ADS. The essential difference is then the timing of the prompt critical burst. The results indicate that axial fuel expansion can stabilize a prompt critical accident in the ADS. But, a word of caution is added as the results are based on the simplified assumption of axial expansion reactivity feedback calculated for an intact core and as being proportional to the temperature rise during the entire accident.

To summarize, the analyses add to the statement that Doppler feedback in the typical minor actinide fueled ADS is too small to influence the development of a prompt critical accident. For slower reactivity insertions, subcriticality could possibly facilitate faster shutdown, but

may be less effective for fast insertions. To some degree axial expansion of the fuel can compensate for a small Doppler coefficient, but it cannot be considered as reliable as the Doppler effect in the general case. It depends on the engineering design and is subject to uncertainties in the thermo-mechanical behaviour of the fuel and overall conditions in the core.

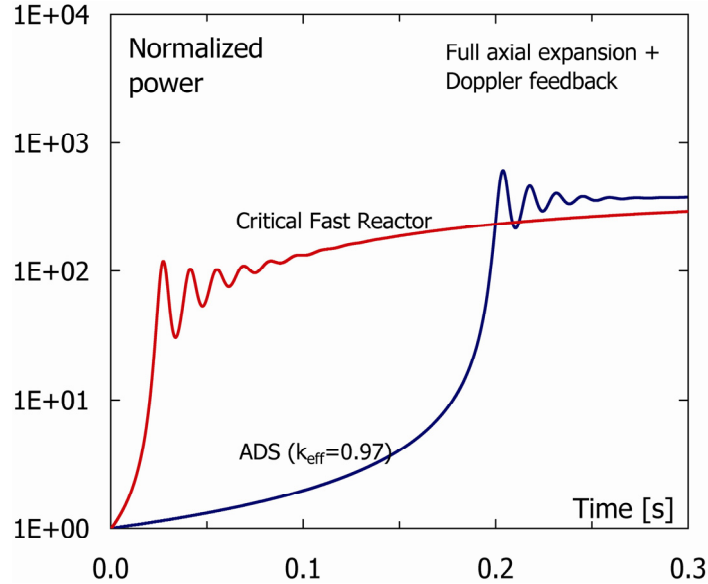


Fig. 23 Prompt critical transients in a conventional fast reactor and ADS ($k_{\text{eff}}=0.97$) with axial expansion reactivity feedback included from the beginning through the entire transient.

Computational performance of the point kinetics method

The so-called “point kinetics approximation” is a widely used method for performing preliminary analyses of dynamic phenomena in nuclear reactors. It has been extensively applied for the transient design analysis of existing reactors and it forms the basis of many transient analysis computational codes. It is based on kinetics theory developed for critical reactor studies. While the utility of the point kinetics methodology for critical reactor analysis is well known, its applicability to source-driven subcritical systems is subject to investigation [77, 78]. Because the neutron balance equations that describe the response in source-driven reactors are fundamentally different from the problem characterizing critical reactors, it has been suggested [79] that the point kinetics technique may be inappropriate for ADS studies; it is nonetheless very popular and often used for analysing such systems. The computational performance of the point model in its application to ADS was investigated in **Paper III**.

Point kinetics theory

The point kinetics equations were first derived by Henry [80]. Their limitations and capabilities for critical reactor analysis have been investigated in great detail [81-83]. The purpose behind the formulation of the kinetics equations is to derive a lumped model that describes the change in the average level of the flux, i.e., the integral of the neutron flux over the energy and the spatial domain. The point-kinetics equations for a source-driven system are derived in Appendix A. The equations are obtained by recasting the time-dependent diffusion (or transport) equation into:

$$\frac{dp(t)}{dt} = \frac{\rho(t) - \beta(t)}{\Lambda(t)} p(t) + \sum_k \lambda_k c_k(t) + s(t)$$

$$\frac{dc_k(t)}{dt} = \frac{\beta_k(t)}{\Lambda(t)} p(t) - \lambda_k c_k(t)$$

The above equations are usually referred to as the “point kinetics equations” or sometimes the “exact point kinetics equations” in a way to distinguish them from the simplifying assumptions applied in the point kinetics approximation. The new quantities, β , Λ , ρ , s , and c_k that emerge in point kinetics equations are integral quantities and they arise only in the derivation of the point kinetics equations (more rigorous definitions of these quantities are given in Appendix A). This is realized since the basic time-dependent neutron diffusion equations do not involve these concepts. As pointed out by Ott [52], that as long as the exact definitions are applied in the calculation of the kinetics parameters (that implies full solution of the space-energy-time problem), the point kinetics equation is exact and completely equivalent to the basic, time-dependent diffusion (or transport) equation, but in a different form. This is true for critical as well as for subcritical systems. The error is introduced when an approximate representation of the time-dependent flux shape, e.g., the point kinetics approximation, is applied. In that case, a prefixed shape representation of the flux is used throughout the entire transient, only the “level” of that flux shape changes, i.e., first-order perturbation theory approach.

Computational model

Numerical testing was performed with coupled core dynamics calculations using the SAS4A/DIF3D-K code [84], see also Appendix B. The “exact” results are obtained from a direct numerical solution of the time-, space-, and energy-dependent multigroup diffusion equation. The direct solution is used as a standard of comparison for the point kinetics solution. One advantage of using the SAS4A/DIF3D-K program for the current task is that the direct solution method and the point kinetics procedure are implemented within the same code. This makes it straightforward to compare the underlying methods without worrying about consistency among different computational procedures and models. For example, the initial steady-state solutions, cross sections, thermal- and hydraulics treatments, and model specifications are all identical. More detailed specifications of the computational methods involved are given in **Paper III**.

The test model used in the present study is based on a previous OECD/NEA benchmark model [85]. The model pertains to an accelerator-driven, lead-bismuth cooled, and minor-actinide loaded transmuter core. The core consists of a central lead-bismuth target region and a homogenized fuel region surrounded by radial and axial reflectors (70% steel and 30% coolant). 114 fuel assemblies are included in the hexagonal-z representation; Fig 1 contains a plan view of a one-sixth symmetry section of the core. The height of the active core is 100 cm. The fuel consists of 2/3 minor actinides and 1/3 plutonium with a ZrN diluent; $(\text{Pu}_{0.1}, \text{MA}_{0.2}, \text{Zr}_{0.7})\text{N}$, where MA represents minor actinides such as Np, Am, and Cm. Fuel compositions correspond to plutonium discharge from UOX-fueled LWRs mixed with MA from a “double strata” strategy. Start-up core loading is used in the simulations. The fuel is further diluted with 71% ZrN.

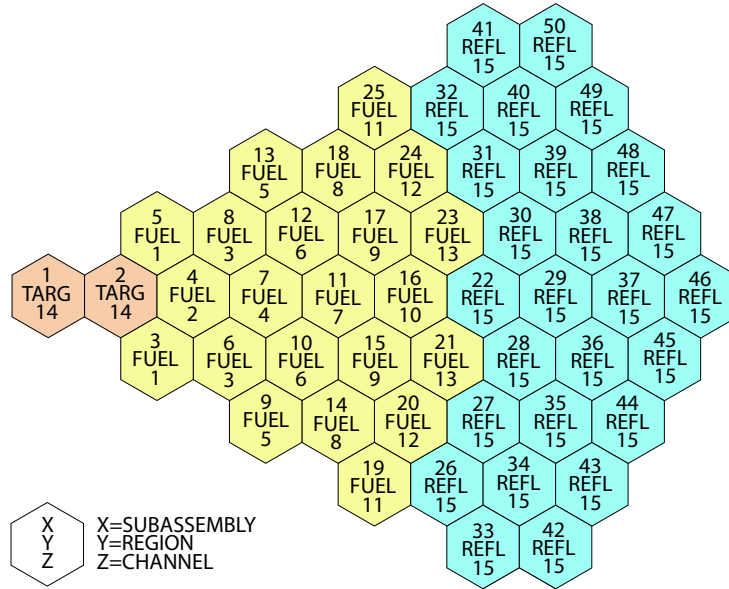


Fig. 24 One-Sixth Core Subassembly and Channel Assignment.

Numerical results

Numerical solutions for three different categories of transients were analyzed. The test problems pertain to accident-type events in ADS's. The first category concerns alterations of the proton beam intensity, i.e., changes in the magnitude of the external neutron source (the spatial and energy distributions for the source neutrons are invariant). Secondly, localized reactivity insertions were examined. Finally, a flow reduction event is analyzed. The total power is extracted as a function of time, i.e., fission power plus decay power, as obtained in the direct solution and in the point kinetics solution. The transients are followed for 20.0 seconds. We further perform calculations at different subcritical levels, i.e., k_{eff} values, to reveal any trends concerning performance characteristics. The initial effective multiplication constant is altered by changing the concentration of fuel diluents (ZrN). It will provide information on the numerical accuracy of the point kinetics solution as function of the level of subcriticality.

For accidents involving external source perturbations (both the source overpower transient and the source trip transient) the point method provided extremely accurate results. In fact, the results are indistinguishable as illustrated in Fig. 25a and Fig. 25b. The maximal deviations are 0.2% and 0.9% for the source overpowers and source trip transients, respectively. Maximum deviation occurs shortly after the source has been fully inserted/removed, followed by better agreement from that point and forward. Deviation from the point kinetics solution is an indication of flux shape changes. An external source perturbation, by itself, does not affect the reactivity. Hence, the only source for spatial distortion is due to reactivity feedbacks. The good agreement implies that the thermal feedbacks are small and/or distributed such that no noticeable flux deformation develops. Based on these results, it is expected that source disturbances can be described accurately by point kinetics.

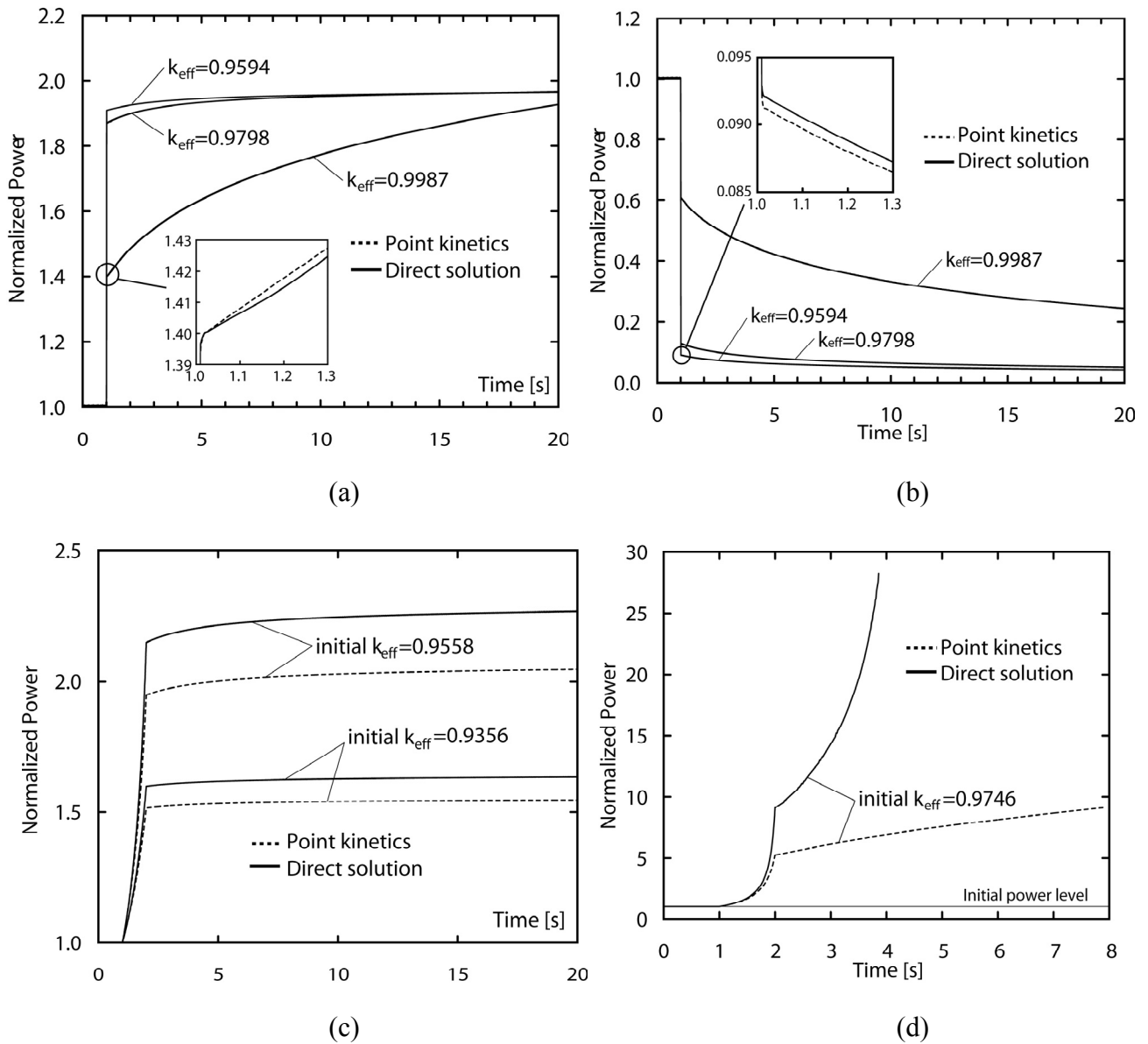


Fig. 25 Source overpower transient problem (a). Source trip transient (b). Reactivity insertion near core-center for cases with initial $k_{\text{eff}}=0.9356$ (c) and $k_{\text{eff}}=0.9558$ (c) and $k_{\text{eff}}=0.9746$ (d).

Next, we consider the effect of local reactivity insertions, i.e., transients in which the point treatment is expected to be a poor approximation. It is assumed that a fuel subassembly is fully withdrawn at initial conditions and subsequently drops into the core during operation. Despite the somewhat remote likelihood of this scenario, it is useful for evaluating the performance of the underlying kinetics methods. The effect of reactivity insertion is investigated at two different positions; in one instant we move a subassembly close to core-center (subassembly no. 4 in accordance with the core map in Fig. 24) and in a second study it is inserted close to the core boundary (subassembly no. 16). The reactivity worth of the fuel subassembly near the core-center is approximately \$13 and \$4 for the subassembly at the core boundary. It is assumed that the region representing the absent subassembly is occupied with coolant at initial conditions. It is well known, from critical system analysis that for local reactivity insertion events, using the point kinetics technique to calculate the response can lead to significant errors. This is because the basic assumption is that the flux shape remains

constant. Comparison with the exact results shows that this is indeed the case. The point approximation severely underestimates the excursion for the case that is closest to the critical state, shown in Fig. 25d, but the results indicate better precision at lower k_{eff} levels, Fig. 25c. While the amount of reactivity insertion is essentially the same for all test configurations, it appears as if the flux spatial distortion decreases when the system is more subcritical. This behavior seems reasonable considering the reduced sensitivity to reactivity inputs in the subcritical state. When the fuel subassembly falls into the reactor, the neutron flux increases near this location due to a local increase in the fission rate. In the near-critical reactor, the neutrons are strongly multiplied, and the increase in the fission source produces a local deformation of the flux shape. In a deeply subcritical core, the neutrons are weakly multiplied therefore; the insertion of the subassembly has an overall smaller effect. Due to this lower sensitivity, flux distortions following a reactivity disturbance diminish as the k_{eff} decreases. In TABLE 17, the relative root-mean-square (*RelRMS*) deviation of the local peak-to-average flux (for all three-dimensional spatial nodes) with respect to the initial distribution is presented. Obviously, the *RelRMS* variation of the flux shape decreases as the core multiplication constant decreases, which gives further support to the previous argument.

TABLE 17

Relative root-mean-square (*RelRMS*) difference of the peak-to-average flux distribution with respect to the initial flux distribution following insertion of the subassembly near the core-center.

Time [s]	RelRMS ^g peak-to-average flux		
	Initial	Initial	Initial
	$k_{\text{eff}}=0.9356$	$k_{\text{eff}}=0.9558$	$k_{\text{eff}}=0.9746$
1.2	0.9%	1.0%	1.2%
1.4	1.8%	2.2%	2.6%
1.6	2.8%	3.4%	4.1%
1.8	4.0%	4.7%	5.7%
2.0	5.2%	6.2%	7.4%
3.0	5.2%	6.3%	7.8%
20.0	5.4%	6.6%	-

$$RelRMS = \sqrt{\frac{1}{N} \sum_{i=1}^N \left(\frac{p_i - p_{0_i}}{p_{0_i}} \right)^2}$$

where N is the number of hex-Z nodes in the three-dimensional space

and p is the local peak-to-average flux in each node. The subscript 0 denotes the initial state.

Concluding remarks on the point kinetics approximation

The results indicate that the point kinetics approximation is capable of providing highly accurate calculations in subcritical systems. The results suggest improved precision at lower k_{eff} levels. The reduced sensitivity to system reactivity perturbations in a subcritical state effectively mitigates any spatial distortions. Because a source-driven subcritical reactor approaches a stationary state (in response to source or reactivity changes), the error of the point kinetics method becomes essentially bounded. Prompt adjustment of the flux shape prevails since the delayed neutrons are less influential (in a critical reactor the delayed neutrons tend to retard the shape transition). In general, the flux shape in a fast neutron spectrum shows strong space-time coupling, i.e., local perturbations will quickly spread throughout the reactor. This is usually attributed to the relatively large mean free path of fast neutrons and to the comparatively compact core size of a fast reactor. All together these characteristics are favorable from a point kinetics view of application to fast spectrum ADS systems.

Accelerator reliability

In accelerator-driven system designs, the neutron source is the controller of the chain reaction. Power fluctuations caused by accelerator beam interruptions (trips) enforces thermal transients to structures. Multiple shutdown events may result in thermal fatigue [86], which can cause premature failure. This problem is of particular concern for ADS's because of the possibility for frequent beam interruptions. ADS applications impose a new requirement on the design and operation of high-power proton accelerators, namely that of extremely high reliability of the beam.

Paper VI examines the reliability and availability of the proton accelerator facility at the Los Alamos Neutron Science Center (LANSCE). Beam trips and failure causes were collected based operational data records, accelerator logbook and beam monitor data. Mean Time Between Failure and Mean Down Time estimates are obtained for typical accelerator components. The availability is expressed as the ratio of the achieved beam time to the scheduled beam time. Reliability has to do with the number and durations of beam interrupts in that interval. It is typically determined by the mean time between failure and the mean down time of a trip. In the case of thermal cycling the reliability to beam trips and fluctuations has a critical influence. The LANSCE system is a linear proton accelerator. The accelerator delivers two proton beams at 800 MeV: the H⁺ and the H⁻ beam. The H⁺ beam may deliver 1.25 mA current (routine operation is at 1 mA) and the H⁻ beam delivers 70 μ A. Each injector system includes a 750 keV Cockcroft-Walton type generator. Both ions are accelerated simultaneously in one and the same structure. The low energy section of the accelerator is an Alvarez Drift Tube Linac (DTL). The drift tube linac accelerate the protons from 750 keV to 100 MeV. The high energy section is a Side Coupled Linac (SCL). The SCL may accelerate protons up to 800 MeV. After acceleration the H⁺ and H⁻ beams are separated and divereted into different target areas.

Beam operational data is reported in Fig. 26. The reliability of the H⁺ and the H⁻ beams are investigated separately. The analysis considers scheduled accelerator operation of the H⁺ beam for 1997 and of the H⁻ beam for 1996 and 1997. From the figure it is obvious that the accelerator is exposed to many beam trips with short duration. The main cause for failure is electric breakdown in the high-voltage column of the injector. The characteristic of injector failure is short outage time, often in the order of 15-20 seconds, the time it takes to reset the trip and re-energize the generator. The annual interrupttion rate in the LANSCE linac is typically on the order of 10^4 per year. But that includes many interruptions of very short duration. Most of these trips are momentary effects, for which the beam has to be interrupted only for a very short period, while the offending system is restored to operation by automated recovery systems. Interruptions with duration shorter than 1 second are not detrimental because the thermal transients in the reactor are then very small. This leaves perhaps 10^3 annual interrupts of duration longer than 1 minut, which require some kind of operator intervention. What beam trip rate is the maximum acceptable limit for a high power subcritical reactor? If we compare the above performance data with an average of 2-3 unscheduled shutdowns per year in LWRs, the necessary reliability improvement appears to be tremendous. On the other hand, if the maximum acceptable trip rate can be relaxed to 10-100 trips/year, the goal seems to be more realistic. One should take into account that current operating proton linacs were designed with high beam availability as a key goal, but the frequency of beam interrupts was not a major issue.

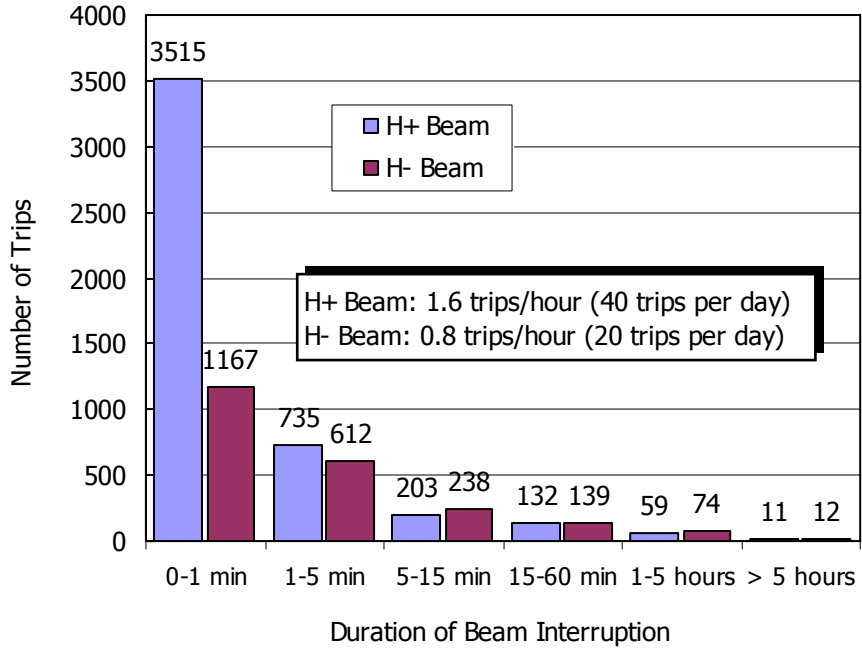


Fig. 26 Beam failure statistics of the LANSCE accelerator facility

Conclusions

The thesis analysed and discussed the safety performance of accelerator-driven nuclear reactors, with emphasis on design features and safety characteristics under normal operation and hypothetical accident sequences. The studies concerned mainly lead-bismuth cooled accelerator-driven reactors operating on a fast neutron spectrum and employing transuranic fuel. Major consideration was given to the potential threat of coolant voiding. The thesis examined the performance of the point kinetics approximation in subcritical systems and also included a study of the proton beam reliability in accelerator facilities.

The ADS is a non-self-sustaining, subcritical reactor driven by an external neutron source, whose kinetics characteristics differ significantly from conventional (critical) nuclear reactors. The critical operating state represents a sensitive balance between the production rate of neutrons through fission and the neutron loss rate and a relatively small off-balance in these two quantities can lead to large deviations in power. In contrast, a subcritical reactor is inherently stable to reactivity changes within the subcritical range or changes in the external neutron source. Under such conditions, the neutron population will adjust to a new stationary level. In the response to a reactivity insertion accident this feature leads to a distinct safety advantage over critical reactor operation, distinguished by high operational stability and additional margins for positive reactivity insertion. In response to accidents featuring negative reactivity feedbacks, however, subcritical operation is less favourable since the power will not drop as much as in a critical reactor.

Given a uranium-free fuel based on minor actinides, the inherent core safety characteristics deteriorate. Parametric analyses indicate that the addition of minor actinides to a fast spectrum reactor lowers the Doppler coefficient and reduces the effective delayed neutron fraction. Critical fast reactors rely heavily on the delayed neutrons and the Doppler effect to achieve smooth power control during normal operation and protection against severe reactivity insertion accidents. In addition, the void reactivity effect becomes increasingly positive in uranium-free and liquid-metal cooled minor actinide cores, especially using sodium coolant. It thus appears that operation of such cores in a critical state would be very difficult. The specific studies of transient operating characteristics and unprotected accident sequences indicate that lead-bismuth cooled accelerator-driven reactors can be effective in addressing the low effective delayed neutron fraction and the high coolant void reactivity that comes with the minor actinide fuel. Here, the elementary factor in preventing supercritical excursion is the built-in subcritical margin. Adjustment of the initial level of subcriticality with regards to the magnitude of the inserted reactivity provides an effective means to overcome the deteriorated effective delayed neutron fraction and the high void value.

The situation with the absent prompt negative Doppler feedback is more complicated. In a conventional fast reactor, the Doppler effect is especially valuable under super prompt critical accidents, in which it will advance the shutdown process and thus reduce the energy release and limit the destructive force on the containment. The first counteractive measure would be to somehow preclude accidents that might lead to prompt-critical conditions from beginning. Obviously, adjustment of initial subcriticality is a step in the right direction. Minimization of the intrinsic reactivity potentials is a second step to preclude prompt critical conditions. Other means could involve adjustment of the fuel design and composition or changes in the

geometrical arrangement of the core to minimize the risk for core compaction and accommodate early dispersal mechanisms. But even beyond such measures, a large negative Doppler effect or some other inherent prompt negative feedback mechanism might ultimately be considered necessary to assure public safety even in the extremely unlikely event of core disruptive accident. Considering the large reactivity vested in a minor actinide core it is always possible to postulate an accident that will proceed into prompt critical conditions, that is a principal difficulty.

The thesis further underlined the importance of a having a low coolant void reactivity value in a lead-bismuth system, despite the high boiling temperature of the coolant. A steam generator tube rupture event was identified as a potential threat, which could lead to extensive voiding in current accelerator-driven design proposals. The design studies found favorable inherent safety features for a molybdenum-based Ceramic-Metal (CerMet) fuel. Detailed analyses found that the point kinetics approximation is capable of providing highly accurate transient calculations of subcritical systems. The results suggest better precision at lower k_{eff} levels, which is an effect of the reduced sensitivity to system reactivity perturbations in a subcritical state. It is recognized that the accelerator is responsible for frequent beam interruptions and this is of concern for accelerator-driven nuclear reactors because of the risk for thermal cycling and premature failure. It is clear that extensive improvement in the mean-time between beam failures is required.

Appendix A:

Reactor Kinetics Equations

Here we review shortly the derivation of the conventional kinetics equations. These were first derived by Henry [80]. The derivation is presented here to serve as a basis for discussion of applications to source-driven systems. For convenience, the derivation proceeds along the lines suggested by Henry [87] with minor modification. An independent source term is incorporated to include neutrons supplied by the external source. The starting-point is the time-dependent continuous energy diffusion equation¹. In shorthand operator notation it can be written as:

$$\frac{1}{v} \frac{\partial \Phi}{\partial t} = (\mathbf{F}_p - \mathbf{M})\Phi + \sum_k \lambda_k C_k \chi_{dk} + S \quad (1a)$$

and completed with the balance equation for the delayed-neutron precursors

$$\frac{\partial C_k}{\partial t} = -\lambda_k C_k + \int_0^\infty v_{dk} \Sigma_f(\mathbf{r}, E', t) \phi(\mathbf{r}, E', t) dE' \quad (1b)$$

$\Phi = \phi(\mathbf{r}, E, t)$ is the time-dependent neutron flux. For simplicity of notation, the functional dependence in Eq (1a) and (1b) has been suppressed. \mathbf{M} and \mathbf{F}_p are the usual “migration and loss operator” and the “prompt neutron production operator”, respectively. These correspond to:

$$\begin{aligned} \mathbf{F}_p \Phi &= \chi_p(E) \int_0^\infty v_p \Sigma_f(\mathbf{r}, E', t) \phi(\mathbf{r}, E', t) dE' \\ \mathbf{M} \Phi &= -\nabla \cdot D(\mathbf{r}, E, t) \nabla \phi(\mathbf{r}, E, t) + \Sigma_t(\mathbf{r}, E, t) \phi(\mathbf{r}, E, t) \\ &\quad - \int_0^\infty \Sigma_s(\mathbf{r}, E' \rightarrow E, t) \phi(\mathbf{r}, E', t) dE' \end{aligned}$$

¹In his original work, Henry derived the reactor kinetics equations starting from the time dependent neutron transport equation, we chose not to proceed along this path, but rather to utilize the diffusion approach as outlined in his textbook.

The purpose behind the formulation of the kinetics equations is to derive a lumped model that describes the change in the average level of the flux, i.e., the integral of $\phi(\mathbf{r}, E, t)$ over the energy and the spatial domain. For that reason, the neutron flux is factorized in the form $\phi(\mathbf{r}, E, t) = p(t) \cdot \psi(\mathbf{r}, E, t)$. It is noted that flux factorization is not an approximation, in contrast to separation of variables. In the former case, the neutron spatial and energy distributions may still depend on time. However, it is necessary to impose a constraint condition to define precisely the two new functions, $p(t)$ and $\psi(\mathbf{r}, E, t)$, that arise in the factorization procedure:

$$\int_V \int_0^\infty \frac{w(\mathbf{r}, E) \psi(\mathbf{r}, E, t)}{v(E)} dE dV = 1 \quad (2)$$

The constraint condition states that the shape function, $\psi(\mathbf{r}, E, t)$, is normalized, for all t , in such a manner that the integral, Eq. (2), over all energy and space is held constant (normally taken as unity) in time. Prior to integration over space and energy, Eq. (1a) and (1b) is multiplied with a weight function, $w(\mathbf{r}, E)$. Introducing a weight function is not a requirement, but it allows manipulation of the kinetics equations in a way that simplifying assumptions (such as the point kinetics approximation) can be applied more effectively. It is emphasized, that the weight function can be any function that is defined over the same energy and spatial domain as the flux. To preserve generality, the following derivation will not employ a specific weight function.

$p(t)$ is sometimes called the amplitude function and it is defined according to:

$$p(t) = \int_V \int_0^\infty \frac{w(\mathbf{r}, E) \phi(\mathbf{r}, E, t)}{v(E)} dE dV \quad (3)$$

Thus, under the constraint condition given in Eq. (2), $p(t)$ can be represented as in Eq. (3) and hence it is proportional to the total number of neutrons present in the reactor at any time.

Next, Eq. (1a) and (1b) are multiplied with the weight function and the neutron flux is substituted with the factorized functions. The equations are then integrated with respect to space and energy. After some manipulations, we arrive at the conventional point kinetics equations:

$$\frac{dp(t)}{dt} = \frac{\rho(t) - \beta(t)}{\Lambda(t)} p(t) + \sum_k \lambda_k c_k(t) + s(t) \quad (4a)$$

$$\frac{dc_k(t)}{dt} = \frac{\beta_k(t)}{\Lambda(t)} p(t) - \lambda_k c_k(t) \quad (4b)$$

The new quantities, ρ , β , Λ , λ_k , s , and c_k that emerge in Eqs. (4) are the integral quantities identified with the following definitions:

$$\beta(t) = \sum_k \beta_k(t)$$

$$\beta_k(t) = \frac{1}{F(t)} \int \int w \sum_k \mathbf{F}_{dk} \psi dE dV$$

$$\rho(t) = \frac{\int \int w(\mathbf{F}_p - \mathbf{M})\psi dEdV}{F(t)}$$

$$\Lambda(t) = \frac{1}{F(t)} \int \int \frac{w\psi}{v} dEdV$$

$$s(t) = \frac{\int \int wSdEdV}{\int \int \frac{w\psi}{v} dEdV}$$

$$c_k(t) = \frac{\int \int wC_k \chi_{dk} dEdV}{\int \int \frac{w\psi}{v} dEdV}$$

The definition of $F(t)$ is:

$$F(t) = \int \int w(\mathbf{F}_p + \sum_k \mathbf{F}_{dk})\psi dEdV$$

where the delayed neutron production operators \mathbf{F}_{dk} are defined similar to the prompt neutron production operator.

Henry [80], called Eqs. (4) the “conventional kinetics equations”. Today they are usually referred to as the “point kinetics equations” or sometimes the “exact point kinetics equations” in a way to distinguish them from the simplifying assumptions applied in the point kinetics approximation.

Appendix B:

Short Summary of the SAS4A Code

The SAS4A/SASSYS-1 [69] code is an integrated safety analysis computer code for the analysis of reactor plant transients in liquid-metal cooled reactors. The development of the SAS family of computer codes began at Argonne National Laboratory in the middle of the 1960's. The acronym SAS is an abbreviation for the Safety Analysis Section of the Reactor Analysis Division at Argonne. Over the years, SASSYS-1 has been employed extensively in the U.S. liquid metal reactor development programs. It has been the principal tool for the analysis of accidents in the licensing of the Fast Flux Test Facility (FFTF) and the Clinch River Breeder Reactor Plant (CRBRP) and in the passive safety design evaluation of the Integral Fast Reactor (IFR). Traditionally, the SAS code is used to track the initial phase of a core disruptive accident, through coolant heat-up and boiling, fuel element failure, and fuel melting and relocation. The information obtained can then be used to determine whether a noncritical and permanently cooled configuration could be established or whether there is a remote possibility for recriticality, and in that case provide the initial conditions for the disassembly phase.

The SAS4A code is built on a multiple-channel thermal-hydraulics core treatment coupled with a point kinetics neutronics model with reactivity feedbacks. Reactivity feedbacks are calculated from each channel. A channel contains a fuel pin, its associated coolant, and a fraction of the structure of the subassembly casing. Usually a channel represents an average pin within a subassembly or a group of similar subassemblies. The SASSYS-1 core treatment is built on the same models as SAS4A. In addition, SASSYS-1 is combined with detailed thermal-hydraulic models of the primary system and secondary coolant circuits and balance-of-plant steam/water circuit, including pumps, plena, pipes, valves, heat exchangers and steam generators. Models for two-phase coolant thermal-hydraulics, fuel and clad melting and relocation events were developed for sodium-cooled reactors with oxide fuel and stainless steel clad or specialized metallic fuel. Many of these models were validated with experimental test data from the EBR-II, FFTF, and TREAT reactors [88-90]. More recently, the code has been adapted to enable the analysis of heavy liquid-metal cooled reactor designs and accelerator-driven systems. The SAS4A has been coupled to the DIF3D-K [91] and VARIANT-K [92, 93] nodal spatial kinetics codes to provide accurate analysis of coupled spatial kinetics and thermal-hydraulics problems [94].

Bibliography

- 1 R. G. Cochran and N. Tsoulfanidis, *The Nuclear Fuel Cycle: Analysis and Management*, Publ. American Nuclear Society, La Grange Park, IL (1990).
- 2 Statens strålskyddsinstitutets föreskrifter om kontroll vid in- och utförelse av radioaktivt avfall (SSI FS 1995:4).
- 3 EU Directive 92/3/Euratom on the supervision and control of shipments of radioactive waste between Member States and into and out of the Community.
- 4 DOE Order 5820.2 (1984) and replaced by 5820.2A in 1988, both titled "Radioactive Waste Management"
- 5 Miljöbalk (1998:808) 15 kap., 1§.
- 6 Statens strålskyddsinstitutets föreskrifter om hantering av radioaktivt avfall och kärnavfall vid kärntekniska anläggningar - bakgrund och kommentarer (SSI FS 2001:18).
- 7 IAEA Classification of radioactive waste. A safety guide. Safety Series No. 111-G-International Atomic Energy Agency.
- 8 M. D. Lowenthal, "Radioactive-Waste Classification in the United States: History and Current Predicaments," Lawrence Livermore National Laboratory Report, 1997, UCRL-CR-128127.
- 9 Power Reactor Information System (PRIS), Operational & Under construction Reactors by Type as of 21st Oct. 2004.
- 10 K. Fukuda, et al., "IAEA Overview of global spent fuel storage," IAEA-CN-102/60, International Conference on Storage of Spent Fuel from Power Reactors, Vienna, 2-6 June (2003).
- 11 "A European Roadmap for Developing Accelerator Driven Systems (ADS) for Nuclear Waste Incineration", ENEA, April 2001, ISBN 88-8286-008-6.
- 12 H. Bailly, D. Menessier, and Prunier C, *The Nuclear Fuel of Pressurized Water Reactors and Fast Neutron Reactors*, p. 167, Lavoisier Publishing, Paris (1999).
- 13 International Commission on Radiological Protection (ICRP), "Age-dependent dose to members of the public from intake of radionuclides: Part 5 compilation of ingestion and inhalation dose coefficients," *Annals of the ICRP*, Volume 26, Issue 1, Pages 1-91 (1996). Also included in ICRP Publication 72.
- 14 W. G. Sutcliffe, et al., "A Perspective on the Dangers of Plutonium," Lawrence Livermore National Laboratory, Livermore, CA, UCRL-JC-118825 (1995).
- 15 G. Choppin, J. O. Liljenzin, and J. Rydberg, *Radiochemistry and Nuclear Chemistry*, 2nd edition, Butterworth-Heinemann, Oxford, 1995.
- 16 International Commission on Radiological Protection (ICRP), ICRP Publication 60, 1990.
- 17 U.S. National Cancer Institute, "Lifetime Risk of Dying From Cancer, U.S. Total 1999-2001"

- 18 D. S. Myers, "The Biological Hazard and Measurement of Plutonium," Lawrence Livermore National Laboratory, Livermore, CA, UCRL-76571 (1975).
- 19 C. M. Koplik, M. F. Kaplan, and B. Ross, "The safety of repositories for highly radioactive wastes," *Reviews of Modern Physics*, Vol. 54, No. 1, January 1982.
- 20 SR 97 - Deep repository for spent nuclear fuel. SR 97 - Post-closure safety. SKB Technical Report TR-99-06, November 1999.
- 21 B. L. Cohen, "High-level radioactive waste from light-water reactors," *Reviews of Modern Physics*, Vol. 49, No. 1, January 1977.
- 22 A.G. Croff et al., A Preliminary Assessment of Partitioning and Transmutation as a Radioactive Waste Management Concept, ORNL/TM-5808, September 1977.
- 23 A.G. Croff and J.O. Blomeke, Actinide Partitioning-Transmutation Program Final Report. I. Overall Assessment, ORNL-5566, (1980).
- 24 OECD/NEA report, Accelerator-driven Systems (ADS) and Fast Reactors (FR) in Advanced Nuclear Fuel Cycles – A Comparative Study, OECD 2002.
- 25 T. E. Marceau, et al., Hanford Site Historic District: History of the Plutonium Production Facilities, 1943-1990. Columbus: Battelle Press, 2003.
- 26 U.S. Department of Energy, Linking Legacies: Connecting the Cold War Nuclear Weapons Production Processes to Their Environmental Consequences. DOE/EM-0319, Washington, D.C (1997).
- 27 P. Seltborg, "External Source Effects and Neutronics in Accelerator-driven Systems," Licentiate Thesis, Royal Inst. of Technology (2003).
- 28 E. P. Horwitz, W. W. Schulz, "The TRUEX Process: A vital tool for disposal of US defense nuclear waste in New separation chemistry for radioactive waste and other specific applications," *Elsevier Applied Science* (1991) 21-29.
- 29 Innovative Technology Summary Reports, *TRUEX/SREX Demonstration*, Prepared for the U.S. Department of Energy, DOE/EM-0419, OST Reference #347, December 1998.
- 30 D. Serrano-Purroy, et al., "Development of a DIAMEX process using high active concentrate," *Proceedings of the International Workshop on P&T and ADS development 2003*, SCK-CEN Club-House, Belgium, October 6-8, 2003.
- 31 OECD/NEA Status and Assessment Report on Actinide and Fission Product Partitioning and Transmutation, May 1999.
- 32 Y. I. Chang, "The Integral Fast Reactor", *Nucl. Technol.*, 88, 129 (1989).
- 33 A. V. Bychkov, et al., "Pyro-electrochemical reprocessing of irradiated FBR-MOX fuel, III. Experiment on high burn-up fuel for the BOR-60 reactor," *GLOBAL'97* (Proc. Int. Conf. Yokohama, Japan, 1997) pp 912-917 (1997).
- 34 C. E. Stevens, *The EBR-II Fuel Cycle Story*, American Nuclear Society, La Grange Park, Ill. (1987).
- 35 IAEA-TECDOC, Implications of Partitioning and Transmutation in Radioactive Waste Management, in publication (2004).
- 36 W. Bernnat, et al., PWR benchmarks from OECD working party on physics of plutonium recycling, in *Proceedings of the International Conference on Evaluation of Emerging Nuclear Fuel Cycle Systems*, GLOBAL'95, page 627, ANS, Versailles, France, September 11-14, 1995.
- 37 D. Albright and K. Kramer, "Plutonium Watch -- Tracking Civil Plutonium Inventories," Institute for Science and International Security, June 2004

- 38 M. Bunn, S. Fetter, J. P. Holdren, B. van der Zwaan, "The Economics of Reprocessing vs. Direct Disposal of Spent Nuclear Fuel," Project on Managing the Atom, Belfer Center for Science and International Affairs, John F. Kennedy School of Government, Harvard University, December 2003.
- 39 Article by C. G. Lawson and C. Krause, "Nuclear Documenting history: Minutes of the New Piles Committee meetings," Nuclear News, November 2004.
- 40 E. Teller, "Fast Reactors: Maybe," Nuclear News, August 1967.
- 41 M. Cometto, Standardisation des outils de calcul pour les ADS et leur application à différents scénarios de transmutation de déchets, Doctoral theses EPFL Lausanne (2002).
- 42 A. E. Waltar and A. B. Reynolds, Fast Breeder Reactors, Pergamon Press, New York (1981).
- 43 T. Wakabayashi, et al., "Feasibility studies of plutonium and minor actinide burning in fast reactors," Nuclear Technology 118 (1997) 14.
- 44 V. Berthou a, C. Degueldre, J. Magill, "Transmutation characteristics in thermal and fast neutron spectra: application to americium," Journal of Nuclear Materials 320 (2003) 156–162.
- 45 J. Tommasi, M. Delpech, J.-P. Grouiller, and A. Zaetta, Nuclear Technology 111, (1995) 133.
- 46 W. Yang and H. Khalil, "Neutronics design studies of an LBE cooled ATW blanket," IAEA-TECDOC--1356, Proc. of the Technical Committee Meeting on Core Physics and Engineering Aspects of Emerging Nuclear Energy Systems for Energy Generation and Transmutation, Argonne (IL), 28 Nov - 1 Dec. (2000).
- 47 H. Murata and T. Mukaiyama, "Fission reactor studies in view of reactor waste programmes," Atomkernenergie – Kerntechnik, 45 (1984) 23-29.
- 48 W. S. Yang, Y. Kim, R. N. Hill, T. A. Taiwo, H. S. Khalil, "Long-Lived Fission Product Transmutation Studies," Nuclear Science and Engineering, 146, 291-318 (2004).
- 49 J. Magill, H. schwoerer, F. Ewald, J. Galy, R. Schenkel, R. Sauerbrey, "Laser transmutation of iodine-129," Appl. Phys. B 77, 387–390 (2003).
- 50 APT Conceptual Design Report, LANL Report LA-UR-97-1329, April 1997.
- 51 G. R. Keeping, Physics of Nuclear Reactors, p. 99, Addison-Wesley Publishing Co., Reading Massachusetts (1965).
- 52 K. O. Ott and R. J. Neuhold, Introductory Nuclear Reactor Dynamics, American Nuclear Society, LaGrange Park, Illinois, USA (1985).
- 53 K. Tucek, Neutronic and Burnup Studies of Accelerator-driven Systems Dedicated to Nuclear Waste, Ph. D. Thesis, Royal Institute of Technology (2004).
- 54 W. Maschek, et al., "Safety Improvements for ADS Transmuters with dedicated Fuel," Proc. of the AccApp/ADTTA 2001 Meeting, Reno, November 11-15, American Nuclear Society (2001).
- 55 K. Tucek, J. Wallenius, and W. Gudowski, "Coolant void worths in fast breeder reactors and accelerator driven transuranium and minor actinide burners," Annals of Nuclear Energy, accepted for publication (2004).
- 56 J. Wallenius, K. Tucek, and W. Gudowski, "Safety analysis of nitride fuels in cores dedicated to waste transmutation," Proc. 6th Information Exchange Meeting on Actinide and Fission Product Partitioning and Transmutation, Madrid, December 11-13, OECD/NEA (2000).

- 57 H.H. Hummel and D. Okrent, *Reactivity Coefficients in Large Fast Power Reactors*, p. 82, American Nuclear Society (1970).
- 58 R. A. Meyer, B. Wolfe, and N. F. Friedman, "A Parameter Study of Large Fast Reactor Meltdown Accidents," Proc. Conf. on Safety, Fuels, and Core Design in Large Fast Power Reactors, ANL-7120, Argonne Natl. Lab., Oct. 11-14 (1965).
- 59 D. D. Freeman, "SEFOR Experimental Results and Applications to LMFBR's," GEAP-13929, General Electric Co., 1973.
- 60 H. K. Fauske, "Some Comments on Cladding and Early Fuel Relocation in LMFBR Core Disruptive Accidents," *Trans. Amer. Nucl. Soc.*, 21 (1975) 322-323.
- 61 K. Tsujimoto, T. Sasa, K. Nishihara, H. Oigawa, and H. Takano. "Neutronics design for lead-bismuth cooled accelerator-driven system for transmutation of minor actinides," *J. Nucl. Sci. Tech.*, 41:21, 2004.
- 62 D. C. Wade and E. K. Fujita. "Trends Versus Reactor Size of Passive Reactivity Shutdown and Control Performance," *Nucl. Sci. Eng.*, 103:182, 1989.
- 63 Nuclear Regulatory Commission, General Design Criterion 11 - Reactor inherent Protection, Appendix A to Part 50--General Design Criteria for Nuclear Power Plants.
- 64 J. Cahalan, Argonne Natl. Lab, Personal communication (January, 2005).
- 65 NUREG-1368, "Preapplication Safety Evaluation Report for the Power Reactor Innovative Small Module (PRISM) Liquid-Metal Reactor," February 1994.
- 66 H. K. Fauske, "The Role of Core-Disruptive Accidents in Design and Licensing of LMFBRs," *Nuclear Safety*, Vol. 17, No. 5 (1976).
- 67 H. A. Bethe and J. H. Tait, "An Estimate of the Order of Magnitude of the Explosion when the Core of a Fast Reactor Collapses," British Report UKAEA-RHM (56)/113, 1956.
- 68 H. K. Fauske, "Assessment of Accident Energetics in LMFBR Core-Disruptive Accidents," *Nuclear Engineering and Design* 42 (1977) 19-29.
- 69 J. E. Cahalan, A. M. Tentner, and E. E. Morris, "Advanced LMR Safety Analysis Capabilities in the SASSYS-1 and SAS4A Computer Codes," Proc. of the International Topical Meeting on Advanced Reactors Safety, Pittsburgh, April 17-21 (1994)
- 70 Y. S. Tang, R. D. Coffield, and R. A. Markley, Thermal Analysis of Liquid Metal Fast Breeder Reactors, p. 277, American Nuclear Society, LaGrange Park, Illinois (1978).
- 71 A. E. Waltar and A. B. Reynolds, *Fast Breeder Reactors*, p. 260 and 540, Pergamon Press, New York (1981).
- 72 J. L. Séran, et al., "Behavior under Neutron irradiation of the 15-15Ti and EM10 Steels Used as Standard Materials of the Phénix Fuel Subassembly," *Effects of Radiation on Materials: 15th Int. Symposium*, ASTM STP 1125, R. E. Stoller, A. S. Kumar, and D. S. Gelles, Eds., American Society for Testing and Materials, p. 1209-1233, Philadelphia (1992).
- 73 A. Fissolo, "Tensile Properties of Neutron Irradiated 316Ti and 15-15Ti Steels," *Effects of Radiation on Materials: 16th Int. Symposium*, ASTM STP 1175, A. S. Kumar, D. S. Gelles, R. K. Nanstad, and E. A. Little, Eds., American Society for Testing and Materials, p. 646-663, Philadelphia (1993).
- 74 N. S. Cannon, F. R. Huang, and M. L. Hamilton, "Transient and Static Mechanical Properties of D9 Fuel Pin Cladding and Duct Material Irradiated to High Fluence," *Effects of Radiation on Materials: 15th Int. Symposium*, ASTM STP 1125, R. E. Stoller, A. S. Kumar, and D. S. Gelles, Eds., American Society for Testing and Materials, p. 1071-1082, Philadelphia (1992).

- 75 R. J. Puigh and M. L. Hamilton, Influence of Radiation on Materials Properties: 13th Int. Symposium (Part II), ASTM STP 956, F. A. Garner, C. H. Henager, N. Igata, Eds., American Society for Testing Materials, p. 22-29 (1987).
- 76 B. F. Gromov, et al., "The Analysis of Operating Experience of Reactor Installations Using Lead-Bismuth Coolant and Accidents Happened," Proc. Heavy Liquid Metal Coolants in Nuclear Technology, Vol. 1, Obninsk, October 5-9, p. 60-66, State Scientific Center of Russian Federation Institute for Physics and Power Engineering (1998).
- 77 A. Rineiski and W. Maschek, "On Application of Quasistatic and Point-Kinetics Schemes for Subcritical Systems With External Neutron Source," Nuclear Mathematical and Computational Sciences: A Century in Review - A Century Anew, M&C 2003, Gatlinburg, Tennessee, USA, April 6-11 (2003).
- 78 S. Dulla, P. Ravetto, M. M. Rostagno, G. Bianchini, M. Carta, A. D'Angelo, "Some Features of Spatial Neutron Kinetics for Multiplying Systems," 149, 88-100 (2005).
- 79 D. G. Cacuci, "On the Neutron Kinetics and Control of Accelerator-Driven Systems," Nuclear Science and Engineering, 148, 55-66 (2004)
- 80 A. F. Henry, "The Application of Reactor Kinetics to the Analysis of Experiments," Nuclear Science and Engineering, 3, 52-70 (1958).
- 81 E. P. Gyftoploulos, Chapter on "General Reactor Dynamics," in The Technology of Nuclear Reactor Safety, Vol. 1, p. 175-204, T. J. Thomson and J. G. Beckerly, Eds., The MIT Press, Cambridge, Massachusetts, USA (1964).
- 82 J. B. Yasinsky and A. F. Henry, "Some Numerical Experiments Concerning Space-Time Reactor Kinetics Behavior," Nuclear Science and Engineering, 22, 171-181 (1965).
- 83 K. O. Ott and D. A. Meneley "Accuracy of the Quasistatic Treatment of Spatial Reactor Kinetics," Nuclear Science and Engineering, 36, 402-411 (1969).
- 84 J. E. Cahalan, T. Ama, G. Palmiotti, T. A. Taiwo, and W. S. Yang, "Development of a Coupled Dynamics Code with Transport Theory Capability," PHYSOR 2000, Pittsburgh, USA, 7-11 May (2000).
- 85 "Comparison Calculations for an Accelerator-driven Minor Actinide Burner," OECD/NEA Nuclear Science Committee, NEA/NSC/DOC(2001)13, OECD (2002). Benchmark prepared by P. WYDLER and H. TAKANO, NEA/NSC/DOC(99)13, Revised 27 Aug. 1999.
- 86 F. E. Dunn and D.C. Wade, "Estimates of Thermal Fatigue Due to Beam Interruptions for an ALMR-Type ATW," Proc. 2nd International Workshop on Utilisation and Reliability of High Power Proton Accelerators, Aix-en-Provence, November 22-24, NEA/OECD (1999).
- 87 A. F. Henry, Nuclear-Reactor Analysis, p. 300-329, The MIT Press, Cambridge, Massachusetts, USA (1975).
- 88 D. J. Hill, "SASSYS Validation Studies," Proc. of the International Topical Meeting on Safety of Next Generation Power Reactors, Seattle, WA, May 1-5, American Nuclear Society, (1988).
- 89 J. P. Herzog, "SASSYS Validation with the EBR-II Shutdown Heat Removal Tests," Trans. Am. Nucl. Soc., 60, 730, 1989.
- 90 F. E. Dunn, "Validation of Detailed Thermal Hydraulic Models Used for LMR Safety and for Improvement of Technical Specifications," Proc. of the American Nuclear Society International Topical Meeting on Safety of Operating Reactors, Seattle (Bellevue), WA, September 17-20, American Nuclear Society (1995).

- 91 T. A. Taiwo, DIF3D-K: A Nodal Kinetics Code for Solving the Time-Dependent Diffusion Equation in Hexagonal-Z Geometry, ANL/NPR-92/17, Argonne National Laboratory, Reactor Analysis Division, October, 1992.
- 92 G. Palmiotti, E. E. Lewis, and C. B. Carrico, VARIANT: VARIational Anisotropic Nodal Transport for Multidimensional Cartesian and Hexagonal Geometry Calculation, ANL-95/40, Argonne National Laboratory, Reactor Analysis Division, October, 1995.
- 93 A. Rineiski, KIN3D: Module de cinetique spatiale et de perturbations pour TGV2, Note technique SPRC/LEPh 97-203, CEA/Cadarache, May, 1997.
- 94 J. E. Cahalan, et al., "Development of a Coupled Dynamics Code with Transport Theory Capability and Application to Accelerator-Driven Systems Transients," Proc. of the ANS International Topical Meeting on Advances in Reactor Physics and Mathematics and Computation into the Next Millennium, PHYSOR 2000, Pittsburgh, Pennsylvania, May 7-12, 2000.

Paper I

INHERENT SAFETY OF FUELS FOR ACCELERATOR-DRIVEN SYSTEMS

M. ERIKSSON*, J. WALLENUS, M. JOLKKONEN
Royal Institute of Technology (KTH), AlbaNova University Center,
Dep. Nuclear & Reactor Physics, 10691 Stockholm, Sweden.

J. E. CAHALAN
Argonne National Laboratory, Nuclear Engineering Division,
9700 South Cass Ave., IL 60439, USA.

Submitted *Nuclear Technology* (Oct, 2004)

Accepted (Jan, 2005)

Transient safety characteristics of accelerator-driven systems (ADS) using advanced minor actinide fuels have been investigated. Results for a molybdenum-based Ceramic-Metal (CerMet) fuel, a magnesia-based Ceramic-Ceramic (CerCer) fuel, and a zirconium-nitride based fuel are reported. The focus is on the inherent safety aspects of core design. Accident analyses are carried out for the response to unprotected loss-of-flow and accelerator beam-overpower transients, and coolant voiding scenarios. An attempt is made to establish basic design limits for the fuel and cladding. Maximum temperatures during transients are determined and compared with design limits. Reactivity effects associated with coolant void, fuel- and structural-expansion, and cladding relocation are investigated. Design studies encompass variations in lattice pitch and pin diameter. Critical mass studies

are performed. The studies indicate favorable inherent safety features of the CerMet fuel. Major consideration is given to the potential threat of coolant voiding in accelerator-driven design proposals. Results for a transient test case study of a postulated steam generator tube rupture event leading to extensive cooling voiding are presented. The study underlines the importance of a having a low coolant void reactivity value in a lead-bismuth system, despite the high boiling temperature of the coolant. It was found that the power rise following a voiding transient increases dramatically near the critical state. The studies suggest that a reactivity margin of a few dollars in the voided state is sufficient to permit significant reactivity insertions.

I. INTRODUCTION

Accelerator-driven systems (ADS) have been proposed for reducing the long-term hazards of spent nuclear fuel disposition [1,2]. The primary objective is to minimize the inventory of americium and curium that, besides plutonium, are responsible for the majority of the long-term radiotoxicity in nuclear waste. If successful, the technology could enable a reduction of the mass and radioactivity of the spent nuclear fuel by a factor of 100, and reduce the required storage time from $\sim 100\,000$ years to ~ 1000 years.

Studies of ADS neutronics and thermal hydraulics have been accomplished, leading to the selection of LBE as main choice for the coolant [3,4]. Concerning the selection of a suitable fuel material, investigations are made in connection with the joint European research programs [5,6]. While some of the originally suggested fuels did not fulfill basic safety and/or design criteria, three fuels have been selected for detailed examination, namely: two composite oxide fuels and one solid solution nitride fuel. The detailed motivation for

selecting these fuels has been outlined in a recent article [7]. In this paper, attention is directed to their inherent safety characteristics and performance during reactor transient conditions. Various accident events of interest in accelerator-driven systems are considered. Reactivity sources are examined with regard to their influence on reactor safety.

II. INHERENT SAFETY

The term “inherent safety” is in widespread use, particularly in discussions of advanced nuclear reactors. Generally, it is used without further definition and sometimes with inconsistent meaning. In most cases, it is meant to denote an applied design approach or to describe a particular system feature and often to indicate a possible safety advantage. According to the IAEA [8], an inherent safety characteristic is a “fundamental property of a design concept that results from the basic choices in the materials used or in other aspects of the design which assures that a particular potential hazard can not become a safety concern in any way”. The potential hazards include the radioactive materials, decay heat, excess reactivity, high temperatures, high pressures, and energetic

*Email: marcus@neutron.kth.se

chemical reactions. An “inherently safe” reactor would require all these hazards to be eliminated, which is impossible for all practical reactor purposes. Nevertheless, a reactor may possess inherent safety characteristics with respect to a particular eliminated hazard and for specific events. To avoid the potential of being misleading, this does not imply absolute safety for all possible situations.

In the following studies, we seek to investigate the inherent safety characteristics of an ADS with respect to specific accident-initiating events. Inherent safety characteristics associated with reactor transients translates into reactor performance when the protective shutdown devices do not perform their function. Studying this specific class of transients is of considerable importance since they describe the fundamental response of the reactor in the absence of safety system intervention. These so-called “unprotected” transients are potentially of the worst kind. Despite their extremely low probability of occurrence, reactor designs must still be protected against such events to assure the health and safety of the general public. Lessons learned from commercial nuclear power operation and reactor accidents recognize that safety should not rest solely on proper operation of the control and safety systems, or even on ideal performance of plant operators. Every mechanical system, electric power supply, instrumentation system, etc., has a non-vanishing probability of failure, and humans make mistakes. Hence, the reactor should be designed such that there is no undue risk for the environment outside the reactor building even in the hypothetical situation that the shutdown system should fail when needed. That implies that the energy releases, reactivities, pressures, and temperatures for critical reactor elements be kept within safe limits under all conditions.

III. FUEL SELECTION PROCESS

The overall mission of the ADS is to maximize the destruction rate of transuranic elements, primarily americium (Am) and curium (Cm). While plutonium is recyclable in fast reactors and to some extent in commercial light water reactors, the amount of Am that can be charged into a critical reactor is limited by safety concerns. The Doppler feedback coefficient and effective delayed neutron fractions decline when americium is added to the fuel [7] and the reactivity effect associated with loss-of-coolant becomes more positive. The ADS is a nuclear reactor operating in a subcritical mode, which provides for the added safety margin to allow for high concentration of Am. With ADS, transmutation of the minor actinides (Am, Cm, and Np) may be confined to a single process, which will improve the operation of critical reactors and ease the burden on recycling in the overall process. Different fuel cycle strategies could be foreseen. The Japan Atomic Energy Research Institute (JAERI) has proposed the double-strata concept [9], utilizing both commercial light-water reactors and fast reactors for plutonium recycling and energy production and ADS's for MA consumption.

The MA based ADS fuel does not require $^{238}\text{U}/^{232}\text{Th}$ for normal operation, but a certain amount of plutonium is necessary for reactivity management. A support material is needed to reduce the power density, and in some cases,

improve thermal properties. The support material constitutes an “inert matrix” in which the fuel particles are embedded (“inert” in this context refers to an inactive material with a high transparency to neutrons). These fuels are then referred to as “inert matrix fuels”. The inert matrix fuel may be of homogeneous (solid solution) and heterogeneous (composite) type and the fuel may be a Ceramic-Ceramic (CerCer) mixture or a combined Ceramic-Metal (CerMet) mixture. CerCer fuels of interest utilize a metal oxide matrix such as magnesia (MgO), spinel (MgAl_2O_4), and alumina (Al_2O_3). CerMet fuels are attractive because of high thermal conductivity. The refractory metals such as molybdenum, chromium, tungsten, and vanadium are of particular interest because of their high melting point. During a pre-selection phase [3], a number of inert matrices have been considered and examined. Among them, the magnesia (MgO) and molybdenum (^{92}Mo) matrices were singled out as potential materials for use with oxide fuels and these are studied in the some more detail in the current paper. The major reason for this selection is a combination of good thermal properties, acceptable neutronics, and solubility in nitric acid. For a detailed account, see ref. [3,7].

Nitride fuel is an alternative to oxide fuels, yet the knowledge on nitride fuels is limited compared to the extensive experience available on oxide fuel. Nitride fuels offer relatively high thermal conductivity and dissolution rate in nitric acid, which makes it compatible with the PUREX reprocessing technique. The nitride fuels of potential use are of the solid solution type; composite nitride fuels are of little interest. Previous studies [10] have indicated that there are a limited number of inert matrices suitable for nitride fuels. So far, the diluents that have been considered are zirconium nitride (ZrN), hafnium nitride (HfN), and yttrium nitride (YN). At this stage of development, ZrN is the primary choice. HfN has high neutron absorption cross-section, and YN is difficult to handle, as it reacts chemically with air and water. ZrN offers relatively high thermal conductivity and high melting point [11]. It forms a solid solution with plutonium nitride [12], has a stabilizing effect on americium nitride [13] and is itself stable in air. Furthermore, it has a high transparency to neutrons, good chemical compatibility with steel, and is soluble in nitric acid. A disadvantage of the nitride fuel is the need for using nitrogen enriched in ^{15}N [14], in order to minimize the production of radioactive ^{14}C during neutron irradiation [by (n, p) reaction in ^{14}N].

In summary, two oxide fuels, one MgO-CerCer and one Mo-CerMet, and one solid solution ZrN-nitride fuel are examined in this article. The materials are listed in TABLE I.

TABLE I.
Minor actinide fuels investigated in this study.

Fuel*	Composition	Form
$\text{AnO}_{2-x}\text{-MgO}$	Oxide	CerCer
$\text{AnO}_{2-x}\text{Mo}$	Oxide	CerMet
$(\text{An,Zr})\text{N}$	Nitride	Solid solution

*“An” denotes a mixture of actinides (Pu, Am, and Cm). The oxide fuels are hypostoichiometric and the chemical formula is referred to as AnO_{2-x} , where x is the deviation from stoichiometry.

IV. FUEL MATERIAL PROPERTIES

Material property data for the minor actinide fuels is limited, particularly at high temperature. Thermophysical properties of minor actinide oxide fuel [15] and nitride fuel [16] were recently reviewed by Thetford and Mignanelli. We have applied their recommendations with minor modification. It is assumed that the correlations depend on temperature, matrix fraction, and porosity. In the case of oxide fuels, the influence of stoichiometry is considered. These are the most important variables. While other parameters also have an effect, these are not reliably established yet. Correlations are based on unirradiated properties (see section IV.B for discussion on irradiation effects). Selected physical properties are presented in TABLE II. Material properties for standard MOX-fuel are included for reference purposes. The values are given at 1000°C and for the fully dense and fresh material. Fuel and matrix proportions correspond to an average fuel pin in the core, as explained later. The fuels contain 40% plutonium, 50% americium, and 10% curium. A more detailed account on this composition is given in later sections. It is seen that the CerCer has considerably lower thermal conductivity, lower density, and much higher specific heat than the nitride and CerMet fuels. It also has a higher coefficient of thermal expansion, which tends to increase the negative reactivity feedback associated with fuel expansion, but may also increase the risk for fuel-cladding mechanical interaction, thermal stresses, and cracking.

TABLE II.
Selected fuel material properties at 1000°C.

Fuel	Properties at 1000°C (100% TD)			α^* 1e+6/K
	ρ g/cm ³	k W/mK	c_p kJ/kgK	
CerCer ^a	6.6	4.7	0.90	14.0
CerMet ^b	10.6	51.2	0.33	9.2
Nitride ^c	9.3	17.0	0.43	9.0
MOX ^d	10.7	2.8	0.33	12.1

*Mean linear coefficient of thermal expansion (300 to 2100 K).

^a0.42(Pu_{0.4},Am_{0.5},Cm_{0.1})O_{1.9}+0.58MgO

^b0.51(Pu_{0.4},Am_{0.5},Cm_{0.1})O_{1.9}+0.49Mo

^c(Pu_{0.13},Am_{0.17},Cm_{0.03},Zr_{0.67})N

^dStandard MOX, U_{0.8}Pu_{0.2}, 95% TD, O/M=2.0.

IV.A. Effect of diluent and porosity

The effect of the diluent on the material properties is approximated using Vegard's law, i.e., sum of the properties of the fissile fuel and diluent phases weighted by their respective atomic fractions. This is a rather crude approximation, but one which we need to accept in the absence of experimental data. Consequently, the fuel thermal conductivity becomes a linear and increasing function of the matrix content. The effect of fuel porosity on the thermal conductivity is modeled with the classical Maxwell-Eucken formula. For oxides and nitrides a pore shape factor of $\beta=2$ has been recommended and is used in our analyses. However, it is noted that the pore geometry depends on the fabrication process and different correction models are in use. The CerCer fuel has a bulk density of 95% of the theoretical value. Hence, the correction factor for the thermal conductivity is 0.86. For the CerMet fuel, the as-fabricated porosity of the

oxide inclusions has a limited effect on the overall conductivity since it is mainly determined by the metallic component, which is fully dense. The porosity has a significant effect on the conductivity of the low-density nitride fuel. The effective thermal conductivity of the nitride fuel is reduced to 65% of the fully dense material. Fig 1 shows the effective thermal conductivity of the investigated fuels as function of temperature. Values are given for the porous material. The CerMet fuel has excellent thermal conductivity. The thermal conductivity of the nitride fuel is quite high, about 4-6 times higher than classical MOX-fuel in the typical reactor operating temperature range. The CerCer fuel has the lowest thermal conductivity of the fuels, however, it is still higher than the standard MOX-fuel (between 1.5 to 3 times higher). The thermal conductivity of the CerCer fuel has a minimum around 1500 K.

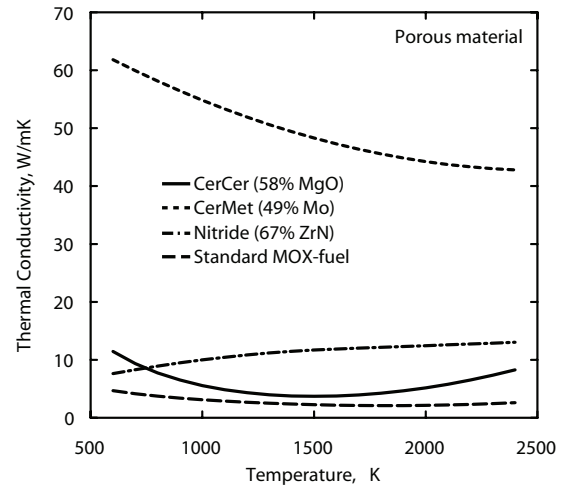


Fig. 1. Effective thermal conductivity of the examined fuels.

IV.B. Effect of irradiation

Fuel properties change during irradiation as a result of restructuring, cracking, chemical redistribution, and introduction of fission products. Such differences play an important role in establishing safety margins as function of temperature and burnup history – both for steady-state operation and during thermal upset conditions. Restructuring (grain growth and pore migration) affects thermal conductivity, void formation, density, volumetric heat generation levels, and hence operating temperatures. An analysis of all the governing processes is beyond the scope of this article. Suffice it to say that restructuring and development of thermal stresses (cracking) depend strongly upon thermal gradients and operating temperatures and is usually small for high-thermal conductivity fuels [17], which suggest limited thermal restructuring for the CerMet and nitride fuels, whereas significant changes may occur in the CerCer fuel. Cracking is further aggravated by a high coefficient of thermal expansion, which suggests more severe cracking for the CerCer fuel. For oxide fuel, decrease in the thermal conductivity due to the introduction of fission products is small in comparison with the larger effects of restructuring. The development of a central void in typical fast reactor mixed-oxide fuel and densification of the restructured regions tend to reduce the maximum fuel

temperature with irradiation time even though the local linear power is constant [18]. Yet, very little in-pile data is available upon which to judge the irradiation behavior for the minor actinide dispersal fuels. Studies have been performed on a $\text{UO}_2+64\%\text{Mo}$ composite fuel irradiated to a burnup of 5 atom% [19]. Post-irradiation examination revealed little or no signs of restructuring, which indicates that molybdenum is a potentially stable matrix material. The reduction of the thermal conductivity with burnup is probably larger for the CerMet fuel because of higher fission gas retention and less pore migration, but it is expected that the net effect of irradiation is to reduce maximum fuel temperatures because of fuel-cladding gap closure early in life. We presume that such a displacement of the fuel surface act to reduce centre line temperatures in the nitride case too, but to a lesser extent as compared to the CerMet fuel. Fission gas (xenon and krypton) mixture effects on the fill gas (helium) conductivity are largely offset by reduced fuel-cladding gap thickness and higher gas pressure. Although restructuring and swelling phenomena may improve fuel thermal performance, for reasons explained above, it is possible that higher burnup negatively affects fuel melting temperatures, fuel-pin mechanical performance as well as power peaking factors. It is apparent that an assessment of the variation of safety margins (power-to-melt, thermo-mechanical limits, etc.) as function of irradiation time would require examination of a wide range of phenomena, each suffering from large uncertainties and, consequently, we find it speculative to extract such limits at this stage.

V. DESIGN LIMITS

We attempt to establish design limits for the fuel and cladding. The fuel failure limit is prescribed by accident conditions and has little constraints on normal operation, whereas the cladding failure limits are defined for steady-state and transient conditions. It should be noted that the design studies are yet in a pre-conceptual stage and it is not meant to imply that the indicated limits are complete. The objective at this point is to describe the analysis methodology involved and to provide a framework for guiding further design work, not to spell out elaborate details on the design criteria or particular failure processes. Inevitably, there are many uncertainties regarding potential failure mechanisms (e.g. mechanical and chemical interactions between fuel components, fission products, and cladding constituents), and, as discussed in Chapter IV.B, further research is required to establish reliable design limits based on in-pile experimental data.

To this end, we have selected Si-modified 15-15Ti austenitic stainless steel as reference cladding material. This class of alloy has demonstrated favourable performance up to 150 dpa [20] and has good high temperature mechanical properties [21].

V.A. Oxide melting

Complications arise in describing the melting behavior of the present oxide fuels. Due to a low solid solubility of the oxide fuel particles in the diluents (MgO and Mo), the two constituents will melt at different temperatures. In addition, eutectic melting may appear at temperatures below the

melting points of the individual materials. The melting point of the mixed actinide oxide, $\text{AnO}_{1.9}$, is estimated to 2640 K, based on the melting points of PuO_{2-x} [22], AmO_{2-x} and CmO_{2-x} [23], and applying Vegard's law. We have assumed a melting point dependence on the oxygen content similar to the recommendations for $(\text{U,Pu})\text{O}_{2-x}$ [24]. It appears that no eutectic reaction occurs between molybdenum and UO_2 [25] If a similar behavior is assumed for $\text{AnO}_{1.9}\text{-Mo}$, then the first sign of melting will occur in the oxide phase (the melting point of pure Mo is 2900 K). The oxygen content may affect the potential for eutectic formation and oxidization of Mo into MoO_2 , however, these effects are not sufficiently known to be taken into account. For the CerCer fuel, complication arises due to the possibility for eutectic reaction below the melting points of AnO_2 and pure MgO ($T_m=3100$ K). Laboratory measurements [26] found no eutectic reaction up to ~ 1923 K, while theoretical calculations [27] predicted that an eutectic may start to form at temperatures as low as 1930 K for low oxygen contents. The same study also estimated that the melting point stabilizes around 2300 K for oxygen-to-metal ratios above 1.62. Keeping low oxygen content, however, is desirable because it reduces corrosion of the cladding. The melting point of $\text{PuO}_{2-x}\text{-MgO}$ [28] ranges from 2341 to 2503 K when the oxygen content changes from 1.61 to 2. Following these results, we estimate the failure limit of the $\text{AnO}_{1.9}\text{-MgO}$ fuel somewhere in the range 2200-2300 K.

V.B. Nitride dissociation

The main concern about nitrides is the dissociation of AmN into metal and nitrogen gas at temperatures around 1600 K [29], which is too low to meet safety requirements under overpower conditions. To investigate this problem, thermo-chemical modeling has been performed on minor actinide nitride compounds in various environments. In this study, an updated version of the ALCHYMY database [30] for Thermo-Calc [31] was used to model the dissociation of AmN in $(\text{Pu}_{0.2}\text{Am}_{0.3}\text{Zr}_{0.5})\text{N}$ heated in a constant-volume system mimicking the dimensions and materials proportions of an actual fuel pin with and without a stabilising addition of 1% N_2 to the filling gas. The assumed pin pressure is that of the bonding gas at the corresponding temperature plus 1.5 times that of americium vapour ($\text{AmN} \rightarrow \text{Am(g)} + 0.5 \text{N}_2$). Up to 2400 K, the contribution from dissociation of PuN is smaller by three orders of magnitude and can be ignored. In the same range, the increase in pressure arising from AmN dissociation is only a few percent of the total pressure and should not be an issue from a purely mechanical point of view. The depletion of Am from the fuel is in itself very small during uniform heating, below 0.01% even in pure helium. Based on these results, we estimate the failure point for the nitride fuel at 2400 K. This failure criteria should be considered applicable only during rapid overpower excursion. For slow transients, one may expect transport effects, with nitride continuously dissociating in hot zones and reforming on colder surfaces, if the overheating would persist for longer time. As the model contains several other simplifications (congruent vaporisation of AmN at stoichiometric composition, ideal solid solution of nitrides) and considering that thermodynamical parameters for AmN are based on

some reasonable but unverified assumptions [32], the results must not be interpreted too literally.

V.C. Cladding transient burst limit

Thermal limits relevant for cladding during thermal upset conditions were established based on transient burst test data. These tests, called Fuel Cladding Transient Test (FCIT), duplicate reactor transient conditions in which the cladding (irradiated or unirradiated) is heated (out-of-pile) until failure occurs. The failure temperature is recorded as function of hoop stress and often related to a particular thermal ramp rate. The FCIT tests are typically carried out for relatively fast ramp rates, in the range 0.5-100 K/s. In our estimates, we have assumed an internal pin pressure of 14 MPa (equivalent to a membrane stress of 100 MPa) and a thermal ramp rate of 5 K/s. This thermal ramp rate was selected because it is similar to the heating rates involved in loss-of-flow conditions. Temperature limits for 15-15Ti are estimated using data for unirradiated D9 pin cladding [33]. The D9 alloy is a titanium modified 316 austenitic stainless steel, which has similar composition as 15-15Ti steel. Tension tests [21] show that the mechanical properties of irradiated 15-15Ti is better than Ti-stabilized 316, indicating that transient/mechanical properties should be no worse than for D9. The failure temperature of irradiated cladding specimens is comparable to the unirradiated cladding [34], as the fuel adjacency effect (FAE) [35] may be negligible in the actual fuel pin environment [36]. Based on these studies, we estimate a failure temperature for 15-15Ti cladding equal to 1330 K.

V.D. Cladding creep rupture limit

For long-term operation, nominal temperatures are limited by thermo-mechanical creep rates. Stress rupture data is scarce for 15-15Ti steels. However, a reasonable amount of data is available for D9. The better tensile properties of 15-15Ti suggest that the thermal creep performance of CW 15-15Ti could be comparable or better than D9. Ongoing studies show that silicon modified CW 15-15Ti stainless steel possesses even better tensile properties, indicating that further improvement might be possible. Tests conducted on 20% CW D9 cladding [37], showed that the in-pile rupture lifetime is lower compared to out-of-pile data, indicating that the pin cladding might fail sooner than predictions based on out-of-core test results. The maximum operating temperature for the CW 15-15Ti cladding, with respect to thermal creep, was estimated to be 920 K (maximum midwall temperature). This limit was determined for a constant plenum pressure loading of 10 MPa (equivalent to a hoop stress of 74 MPa) and an expected in-pile service of 3 years (exposure time 30,000 h).

V.E. Cladding corrosion limit

Corrosive attack by the coolant imposes additional constraints. The effect of LBE corrosion is manifest as wall thinning, as structural material dissolves in the coolant, and higher stresses, which altogether leads to reduced cladding lifetime. The corrosion rate shows a strong dependence on temperature and some correlation with fluid velocity. It has been demonstrated that, for non-protected stainless steels, nominal temperatures must not exceed 670 K for austenitic steels and 720 K for ferritic steels [38]. In an oxygen-controlled environment, however, a protective oxide film may

form on the surface of the structure, which may slow down the dissolution rate. The protective film is formed by oxidation reactions between the oxygen dissolved in the coolant and steel alloy elements (Fe, Cr, Si, and others with high affinity to O₂). Using this technique, operating temperature can be raised by 150-200 degrees. In Russia, where most corrosion studies with Pb/Bi have been carried out, the results indicate that the ferritic/martensitic steels offer the best performance. This appears to be due to the low nickel content of the ferritic steels compared to the austenitic steels [38]. Nickel shows high solubility in Pb/Bi alloy, which has an impairing effect on the stability of the oxide film and increases the corrosion rate. At this stage of development, long-term operation ($\geq 30,000$ hours) at temperatures above 890 K appears to be difficult [38], even for the most promising corrosion resistant steel, i.e., Russian type silicon-alloyed ferritic-martensitic steel (EP823). With reference to austenitic 15-15Ti steels, we assume that the operating clad temperature is to be kept below 840 K (surface temperature). TABLE III summarizes the current estimates of the design limits for the investigated fuels and cladding materials. It is cautioned that these limits are preliminary estimates and may change in the light of further testing.

TABLE III.
Summary of thermal limits for fuel and cladding.

Component	Failure temp. (K)	Failure mechanism
Fuel		
CerCer	2200-2300	Eutectic melt
CerMet	2640	Oxide melting
Nitride	2400	AmN dissociation
Cladding (type 15-15Ti)		
Surface (steady-state)	840	Corrosive thinning
Midwall (steady-state)	920	Creep rupture
Midwall (transient)	1330	Mech. burst limit

VI. COMPUTATIONAL METHODS

The continuous energy Monte Carlo code MCNP4C [39] together with the JEF2.2 nuclear data library is used for neutronic calculations. A three-dimensional pin-by-pin model is employed. The MCNP code is used to calculate neutronics input data required for transient modeling (kinetics parameters, reactivity coefficients, power distributions, and gamma heating).

The SAS4A/SASSYS-1 computer code [40] is used for thermal- and hydraulic calculations at steady-state and transient conditions. The SASSYS-1 code is an integrated safety analysis computer code for the analysis of reactor plant transients in liquid-metal cooled reactors. A detailed description of the SAS code is outside the scope of this paper. The code has been adapted to enable the analysis of heavy liquid-metal cooled reactor designs and accelerator-driven systems. The calculational model used in this study employs two thermal-hydraulic channels. One channel represents an average pin within the core and a second channel represents the hottest pin in the core (with a power peaking factor of 1.3). The primary system includes models of the core, primary pumps, shell side of the steam generators, connecting piping,

and compressible pool volumes with cover-gas surfaces. The fuel-cladding gap conductance model accounts for gas conduction, radiative heat-transfer, surface roughness, and differential thermal expansion of fuel and cladding during transient conditions. Reactivity feedbacks are calculated for coolant expansion, fuel elongation, radial core expansion, and Doppler effect. Changes in power level are computed with point kinetics theory. The performance of the point kinetics approximation for transient analysis of ADS's was considered in a previous assessment [41] and found adequate for similar problems.

VII. CORE MODEL

A reference core was constructed largely based on previous parametric studies. The core model pertains to a LBE-cooled accelerator-driven system with a thermal rating of 800 MW. The core consists of a central lead-bismuth spallation target surrounded by a fuel region. The active core is 1 m high with a diameter of 1.6 to 2.2 m, depending on the core configuration. The core is surrounded by axial and radial reflectors 0.5 m thick. The reflectors consist of subassemblies filled with coolant and empty cladding tubes. The pitch-to-diameter (P/D) ratio and the pin diameter are design parameters. The reference configuration uses a P/D equal 1.50 and a pin diameter of 5.72 mm. In a second configuration, the P/D value is increased to 1.75 by changing the pin pitch. In a third modification, the pin diameter is increased to 6.8 mm while holding the P/D ratio at 1.50. In all the cases the flat-to-flat distance is fixed while the number pins per subassembly is either 91 or 127. A summary of design parameters is given in TABLE IV.

TABLE IV.
Core lattice configurations

SA pitch	10.2 cm
FTF outer	10.0 cm
FTF inner	9.6 cm
P/D	1.50/1.75
Pins per SA (1.50/1.75)	127/91
Volume fractions	27/16/52 % (P/D=1.50)
(fuel/steel/coolant)	19/14/63 % (P/D=1.75)
Cladding o.d.	5.7/6.8
Cladding i.d.	5.0/6.0
Active core height	1.0 m
Core diameter	~1.6-2.2 m
Spallation target diameter	0.4 m
Gas plenum height	1.50 m

The core is partitioned into three regions of different matrix fractions. The purpose is to level out the radial power distribution. Matrix fractions are adjusted to obtain an initial k_{eff} equal 0.97 and a radial peak-to-average power ratio factor of 1.3. Matrix contents drop towards the edges, as shown in TABLE V. The poorer neutron economy of the oxides result in matrix contents lower compared to the nitride, which has an adverse effect on the fuel performance. A high volume fraction of diluents is favorable from the viewpoint of thermal performance, stability, and fuel fabrication. Increasing the P/D ratio requires lower concentration of diluents while increasing the pin diameter enables a slightly larger fraction of

matrix to be used. The plutonium fraction is fixed at 40%, which is similar to the initial Pu loading in the double-strata cycle studied by JAERI. It was shown that this plutonium content provides minimal burnup reactivity swing over a large number of irradiation cycles [42]. The fuel has total americium content of 50% and 10% curium. Neptunium is not considered because it is not an important contributor to the long-term radiotoxicity. The americium vector consists of two thirds ^{241}Am and one third of ^{243}Am . Curium is composed of 87% ^{244}Cm and 13% ^{245}Cm . The isotopic vector of plutonium (5% ^{238}Pu , 38% ^{239}Pu , 30% ^{240}Pu , 13% ^{241}Pu , and 14% ^{242}Pu) corresponds to discharged MOX fuel from LWRs after 7 years cooling. The isotopic composition of americium and curium derives from a mixture of spent UOX and MOX fuel. Burnup reactivity losses are compensated by increasing the proton beam current by a factor of 1.5 at end-of-life. Delayed neutron parameters and prompt neutron generation times are shown in TABLE VI. Clearly, there is a large difference between the effective delayed neutron fraction (β_{eff}) and the actual delayed neutron fraction (β). The β_{eff} is around 180 pcm, while the corresponding β value is in the range of 230-280 pcm. The reason for this variation is that delayed neutrons are emitted with much smaller average energy (~ 0.5 MeV) and thus with lower chance of causing fission in the even neutron numbered nuclei (^{241}Am , ^{243}Am , ^{240}Pu , and ^{242}Pu) than prompt neutrons. The prompt neutron generation time (Λ) varies between 0.5-0.8 μs and increases for higher P/D.

TABLE V.
Inert matrix volume fractions.

Fuel	D_{clad}	P/D	Zone 1	Zone 2	Zone 3
CerCer	5.7	1.50	0.65	0.58	0.42
	5.7	1.75	0.56	0.51	0.41
	6.8	1.50	0.68	0.62	0.52
CerMet	5.7	1.50	0.54	0.48	0.37
	5.7	1.75	0.47	0.41	0.31
Nitride	6.8	1.50	0.60	0.54	0.45
	5.7	1.50	0.73	0.67	0.54
	5.7	1.75	0.66	0.61	0.50
	6.8	1.50	0.76	0.71	0.60

TABLE VI.
Delayed neutron fractions (β and β_{eff}) and neutron generation times (Λ).

Fuel	D_{clad}	P/D	β (pcm)	β_{eff} (pcm)	Λ (μs)
CerCer	5.7	1.50	250	180	0.65
	5.7	1.75	250	190	0.81
	6.8	1.50	250	190	0.76
CerMet	5.7	1.50	240	170	0.50
	5.7	1.75	230	180	0.67
	6.8	1.50	270	190	0.60
Nitride	5.7	1.50	280	180	0.55
	5.7	1.75	240	180	0.71
	6.8	1.50	260	170	0.67

Additional fuel pin specifications are given in TABLE VII. Because of lower thermal conductivity, the CerCer fuel is required to operate at lower linear powers; 25 kW/m compared to 35 kW/m for the CerMet and the nitride fuel.

The initial gap thickness is chosen so that direct solid-to-solid contact is prevented during transients (assuming unirradiated geometry). As oxide fuels have a high plasticity and low swelling characteristics, pellet cladding mechanical interactions (PCMI) are less acute, and hence a rather small pre-fabricated porosity is sufficient. In the case of the nitride and the CerMet, PCMI cannot be tolerated, and hence a larger porosity of the nitride and a larger fuel-cladding gap of the CerMet have been adopted. The smear density for the CerCer, CerMet, and the nitride fuels are 91%, 88%, and 82%, respectively.

TABLE VII.

Fuel pin description (at operating condition).

Fuel	CerCer	CerMet	Nitride
Average linear power, kW/m	25	35	35
Smear density (%)	91	88	82
Fuel-clad gap width, μm	50	100	50

VII.A. Temperature profile

The temperature distribution in structural components and fuel elements depend on the surface heat transfer conditions. Following recommendations by the IPPE (Obninsk), the heat-transfer coefficient between element and lead-bismuth coolant is determined using the following Lyon-Martinelli correlation [43]:

$$Nu = 5 + 0.025Pe^{0.8}$$

In Fig. 2, the steady-state temperature profile in the fuel rod is shown. The plot reproduces the profile for the hottest pin at core midplane and for the configuration using a pin diameter of 5.7 mm. Because of the low thermal conductivity, the CerCer fuel suffers from a steep temperature gradient (more than 300 K/mm). Despite that the CerCer fuel is operating with a lower specific power, it is the hottest of the three fuels. The CerMet fuel remains relatively cold, reaching a maximum temperature of 1690 K. The margin to melting is 950 K. The larger gap size for the CerMet eliminates some of the advantage of its high conductivity. Use of a liquid-metal bonding material could reduce fuel surface temperatures further, but at the risk of introducing additional problems, e.g., compatibility issues with fuel and cladding, bond vaporization, practical problems associated with manufacturing and reprocessing. Considering the small temperature gradient in the CerMet fuel (approaching 50 K/mm) suggests lower tendency for thermal restructuring and cracking, and the relatively low operating temperature implies lower fission gas release rates. Peak fuel and cladding temperatures as function of P/D and pin diameter are tabulated in TABLE VIII. It is seen that the reference case, with a tight pin lattice and thin pin diameter, is not consistent with a permissible cladding surface temperature of 840 K as dictated by long-term cladding corrosion damage. Cladding temperatures reported in TABLE VIII refer to the cladding midpoint. The surface temperature, which is of interest for the corrosion rate, is approximately 10-20 degrees lower. Maximum cladding temperatures occur at the outlet where coolant temperatures are highest. To maintain the cladding temperature within the given limit, a higher coolant mass flow rate is desirable. This may be achieved by increasing the P/D ratio. The reason the steady-state temperatures are lower for

the cases with larger pin diameter is twofold: coolant temperatures are lower because the coolant flow area is larger and the thermal conductivity of the fuel is better because matrix fractions are generally higher.

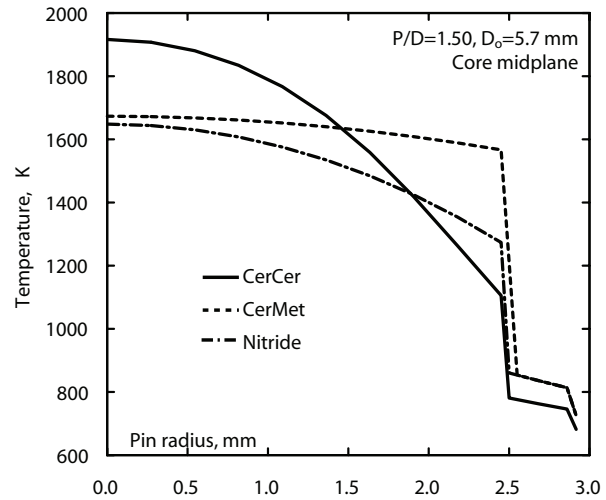


Fig. 2 Steady-state temperature profile at core midplane.

TABLE VIII.

Peak fuel and cladding (midpoint) temperatures in the hottest channel at normal operating conditions.

Fuel	P/D=1.50, D _o =5.7 mm		P/D=1.75, D _o =5.7 mm		P/D=1.50, D _o =6.8 mm	
	Fuel	Clad	Fuel	Clad	Fuel	Clad
CerCer	1920	840	1920	770	1740	770
CerMet	1690	940	1690	840	1530	850
Nitride	1660	940	1650	840	1540	850

VIII. REACTOR PLANT SYSTEM

TABLE IX contains major specifications of the lead-bismuth cooled ADS plant. The primary system is of pool type design. Due to high corrosion activity, coolant temperatures and velocities are limited. The coolant flow velocity in the pin bundle is limited to 2.5 m/s and the reactor inlet temperature is set at 573 K. LBE is chemically inert with water/steam. Hence, a two-circuit system is utilized, with the steam generator located in the primary system, which simplifies the overall plant design and reduces the cost. The primary system includes four centrifugal pumps (two for each loop) and four steam generators (two for each loop). Based on a seismic analysis, as discussed in the next section, a vessel height of 10 m is selected. The elevation difference between the core midplane and the thermal center of the steam generators should be as large as possible to increase natural circulation contribution. To allow room for cover gas and bottom support, however, the separation distance is limited to 5.5 m. The pump design includes flywheels to prolong the coast-down time in the event of a loss-of-flow accident. The size of the flywheel was optimized to provide a smooth transition to natural circulation. A pump inertia (pump, motor, and flywheel) equal to 400 kg m² was found appropriate. As a

comparison, the FFTF reactor, which is a sodium-cooled 400 MWth reactor, had a primary pump inertia of 700 kg m² [44].

VIII.A. Seismic analysis

A tall vessel is desirable to promote natural circulation. On the other hand, a large vessel increases the cost and decreases seismic stability. The vessel thickness increases with the vessel size and weight of the contained liquid. According to one report [45], wall thickness for type 316SS is limited to 130 mm by manufacturing capability. Thus, to ensure acceptable stress levels under a seismic event, it is necessary to limit the size of the vessel. A rough estimate of the allowable vessel height was calculated based on a seismic model suggested by Buongiorno [46]. We assume that the vessel has an outer diameter of 6 m and contains lead-bismuth with an average density of 10.2 g/cm³. The vessel is made of grade 316 stainless steel with a steady-state operating temperature of 693 K. Following Buongiorno's example, the vessel is subject to an earthquake with a peak ground acceleration of 0.5g (horizontal motion). This criterion is adequate for licensing purposes of most sites in the U.S. The calculated peak stress intensity is compared with limits specified by the ASME code for 316SS. The analysis suggests an allowable vessel height in the range 10-12 m. It should be noted that this estimate is based on a tentative maximum wall thickness of 130 mm for a vessel made of 316SS, as compared to thicknesses around 200-250 mm for PWR systems (utilizing carbon steels). It is found that, a wall thickness of 250 mm should admit a vessel height around 15-16 m, which indicates a rather high sensitivity of the stress level on the vessel height. The dependence on the vessel diameter is not strong, however. The study also depends on seismic load conditions, which are site dependent. Use of bottom horizontal structure support and/or base isolation could enhance seismic performance. The effect of seismic isolation is a reduction of the natural frequency of the structure, which may lead to significant reduction of building accelerations in an earthquake. This was recently shown in the application to an ADS plant [47].

TABLE IX.
Plant specification

General	
Type of plant	Pool type
Reactor power	800 MWth
Coolant	LBE (44.5%Pb+55.5%Bi)
Reactor inlet temperature	573 K
Coolant inlet velocity	2.5 m/s
Reactor vessel	
Height	10 m
Diameter	6 m
Wall thickness	13 cm
Weight (incl. coolant)	~2500 ton
Primary system	
Steam generators	4 (integrated)
No. of pumps	4
Pump mass of inertia	400 kg·m ²
Distance between thermal centers of core and SG's	5.5 m

VIII.B. Thermal- and hydraulics analysis

Plant thermal-hydraulics data are presented in TABLE X. Because of different linear power ratings, the exit temperature for the CerCer core is lower than the CerMet and nitride cores. It is noted that the coolant mass flow rate is higher and the exit temperatures are lower for the configurations using a pin diameter of 6.8 mm, which is a geometrical effect of maintaining a constant P/D ratio while the pin diameter is increased. Friction factors for the calculation of the pressure drop in the rod bundle are determined from the Blasius relation for turbulent flow:

$$f = 0.316 \text{Re}^{-0.25}$$

The pressure drop through the core depends on the pitch-to-diameter ratio and on the cladding diameter. It is found that for P/D=1.50 it accounts for 90% of the total system pressure loss at normal forced flow operation; at P/D=1.75 it is responsible for about 60% of the pressure loss.

TABLE X
Thermal-hydraulics data during steady-state.

Fuel	D_{clad}	P/D	CerCer	CerMet	Nitride
Coolant exit temp. (K)	5.7	1.50	740	810	810
	5.7	1.75	680	720	720
	6.8	1.50	690	740	740
Hot channel exit temp. (K)	5.7	1.50	790	880	880
	5.7	1.75	710	760	760
	6.8	1.50	730	790	790
Mass flow rate (kg/s)	5.7	1.50	0.96	0.96	0.96
	5.7	1.75	1.61	1.61	1.61
	6.8	1.50	1.33	1.33	1.33
SA friction, Δp (Pa)	5.7	1.50	$2.8 \cdot 10^5$	$2.8 \cdot 10^5$	$2.8 \cdot 10^5$
	5.7	1.75	$1.6 \cdot 10^5$	$1.6 \cdot 10^5$	$1.6 \cdot 10^5$
	6.8	1.50	$2.4 \cdot 10^5$	$2.4 \cdot 10^5$	$2.4 \cdot 10^5$
Primary loop, Δp (Pa)	5.7	1.50	$3.1 \cdot 10^5$	$3.1 \cdot 10^5$	$3.1 \cdot 10^5$
	5.7	1.75	$2.5 \cdot 10^5$	$2.5 \cdot 10^5$	$2.5 \cdot 10^5$
	6.8	1.50	$3.0 \cdot 10^5$	$3.0 \cdot 10^5$	$3.0 \cdot 10^5$

IX. REACTIVITY SOURCES

Identification of potential reactivity sources is an important element influencing the inherent safety characteristics of the reactor. These sources may come into play because of temperature changes during normal operation or as a result of displacement of core materials under accident conditions. Because of the built-in subcritical margin, reactivity feedbacks involving only temperature changes have a limited role in ADS's [48]. We have chosen to include them in the discussion for completeness.

IX.A. Temperature coefficients

The main reactivity feedback mechanisms and their numerical values are shown in TABLE XI. These coefficients are whole core values and reflect the effect of changes in temperature about the normal operating point. The reactivity coefficients are calculated through two successive eigenvalue calculations, one for the initial state, and one for a perturbed state (involving a certain change in density, temperature, or geometric configuration around the operating point). The coefficient for thermal expansion of the associated material (fuel, coolant, steel) is used to define the appropriate relationship with the temperature coefficient of reactivity. The radial expansion reactivity is calculated by expanding the core grid in the horizontal direction. The fuel expansion reactivity effect is determined based on elongation of the fuel column; any contact between the fuel and the cladding is ignored. It is seen that the coolant density coefficient is somewhat stronger in the CerCer core than in the CerMet and nitride cases. Literature values for the typical sodium-cooled and MOX-fueled fast breeder reactor (FBR) are included for comparison. It is noteworthy that the positive reactivity effect due to sodium expansion in the FBR is about twice the LBE-expansion coefficient in the investigated cores. The Doppler coefficient is around 0.05 pcm/K for the studies cores, which is an order of magnitude smaller than in the FBR. The integrated effect (up to fuel failure) due to Doppler feedback is in the range -0.2 - 0.3% , which is unimportant for transients in ADS's. Reactivity feedback due to axial expansion is

approximately 5 times the Doppler coefficient, but usually it has a small effect. It may be compared with subcriticality levels around 16-18 dollars for the examined cores. All cores feature a net negative temperature coefficient, assuming isothermal heatup. Radial core expansion is by far the most important feedback effect in this respect. However, radial core expansion effect is determined by temperature changes of the grid support structure and heating of the duct walls at the above-core load pads, so the overall effect depends on the heating rate and local temperature distribution.

TABLE XI.

Whole-core temperature reactivity coefficients for reference core P/D=1.5, D=5.7 mm (as calculated around the operating point).

Reactivity coefficients	$\Delta k / \Delta T \cdot 10^5$ (pcm)			
	CerCer	CerMet	Nitride	FBR
Coolant expansion	+0.43	+0.32	+0.35	+0.80 ^a
Axial fuel expansion	-0.28	-0.18	-0.25	-0.18 ^b
Radial core expansion	-0.94	-0.97	-1.01	-1.10 ^a
Doppler effect	-0.05	-0.05	-0.05	-0.40 ^a
Net (isothermal heatup)	-0.84	-0.88	-0.96	-0.88

^aSuper-Phénix, sodium cooled, UO₂-PuO₂ fuel.

^bFFTF, sodium cooled, UO₂-PuO₂ fuel.

IX.B. Coolant void

Considerable attention is given to the reduction of the coolant void worth in current ADS designs. It has been shown that coolant voiding could introduce reactivities that may override the subcritical reactivity for certain combinations of fuel and liquid-metal coolant [3,4,49]. A parametric study of the effect of americium content on the void worth was made by Tucek, et al. [50]. It was found that the void reactivity effect increases with the americium content. LBE yields lower void worths than sodium for a wide range of fuel types and core sizes [3,51]. The low void worth and high boiling point in comparison with sodium are principal advantages that favour the selection of LBE. The higher sodium void worth is partly due to its higher moderating power, which causes a larger spectrum shift during voiding. The void worths associated with the present fuels were calculated in a previous paper [7]. For convenience, these results are listed in TABLE XII. The effect of changing the core size and pin diameter is shown. The negative leakage component tends to decrease with increasing reactor size, while the spectrum hardening effect increases for higher coolant volume fractions. The net effect is that the void effect becomes more positive when the core size increases. The calculations indicate an increase in void worth for larger pin diameters. The effect of separately voiding the core region and plenum region was investigated. The spectral contribution to the void reactivity is usually more positive near the center of the core, while the leakage component is more negative near the edges where the flux gradient is stronger. As a result, expulsion of coolant from the central region results in a positive reactivity gain. However, if the plenum region is voided simultaneously, the reactivity effect may decrease considerably. Evidently, the CerMet fuel offers low void worths. For tight lattice configurations with this fuel, even central voiding can be accommodated. The void worth of the CerCer core is considerably higher than the

CerMet and nitride. The reason is the larger core size (more fuel pins) of the CerCer core, which is an effect of the lower linear rating requirement of this fuel. It is noted, however, that all three fuels provide acceptable void values when the core and plenum is voided simultaneously.

TABLE XII.

Coolant void reactivity worth (in pcm) computed for the examined fuels in various lattice configurations.

Fuel	P/D=1.50, D _o =5.7 mm		P/D=1.75, D _o =5.7 mm		P/D=1.50, D _o =6.8 mm	
	Core	Core+ plenum	Core	Core+ plenum	Core	Core+ plenum
CerCer	4060	1790	5300	2300	4570	2250
CerMet	2460	220	3580	470	2990	520
Nitride	2960	680	4150	880	3610	1080

IX.C. Cladding relocation

Theoretically, molten cladding could be ejected into the coolant and swept upwards with a consequent positive reactivity effect. Such a scenario has been suggested by Maschek et al. [52] in a previous paper. The effect is important if the cladding leaves the core ahead of the fuel. For transient events, it is likely to be associated with coolant overheating, e.g., due to a reduction in flow. On a longer timescale, positive reactivity could be inserted because of dissolution of structural materials in the coolant. In this study, we calculated the reactivity effect assuming all cladding is removed from core, which enables a rough estimate of the reactivity values involved. The results are presented in TABLE XIII. It can be seen that cladding removal leads to a net positive reactivity insertion around 3000 pcm. Note that this value is more or less the same for all fuels. It is further seen that the cladding reactivity worth is largely insensitive to the size of the pin, but decreases for larger pitches as the volume fraction of cladding is lower. Evidently, a larger core size may reduce the cladding worth, but at the cost of a higher void worth. Use of a thinner cladding could further reduce the positive reactivity effect, but it would also degrade mechanical strength.

TABLE XIII.

Reactivity changes (in pcm) following removal of the cladding from the core.

Fuel	P/D=1.50, D _o =5.7 mm	P/D=1.75, D _o =5.7 mm	P/D=1.50, D _o =6.8 mm
	CerCer	3170	2610
CerMet	3360	2750	3310
Nitride	3350	2790	3400

IX.D. Fuel relocation

Reactivity might be introduced in a fast reactor if the fuel would collect in a denser configuration. This is a fundamental distinction between reactors operating on a fast neutron spectrum and thermal systems. The latter is arranged in nearly an optimum configuration to maximize neutron multiplication and any change to the configuration is likely to shut down the chain reaction. By comparison, if the fuel in an ADS melts or the structure collapses, it is possible that criticality would occur. Neutronic calculations have been

performed to determine critical fuel geometries. TABLE XIV shows critical mass, critical volume, and theoretical number of critical assemblies available. The critical mass is sensitive to the material composition (additions of steel, neutron absorbing materials, reflective conditions, etc.) and the fuel geometry. The calculations were carried out for a cylinder containing pure fuel material (fresh fuel) at its normal density. The height-to-diameter (H/D) ratio of the cylinder is 1. It was further assumed that the cylinder is surrounded by LBE on all surfaces. Of course, the assumed critical geometry is an idealized form of the actual configuration of a hypothetical core melt. Calculations for standard fast reactor fuel (U_{0.8}Pu_{0.2}O₂ surrounded by Na) were also performed to enable comparison. It is seen that the critical mass of the minor actinide fuels is quite small in comparison with standard fast reactor fuel, however, variations occur. The nitride fuel has the smallest critical mass (70 kg), which is approximately 20 times smaller than classical MOX-fuel surrounded by sodium. This corresponds to the fuel mass contained in three subassemblies (127-pin bundles). The critical mass of the CerMet fuel is 340 kg, which is a factor of 5 larger than the nitride fuel. The critical mass of the CerCer fuel is somewhat smaller than for the CerMet. Clearly, an ADS core contains sufficient fuel to assemble several critical masses. About 69 critical masses were calculated for the nitride core while the oxide cores contain 18 critical masses each. By comparison, Super-Phénix held about 17 critical masses. Given that the total fuel mass in the French reactor is about 4 times larger than for the present ADS cores, a direct comparison is not appropriate. Based solely on the critical mass, it would seem desirable to use a neutron absorbing matrix material, such as molybdenum or magnesia. However, the recriticality question is complex and in comparison with fast reactors, the behavior of an ADS under these conditions is not well known. The critical size of the fuel is merely one element affecting the recriticality potential.

TABLE XIV.

Critical mass studies.

Fuel	Critical mass* (kg)	Critical volume (dm ³)	Reactor total (critical masses)
CerCer	290	47	18
CerMet	340	33	18
Nitride	70	9	69
Super-Phénix	1370	130	17**

*Cylindrical volume element (H/D=1) surrounded by LBE.

**Based on (U_{0.8}Pu_{0.2})O₂, 3000 MWth (23 tons of fuel).

X. UNPROTECTED LOSS-OF-FLOW

This section presents results for a flow coastdown transient. It is assumed that all primary pumps are tripped in conjunction with failure of the shutdown system, i.e., the proton beam remains on. It is further assumed that the heat rejection system maintains core inlet temperature at the pre-transient value. This is a reasonable assumption, since negligible changes in the inlet temperature typically occur during a loss-of-flow event. During the transition to natural circulation condition, the flow rate is determined by the inertia of the pump and the thermal buoyant drive, which is

counterbalanced by the system pressure losses. It was mentioned earlier that the pump moment of inertia was optimized to soften the cladding-heating rate following pump trip. The cladding-heating rate gradually decreases for longer flow coast-down time, which implies longer grace periods with ever increasing pump inertia. There are, however, operational problems associated with high inertia pumps that impose an upper limit on the pump mass. Besides mechanical problems on the pump shaft, an adverse negative effect is sluggish speed control. In a controlled shutdown event, it is desirable to match the flow and power to avoid thermal cold shock in reactor components (mainly in upper internal structures and heat exchangers). In that case, a large rotating mass is a drawback. Multiple shutdown events may result in thermal fatigue [53], which can cause premature failure. This problem is of particular concern for ADS's because of the possibility for frequent beam interruptions [54]. Therefore, a balance must be struck in the selection of the flywheel size.

X.A. Transient results

Examination of Fig. 3, which shows the coolant flow rate in the average channel for the case with $P/D=1.75$, reveals that the natural circulation flow reaches a quasi-steady value of 23-27% of initial flow at 50-60 seconds after the pump trip. From this data plus the thermal response for the cladding shown later, it is apparent that the transition to natural circulation is smooth. Because the CerCer system operates with a lower coolant ΔT , the fluid density difference between the hot leg and the cold leg is smaller, which provides for a lower circuit buoyant head. As a result, the natural circulation flow level is lower in the CerCer reactor. Fig. 3 shows the power history. All three cores feature overall negative temperature-induced reactivity feedbacks. The power decreases steadily during the entire transition to natural circulation conditions. The overall effect of the reactivity feedbacks is not great, however. The power falls to approximately 95% of the initial value of 800 MWth when equilibrium is reached. The power response behavior is similar among the cores.

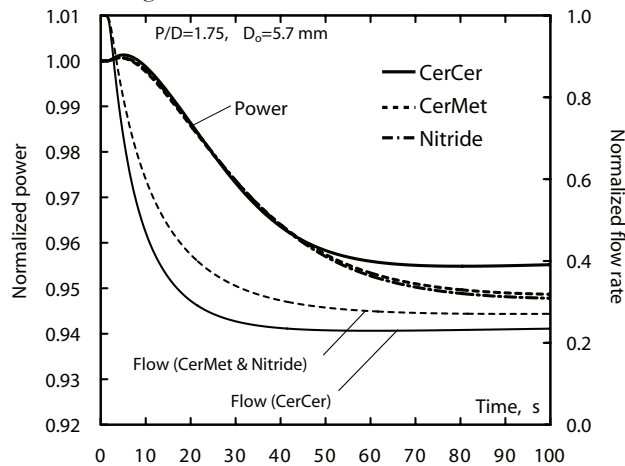


Fig. 3. Transient power and flow conditions for unprotected loss-of-flow transient.

Reactivity feedbacks are illustrated in Fig. 4. For simplicity only the case with CerCer fuel and $P/D=1.75$ is shown. Reactivity feedback from radial expansion of the core is the

dominant negative feedback mechanism – it contributes about minus one dollar at equilibrium conditions. A brief description on the radial expansion reactivity model is in place. The radial growth of the core is determined by the expansion of the grid support structure and by the expansion of the hexcan duct walls and the above-core load pads. The model does not explicitly account for subassembly bowing or for subassembly clearance at the upper load pads. Since the coolant inlet temperature is constant during the transient, the reactivity feedback is determined solely by the temperature rise of duct walls and the structure in the upper load pad region. Axial fuel expansion reactivity differs somewhat between the fuels, where the coefficient of thermal expansion for the CerCer fuel is larger by a factor 1.6 in comparison with the CerMet and nitride. The smaller axial expansion reactivity coefficient for the CerMet fuel tends to reduce the reactivity effect associated with this feedback. As the coolant temperature increases it produces a positive reactivity effect. The resulting reactivity increment due to coolant expansion amounts to +0.5\$ for the CerCer core and +0.4\$ for the nitride. The coolant reactivity is however exceeded by the reactivity losses due to radial expansion and fuel elongation. The positive coolant expansion effect is largely compensated by the negative feedback from fuel elongation. The Doppler effect is insignificant.

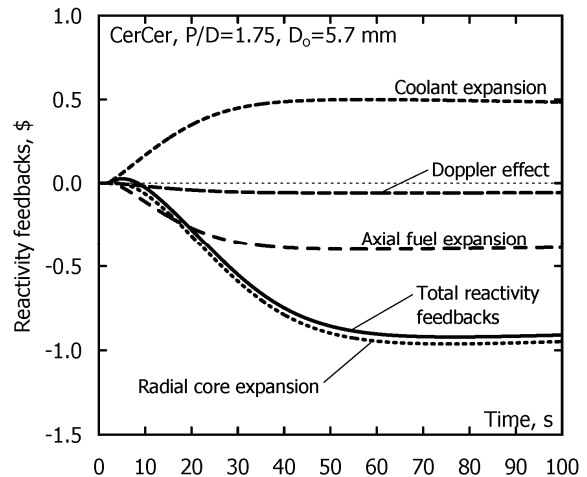


Fig. 4. Reactivity feedback contributions plotted for unprotected loss-of-flow transient.

The immediate effect of the flow reduction is a temperature rise in the coolant, and this in turn leads to higher cladding and fuel temperatures. Coolant boilout is not an issue with lead/bismuth. The major concern is whether the cladding exceeds design limits. Lower cladding temperatures are promoted by higher coolant volume fractions. Larger distance between the fuel pins reduces the core pressure drop and in turn increases contribution from natural circulation. As a result, less forced flow is lost in a pump failure event. Cladding temperature is highest for the CerMet and nitride cores because of their higher power rating. A comparison of cladding temperatures for these cores corresponding to $P/D=1.50$ and $P/D=1.75$ is shown in Fig. 5. The burst temperature for the cladding is 1330 K, as discussed previously. Thus, for the smaller pitch design, the cladding exceeds the failure point within 30-40 seconds after pump

failure, which leaves small safety margins. On the other hand, increasing the P/D ratio to 1.75 reduces cladding temperatures by more than 200 degrees. In that case, early cladding failure can be avoided. It is noted however, that a safe state cannot be assured indefinitely. The burst limit is applicable in transients in which the cladding is heated, without interruption, until failure. Thermal creep rates increase rapidly at high temperatures. Based on creep rupture data for D9 alloy [37], the lifetime at 1280 K is in the minute-scale. Thus, damage prevention will eventually require the need for shutdown and restored cooling capability.

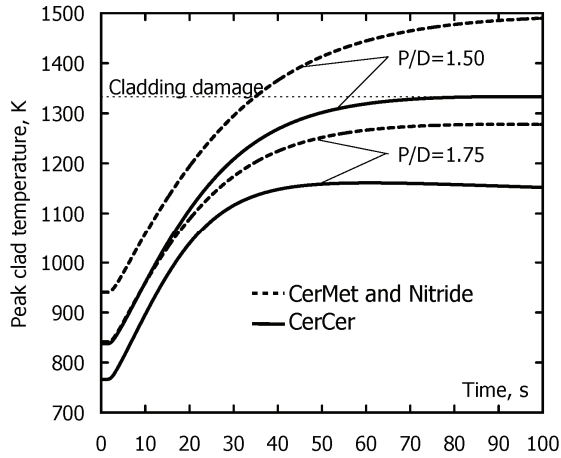


Fig. 5. Peak cladding temperatures for unprotected loss-of-flow transient. Effect of P/D is illustrated.

Maximum fuel and cladding temperatures as function of pitch-to-diameter ratio and pin diameter are presented in TABLE XV. Since the fuel temperature increases along with the coolant temperature, the potential for fuel damage must also be considered. The CerCer temperature reaches close to the damage limit for the cases of the smaller pins. Increasing the pin diameter should be considered in this case.

TABLE XV.

Peak fuel and cladding temperatures at a time $t=100$ seconds during unprotected loss-of-flow transient as function of P/D and pin diameter.

Fuel	P/D=1.50		P/D=1.75		P/D=1.50	
	D _o =5.7 mm	Clad	D _o =5.7 mm	Clad	D _o =6.8 mm	Clad
CerCer	2160	1330	2130	1160	1970	1200
CerMet	2120	1490	2030	1280	1920	1340
Nitride	2080	1490	1980	1280	1920	1340

XI. BEAM OVERPOWER

In accelerator-driven system designs, fission reactions are maintained through multiplication of neutrons from a spallation neutron source, which is driven by a proton accelerator. In such systems, the neutron source is the controller of the chain reaction [55]. Thus, it is appropriate to consider transients in which the source intensity suddenly changes. This could for example happen due to a control system failure, accelerator malfunction, or operator error. In the study, it is assumed that the source intensity increases by a factor of 1.5 times the initial strength, which corresponds to

the beam output capability at end-of-cycle. The ramp is initiated at $t=1$ second and halted at 1.001 seconds. The source is held constant thereafter. It is noted that the source strength in an ADS may change rapidly while transients in a traditional reactor are limited by mechanical speeds. Since the prompt adjustment time in an ADS is very short (tens of Λ), the power will instantaneously respond to any source variation, which permits accidents with very short initial ramp times in comparison with transients in critical reactors. No safety system can act instantaneously; there are always time delays involved. For a traditional safety rod based shutdown system, there is typically a 200 ms delay from detection to control rod motion [56], and then an insertion time of the order of a second. This is fast enough to detect all accident initiators identified for fast reactors [17], which always appear as gradual changes. A beam overpower accident, however, can produce a considerable power change before the malfunction has been detected. Hence, failure prevention should be precluded by the design, and not simply rely on proper control system action.

XI.A. Transient results

Power variation and fuel hot-channel temperatures are illustrated in Fig. 6. It shows the case with a pin diameter of $D=6.8$ mm. Beam overpower transients are characterized by higher fuel temperatures and the primary concern is fuel melting. As indicated in TABLE XVI, the configuration with the smaller P/D and smaller pin diameter is unacceptable for the CerCer fuel. The melting point is reached at 3 seconds after the beam insertion, which leaves little room for control action. Transient temperatures drop when a larger pin diameter is used because steady-state temperatures are lower with this configuration, for reasons discussed previously. It seems that the CerCer fuel needs to employ a larger pin diameter to avoid premature fuel failure. The temperature of the CerMet fuel reaches 2130 K for the same configuration, which corresponds to a margin to melting of 500 degrees. The nitride fuel, which has lower thermal conductivity than the CerMet fuel but smaller gap size, is slightly colder (2080 K) leaving a margin to dissociation of 320 degrees. As seen in TABLE XVI, the cladding remains well below the damage limit for all three fuel-systems and core configurations.

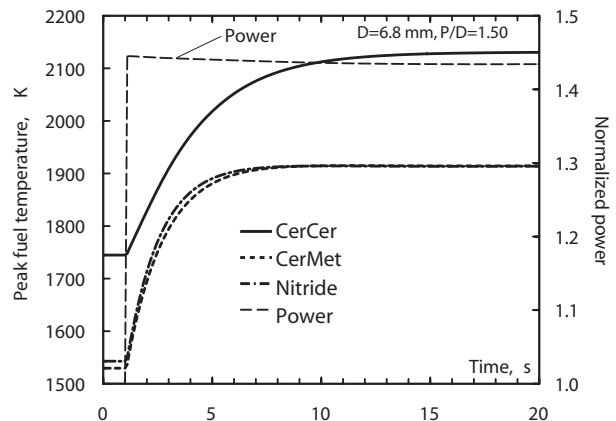


Fig. 6. Transient power and fuel temperatures for beam overpower transient.

TABLE XVI.

Peak fuel and cladding temperatures at a time $t=20$ seconds during beam overpower accident.

Fuel	P/D=1.50		P/D=1.75		P/D=1.50	
	D _o =5.7 mm		D _o =5.7 mm		D _o =6.8 mm	
	Fuel	Clad	Fuel	Clad	Fuel	Clad
CerCer	2290	950	2300	850	2130	860
CerMet	2130	1090	2130	950	1920	970
Nitride	2080	1090	2070	950	1910	970

XII. COOLANT VOIDING

The purpose is to investigate transient response associated with coolant voiding. Extensive voiding in a liquid-metal reactor (LMR) may, for example, be caused by a leak in the primary system, sudden release of fission gases, failure in the heat-transport system that causes gas bubbles to enter the coolant, or coolant overheating and vaporization. Usually, LMR plant designs are arranged with backup protection to mitigate the impact of vessel leakage or rupture, to the degree that large-scale loss-of-coolant accidents (LOCA) are extremely unlikely. Pool systems typically have a second guard vessel, and loop systems are normally double pipe and tank designs. Since the liquid-metal coolant is not pressurized under normal operation, a leak in the primary system will not automatically result in coolant boiling, as opposed to the situation in LWR's. In a sodium-cooled reactor, voiding may arise due to boiling out of coolant. This is prevented in a LBE system. In order for the LBE to get hot enough to boil ($T_b=1940$ K), temperatures have to be above the melting point of steel ($T_m=1700$ K). In that case, much larger reactivity changes may become available due to fuel or cladding relocation. Coolant can be expelled by the rapid escape of fission gases from ruptured fuel pins. Such an accident has been analyzed by Maschek in a previous study [57]. Fission gas release is of concern for unvented and high burnup ADS fuels. Significant amounts of helium are produced due to production of ^{242}Cm through neutron capture in ^{241}Am , and its subsequent alpha-decay into ^{238}Pu . Another possible mechanism for coolant voiding, without the precondition of steel melting, is the possibility of entrainment of air into the core from the cover gas region or steam/water during a failure in the steam generator, i.e., a so-called steam generator tube rupture (SGTR) event. In sodium plants, intermediate sodium-loops are introduced as a second physical barrier to minimize the consequences of SGTRs and to avoid violent chemical reactions between water and sodium in the primary system. Because lead/bismuth is chemically inert with water/steam, two-circuit designs are suggested, with the steam generators located in the primary system. In such designs, there will only be one barrier to fail in order to get high-pressure steam into the primary system. It is noted that the pressure on the steam side can be as high as 100-150 bars and low pressure on the metal side, about 1 bar. Thus, a significant head is available to push steam into the primary system or cause overpressurization in the circuit, which could open further leakage paths. Normally, steam generator tube failures have a high enough probability occurrence to be considered in the licensing procedure. It is noteworthy that a steam-generator failure was the cause of a LOCA and

radioactive contamination in a Russian LBE-cooled nuclear submarine in 1982 [58].

XII.A. Modeling approach

The steam transfer in the circuit and the rate of coolant removal depends on the hydraulic design of the reactor and the size of leak (i.e. number of ruptured steam generator tubes). In this study, we have assumed that the coolant is swept upwards through the core, beginning at the lower cold-leg region, and that the void front moves at the average coolant velocity through the core (2.5 m/s). Since the total height of the core plus plenum regions is 2.5 m, the passage occurs in 1 second. The transient calculation uses a reactivity history based on progressive axial voiding of the core. It is assumed that the void spreads axially and simultaneously in all subassemblies. The reactivity effect, as function of axial void level, is pre-calculated using the MCNP code. The results are illustrated in Fig. 7. Based on this information, a time pattern for the reactivity change is constructed, which is applied in the transient calculation. The configuration employing P/D=1.75 is investigated, which poses the largest positive void reactivity effect. Note that the reactivity effect is strongest for the CerCer fuel and most positive when the core has been voided up to slightly below the top of the active fuel region. The reactivity insertion rate is highest at core midlevel. As a coincidence, the maximum reactivity insertion due to coolant void corresponded to the initial subcritical reactivity of the CerCer core.

The model is intended for scoping evaluations on a shorter time scale. It is noted that the coolant could not be removed from the channel in a physical sense; only the associated reactivity effect is reproduced. As a result, the insulating effect of the gas is neglected. This will affect fuel pin temperatures. The cladding will be subject to the largest uncertainty since it has the shortest time response to changes in convective conditions. The effect on the fuel is expected to be limited during the time frame studied. Power estimates are not affected since all thermal feedback effects are small in comparison with the void reactivity.

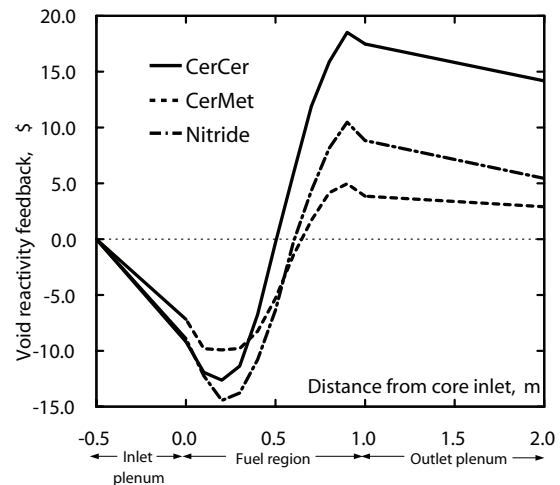


Fig. 7. Reactivity effect (\$) following progressive axial voiding of coolant beginning at the lower plenum.

XII.B. Transient results

The resulting power history is presented in Fig. 8. It is assumed that the steam bubble reaches the lower plenum at 1 second after the steam generator failure. Initially, the bubble passage produces a negative reactivity effect due to increased neutron leakage, as the lower plenum is voided first. The power will find its peak as the reactivity reaches its maximum. The reactivity at peak power, is -0.2% , -12.3% , and -6.8% , respectively for the CerCer, CerMet, and nitride cores, the corresponding peak power is 15.3, 1.3, and 2.1, times the initial power. The power rise in the nitride and CerMet fueled cores is quite modest. The CerCer core, on the other hand, suffers from a sharp power peak. Except from coolant void, axial fuel expansion is the only feedback effect that has some impact on the transient. At peak conditions, the contribution from axial expansion provided an extra reactivity margin, which was sufficient to maintain the reactor in the subcritical state, thereby limiting the magnitude of the peak. Radial core expansion is too slow to be of any significance. It was found that the flux shape in the voided state was similar to the initial shape, and power peaking factors were even lower. The power rise is halted when the void has extended to the top of the core and begins to void the upper plenum region. Judging from Fig. 8, voiding of the upper plenum plays a vital role in reversing the accident. It is assumed that the beam is shutdown after 2 seconds. After shutdown, heat is generated by fissions produced by delayed neutrons plus the reactor decay heat. The delayed neutron source dies away in about 80 seconds (which is the mean life of the longest living precursor ^{87}Br).

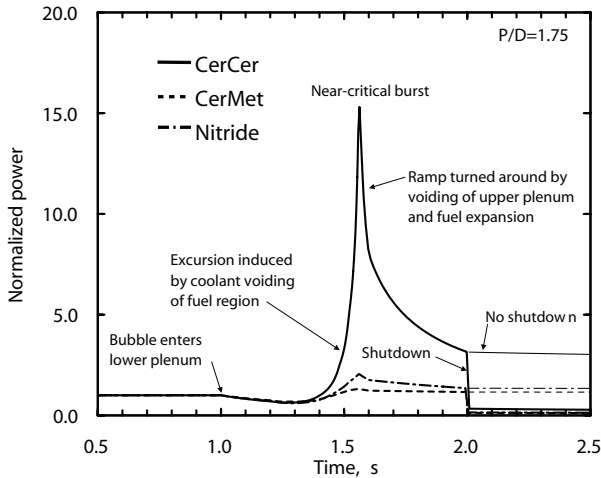


Fig. 8. Transient power for coolant voiding transient.

It is interesting to see that the power in the CerMet and nitride cases is only slightly affected, despite that the reactivity input is of the order of 5-10 dollars. This is a consequence of the fact that these two systems maintain a considerable margin to criticality during the entire transient. The power following a reactivity insertion in a subcritical reactor is inversely proportional to the reactivity in the perturbed state, which tends to zero as the reactor approaches the critical state. Thus, in the presence of an external source, the power approaches infinity as the reactor approaches critical conditions (a $1/\rho$ approach). As a result, the majority of the

power rise will occur near the critical state. The analysis shows that it can be extremely productive to adjust the initial multiplication constant even by a relatively small amount. For example, if the CerCer core would be designed with an initial $k_{\text{eff}}=0.96$ instead of $k_{\text{eff}}=0.97$, then the same voiding scenario (subject to an equivalent reactivity input) would cause a mild peak of approximately 3 times the initial value, instead of 15.

Fig. 9 illustrates the maximum fuel temperature during the accident. The temperature of the CerCer fuel rises considerably; reaching over 2500 K at the time when the reactor is shutdown (the thicker curve represents the temperature evolution after shutdown takes place). The temperature exceeds the assumed melting point of 2200 K at 1.6 seconds. Unless shutdown is initiated, fuel temperatures would continue to rise according to the thinner curve depicted in Fig 9. The temperature of the CerMet and nitride fuels is well below their failure limits. In these systems, the main effect of the coolant expulsion is the loss in heat removal capability on the surface, which presents greatest hazard to the cladding. The temperature rise in the CerCer fuel is overshadowed by the power rise caused by the positive void reactivity insertion. When the power falls during the shutdown phase, the temperature profile tends to level out across the fuel rod. Thus, fuel centerline temperatures decrease, according to Fig 9. Nevertheless, the average temperature of the core continues to rise even after the reactor has been shutdown since the core is deprived of cooling (assuming no coolant reentry). Beam shutdown alone does not prevent the reactor from reaching a failure point, as it would require restored cooling capability. Because of the limited power rise in the nitride and CerMet cores, it is predicted that cladding failure will occur prior to fuel failure.

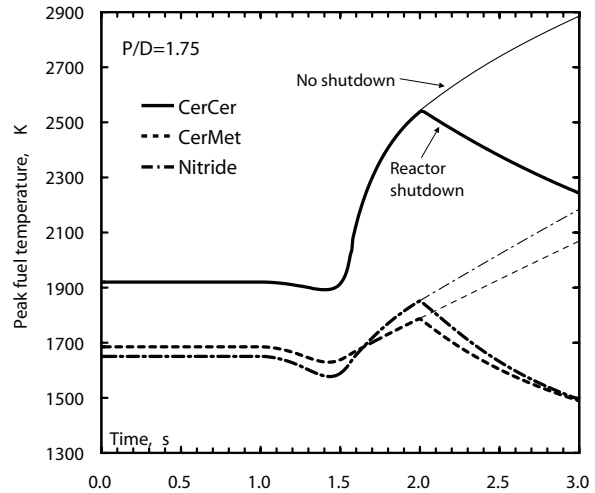


Fig. 9. Peak fuel temperatures for coolant voiding transient.

XIII. CONCLUSIONS

The objective was to study transient safety characteristics of lead-bismuth cooled accelerator-driven systems (ADS) with CerCer-, CerMet-, or nitride-fueled cores. Major consideration was given to the inherent safety aspects of core design. Analyses were carried out for the short-term transient response to unprotected loss-of-flow and accelerator beam-overpower accidents, and a coolant voiding scenario. The

effect of design changes involving variations in the lattice pitch and pin diameter was investigated. Design limits for the fuel and selected cladding materials were compiled. Fuel thermophysical properties were updated according to recently published review articles. Maximum temperatures were determined and compared with design limits. Reactivity effects associated with the relocation of core materials were investigated.

In summary, the better thermal conductivity, higher melting point, and lower coolant void worth of the CerMet fuel combine to contribute to better inherent safety features. In none of the studied transients was the CerMet fuel close to melting. The swelling behavior and hardness of the molybdenum metal raise safety concerns regarding fuel-cladding mechanical interactions. The approach so far has been to increase the initial fuel-cladding gap to accommodate fuel swelling. Although, the results indicate favorable safety performance of the CerMet fuel, many questions still need to be answered and irradiation performance remains to be demonstrated. The CerCer fuel suffers from low thermal conductivity and uncertain melting behavior, which limits both the achievable power density and predicted performance during overpower conditions. Even though the fuel is set to operate at a lower linear power, hot channel fuel temperatures are fairly high, leaving a limited margin to melting. This margin is easily exceeded in an overpower accident and the fuel reaches close to melting during unprotected loss-of-flow conditions. Further measures must be taken to lower the fuel temperature, e.g., increasing the coolant flow area. Increasing the pin diameter will enable lower operating temperature as it allows larger matrix fractions to be used. In addition, the reactivity void worth of this fuel is relatively high in comparison with the other fuels, which is a safety dilemma. It is noted that the specific power density has a critical impact on the achievable burnup level, recycling requirements, overall transmutation efficiency, etc., and, thus, has a strong influence on the economics of the entire fuel cycle. The lower power rating capability of the CerCer fuel leads to obvious performance penalties. The principal problem with the nitride fuel, with regards to the safety performance, is its tendency to dissociate at low temperatures. However, recent studies have shown that decomposition could be suppressed in a nitrogen atmosphere. Whether this is an effective solution under accident conditions, is subject to further investigation. Efforts to increase the understanding of nitride dissociation phenomena are underway. The cladding reactivity worth was essentially the same for all fuels and comparable to the maximum void reactivity available. The study showed that the fuels possess smaller critical masses in comparison with classical fast reactor fuel, but significant variations were observed. The studies point to a particular small critical mass for the low absorbing nitride fuel, about 70 kg, which corresponds to the fuel inventory contained in three individual subassemblies. The critical mass is much larger for the oxide fuel versions, by a factor of ~5. The higher melting point of the CerMet fuel in combination with its larger critical mass is favorable characteristics from the recriticality point of view.

Standard type 316 stainless steel is excluded as potential cladding material because of unacceptable radiation swelling.

HT-9 cladding, which has excellent irradiation performance, is rejected because of unsatisfactory high-temperature mechanical performance. At this point, type 15-15Ti austenitic stainless steel is the suggested cladding material. While previous studies indicate high reliability for this material, experimental confirmation of corrosion stability and transient mechanical performance is necessary. For a lead/bismuth-cooled reactor, cladding corrosion leading to wall thinning is a major life-limiting factor. The corrosion rate is strongly dependent on temperature. Cladding temperatures during normal operation are essentially determined by the coolant outlet temperature, which is given by the linear power and the coolant mass flow rate. For a given geometrical arrangement, the coolant mass flow rate is the same for all three fuels; only the linear power rating varies. It was found that the higher rated CerMet and nitride fuels required a higher coolant mass flow rate in order to achieve acceptable cladding temperatures for normal operation. This suggests the use of a higher pin pitch. A higher lattice pitch is also necessary to avoid mechanical failure during unprotected loss-of-flow.

Finally, a steam generator tube rupture event was identified as a potential threat, which could lead to extensive voiding in current accelerator-driven design proposals. A preliminary transient test case study was performed. Due to the strong positive reactivity effect, the CerCer system was subject to a sharp power peak, while the power rise in the nitride and CerMet fueled cores was quite modest, which simply confirms the importance of having a low coolant void reactivity value in a lead/bismuth system, despite of its high boiling temperatures.

REFERENCES

1. D. G. FOSTER, et al., "Review of PNL Study on Transmutation Processing of High Level Waste," LA-UR-74-74, Los Alamos Scientific Laboratory (1974).
2. T. TAKIZUKA, et al., Proc. 5th Int. Conf. Emerging Nuclear Energy Systems 1989, ICENES '89, Karlsruhe, July 3-6 (1989).
3. J. WALLENIS, "Neutronic aspects of inert matrix fuels for application in ADS," J. Nucl. Mater. **320** (2003) 142-146.
4. M. ERIKSSON, J. WALLENIS, J. E. CAHALAN, K. TUCEK, and W. GUDOWSKI, "Safety analysis of Na and Pb-Bi coolants in response to beam instabilities," Proc. 3rd International Workshop on Utilisation and Reliability of High Power Proton Accelerators, Santa Fe, May 12-16, NEA/OECD (2002).
5. J. WALLENIS, "CONFIRM: Collaboration on Nitride Fuel Irradiation and Modelling," Proc. of the AccApp/ADTTA 2001 Meeting, Reno, November 11-15, American Nuclear Society (2001).
6. S. PILLION and J. WALLENIS, "Oxide and nitride TRU-fuels: lessons drawn from the CONFIRM and FUTURE projects of the 5th European framework

- programme,” Nucl. Sci. Eng., Accepted for publication (2004).
7. J. WALLENIS and M. ERIKSSON, “Neutronic design of minor actinide burning accelerator driven systems,” Nucl. Technol., Submitted (2004).
 8. “Safety related terms for advanced nuclear plants,” IAEA-TECDOC-626, September (1991).
 9. H. MURATA and T. MUKAIYAMA, “Fission reactor studies in view of reactor waste programmes,” Atomkernenergie – Kerntechnik, **45** (1984) 23-29.
 10. H. KLEYKAMP, “Selection of materials as diluents for burning of plutonium fuels in nuclear reactors,” J. Nucl. Mater. **275** (1999) 1-11.
 11. M. BURGHARTZ, G. LEDERGERBER, H. HEIN, R. R. VAN DER LAAN, and R. J. M. KONINGS, “Some aspects of the use of ZrN as an inert matrix for actinide fuels,” J. Nucl. Mater. **288** (2001) 233-236.
 12. K. MINATO, M. AKABORI, M. TAKANO, Y. ARAI, K. NAKAJIMA, A. ITOH, and T. OGAWA, “Fabrication of nitride fuels for transmutation of minor actinides,” J. Nucl. Mater. **320** (2003) 18-24.
 13. M. TAKANO, “Study on The Stability of AmN and (Am,Zr)N,” Proc. GLOBAL 2003, New Orleans, Louisiana, November 16-20 (2003).
 14. J. WALLENIS and S. PILLON, “N-15 Requirement for 2nd Stratum ADS Nitride Fuels,” Proc. of the AccApp/ADTTA 2001 Meeting, Reno, November 11-15, American Nuclear Society (2001).
 15. M. A. MIGNANELLI and R. THETFORD in Proc. on Advanced Reactors with Innovative Fuels, ARWIF-2001, Chester, October 22-24 (2001).
 16. R. THETFORD and M. MIGNANELLI, “The chemistry and physics of modeling nitride fuels for transmutation,” J. Nucl. Mater. **320** (2003) 44-53.
 17. A. E. WALTAR and A. B. REYNOLDS, Fast Breeder Reactors, p. 260 and 540, Pergamon Press, New York (1981).
 18. D. R. OLANDER, Fundamental Aspects of Nuclear Reactor Elements, p. 131-135, Published by Technical Information Center, Office of Public Affairs, Energy Research and Development Administration, Springfield, VA (1976).
 19. Ph. DEHAUDT, A. MOCELLIN, G. EMINET, L. CAILLOT, G. DELETTE, M. BAUER, and I. VIALLARD, “Composite Fuel Behaviour Under and After Irradiation,” IAEA Technical Committee Meeting on Research of Fuel Aimed at Low Fission Gas Release, Moscow, October 1-4 (1996).
 20. J. L. SÉRAN, V. LÉVY, P. DUBUISSON, D. GILBON, A. MAILLARD, A. FISSOLO, H. TOURON, R. CAUVIN, A. CHALONY, and A. LE BOULBIN, “Behavior under Neutron irradiation of the 15-15Ti and EM10 Steels Used as Standard Materials of the Phénix Fuel Subassembly,” Effects of Radiation on Materials: 15th Int. Symposium, ASTM STP **1125**, R. E. Stoller, A. S. Kumar, and D. S. Gelles, Eds., American Society for Testing and Materials, p. 1209-1233, Philadelphia (1992).
 21. A. FISSOLO, V. LÉVY, J. L. SÉRAN, A. MAILLARD, J. ROYER, and O. ARBOUILLE, “Tensile Properties of Neutron Irradiated 316Ti and 15-15Ti Steels,” Effects of Radiation on Materials: 16th Int. Symposium, ASTM STP **1175**, A. S. Kumar, D. S. Gelles, R. K. Nanstad, and E. A. Little, Eds., American Society for Testing and Materials, p. 646-663, Philadelphia (1993).
 22. E. H. P. CORDFUNKE and R. J. M. KONINGS, Thermochemical Data for Reactor Materials and Fission Products, North-Holland, Amsterdam (1990).
 23. J. J. KATZ, G. T. SEOBORG, and L. R. MOSS, The chemistry of the actinide elements, 2nd ed., Vols. 1 and 2, Chapman and Hall, London (1986).
 24. J. EDWARDS, et al., “Fast Reactor Manual,” Fast Reactor European Collaboration report (1990).
 25. R. KONINGS, Personal Communication (January, 2004).
 26. S. CASALTA, HJ. MATZKE, and C. PRUNIER, Proc. Int. Conf. On Evaluation of Emerging Nuclear Fuel Cycle Systems, GLOBAL’95, Versailles, September 11-14, p. **1725** (1995).
 27. H. ZHANG, R. J. M. KONINGS, M. E. HUNTELAAR, and E. H. P. CORDFUNKE, “Melting behaviour of oxide systems for heterogeneous transmutation of actinides. III. The system Am-Mg-O,” J. Nucl. Mater. **250** (1997) 88-95.
 28. H. ZHANG, R. J. M. KONINGS, M. E. HUNTELAAR, and E. H. P. CORDFUNKE, “Melting behaviour of oxide systems for heterogeneous transmutation of actinides. I. The systems Pu-Al-O and Pu-Mg-O,” J. Nucl. Mater. **249** (1997) 223-230.
 29. M. TAKANO, A. ITOH, M. AKABORI, et al., “Synthesis of americium mononitride by carbothermic reduction method,” Proc. Int. Conf. On Future Nuclear Energy Systems, GLOBAL’99, Jackson Hole, Wyoming, Aug. 29 – Sep. 33, p. 110, American Nuclear Society (1999).
 30. M. JOLKKONEN, M. STREIT, and J. WALLENIS, “Thermo-chemical modelling of uranium-free nitride fuels,” J. Nucl. Sci. Technol. **41**(4), 457 (2004).
 31. J.-O. ANDERSSON, et al., “Thermo-Calc and DICTRA, computational tools for materials science,” Calphad **26**, 273 (2002).
 32. T. OGAWA, T. OHMACHI, A. MAEDA, et al., “Vaporization behaviour of (Pu,Am)N,” J. Alloys and Compounds, **224**, 55 (1995).
 33. N. S. CANNON, F. R. HUANG, and M. L. HAMILTON, “Transient and Static Mechanical Properties of D9 Fuel Pin Cladding and Duct Material Irradiated to High Fluence,” Effects of Radiation on Materials: 15th Int.

- Symposium, ASTM STP 1125, R. E. Stoller, A. S. Kumar, and D. S. Gelles, Eds., American Society for Testing and Materials, p. 1071-1082, Philadelphia (1992).
34. I. SHIBAHARA, T. OMORI, Y. SATO, S. ONOSE, and S. NOMURA, "Mechanical Property Degradation of Fast Reactor Fuel Cladding During Thermal Transients," Effects of Radiation on Materials: 16th Int. Symposium, ASTM STP 1175, A. S. Kumar, D. S. Gelles, R. Nanstad, and E. A. Little, Eds., American Society for Testing and Materials, p. 664-678, Philadelphia (1994).
 35. M. G. ADAMSON, E. A. AITKEN, and S. VAIDYANATHAN, "Synergistic tellurium-caesium embrittlement of Type 316 stainless steel", Nature, **295**, 49 (1982).
 36. S. TANI, S. NOMURA, and I. SHIBAHARA, "Fuel Cladding Mechanical Property Degradation Mechanisms and Fuel Reliability Under Transient Conditions," Int. Conf. on Reliable Fuels for Liquid Metal Reactors, Sep. 7-11, Tucson (1986).
 37. R. J. PUGH and M. L. HAMILTON, Influence of Radiation on Materials Properties: 13th Int. Symposium (Part II), ASTM STP 956, F. A. Garner, C. H. Henager, N. Igata, Eds., American Society for Testing Materials, p. 22-29 (1987).
 38. G. S. YACHMENYOV, A. YE. RUSANOV, B. F. GROMOV, YU. S. BELOMYTSEV, N. S. SKVORTSOV, and A. P. DEMISHONKOV, "Problems of structural materials' corrosion in lead-bismuth coolant," Proc. Heavy Liquid Metal Coolants in Nuclear Technology, Vol. 1, Obninsk, October 5-9, p. 133-140, State Scientific Center of Russian Federation Institute for Physics and Power Engineering (1998).
 39. J. F. BRIESMEISTER, "MCNP - A general Monte Carlo N-Particle transport code," LA-13709-M, Los Alamos National Laboratory (2000).
 40. J. E. CAHALAN, A. M. TENTNER, and E. E. MORRIS, "Advanced LMR Safety Analysis Capabilities in the SASSYS-1 and SAS4A Computer Codes," Proc. of the International Topical Meeting on Advanced Reactors Safety, Pittsburgh, April 17-21 (1994).
 41. M. ERIKSSON, J. E. CAHALAN, and W. S. YANG, "On the Performance of Point Kinetics for the Analysis of Accelerator Driven Systems," Accepted for publication in the March Issue of Nucl. Sci. Eng. (2005).
 42. K. TSUJIMOTO, T. SASA, K. NISHIHARA, H. OIGAWA, and H. TAKANO, "Neutronics Design for Lead-Bismuth Cooled Accelerator-Driven System for Transmutation of Minor Actinides," J. Nucl. Sci. & Technology, **41** (2004) 21.
 43. P. A. USHAKOV, "Hydrodynamics and Heat Transfer in Reactor Cooled by Lead-Bismuth Alloy," Proc. Heavy Liquid Metal Coolants in Nuclear Technology, Vol. 2, Obninsk, October 5-9, p. 612-626, State Scientific Center of Russian Federation Institute for Physics and Power Engineering (1998).
 44. F. E. DUNN and D. J. MALLOY, "LMR Centrifugal Pump Coastdowns," Proc. Anticipated and Abnormal Transients In Nuclear Power Plants, Vol. 1, American Nuclear Society Topical Meeting, Atlanta, Georgia, April 12-15 (1987).
 45. H. TAKANO, et al., "A Design for Inherent Safety Core, Aseismicity and Heat Transport System in Lead-Cooled Nitride-Fuel Fast Reactor," Proc. Int. Topical Meeting on Advanced Reactor Safety, Pittsburgh, April 17-21 (1994).
 46. J. BUONGIORNO and B.D. HAWKES, "Seismic analysis of heavy-liquid-metal-cooled reactor vessels", Nuclear Engineering and Design **228** (2004) 305-317.
 47. I. MICHELI, S. CARDINI, A. COLAIUDA, P. TURRONI, "Investigation upon the dynamic structural response of a nuclear plant on aseismic isolating devices," Nuclear Engineering and Design **228** (2004) 319-343.
 48. M. ERIKSSON and J. E. CAHALAN, "Inherent shutdown capabilities in accelerator-driven systems," Annals of Nuclear Energy, vol. 29/14 pp 1689-1706, (2002).
 49. W. MASCHEK, et al., "Safety Improvements for ADS Transmuters with dedicated Fuel," Proc. of the AccApp/ADTTA 2001 Meeting, Reno, November 11-15, American Nuclear Society (2001).
 50. K. TUCEK, J. WALLENIUS, and W. GUDOWSKI "Coolant void worths in fast breeder reactors and accelerator driven transuranium and minor actinide burners," Annals of Nuclear Energy, accepted for publication (2004).
 51. J. WALLENIUS, K. TUCEK, and W. GUDOWSKI, "Safety analysis of nitride fuels in cores dedicated to waste transmutation," Proc. 6th Information Exchange Meeting on Actinide and Fission Product Partitioning and Transmutation, Madrid, December 11-13, OECD/NEA (2000).
 52. W. MASCHEK, T. SUZUKI, X. CHEN, MG. MORI, C. M. BOCCACCINI, M. FLAD, K. MORITA, "Behavior of Transmuter Fuels of Accelerator Driven Systems under Severe Accident Conditions," GENES4/ANP2003, Kyoto, September 15-19 (2003).
 53. F. E. DUNN and D.C. WADE, "Estimates of Thermal Fatigue Due to Beam Interruptions for an ALMR-Type ATW," Proc. 2nd International Workshop on Utilisation and Reliability of High Power Proton Accelerators, Aix-en-Provence, November 22-24, NEA/OECD (1999).
 54. M. ERIKSSON, "Reliability Assessment of the LANSCE Accelerator System," M.Sc. Thesis, Royal Institute of Technology, Dep. Nuclear and Reactor Physics (Nov. 1998).
 55. J. E. CAHALAN and M. ERIKSSON, "Active and Passive Safety Control Performance in Sub-critical, Accelerator-Driven Nuclear Reactors," Proc. 3rd International Workshop on Utilisation and Reliability of High Power Proton Accelerators, Santa Fe, May, NEA/OECD (2002).
 56. Y. S. TANG, R. D. COFFIELD, and R. A. MARKLEY, Thermal Analysis of Liquid Metal Fast Breeder Reactors, p.

277, American Nuclear Society, LaGrange Park, Illinois (1978).

57. W. MASCHKEK, et al., "Safety Analyses for ADS Cores with Dedicated Fuel and Proposals for Safety Improvements," IAEA-TECDOC-1356, IAEA (2000).

58. B. F. GROMOV, O. G. GRIGORIEV, A. V. DEDOUL, G. I. TOSHINSKY, V. S. STEPANOV, "The Analysis of Operating Experience of Reactor Installations Using Lead-Bismuth Coolant and Accidents Happened," Proc. Heavy Liquid Metal Coolants in Nuclear Technology, Vol. 1, Obninsk, October 5-9, p. 60-66, State Scientific Center of Russian Federation Institute for Physics and Power Engineering (1998).

Paper II

Neutronics of minor actinide burning accelerator driven systems with ceramic fuel

J. Wallenius and M. Eriksson

Department of Nuclear and Reactor Physics, Royal Institute of Technology, Stockholm, Sweden

(Dated: February 2, 2005)

We have investigated neutronic properties of lead-bismuth cooled accelerator driven systems (ADS) with different minor actinide based ceramic fuels (two composite oxides and one solid solution nitride). Adopting a TRU composition with 40% plutonium in the initial load, transmutation rates of higher actinides (americium and curium) equal to 265-285 kg per $GWth \times y$ are obtained. The smallest reactivity swing is provided by the magnesium oxide based cercer fuel. The cercer cores however exhibit large coolant void worths, which is of concern in case of gas bubble introduction into the core. Nitride and cermet cores are more stable with respect to void formation. The poorer neutron economy of the molybdenum based cermet makes it however difficult to accommodate an inert matrix volume fraction exceeding 50 percent, a lower limit for fabricability. Higher plutonium fraction is thus required for the cermet, which would lead to lower actinide burning rates. The nitride core yields high actinide burning rates, low void worths and acceptable reactivity losses.

I. INTRODUCTION

Separating plutonium and minor actinides from spent nuclear fuel, these elements may be recycled in fission reactors. If the amount of these elements destined for geological repository can be reduced by more than a factor of 100, the time needed to store the residual waste until it reaches the toxicity of uranium ore is shortened to less than 1000 years [1]. Multi-recycling of americium and curium, in addition to plutonium, is necessary in order to obtain such reduction factors [2]. The introduction of americium into the fuel of critical reactors however leads to deterioration of safety parameters [3]. Hence, already in 1974, it was suggested by Los Alamos that the higher actinides should be recycled in accelerator driven systems (ADS) [4]. Later, JAERI proposed the Double Strata fuel cycle, where the management of minor actinides would take place in dedicated facilities, separated from the commercial fuel cycle [5, 6]. Adopting fast reactors for recycling of plutonium, such a strategy would allow for a very small fraction of the nuclear power park to be penalised by the handling of strong alpha and neutron emitters, as shown in a study by CEA [7].

Previous design studies of accelerator driven systems were made using a fixed core concept, with coolant and fuel selected on the basis of chemical and physical properties, choice of reprocessing method or fast reactor experience [6, 8–11]. To our knowledge, no consistent comparison between different fuel options for ADS has been published. It is the purpose of the present paper to perform such a comparison. The focus will be on neutronic characteristics, while thermo-hydraulic studies are presented in forthcoming paper [12].

In what follows we will show why a uranium matrix does not significantly improve the neutronic safety parameters of americium bearing fuels, corroborating the selection of inert matrix fuels and sub-critical operation for minor actinide burning. We will briefly motivate the selection of lead-bismuth coolant and recapitulate a scoping study leading to selection of three fuel

form/compositions to be investigated in detail. Then we account for detailed calculations of neutronic properties for 800 MWth cores with two composite oxide fuels and one solid solution nitride fuel, as function of core geometry. Finally we discuss the relative performance and safety characteristics pertaining to the fuels.

II. FERTILE VS INERT MATRIX

When designing a dedicated minor actinide burner a small reactivity swing is desired for reasons of safety and economy, irrespective of whether the reactor is operated in critical or sub-critical mode. Therefore some plutonium should be present in the fuel. For a uranium free core, a ratio of americium to plutonium of about 3:2 was shown to provide a minimum reactivity swing when approaching equilibrium [13]. The question then may be raised whether such a core can be operated in a critical mode, or if sub-criticality is an absolute requirement. A complete answer can only be given by time-dependent analysis of all relevant accident conditions. However, an indicator of the potential for critical operation may be provided by quasi-static analysis.

Among the neutronic parameters of importance for the safety of critical reactors are

- The effective delayed neutron fraction β_{eff}
- The fuel Doppler coefficient $\alpha_D = \left(\frac{\Delta k}{\Delta T}\right)_{\text{Doppler}}$
- The coolant temperature coefficient $\alpha_c = \left(\frac{\Delta k}{\Delta T}\right)_{\text{cool}}$

When introducing minor actinides into the fuel, these parameters are deteriorated, and margins to failure under design extension conditions decrease. Wade and Fujita defined the following safety indicators for passive shutdown behavior in sodium-cooled fast reactors [14]:

$$\begin{aligned} A &= (\alpha_D + \alpha_l) \overline{\Delta T_{\text{fuel}}} \\ B &= (\alpha_D + \alpha_l + \alpha_c + 2\alpha_R) \Delta T_{\text{cool}} / 2 \\ C &= \alpha_D + \alpha_l + \alpha_c + \alpha_R \end{aligned} \quad (1)$$

where α_l and α_r are axial and radial expansion coefficients, respectively. $\overline{\Delta T_{\text{fuel}}}$ is the difference between the average fuel and coolant temperature and ΔT_{cool} is the difference between coolant inlet and outlet temperatures.

In the quasi static approximation, the asymptotic rise in coolant outlet temperature is then given by

$$\Delta T_{\text{out}} = \frac{A}{B} \Delta T_{\text{cool}} \quad (2)$$

for the un-protected loss of flow (LOF) event. In the case of a total loss of heat-sink (LOHS), the maximum temperature increase in core inlet temperature is given by $(A + B)/C$, which may be rewritten as

$$\Delta T_{\text{out}} = \left(\frac{1 + A/B}{C \Delta T_{\text{cool}}/B} - 1 \right) \Delta T_{\text{cool}} \quad (3)$$

An estimate for the asymptotic increase in core outlet temperature during a control rod runout transient over power event (TOP) is given by

$$\Delta T_{\text{out}} = \left(\frac{-\Delta \rho_{\text{TOP}}/B}{1 + A/B} \right) \Delta T_{\text{cool}} \quad (4)$$

where $\Delta \rho_{\text{TOP}}$ is the reactivity worth of the most efficient control rod. To preclude coolant boiling and ensure integrity of the cladding and structural materials during passive shutdown, the following set of conditions may be derived from (2), (3) and (4), under the assumption that $\Delta T_{\text{out}} \leq M \Delta T_{\text{cool}}$:

$$\frac{A}{B} \leq M \quad (5)$$

$$\frac{C \Delta T_{\text{cool}}}{B} \geq 1 \quad (6)$$

$$\frac{\Delta \rho_{\text{TOP}}}{|B|} \leq M \quad (7)$$

where A , B and C are all negative. The margin to clad failure is thus $M \Delta T_{\text{cool}}$. In a conventional sodium cooled reactor we have $\Delta T_{\text{cool}} \simeq 150$ K. Ferritic steels like HT-9, have a 24 hour creep limit of about 950 K [15], giving $M \simeq 1$. The corresponding limit for austenitic steels is 1100 K [16], leading to $M \simeq 2$.

Values of axial expansion coefficients range from -0.2 pcm/K for oxide to -0.6 pcm/K for metal fuel. Radial expansion coefficients are independent of fuel type, but vary with core size between -1.1 pcm/K for large reactors like Super-Phenix to -1.4 pcm/K for smaller cores, assuming that austenitic steels are used for the diagrid. [14, 17, 18]. A ferritic diagrid would yield 30% smaller radial expansion coefficients.

For a conventional sodium cooled reactor with oxide fuel we have $\Delta T_{\text{cool}} \simeq 150$ K and $\overline{\Delta T_{\text{fuel}}}/\Delta T_{\text{cool}} \simeq 5$. Temperature coefficients calculated for Super-Phenix: $\alpha_D = -0.6$ pcm/K, $\alpha_c = +0.8$ pcm/K, $\alpha_l = -0.2$ pcm/K and $\alpha_r = -1.1$ pcm/K yields $C \Delta T_{\text{coolant}}/B = 1.0$ and

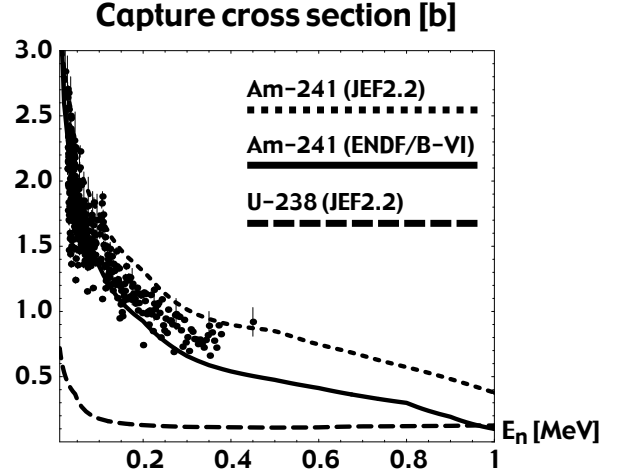


FIG. 1: Capture cross section of ^{241}Am . Solid line: ENDF/B-VI, dotted line JEF2.2. Experimental data from EXFOR are denoted with error bars. The capture cross section of ^{238}U (dashed line) is included for comparison.

$A/B = 1.8$. These numbers indicate that clad and structural material have to be made from austenitic steels if a Super-Phenix core is to survive an un-protected LOF.

The negative temperature coefficients (Doppler plus expansion) must compensate for the magnitude of the positive coolant void coefficient for the total inlet temperature coefficient C to be negative. This is typically the case for reactors with $(\text{U}, \text{Pu})\text{O}_2$ fuel. As we shall see, it may not be so for americium based fuels. Further, the magnitude of B is drastically reduced, leading to very small upper limits for control rod worths.

The relatively high capture cross section of americium in the energy range of 10-500 keV leads to a decrease in Doppler feedback. As shown in Fig. 1, the capture cross section of ^{241}Am is 10 times higher than that of ^{238}U at $E = 100$ keV. Even with a large fraction of ^{238}U in the fuel, most captures will take place in americium, at energies above the resolved resonance region.

In order to quantify the impact, we have calculated the fuel Doppler constant K_D with the Monte Carlo code MCNP4C, for an hexagonal pin cell with oxide fuel and sodium coolant. Clad inner/outer diameters of 5.8/6.6 mm and $P/D = 1.20$ were assumed. Fitting the function $k = c + K_D \times \log(T)$ to k-eigenvalues obtained with cross sections Doppler broadened with NJOY at 900, 1200, 1500 and 1800 Kelvin, the statistical error could be minimised. Probability tables were used above the resolved resonance region. Table I shows how the Doppler constant vanishes with large fractions of americium present in the core.

It can be seen that the addition of 30% americium in the fuel completely suppresses the Doppler feedback, even in the presence of uranium. This fact is reflected in the average neutron flux energy, increas-

TABLE I: Fuel Doppler constant K_D ($\partial k/\partial T = -K_D/T$) for oxide fuels in a sodium cooled hexagonal pin cell with P/D = 1.20. ENDFB/VI data were used.

U [%]	Pu [%]	Zr [%]	Am [%]	K_D [pcm]
80	20	-	-	-810 ± 20
50	20	-	30	-20 ± 20
-	20	80	-	-420 ± 20
-	20	50	30	-20 ± 20

TABLE II: Sodium temperature coefficient in an oxide fuel hexagonal pin cell with P/D = 1.20. $\Delta k/\Delta T$ was calculated as an average between 700 and 900 K, using the ENDFB/VI library. The statistical error corresponds to one standard deviation.

U [%]	Pu [%]	Zr [%]	Am [%]	$\Delta k/\Delta T$
80	20	-	-	$+1.07 \pm 0.02$
50	20	-	30	$+1.79 \pm 0.02$
-	20	80	-	$+0.72 \pm 0.03$
-	20	50	30	$+2.02 \pm 0.02$

ing from 480 keV in the americium free fuels to above 620 keV in the americium bearing fuels. Note that fertile plutonium nuclides may provide a substantial negative Doppler feedback, if americium is absent. The plutonium vector used in the pin cell calculation was $238/239/240/241/242 = 1.0/69.0/25.0/3.0/2.0$, corresponding to that of fast spectrum equilibrium in IFR [19].

Table II displays the coolant temperature coefficient in the pin cell model, obtained using perturbation techniques, as function of uranium and americium content. We see a strong increase in the coolant temperature coefficient with americium content. The pure plutonium fuel, on the other hand, gives a smaller temperature coefficient.

The presence of ^{238}U in the fuel of FBRs has been thought to be a major contributor to β_{eff} [20]. It is true that the use of ^{238}U as matrix for an americium bearing fuel increases the production of delayed neutrons, comparing to an inert (non-fissionable) matrix. However,

TABLE III: Delayed and effective delayed neutron fractions for fresh oxide fuels in a sodium cooled hexagonal pin cell with P/D = 1.20. The ENDF/B-VI library was used. The statistical error corresponds to one standard deviation.

U [%]	Pu [%]	Zr [%]	Am [%]	β [pcm]	β_{eff} [pcm]
80	20	-	-	399 ± 11	342 ± 10
50	20	-	30	307 ± 10	204 ± 11
-	20	80	-	221 ± 11	206 ± 13
-	20	50	30	213 ± 11	143 ± 11

the *effective* delayed neutron fraction will not be raised by the same magnitude. The reason is that the spectrum of the delayed neutrons has a median energy below the fast fission threshold and hence leads to a higher probability for absorption of delayed neutrons in americium, as compared to prompt fission neutrons.

In order to quantify the impact, we have calculated β (the fraction of delayed neutrons emitted in an average fission) and β_{eff} using the same pin cell model. As can be seen, β_{eff} is reduced more than β when substituting 3/8 of the initial uranium with americium. Note further that β_{eff} for a uranium free fuel may be of the same magnitude as a fuel with 50% ^{238}U , as long as americium is not present.

Safety indicators estimated on the basis of the above pin cell calculations are shown in Table IV. The axial and radial expansion coefficients were taken to be $\alpha_l = -0.2 \text{ pcm/K}$ and $\alpha_R = -1.2 \text{ pcm/K}$.

The first thing to note is the very small absolute value of B for the americium bearing fuels. Condition (7) means that the individual control rod worth should be less than $|B|$. To achieve a similar total control bank worth one would need 2.5 times more control rods in the $(U_{0.5}, Pu_{0.2}, Am_{0.3})O_2$ fueled core than in a standard FBR.

Second, the inlet temperature coefficient C is positive for the americium loaded cores. This is clearly unacceptable if passive shutdown capability is a required feature.

It thus appears that a uranium free, americium based fuel should not be used in a oxide fueled critical reactor with sodium coolant. The use of a uranium matrix does not provide us with a Doppler feedback sufficient to compensate for the increase in coolant temperature coefficient caused by the fast fission in even neutron number nuclides. In addition, absorption of delayed neutrons in americium quenches the effective delayed neutron fraction. We thus conclude that for core configurations and fuel compositions similar to the ones here investigated, the use of a fertile matrix for minor actinide burning does not improve safety indicators to the extent that such cores may be operated in a critical mode. Plutonium fuels (or fuels with high Pu/Am ratios) might be operated in critical configurations without support of uranium. Their large reactivity loss however leads to problem with condition (7). Inert matrix supported americium based fuels, on the other hand, may provide acceptable safety parameters during sub-critical operation. In the following sections we will discuss conditions for selection of coolant and fuel composition of a sub-critical system operating on americium based fuels.

III. CHOICE OF COOLANT FOR THE ACCELERATOR DRIVEN REACTOR

As seen in Table II, the sodium temperature coefficient becomes very large for americium bearing fuels.

TABLE IV: Safety indicators estimated for a sodium cooled oxide fuel pin channel with P/D = 1.2.

U [%]	Pu [%]	Zr [%]	Am [%]	A [pcm]	B [pcm]	C [pcm/K]	A/B	$\Delta T_{\text{cool}}C/B$
80	20	-	-	-280	-160	-0.88	1.8	+0.8
50	20	-	30	-80	-60	+0.38	1.3	-0.9
-	20	80	-	-180	-160	-0.97	1.1	+0.9
-	20	50	30	-80	-40	+0.64	2.0	-2.3

The probability of reaching the boiling point of sodium during a LOHS event grows if the inlet temperature coefficient is positive. In a previous study, we have shown that the sodium void worth exceeds 4000 pcm for several kinds of inert matrix fuels [21]. We further found that certain accelerator over power transients in cores with such fuels result in sodium boiling followed by a prompt excursion [22]. An alternative coolant providing a fast neutron spectrum should thus be chosen for the system under consideration. While lead and gas cooling have been suggested [8, 23], problems related to clad durability during transients (He) and extended operation at high temperature (Pb) lead us to adopt lead-bismuth eutectic (LBE) as the reference coolant. LBE features a combination of relatively low melting temperature and high boiling point that makes it suitable for application in ADS. Corrosion control is more delicate than in sodium. A core melt due to corrosion product blockage of the coolant occurred in the first LBE cooled submarine reactor put into operation. Subsequently, oxygen control systems were developed and 80 years of reactor operation were accumulated in Soviet sub-marines without any incident related to corrosion problems [24]. Finally, synergy effects with the spallation target are evident.

IV. CHOICE OF FUEL

Having selected lead-bismuth as coolant, we need to find an inert matrix fuel that provides us with the following features:

- A high linear rating, in order to achieve a high burnup within the short residence time set by LBE induced corrosion.
- At least 50 percent inert matrix volume fraction, to ensure fabricability and/or stability at high temperature.
- A low void worth, in order to ensure that the core remains sub-critical during steam blow down or fission and helium gas leakage events.
- Reasonable solubility rate in nitric acid, to retain compatibility with existing industrial scale reprocessing facilities in Europe.

Recently, americium bearing metal alloy fuels have successfully been fabricated [25]. Metallic fuels feature a large solid fission product swelling rate, and are thus fabricated with a large pellet clad gap, that is filled with sodium [26]. Consequently, aqueous reprocessing is not applicable. We therefore consider metal alloys to be out of scope of the present work, and focus on ceramic fuels.

A. Oxide fuels

The condition of high linear rating directly excludes solid solution oxide fuels from our list of candidates. Not only do most oxides have low conductivity. The oxygen to metal ratio of compounds with americium and curium must be considerably less than 2.0, in order to ensure stability at high temperatures [27, 28]. Consequently, the thermal conductivity will be lower than for standard oxide fuels. Composite oxide fuels, where the matrix provides heat conduction is however a relevant option. The host phase may be either ceramic (cercer) or metallic (cermet).

Several ceramic matrices with high thermal conductivity have been investigated, like MgO and MgAl₂O₄ (spinel). Low temperature irradiation tests of AmO_{2-x} micro-dispersed in spinel have however shown that this matrix is prone to radiation damage [29, 30]. PuO₂-MgO fuels have successfully been irradiated at linear ratings up to 165 kW/m [31]. AmO_{1.6}-MgO targets have been fabricated and are currently under irradiation in Phenix [32]. Some concerns for a possible formation of a low melting eutectic between americium oxide and magnesia were raised [27], but the issue remains to be clarified experimentally.

At first glance, one may consider all metals with high melting temperature as candidates for cermet fuels; the possible choices are however limited by the cross section for neutron absorption of the matrix.

In the present design study, we assume that the Pu-fraction in the actinide vector is 40%, in order to minimise the reactivity swing. It has been shown that 20% burnup of this type of fuel can be achieved with a reactivity swing less than 2000 pcm [13, 33]. Consequently, it will be possible to avoid any fuel shuffling during irradiation, which is an important advantage in liquid metal cooled systems, both for safety and cost. In any case, the content of plutonium in the oxide phase is limited to less than 40% by the solubility of plutonium oxide in

nitric acid. Therefore, we may not compensate a high cross section for absorption in the matrix by increasing the fissile content of the fuel too much.

In a scoping study performed by one of the present authors, it was shown that for a Pu fraction of 40%, the matrix fraction of tungsten and natural molybdenum must be less than 50 volume percent, to achieve a k-eigenvalue of 0.97 in 800 MWth cores with LBE coolant [21]. Tungsten is thus of less interest for application in the present context. Molybdenum, on the other hand, may be enriched in ^{92}Mo , which has a full neutron shell, and hence a lower cross section for neutron absorption.

Among the metallic matrices with high melting temperature that satisfy the matrix volume fraction condition, chromium appears to be most interesting from the neutronic viewpoint, yielding a very low void worth. Recent fabrication tests however indicate that a low melting eutectic may form between Cr and rare earth oxides [34].

Hence two composite oxide fuel candidates remain that fulfill the above listed criteria, one cermet and one cermet:

- $(\text{Pu,Am,Cm})\text{O}_{2-x}\text{-MgO}$
- $(\text{Pu,Am,Cm})\text{O}_{2-x}\text{-}^{92}\text{Mo}$

Irradiation experience of Mo based cermet fuels is limited to $\text{UO}_2\text{-Mo}$ [35]. Pure molybdenum has been irradiated under a wide variety of conditions in the context of fusion, and has shown to exhibit the classical increase of ductile to brittle transition temperature of BCC metals.

B. Nitride fuels

Nitride fuels intrinsically have a high thermal conductivity, but are more complex to fabricate. Nitrogen enriched to 98% in ^{15}N is required for the fabrication, in order to limit production of ^{14}C in the fuel during irradiation [36].

Actinide nitrides unfortunately tend to dissociate into metal and nitrogen at temperatures below their melting point [37, 38]. Especially americium nitride is unstable under sintering conditions [39–42]. Hence, a stabilizing matrix is necessary, and it has been shown that UN in solid solution with ZrN remains stable up to melting [38].

$(\text{Pu,Zr})\text{N}$ has successfully been fabricated by several methods [43, 44]. When performing sintering of $(\text{Pu,Am,Zr})\text{N}$ under inert gas, considerable vapourisation of Am was reported [40]. Such losses may be avoided by sintering under nitrogen [42], and recent sintering tests of $(\text{Am,Zr})\text{N}$ performed at JAERI showed that the losses of Am could be reduced by an order of magnitude [41].

Nitrides are in general more easily soluble in nitric acid than corresponding oxides, and the above mentioned scoping study showed that a molar fraction of

ZrN in excess of 50% can be maintained even for relatively large pin pitches.

$(\text{Pu,Zr})\text{N}$ has been irradiated at low rating (25 kW/m) up to 11% burnup in BOR-60 [45]. Similar ratings are used for JAERI's irradiation of $(\text{Pu,Zr})\text{N}$ in JMTR [43]. Recently irradiation of $(\text{Pu,Am,Zr})\text{N}$ started in ATR [46]. Irradiation of $(\text{Pu,Zr})\text{N}$ at high linear rating (40-50 kW/m) is planned to take place in Studsvik [44].

Other nitride matrices could be considered, like YN and HfN. YN is however extremely hygroscopic, and hafnium nitride has a much higher cross section for absorption than zirconium nitride. The solid solution fuel candidate best suited for application in ADS thus appears to be

- $(\text{Pu,Am,Cm,Zr})^{15}\text{N}$

the main question-mark being loss of clad integrity leading to un-inhibited dissociation of the ceramic phase.

V. METHOD

The core design was made in a series of iterative steps. First, the core power was chosen on the basis of the heat removal capacity of the spallation target and an assumed maximum level of the source multiplication factor. Then, a rough estimation of the maximum linear rating of each fuel was made, based on assessments of the effective thermal conductivity for the three selected fuel candidates. The approximate number of fuel pins in the core was obtained from the ratio of core to pin power, assuming that a radial power peaking factor of 1.3 would be achievable by dividing the core into three fuel zones with different inert matrix fraction. Adopting a spallation target radius of 20 cm, the dimensions of the fuel sub-assembly was fixed by fitting the spallation target into the empty space left by removing 19 central sub-assemblies. For a fixed pin diameter and sub-assembly FTF, only discreet values of P/D are possible. A small pin diameter is preferred in order to provide a short residence time to reach a target burnup of 20%. We decided to study two different values of P/D resulting from the selected pin diameter, each P/D corresponding to a different average inert matrix fraction in the fuel. Finally, the inert matrix fraction in the three fuel zones was adjusted to yield a radial power peaking factor smaller than 1.3, while maintaining a k-eigenvalue of 0.97 at BOL. A more detailed description of each step taken is given below. The resulting core geometry and fuel composition is displayed in Tables VI, VII and VIII.

A. Core power

The thermal power of an ADS is limited by the source strength and multiplication. A heavy liquid metal spallation target would allow for dissipation of a proton

beam power of the order of 10 MW. Lead bismuth eutectic has been selected as the reference material in the ADS programs in Europe, Unites States and Japan. Using a beam window in contact with the molten LBE, the lifetime of the window material however becomes very short [47, 48]. A "windowless" solution, where a cold window is separated by vacuum from a free surface of LBE, appears thus to be the best solution for a high power target. With a windowless design, the heat deposition P_{dep} possible to remove may be estimated from the temperature rise in the molten metal:

$$\Delta T = \frac{P_{\text{dep}}}{\rho C_p \bar{v} A}. \quad (8)$$

For LBE we have $\rho \simeq 10^4 \text{ kg/m}^3$, $C_p \simeq 150 \text{ J/(kg} \times \text{K)}$ and $\bar{v} \leq 2.5 \text{ m/s}$, the velocity being limited by erosion rates of structural material [49]. For long term durability of these components, we would like to keep LBE temperatures below 720 K. Assuming that ΔT should not exceed 100 K and that the effective flow area equals 350 cm^2 , we find that $P_{\text{dep}} \leq 13 \text{ MW}$. As about 50% of the proton beam energy is consumed by the spallation process, this corresponds to a proton beam power of 26 MW. Hence we adopt $P_{\text{beam}}^{\text{max}} = 26 \text{ MW}$ for the present design.

The fission power P_f in the core of an accelerator driven sub-critical system is a function of the proton source efficiency ψ^* [50]:

$$P_f = \langle S_p \rangle \frac{\bar{E}_f}{\bar{v}} \frac{k}{1-k} \psi^* \quad (9)$$

where $S_p = P_{\text{beam}}/E_p$ is the proton current, \bar{E}_f and \bar{v} are the average energy and number of neutrons released in a fission, and k is the k -eigenvalue of the core. Safety considerations will lead us to demand $k \leq 0.97$. With a reactivity loss of 2000 pcm, the maximum proton beam current (at EOL) is inserted for $k \simeq 0.95$. For a proton energy of 1000 MeV, an average fission energy of 200 MeV, and $\bar{v} = 3.0$, we thus get at EOL

$$P_f \simeq P_{\text{beam}} 1.3 \psi^* \quad (10)$$

The LBE cooled cores here studied yield EOL proton source efficiencies of about 25. A maximum beam power of 30 MW then corresponds to a core fission power of 800 MW. We hence fix the core power to 800 MWth for all fuels.

B. Linear Power

Having selected three fuel candidates to be used in detailed design studies, the linear rating of each fuel was assessed. In deeply sub-critical systems, feedbacks are not able to reduce power as they are in critical reactors [51]. Hence, beam over-current accidents may have severe consequences in ADS:s. Further, if the core power

is regulated by adjusting the proton source strength, the possible overpower insertion is given by

$$\Delta P \simeq \frac{1 - k_s^{\text{max}}}{1 - k_s^{\text{min}}} \quad (11)$$

where k_s is the source multiplication eigenvalue. If k_s varies between 0.967 and 0.95, an overpower insertion of 50% is theoretically possible. Therefore, one should set the operational rating lower than 2/3 of the maximum permissible power density.

The failure temperatures of americium bearing inert matrix fuels are unfortunately not precisely known. The cercer fuel here studied is expected to undergo eutectic melting. Eutectic melting of $\text{PuO}_2\text{-MgO}$ has been detected at $T = 2530 \pm 30 \text{ K}$ [52], in good agreement with theoretical assessments [53]. Decreasing the oxygen to metal ratio lowers the melting temperature, and $\text{PuO}_{1.61}\text{-MgO}$ melts at $T \simeq 2300 \pm 80 \text{ K}$ [53, 54]. With americium in the fuel, a certain degree of hypo-stoichiometry is mandatory to ensure sufficiently vapour pressure of oxygen at operating temperature. No measurements on the eutectic melting temperature of $\text{AmO}_{2-x}\text{-MgO}$ have been reported. The assessment of Zhang and Konings indicates that the melting temperature would vary between 1930 K for $\text{AmO}_{1.5}\text{-MgO}$ and 2360 K for $\text{AmO}_{1.8}\text{-MgO}$ [27]. The $(\text{Pu,Am})\text{O}_{2-x}\text{-MgO}$ fuel of interest in the present context will be fabricated with $x \simeq 0.10$ [55]. Judging from the data for its components, we adopt a failure temperature of $2300 \pm 100 \text{ K}$ for this composite fuel.

Concerning the molybdenum based cermet, the failure temperature may be identified with the melting temperature of the oxide inclusions. As in the case of the cercer, these will be hypostoichiometric, lowering their melting temperature. Using Vegard's law, the melting point of $(\text{Pu}_{0.4}\text{,Am}_{0.5}\text{,Cm}_{0.1})\text{O}_{1.9}$ is estimated to 2640 K.

In the case of the nitride, it is known that AmN dissociates in inert gas atmosphere when temperatures exceed 1600 K [40]. In a closed volume, the nitrogen pressure buildup will however stabilise the solid phase [41, 42]. At $T = 2200 \text{ K}$, the vapour pressure of americium in a fuel pin is negligible and there should be little concern about material transport to cold spots [12, 42]. Although the fuel most likely could survive transients to higher temperature, we use 2200 K at upper limit for the nitride in the present study.

In order to arrive at an operative rating for the three fuels, we need to make assumptions about clad temperature, gap conductance and fuel thermal conductivity.

An upper limit for the clad outer temperature is set by LBE corrosion rates. Using oxygen control techniques, the performance of austenitic stainless steels seems to be satisfactory up to 820 K [56, 57]. Ferritic steels with high silicon content developed in Russia feature good corrosion resistance up to 870-890 K [58]. Ferritic steels unfortunately have poorer mechanical properties under transient conditions [59, 60]. Standard stainless steels

(e.g. SS316) on the other hand have a low incubation threshold for swelling. Austenitics with composition especially tailored for high radiation resistance were therefore developed in the fast reactor programs, and Si-modified 15-15Ti have been shown to withstand doses up to 150 DPA. We therefore select Si-modified 15-15Ti as reference material, leading to an upper temperature limit of the clad equal to 820 K.

The biggest uncertainty in the fuel temperature calculation at BOL is the gap conductance. While the contribution from heat conduction in helium for a well defined open gap can be calculated with a small error, radiative contributions may be of significance. In Fig. 2, temperature gradients over the gap resulting from neglecting radiative heat transport and surface roughness are plotted as function of radial gap size and linear power.

In the absence of thermo-mechanical calculations of pellet-clad mechanical interaction, we adopt a hot radial gap of 50 microns at BOL for the oxide cercer and the nitride fuel. In the case of cermet fuel a larger initial gap is required to allow for swelling. As the fuel failure temperature is comparatively high, we settle for a radial gap of 100 microns for the cermet.

For the composite fuels, the effective thermal conductivity of a matrix with spherical inclusions having negligible conductivity, was estimated using the standard formula for a material with spherical porosity P :

$$\lambda_{\text{eff}} = \lambda(1 - P)^{3/2} \quad (12)$$

For a matrix volume fraction of 50%, we get $\lambda_{\text{eff}} = 0.35\lambda$.

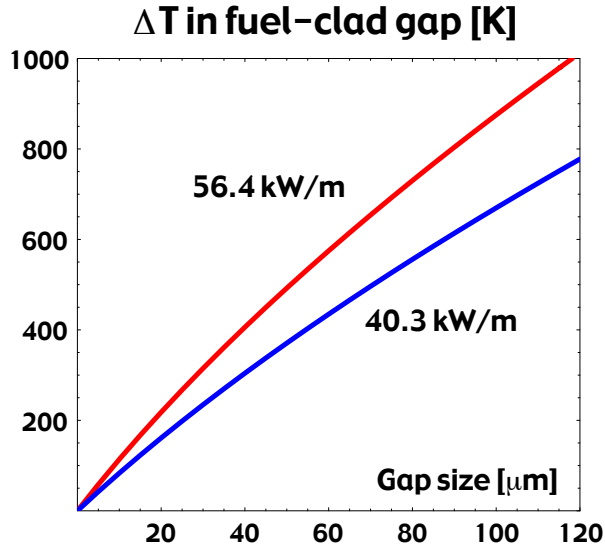


FIG. 2: Temperature gradient in the fuel clad gap as function of radial gap size, for a pellet diameter of 4.9 mm. Radiative contributions to heat transport are neglected.

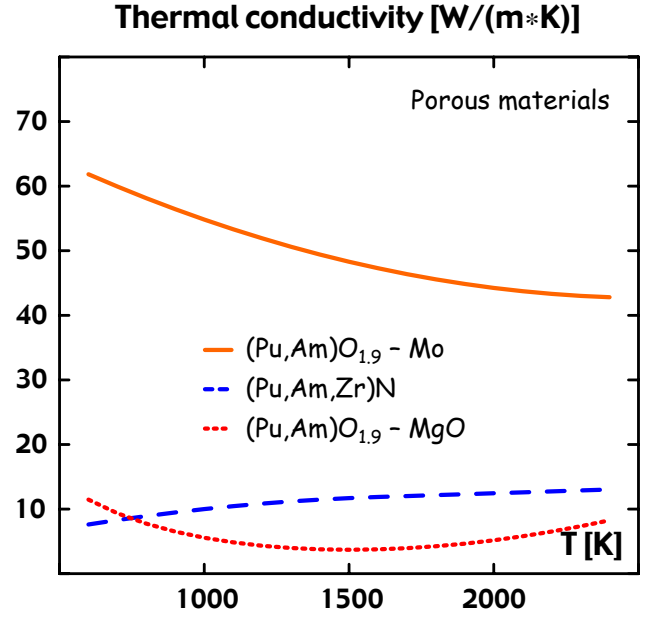


FIG. 3: Effective thermal conductivity for the three inert matrix fuels here investigated. The porosity of the ceramic phase was assumed to be 5% for the Cercer fuel, 10% for the Cermet and 15% for the nitride.

The metallic matrix in the Cermet fuel will be 100% dense. For magnesia, we assume that a density of 95% TD is possible to achieve. For the nitride fuel, a porosity of 15% was adopted to allow for solid fission product swelling. The resulting effective conductivity in a fuel pin with 50 volume percent inert matrix is displayed in Fig. 3, for each of the fuel candidates.

From the above data, the temperature gradient ΔT_{fuel} over a solid fuel pellet as function of linear rating can be evaluated in terms of the conductivity integral. If we make the rough approximation that temperature gradients scale linearly with power, we may set the condition that the temperature difference between coolant inlet and fuel temperature during normal operation should be less than 2/3 of the allowed difference during a transient. Doing so, we may estimate an upper limit for the linear power during normal operation. With an inlet coolant temperature of 570 K, this limit becomes 1660 K for the nitride fuel, 1730 K for the cercer and 1950 K for the cermet fuel. In table V linear ratings yielding these steady state temperatures for fuels with 50 volume percent inert matrix fraction are tabulated. With a total power peaking factor of 1.6, these number correspond to average pin powers of 24, 36 and 40 kW/m.

More detailed temperature calculations, including transient performance, will be provided in a forthcoming paper [12].

TABLE V: BOL fuel temperatures at core mid-plane for the maximum linear ratings of the fuels here investigated. A coolant inlet temperature of 570 K. was assumed. For the nitride and cermet fuels a clad outer diameter of 5.7 mm and $P/D = 1.75$ was used. For the Cercec fuel 6.8 mm and $P/D = 1.50$ was adopted. Temperatures are given in Kelvin, ratings in kW/m .

Fuel type	χ	ΔT_{clad}	ΔT_{gap}	ΔT_{fuel}	T_{max}
Nitride	58	65	495	350	1660
Oxide Cercec	38	45	310	600	1730
Oxide Cermet	65	75	970	145	1950

While the molybdenum based Cermet fuel would appear to be outstanding from the terms of linear rating, it will be evident that this potential cannot be fully utilised in an ADS, as the relatively high neutron absorption cross section of molybdenum cripples the neutron balance. Thus a larger actinide inventory is required in the Cermet core to achieve similar reactivity. In the present study, we therefore adopt identical linear rating for the nitride and the Cermet fuels (35 kW/m core average), letting the margin to melt of the Cermet fuel increase by several hundred degrees.

C. Core geometry

In the present study, we adopt a classical hexagonal fuel bundle geometry. Due to sub-criticality, three fuel zones are required to achieve an acceptable radial power peaking factor, as compared to two zones in a standard FBR. Hence we choose a comparatively small wrapper tube flat to flat (FTF) distance, of the order of 10 cm. 19 central fuel assemblies are removed to make space for the spallation target, having an outer radius of 21 cm. The impact of the proton beam is set to 18 cm above core mid plane to make the axial power profile symmetric, and the radius of beam guide tube is set to 15 cm to allow for spreading of the beam.

In order to reduce the reactivity potential related to core compaction, the fuel pin pitch to diameter ratio (P/D) should ideally be set to the smallest value ensuring sufficient heat removal under transient conditions. As the detailed accident analysis will be presented in another paper [12], we here choose to investigate the neutronic performance for two limiting cases, one *small* pitch ($P/D = 1.50$), expected to yield higher inert matrix fraction and lower void worth [21], and one *large* pitch ($P/D = 1.75$), providing better coolability under design extension conditions [22].

For a fixed linear rating, the burnup rate of the fuel increases with decreasing pellet diameter. Since the fuel residence time is limited by LBE corrosion rates, small pellet diameters are preferable. On the other hand, neutron leakage increases with decreasing pellet radius,

TABLE VI: Core geometry parameters used for the present study. A total core power of 800 MWth is assumed. The higher number of fuel pins in the Cercec core is thus due to the lower linear rating of this fuel. The combination of a large pin diameter with a large pin pitch is not investigated.

Spallation target radius	21 cm
Proton beam impact (relative to mid plane)	18 cm
Beam tube radius	15 cm
Sub-assembly inner flat to flat	96 mm
Sub-assembly outer flat to flat	100 mm
Sub-assembly pitch	102 mm
Pin pitch to diameter ratio	1.50/1.75
Clad outer diameter	5.7/6.8 mm
Clad inner diameter	5.0/6.0 mm
Pins per sub-assembly	91/127
Nitride/Cermet core fuel sub-assemblies	180/246
Nitride/Cermet core fuel pins	22386/22860
Cercec core fuel sub-assemblies	252/348
Cercec core fuel pins	32004/31668
Active core height	100 cm
Upper gas plenum height	100 cm
Lower gas plenum height	50 cm

making it more difficult to meet the requirement of at least 50 volume percent matrix fraction set by fabricability. Especially for oxide fuels, this becomes an issue of concern. Thus, beside making core calculations for a small diameter pellet, we also investigate the case of a larger pellet combined with the smaller P/D .

Since the FTF distance of the sub-assemblies has been fixed by the spallation target radius, only discrete combinations of fuel clad diameters and pin pitches are possible. $D_{\text{clad}} = 5.7 \text{ mm}$ and $D_{\text{clad}} = 6.8 \text{ mm}$ may be combined with the selected P/D ratios for an inner FTF of 96 mm. Assuming that the 15-15Ti clad should be thick enough to withstand an internal gas pressure of 20 MPa at a temperature of 1000 K, the corresponding inner clad diameters become 5.0 mm and 6.0 mm , respectively.

Table VI summarises the geometrical parameter of the cores here investigated. Note that a relatively large gas plenum is present to provide space for release of helium arising from decay of ^{242}Cm .

The radial reflector was assumed to consist of two sub-assembly rows filled with steel pins, cooled by lead bismuth. The LBE fraction in the radial reflector was set to 10 volume percent. In Fig. 4, a core map for the nitride/cermet configuration with 246 sub-assemblies is displayed.

VI. COMPUTATIONAL MODEL

Beginning of life (BOL) core calculations were made with the continuous energy Monte Carlo code

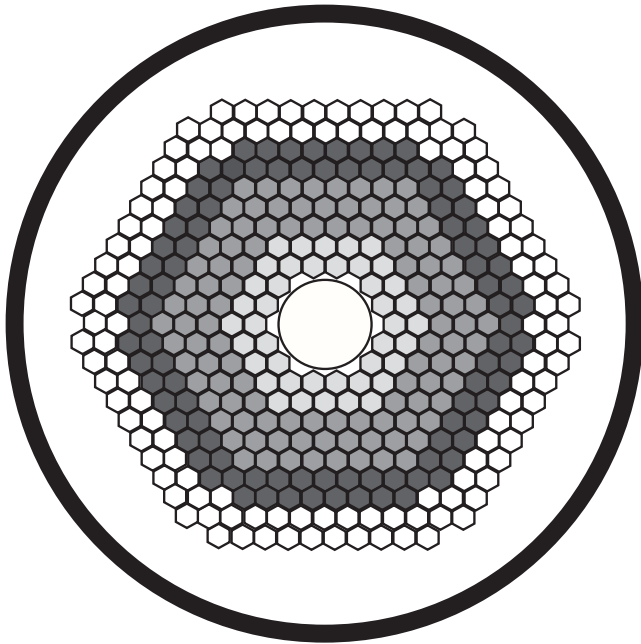


FIG. 4: Example of core map with 246 sub-assemblies for the cermet and nitride cores here studied. Around the central spallation target, the three fuel zones are distinguished by different shades of grey. Outside of the fuel, two sub-assembly rows filled with steel pins function as radial shield/reflector.

MCNP4C, using the JEF2.2 nuclear data library. Fully three dimensional, pin by pin models were constructed. The plutonium, americium and curium vectors used are shown in Table VII. The Pu vector is that of spent light water reactor MOX fuel after seven years of cooling. The higher actinide vectors represent a mixture of Am and Cm deriving from spent UOX and MOX fuel.

The relative fractions of Am and Cm was set to 5/1, corresponding to their concentration in spent LWR fuel. The plutonium fraction in these start-up cores was set to 40% in order to minimise the burnup reactivity swing

TABLE VII: Isotope vectors used for the present design study. The Pu vector is that of spent LWR MOX fuel after seven years of cooling. The higher actinide vectors represent a mixture of Am and Cm deriving from spent UOX and MOX fuel.

Nuclide	Atom fraction
^{238}Pu	0.050
^{239}Pu	0.379
^{240}Pu	0.303
^{241}Pu	0.132
^{238}Pu	0.135
^{241}Am	0.666
^{243}Am	0.334
^{244}Cm	0.873
^{245}Cm	0.127

over a large number of irradiation cycles where the plutonium feed comes from spent ADS fuel, starting with the second core load [13].

Burnup simulations of the first irradiation cycle were made using the Monte Carlo burnup code MCB, for cores with $P/D = 1.75$. The accumulation and decay heat of about 300 fission products was taken into explicit account. For source calculations, the high energy particle transport code MCNPX was used to write a neutron source on the surface of the target with a cut-off at 20 MeV, which then was used for neutron transport in MCB. The statistical uncertainty for the major transmutation rates was calculated to be less than 0.1% in each burnup step, indicating less than 1% uncertainty in the final composition averaged over each burnup zone.

VII. RESULTS

Inert matrix volume fraction in the inner, middle and outer fuel zones yielding a radial power peaking factor less than 1.3 at BOL are given in Table VIII.

One may note the following: In the case of the nitride core, all geometries are compatible with an inert matrix fraction above 50 volume percent in all fuel zones. The poorer neutron economy pertaining to the composite oxide fuels results in matrix fractions below this limit with exception for the small pitch, large pin cermet core. Especially the cermet has a too high neutron absorption cross section, in spite of the use of depleted Molybdenum. In the latter case, one would either have to increase the relative concentration of plutonium in the fuel, or increase the actinide inventory in the core. Neither of these solutions are optimal. Increasing the Pu concentration in the feed stream would lead to a larger reactivity swing, which could require the introduction of fuel shuffling to reach the target burnup. The economic penalty related to shuffling of fuel elements in liquid metal cooled reactors is significant. Concerning an increase of fuel inventory, example given by increasing the number of fuel assemblies, the operating power

TABLE VIII: Inert matrix volume fractions yielding a radial power peaking factor less than 1.3 at BOL.

Fuel type	D_{clad} [mm]	P/D	Zone 1	Zone 2	Zone 3
Oxide Cermet	5.7	1.50	0.65	0.58	0.42
	6.8	1.75	0.56	0.51	0.41
Oxide Cermet	5.7	1.50	0.68	0.62	0.52
	6.8	1.50	0.68	0.62	0.52
Oxide Cermet	5.7	1.50	0.54	0.48	0.37
	6.8	1.75	0.47	0.41	0.31
Nitride	5.7	1.50	0.60	0.54	0.45
	6.8	1.50	0.60	0.54	0.45
Nitride	5.7	1.50	0.73	0.67	0.54
	6.8	1.75	0.66	0.61	0.50
Nitride	5.7	1.50	0.76	0.71	0.60
	6.8	1.50	0.76	0.71	0.60

density of the cermet fuel would go down, as the total core power is limited by the source strength. An even higher margin to failure would result, but also a longer residence time. The ultimate limit for the fuel burnup would then be set by corrosion damage to the clad, rather than by irradiation induced swelling. These conclusions are however preliminary, as the absorption cross section of molybdenum appears to differ significantly from one evaluation to the other.

A. Power profiles

In Fig. 5, the radial power profile for the nitride core with small pins and large pitch is shown. The number of sub-assembly rows in each fuel zone was set to minimise the difference in power between adjacent assemblies on the interface between the fuel zones. Between zone two and three, twenty percent difference in power density remains, which roughly translates into forty degrees temperature difference between neighbouring hot and cold channels. Thermal striping should thus not be an issue. The axial peaking factor remains modest (less than 1.22), thanks to the better reflective properties of LBE, as compared to sodium.

B. Safety parameters

Neutronic safety parameters calculated for each of the core configurations are tabulated in Table IX. The coolant core void worth W_{core} was calculated by removing the

coolant from the active zone only, while the total void worth W_{tot} was calculated by removing the coolant from the active zone and the upper plenum. As expected, the effective delayed neutron fraction is very small. If these cores were to be operated in a critical mode, they would be extremely sensitive to any reactivity perturbation. Example given, the coolant void worths vary between 15 and 25 dollars, which may be compared to the upper limit of 3-4 dollars usually considered to be appropriate for critical sodium cooled reactors. Judging from the quoted numbers only, it would appear that a sub-criticality margin of 3000 pcm is sufficient to ensure that the cores could not go prompt critical, as long as the coolant density in the plenum is reduced proportionally to the density in the active zone. However, a localised void, potentially arising from introduction of gas bubbles into the core, could yield a reactivity insertion in excess of 3000 pcm, especially in the case of the oxide cercer fuel. Here, one should keep mind that the nuclear data libraries yield significantly different values of LBE void worths, mainly due to differences in the inelastic scattering of lead [61]. The ENDF/B-VI evaluation, for instance, yield about 1000 pcm higher void worths for the present cases.

The variation of β_{eff} between different core configurations appears to be insignificant, considering the estimated statistical uncertainty. Neutron generation times are slightly larger than typically found for classical FBRs, which may be attributed to the larger pin pitch.

The coolant and fuel temperature coefficients are of much less significance in a sub-critical system than in a critical reactor [51]. Still, they might play a role to mitigate excursions into the prompt critical regime. Table X gives core averaged values for coolant and fuel expansion coefficients for each of the configurations here studied. The coolant expansion was calculated assuming a uniform temperature rise in the active zone and upper plenum. The fuel grid radial expansion coefficient was calculated by increasing pin P/D and the sub-

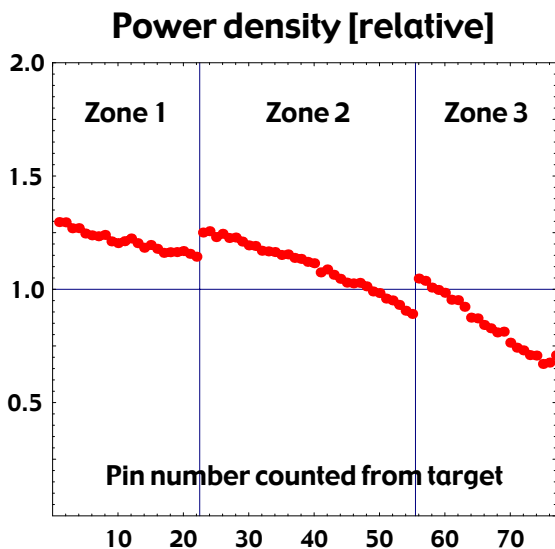


FIG. 5: Radial power profile (relative to the average pin power) in the nitride core with small pin diameter and large pitch. Each point corresponds to a single fuel pin. The radial peaking factor equals 1.29.

TABLE IX: BOL neutronic safety parameters. Delayed neutron fractions and void worths are given in pcm, neutron generation times in μs . The estimated uncertainty arising from the Monte Carlo procedure is ± 15 pcm for the delayed neutron fractions and ± 25 pcm for the void worths.

Fuel	D_{clad}	P/D	β	β_{eff}	Λ	W_{core}	W_{tot}
Cercer	5.7	1.50	250	180	0.65	4060	1790
	5.7	1.75	250	190	0.81	5300	2300
	6.8	1.50	250	190	0.76	4570	2250
Cermet	5.7	1.50	240	170	0.50	2460	220
	5.7	1.75	230	180	0.67	3580	470
	6.8	1.50	270	190	0.60	2990	520
Nitride	5.7	1.50	280	180	0.55	2960	680
	5.7	1.75	240	180	0.71	4150	880
	6.8	1.50	260	170	0.67	3610	1080

TABLE X: BOL temperature coefficients of coolant, fuel and grid, given in pcm/K . The fuel Doppler coefficient was estimated to be negligible (i.e. less than 0.05 pcm/K) for all core configurations. The estimated uncertainty arising from the Monte Carlo procedure is ± 0.02 pcm/K.

Fuel	D_{clad}	P/D	$(\frac{\Delta k}{\Delta T})_{\text{LBE}}$	$(\frac{\Delta k}{\Delta T})_{\text{fuel}}^{\text{axial}}$	$(\frac{\Delta k}{\Delta T})_{\text{grid}}^{\text{radial}}$
Cercer	5.7	1.50	+0.43	-0.28	-0.94
	5.7	1.75	+0.59	-0.28	-0.99
	6.8	1.50	+0.53	-0.26	-0.97
Cermet	5.7	1.50	+0.32	-0.18	-0.97
	5.7	1.75	+0.46	-0.17	-1.04
	6.8	1.50	+0.36	-0.18	-1.05
Nitride	5.7	1.50	+0.35	-0.25	-1.01
	5.7	1.75	+0.50	-0.24	-1.11
	6.8	1.50	+0.42	-0.23	-0.99

assembly FTF and pitch uniformly. As expected, the coolant temperature coefficient increases with increasing coolant volume fraction. Still the calculated LBE expansion reactivity coefficient is significantly smaller for all pitches than corresponding sodium expansion coefficients, approaching +2 pcm/K even for small pitches, as shown in Table II. The fuel axial expansion coefficient is smallest for the cermet fuel, due to the relatively small thermal expansion coefficient of metallic molybdenum. The fuel grid radial expansion coefficient has a magnitude similar to that of critical cores, as expected.

C. Burnup simulations

Table XI compares the accumulated burnup, higher actinide transmutation rate, damage fluence, reactivity loss and proton beam power after 300 full power days for the three different fuels. The spread in burnup is less than one might expect from the variation in linear rating. This can be attributed to the different inert matrix fractions and light atom content, leading to roughly equal actinide inventories in the three cores.

TABLE XI: Burnup characteristics after 300 EFPD for cores with outer clad diameter of 5.7 mm and P/D = 1.75. The burnup B is given in percent TRU. The higher actinide transmutation rate $R_{\text{Am+Cm}} = \Delta M_{\text{Am+Cm}} / \Delta M_{\text{TRU}}$ is given relative to the TRU consumption of the core. The damage fluence F_{dam} is estimated for the most exposed pin.

Fuel	B [%]	$R_{\text{Am+Cm}}$	F_{dam} [m^{-2}]	$\Delta k/B$	P_{beam}
Cercer	9.1	0.77	1.2×10^{27}	-70 pcm/%	16 MW
Cermet	9.3	0.82	1.7×10^{27}	-290 pcm/%	25 MW
Nitride	9.6	0.81	1.6×10^{27}	-250 pcm/%	23 MW

The higher actinide transmutation rate $R_{\text{Am+Cm}} = \Delta M_{\text{Am+Cm}} / \Delta M_{\text{TRU}}$ equals about 80%, being slightly higher for cores with harder spectrum. In terms of mass, the cores are capable of transmuted 265-285 kg higher actinides per $GWth \times y$, which may be compared to the theoretical maximum of 345 kg per $GWth \times y$. Assuming a capacity factor of 80%, 14-15 of these cores may then consume the entire higher actinide production of the 130 GWe European LWR park, being about 2.5 tons per year (after four years of cooling). The corresponding fraction of nuclear electricity produced in the accelerator driven reactors would be about three percent.

Note the lower damage fluence of the cercer core. The reason is the considerably softer spectrum of this oxygen rich core, also being reflected in a remarkably small reactivity loss. At BOL, the number averaged neutron energy in zone 2 of the cercer core is 115 keV, which may be compared with 169 keV for the nitride and 187 keV for cermet core. The corresponding fission probabilities of ^{243}Am are 13, 17 and 20%, respectively. Consequently, the curium build-up in the magnesia supported oxide fuel is larger, leading to higher heat loads.

Assuming a damage fluence limit for 15-15Ti of $3.2 \times 10^{27} n/m^2$, the core averaged dose limitation to burnup for the cercer fuel would be about 25 %, even without fuel shuffling. The corresponding limits for the nitride and cermet fuels are 19% and 18%, respectively. The ultimate limitation to burnup may however be corrosion damage rather than radiation damage. With typical LBE corrosion damage rates of 20 microns per year [56, 57], more than 10% of the clad thickness would be oxidised after 700 full power days. It remains to be seen whether this is acceptable or not.

The reactivity loss for cercer core may remain within 1500 pcm for 20% burnup. The concomitant increase in proton beam power would in this case remain below 50%. For the other fuels the reactivity swing and increase in proton beam power becomes too large when the burnup exceeds 10%. It is however known that the reactivity swing is reduced in consecutive core loads, as to the poorer Pu quality of recycled ADS fuel comes into play [13]. Hence it should be possible to reach 20% burnup with a source strength increase less than 50% also for the cermet and the nitride cores, starting from the second core load.

VIII. CONCLUSIONS

We have presented detailed neutronic studies of lead-bismuth cooled, sub-critical minor actinide burners with different inert matrix ceramic fuels. Assuming an TRU composition with 40% Pu in the initial load, higher actinide transmutation rates of 265-285 kg per $GWth \times y$ are obtained, being about 80% of the theoretical maximum. The fraction of nuclear power that has to be produced in such cores in order to fission the entire higher actinide production from present LWR fleets is about

three percent.

The reactivity swing for the initial load varies between 70 and 300 pcm per percent burnup. The smallest reactivity loss was provided by the magnesium oxide based cermet fuel, which also featured the softest spectrum and lowest damage rate.

Among neutronic safety indicators, the coolant void worth proves to be the most delicate issue. Even though coolant boiling is virtually excluded in LBE cooled systems, fission and helium gas release or steam blow down from failing heat exchangers may lead to void formation in cores of the present type. In this case, the cermet fuel exhibits the least benign characteristics, with core and upper plenum combined void worth exceeding 2000 pcm due to a combination of softer spectrum and larger core size. Recently we have shown that such void worths may produce a sharp power increase followed by fuel failure within a few seconds after an introduction of a gas bubble through the core, even if the core remains sub-critical [12]. The bubble scenario is also the main reason why these cores should not be operated in a critical mode, even though they fulfill the A-B-C criteria (5,6 & 7). A conventional FBR with a nominal Doppler feedback around -0.5 pcm/K is designed to avoid superprompt criticality for a boiling initiator, delivering reactivity ramp rates in the neighbourhood of $1\$/s$ to $5\$/s$ [62]. Thus it appears that a prompt temperature feedback coefficient of less than -0.2 pcm/K is not sufficient to avoid a prompt super-excursion for ramp rates exceeding $10\$/s$. Reactivity potentials of such magnitude

violate the NRC requirement that the reactor core and associated coolant systems should be designed so that in the power operating range the net effect of the prompt inherent nuclear feedback characteristics tends to compensate for a rapid increase in reactivity [63].

The nitride and the cermet cores are more stable with respect to coolant void formation. The poorer neutron economy of the composite oxide fuels makes it however difficult to combine an inert matrix volume fraction exceeding 50 volume percent with the suggested plutonium concentration (40% of actinides) for the molybdenum based cermet. Since fabrication of composite fuel requires an inert matrix fraction of at least 50 volume percent, a higher plutonium fraction may be required for the cermet, leading to larger reactivity losses and lower performance in terms of actinide burning rates.

The nitride core yields high actinide burning rates, low void worths and acceptable reactivity losses.

IX. ACKNOWLEDGEMENTS

The authors would like to thank P. Smith and J. Cahalan for fruitful discussions and advice, and W. Gudowski for providing cross section libraries in MCNP format. Financial support from SKB and the European Commission CONFIRM and FUTURE projects is acknowledged.

-
- [1] A roadmap for developing accelerator transmutation of waste (ATW) technology: A report to congress, US DOE, 1999.
- [2] M. Delpech. The Am and Cm transmutation, physics and feasibility. In *Proc. Int. Conf. Future Nuclear Systems, GLOBAL 99*. American Nuclear Society, 1999.
- [3] J. Tommasi, M. Delpech, J-P. Grouiller, and A. Zaetta. Long-lived waste transmutation in reactors. *Nucl. Tech.*, 111:133, 1995.
- [4] D.G. Foster, editor. Review of PNL study on transmutation processing of high level waste. Technical Report LA-UR-74-74, Los Alamos Scientific Laboratory, 1974.
- [5] H. Murata and T. Mukaiyama. Fission reactor studies in view of reactor waste programs. *Atomkernenergie-Kerntechnik*, 45:23, 1984.
- [6] T. Takizuka, I. Kanno, H. Takada, T. Ogawa, T. Nishida, and Y. Kaneko. A study on incineration target system. In *Proc. 5th Int. Conf. Emerging Nuclear Energy Systems, ICENES 89*, page 70. World Scientific, 1989.
- [7] M. Salvatores, I. Slessarev, G. Ritter, P. Fougeras, A. Tchistiakov, G. Youinou, and A. Zaetta. Long-lived radioactive waste transmutation and the role of accelerator driven (hybrid) systems. *Nucl. Inst. Meth. A*, 414:5, 1998.
- [8] C. Rubbia. Fast neutron incineration in the energy amplifier as alternative to geologic storage. Technical Report LHC/97-01 (EET), CERN, 1997.
- [9] K. Tsujimoto, T. Sasa, K. Nishihara, T. Takizuka, and H. Takano. Accelerator-driven system for transmutation of high-level waste *Prog. Nucl. Energy.*, 37:339, 2000.
- [10] J. Wallenius, K. Tucek, J. Carlsson, and W. Gudowski. Application of burnable absorbers in an accelerator driven system. *Nucl. Sci. Eng.*, 137:96, 2001.
- [11] W. Yang and H. Khalil. Blanket design studies of a lead-bismuth eutectic-cooled accelerator transmutation of waste system. *Nucl. Tech.*, 135:162, 2001.
- [12] M. Eriksson, J. Wallenius, M. Jolkkonen, and J.E. Cahalan. Safety properties of minor actinide bearing inert matrix fuels. *Nucl. Tech.*, 2005. accepted for publication.
- [13] K. Tsujimoto, T. Sasa, K. Nishihara, H. Oigawa, and H. Takano. Neutronics design for lead-bismuth cooled accelerator-driven system for transmutation of minor actinides. *J. Nucl. Sci. Tech.*, 41:21, 2004.
- [14] D.C. Wade and E.K. Fujita. Trends Versus Reactor Size of Passive Reactivity Shutdown and Control Performance. *Nucl. Sci. Eng.*, 103:182, 1989.
- [15] T.H. Bauer, G.R. Fenske, and J.M. Kramer. Cladding failure margin for metallic fuel in the integral fast reactor. In *9th Int. Conf. on structural mechanics in reactor technology*, volume C, 1987.
- [16] R.J. Puigh and M.L. Hamilton. In *Influence of Radiation on Materials Properties: 13th Int. Symposium, ASTM STP*, volume 956. ASTM, 1987.
- [17] Y.S. Tang. *Thermal analysis of liquid metal fast breeder reactors*. ANS, 1978.

- [18] M.A. Smith, E.E. Morris, and R.N. Hill. Physics and safety studies of low conversion ratio sodium cooled fast reactors. In *Proc. Int. Conf. Future Nuclear Systems, GLOBAL 03*. American Nuclear Society, 2003.
- [19] D.C. Wade and R.N. Hill. The design rationale of the IFR. *Prog. Nucl. Energy.*, 31:27, 1997.
- [20] A. Waltar and A. Reynolds. *Fast Breeder Reactors*. Pergamon Press, 1981.
- [21] J. Wallenius. Neutronic aspects of inert matrix fuels for application in ADS. *J. Nucl. Mat.*, 320:142, 2003.
- [22] M. Eriksson, J. Wallenius, J. Cahalan, K. Tucek, and W. Gudowski. Safety analysis of Na and Pb-Bi coolants in response to beam instabilities. In *Proc. 3rd Int. workshop on utilisation and reliability of high power proton accelerators, HPPA02*. American Nuclear Society, 2002.
- [23] B. Carluec and P. Anzieu. Proposal for a gas cooled ADS demonstrator. In *Proc. Int. Conf. Accelerator Driven Transmutation Technologies and Application, ADTTA 99*, 1999.
- [24] B.F. Gromov, Yu. S. Belomitcev, E. I. Yefimov, M. P. Leonchuk, P. N. Martinov, Yu. I. Orlov, D. V. Pankratov, Yu. G. Pashkin, G. I. Toshinsky and V. V. Chekunov. Use of lead-bismuth coolant in nuclear reactors and accelerator-driven systems. *Nucl. Eng. Des.*, 173:207, 1997.
- [25] M. K. Meyer. Development and testing of metallic fuels with high minor actinide content. In *Proc. 11th International Conference on Nuclear Engineering, ICONE-11*, 2003.
- [26] G.L. Hofman, L.C. Walters, and T.H. Bauer. Metallic fast reactor fuels. *Prog. Nucl. Energy.*, 31:83, 1997.
- [27] R.J.M. Konings, H. Zhang, M.E. Huntelaar, and E.H.P. Cordfunke. Melting behaviour of oxide systems for heterogeneous transmutation of actinides. III. the system Am-Mg-O. *J. Nucl. Mat.*, 250:88, 1997.
- [28] R.J.M. Konings. Thermochemical and thermophysical properties of curium and its oxides. *J. Nucl. Mat.*, 298:255, 2001.
- [29] F. Klaassen, K. Bakker, R.P.C. Schram, R. Klein Meulekamp, R. Conrad, J. Somers, and R.J.M. Konings. Post irradiation examination of irradiated americium oxide and uranium dioxide in magnesium aluminate spinel. *J. Nucl. Mat.*, 319:108, 2003.
- [30] T. Wiss, R.J.M. Konings, C.T. Walker, and H. Thiele. Microstructure characterisation of irradiated am-containing $MgAl_2O_4$ (EFTTRA-T4). *J. Nucl. Mat.*, 320:85, 2003.
- [31] M.D. Freshley and D.F. Carroll. The irradiation performance of PuO_2/MgO fuel material. In *Trans. Amer. Nucl. Soc.*, volume 6, page 396. ANS, 1963.
- [32] Y. Croixmarie, E. Abonneau, A. Fernandez, R.J.M. Konings, F. Desmouliere, and L. Donnet. Fabrication of transmutation fuels and targets: the ECRIX and CAMIX-COCHIX experience. *J. Nucl. Mat.*, 320:11, 2003.
- [33] P. Smith. Detailed core design of a reference ADT for safety analyses. In S. Pillon, editor, *2nd annual report of the FUTURE project*. CEA, 2004.
- [34] A. Fernandez. Institute of Transuranium Elements, Personal communication (2003).
- [35] P. Dehaut. Composite fuel behaviour under and after irradiations. In *Studies on fuels with low fission gas release*. IAEA-TECDOC-970, 1996.
- [36] J. Wallenius and S. Pillon. N-15 requirement for 2nd stratum ADS fuels. In *Proc. ANS Meeting on Accelerator Applications/ Accelerator Driven Transmutation Technology Applications, AccApp/ADTTA01*. ANS, 2001.
- [37] K. Richter and C. Sari. Investigation of the operational limits of uranium-plutonium nitride fuels. *J. Nucl. Mat.*, 184:167, 1991.
- [38] R. Thetford and M. Mignanelli. The chemistry and physics of modelling nitride fuels for transmutation. *J. Nucl. Mat.*, 320:44, 2003.
- [39] T. Ogawa, T. Ohmichi, A. Maeda, Y. Arai, and Y. Suzuki. Vaporization behaviour of (Pu,Am)N. *J. Alloys and Compounds.*, 224:55, 1995.
- [40] R. Margevicius. AFC fuels development update. Technical Report LA-UR-03-0415, Los Alamos National Laboratory, 2003.
- [41] M. Takano, A. Itoh, M. Akabori, K. Minato, and M. Numata. Study on the stability of AmN and (Am,Zr)N. In *Proc. Int. Conf. Future Nuclear Systems, GLOBAL 03*. American Nuclear Society, 2003.
- [42] M. Jolkkonen, M. Streit, and J. Wallenius. Thermochemical modelling of uranium-free nitride fuels. *J. Nucl. Sci. Tech.*, 41, 2004.
- [43] K. Minato, M. Akabori, M. Takano, Y. Arai, K. Nakajima, A. Itoh, and T. Ogawa. Fabrication of nitride fuels for transmutation of minor actinides. *J. Nucl. Mat.*, 320:18, 2003.
- [44] J. Wallenius. CONFIRM: status and perspectives. In *Proc. Int. Conf. Future Nuclear Systems, GLOBAL 03*. American Nuclear Society, 2003.
- [45] A. Mayorshin. Irradiation of oxide and nitride fuels in BOR-60. In *Proc. Int. Conf. Future Nuclear Systems, GLOBAL 03*. American Nuclear Society, 2003.
- [46] B. Hilton, S. Hayes, M.K. Meyer, D. Crawford, G.S. Chang, and R.G. Ambrosek. The AFC-1 and AFC-1F irradiation tests of metallic and nitride fuels for actinide transmutation. In *Proc. Int. Conf. Future Nuclear Systems, GLOBAL 03*. American Nuclear Society, 2003.
- [47] Y. Dai, X.J. Dia, and K. Farrell. Mechanical properties of modified 9Cr1Mo (T91) irradiated at 300 C in SINQ target-3. *J. Nucl. Mat.*, 318:192, 2003.
- [48] C. Fazio, R. Stieglitz, J. Knebel, F. Groeschel, W. Wagner, A. Strinning, H. Heyck, Y. Dai, B. Smith, W. Leung, G. Laffont, T. Kirchner, A. Guertin, P. Agostini, D. Gorse, T. Auger, J. Vogt, and A. Al Mazouzi. The MEGA-PIE test project. In *InWor03*. SCK-CEN, 2003.
- [49] N.N. Novikova, Y. Pashkin, and V.V. Chekunov. Some features of sub-critical blankets cooled with lead-bismuth. In *Proc. Int. Conf. on Accelerator Driven Transmutation Technologies and Applications, ADTTA99*, 1999.
- [50] P. Seltborg, J. Wallenius, K. Tucek, and W. Gudowski. Definition and application of proton source efficiency in accelerator driven systems. *Nucl. Sci. Eng.*, 145:390, 2003.
- [51] M. Eriksson and J.E. Cahalan. Inherent shutdown capabilities in accelerator driven systems. *Ann. Nucl. Energy*, 29:1689, 2002.
- [52] A. Hough and J.A.C. Marples. The pseudo binary phase diagrams of PuO_2 with alumina, beryllia and magnesia and the pseudo ternary PuO_2-ThO_2-BeO . *J. Nucl. Mat.*, 15:298, 1965.
- [53] R.J.M. Konings, H. Zhang, M.E. Huntelaar, and E.H.P. Cordfunke. Melting behaviour of oxide systems for heterogeneous transmutation of actinides. I. the systems Pu-Al-O and Pu-Mg-O. *J. Nucl. Mat.*, 249:223, 1997.
- [54] D.F. Carroll. *J. Am. Ceram. Soc.*, 47:650, 1964.
- [55] R. Konings. Institute of Transuranium Elements, Personal communication (2003).
- [56] F. Barbier, G. Benamati, C. Fazio, and A. Rusanov. Compatibility tests of steels in flowing liquid lead-bismuth. *J. Nucl. Mat.*, 295:149, 2001.

- [57] N. Li. Corrosion tests of US steels in lead-bismuth eutectic (LBE). In *Proc. ANS Meeting on Accelerator Applications/ Accelerator Driven Transmutation Technology Applications, AccApp/ADTTA01*. ANS, 2001.
- [58] A. Rusanov. Developing and studying the cladding steels for the fuel elements of NPLs with heavy coolant. In *Heavy liquid metal coolants in Nuclear technology, HLMC98*. IPPE, 1998.
- [59] N.S. Cannon, F.H. Huang, and M.L. Hamilton. Simulated transient behaviour of HT-9 cladding. In *Effects on radiation on materials: 14th Int. Symposium*, volume 2. ASTM STP 1046, 1990.
- [60] N.S. Cannon, F.H. Huang, and M.L. Hamilton. Transient and static mechanical properties of D9 fuel pin cladding and duct material irradiated to high fluence. In *Effects on radiation on materials: 15th Int. Symposium*. ASTM STP 1125, 1992.
- [61] M. Embid, R. Fernandez, and E. Gonzales. In *Proc. 5th Int. Information Exchange Meeting on Actinide and Fission Product Partitioning and Transmutation*. OECD/NEA, 1998.
- [62] J. Cahalan. Argonne National Laboratory, Personal communication (2005).
- [63] NRC general design criterion 11 - reactor inherent protection, appendix a to part 50 - general design criteria for nuclear power plants, 1999.

Paper III

On the Performance of Point Kinetics for the Analysis of Accelerator Driven Systems

M. Eriksson*

Royal Institute of Technology (KTH), AlbaNova University Center,
Dep. Nuclear & Reactor Physics, 10691 Stockholm, Sweden.
and

J. E. Cahalan and W. S. Yang

Argonne National Laboratory, Nuclear Engineering Division,
9700 South Cass Ave., IL 60439, USA.

Accepted *Nuclear Science and Engineering* (2004).

Abstract – *The ability of point kinetics to describe dynamic processes in accelerator-driven systems (ADS) is investigated. Full three-dimensional energy-space-time dependent calculations, coupled with thermal- and hydraulic feedback effects, are performed and used as a standard of comparison. Various transient accident sequences are studied. Calculations are performed in the range of $k_{\text{eff}} = 0.9594$ to 0.9987 , to provide insight into the dependence of the performance on the subcritical level. Numerical experiments are carried out on a minor-actinide loaded and lead-bismuth cooled ADS. It is shown that the point kinetics approximation is capable of providing highly accurate calculations in such systems. The results suggest better precision at lower k_{eff} -levels. It is found that subcritical operation provides features that are favorable from a point kinetics view of application. For example, reduced sensitivity to system reactivity perturbations effectively mitigates any spatial distortions. If a subcritical reactor is subject to a change in the strength of the external source, or a change in reactivity within the subcritical range, the neutron population will adjust to a new stationary level. Therefore, within the normal range of operation, the power predicted by the point kinetics method and the associated error in comparison with the exact solution tends to approach an essentially bounded value. It was found that the point kinetics model is likely to underestimate the power rise following a reactivity insertion in an ADS, which is similar to the behavior in critical systems.*

I. INTRODUCTION

In recent years, there has been an increasing interest in the application of accelerator-driven systems (ADS) for the purpose of incinerating long-lived radionuclides in high-level waste. The ADS is a non-self-sustaining, subcritical reactor driven by an external neutron source that is maintained by a charged-particle accelerator. Appropriate neutron kinetics models are required for predicting the consequences of operational disturbances and accidents in these systems. The so-called “point kinetics approximation” is a widely used method for performing preliminary analyses of dynamic phenomena. It has been extensively applied for the transient design analysis of existing reactors and it forms the basis of many transient analysis computational codes. It is based on kinetics theory developed for critical reactor studies. While the utility of the point kinetics methodology for critical reactor analysis is well known, its applicability to source-driven

subcritical systems is subject to investigation¹. Because the neutron balance equations that describe the response in source-driven reactors are fundamentally different from the problem characterizing critical reactors, it has been suggested² that the point kinetics technique may be inappropriate for ADS studies; it is nonetheless very popular and often used for analysing such systems.

In the present paper, we investigate the precision of the point model in its application to ADS in some more detail. The objective is to estimate the magnitude of the errors encountered in the analysis of certain accidents under physically realistic conditions, i.e., including thermal- and hydraulic feedbacks. The basic approach is by comparison with an “exact” numerical solution. Results are obtained as function of the subcritical level. First, we make a short review of point kinetics theory and discuss its implications in a source-driven, subcritical operating mode. We then describe the test models and the computational techniques involved in the study. Problems and results are then summarized, followed by a brief conclusion in the last section.

*E-mail: marcus@neutron.kth.se

II. REACTOR KINETICS EQUATIONS

In this section, we review shortly the derivation of the conventional kinetics equations. These were first derived by Henry³. Their limitations and capabilities for critical reactor analysis have been investigated in great detail^{4,6}. The derivation is presented here to serve as a basis for discussion of applications to source-driven systems. For convenience, the derivation proceeds along the lines suggested by Henry⁷ with minor modification. An independent source term is incorporated to include neutrons supplied by the external source. The starting-point is the time-dependent continuous energy diffusion equation^a. In shorthand operator notation it can be written as:

$$\frac{1}{v} \frac{\partial \Phi}{\partial t} = (\mathbf{F}_p - \mathbf{M})\Phi + \sum_k \lambda_k C_k \chi_{dk} + S \quad (1a)$$

and completed with the balance equation for the delayed-neutron precursors

$$\frac{\partial C_k}{\partial t} = -\lambda_k C_k + \int_0^\infty v_{dk} \Sigma_f(\mathbf{r}, E', t) \phi(\mathbf{r}, E', t) dE' \quad (1b)$$

$\Phi = \phi(\mathbf{r}, E, t)$ is the time-dependent neutron flux. For simplicity of notation, the functional dependence in Eq (1a) and (1b) has been suppressed. \mathbf{M} and \mathbf{F}_p are the usual “migration and loss operator” and the “prompt neutron production operator”, respectively. These correspond to:

$$\mathbf{F}_p \Phi = \chi_p(E) \int_0^\infty v_p \Sigma_f(\mathbf{r}, E', t) \phi(\mathbf{r}, E', t) dE'$$

$$\mathbf{M}\Phi = -\nabla \cdot D(\mathbf{r}, E, t) \nabla \phi(\mathbf{r}, E, t) + \Sigma_t(\mathbf{r}, E, t) \phi(\mathbf{r}, E, t) - \int_0^\infty \Sigma_s(\mathbf{r}, E' \rightarrow E, t) \phi(\mathbf{r}, E', t) dE'$$

The purpose behind the formulation of the kinetics equations is to derive a lumped model that describes the change in the average level of the flux, i.e., the integral of $\phi(\mathbf{r}, E, t)$ over the energy and the spatial domain. For that reason, the neutron flux is factorized in the form $\phi(\mathbf{r}, E, t) = p(t) \cdot \psi(\mathbf{r}, E, t)$. It is noted that flux factorization is not an approximation, in contrast to separation of variables. In the former case, the neutron spatial and energy distributions may still depend on time. However, it is necessary to impose a constraint condition to define precisely the two new functions, $p(t)$ and $\psi(\mathbf{r}, E, t)$, that arise in the factorization procedure:

$$\int_V \int_0^\infty \frac{w(\mathbf{r}, E) \psi(\mathbf{r}, E, t)}{v(E)} dEdV = 1 \quad (2)$$

The constraint condition states that the shape function, $\psi(\mathbf{r}, E, t)$, is normalized, for all t , in such a manner that the integral, Eq. (2), over all energy and space is held constant (normally taken as unity) in time. Prior to integration over space and energy, Eq. (1a) and (1b) is multiplied with a weight function, $w(\mathbf{r}, E)$. Introducing a weight function is not a requirement, but it allows manipulation of the kinetics equations in a way that simplifying assumptions (such as the point kinetics approximation) can be applied more effectively. It is emphasized, that the weight function can be any function that is defined over the same energy and spatial domain as the flux. To preserve generality, the following derivation will not employ a specific weight function.

$p(t)$ is sometimes called the amplitude function and it is defined according to:

$$p(t) = \int_V \int_0^\infty \frac{w(\mathbf{r}, E) \phi(\mathbf{r}, E, t)}{v(E)} dEdV \quad (3)$$

Thus, under the constraint condition given in Eq. (2), $p(t)$ can be represented as in Eq. (3) and hence it is proportional to the total number of neutrons present in the reactor at any time.

Next, Eq. (1a) and (1b) are multiplied with the weight function and the neutron flux is substituted with the factorized functions. The equations are then integrated with respect to space and energy. After some manipulations, we arrive at the conventional point kinetics equations:

$$\frac{dp(t)}{dt} = \frac{\rho(t) - \beta(t)}{\Lambda(t)} p(t) + \sum_k \lambda_k c_k(t) + s(t) \quad (4a)$$

$$\frac{dc_k(t)}{dt} = \frac{\beta_k(t)}{\Lambda(t)} p(t) - \lambda_k c_k(t) \quad (4b)$$

The new quantities, ρ , β , Λ , s , and c_k that emerge in Eqs. (4) are the integral quantities identified with the following definitions:

$$\beta(t) = \sum_k \beta_k(t)$$

$$\beta_k(t) = \frac{1}{F(t)} \int \int w \sum_k \mathbf{F}_{dk} \psi dEdV$$

$$\rho(t) = \frac{\int \int w(\mathbf{F}_p - \mathbf{M}) \psi dEdV}{F(t)}$$

$$\Lambda(t) = \frac{1}{F(t)} \int \int \frac{w \psi}{v} dEdV$$

$$s(t) = \frac{\int \int w S dEdV}{\int \int \frac{w \psi}{v} dEdV}$$

$$c_k(t) = \frac{\int \int w C_k \chi_{dk} dEdV}{\int \int \frac{w \psi}{v} dEdV}$$

^aIn his original work³, Henry derived the reactor kinetics equations starting from the time dependent neutron transport equation, we chose not to proceed along this path, but rather to utilize the diffusion approach as outlined in his textbook⁷, mainly to be in better accordance with the terms of our computational exercises and to avoid the potential of being misleading. In general, the reactor kinetics equations involve angular dependence and as shown by Henry, the equations may be extended to a transport formulation in a straightforward manner.

The definition of $F(t)$ is:

$$F(t) = \int \int w(\mathbf{F}_p + \sum_k \mathbf{F}_{dk}) \psi dE dV$$

where the delayed neutron production operators \mathbf{F}_{dk} are defined similar to the prompt neutron production operator. It is in the cross sections (that depend on temperature, material density, and composition) in the operators \mathbf{F}_p and \mathbf{M} that thermal and hydraulic feedbacks are accounted for during a transient.

Henry³, called Eqs. (4) the ‘‘conventional kinetics equations’’. Today they are usually referred to as the ‘‘point kinetics equations’’ or sometimes the ‘‘exact point kinetics equations’’ in a way to distinguish them from the simplifying assumptions applied in the point kinetics approximation.

It is stressed that Eqs. (4) are exact and completely equivalent to Eqs. (1), but in a different form. The basic, time-dependent equations, Eqs. (1), are recast into Eqs. (4) without simplifying approximations. Henry⁷ clearly states that as long as the rigorous definitions of the kinetics parameters are used, i.e., the actual time-dependent flux shape is calculated, the solution of Eqs. (4) for $p(t)$ with any arbitrary weighting function will be *exactly* the same as the solution of Eqs. (1) for $\phi(\mathbf{r}, E, t)$ and then the application of Eq. (3). This is true for critical as well as for subcritical systems. The error is introduced when we modify the equations to better cope with an approximate representation of the time-dependent flux shape, e.g., the point kinetics approximation. In that case, the weight function becomes useful because it leaves us with the possibility of freely choosing $w(\mathbf{r}, E)$ in a manner to better suit a point kinetics approximation. Within a perturbation theory approach it is shown⁷ for a critical reactor, that adjoint flux weighting eliminates the influence of first-order flux shape changes on the reactivity, and therefore also reduces the error in the approximation of $p(t)$. Consequently, the estimation for $p(t)$ may tolerate a less precise description of the flux shape. This fact facilitates the use of the initial flux shape throughout the entire transient, i.e., first-order perturbation theory approach. In first-order perturbation theory, the weight function corresponds to the initial adjoint flux, $\Phi_{\lambda_0}^*$, i.e., the solution of the initial adjoint eigenvalue problem:

$$(\mathbf{M}_0^* - \lambda_0 \mathbf{F}_0^*) \Phi_{\lambda_0}^* = 0 \quad (5)$$

Where \mathbf{F}_0^* and \mathbf{M}_0^* are the adjoint operators of the total neutron production operator, $\mathbf{F}_0 = \mathbf{F}_{p0} + \sum_k \mathbf{F}_{dk0}$, and the loss operator \mathbf{M}_0 . In the point kinetics approximation, the basic assumption is that the time dependence is separable from the (\mathbf{r}, E) dependence, i.e., the space-energy flux shape is fixed at all times. For a critical reactor, it permits the use of first-order perturbation theory to calculate the reactivity changes. The neutron balance equation for a reactor with an independent source is mathematically an inhomogeneous problem. In strict terms, separation of variables is not

possible for such cases. Thus, the point kinetics approximation becomes questionable. Moreover, the adjoint flux is not uniquely defined for a source-driven system. This invalidates the use of the standard first-order perturbation formula. The usual procedure for generating a weight function for a source-driven reactor is to employ an artificial initial λ -mode adjoint weighting function, i.e., the solution to the source-free adjoint equation, Eq. (5). As was shown by Ott⁸, the error cancellation property of the first-order perturbation formula is preserved in a source-driven system if the real flux shape is calculated from the initial inhomogeneous problem and not the initial λ -mode shape.

The integral kinetics parameters ρ , β , and Λ arise only in the derivation of lumped models such as the kinetics equations. This is realized since Eqs. (1) do not involve these concepts. It is noted that the point kinetics parameters depend on the weighting function and for that reason their definition is entirely arbitrary. Therefore, the kinetics parameters do not necessarily correspond to any physically meaningful quantities. According to Henry³, the kinetics parameters have a meaningful interpretation only when the reactor is on a constant reactivity level and when the independent source term is negligible in comparison with the fission rate. These conditions are fulfilled automatically in a critical reactor when the time dependence is separable from the (\mathbf{r}, E) dependence. If the weighting function is unity then a clear physical interpretation can be defined. If $w(\mathbf{r}, E) \neq 1$ then the kinetics parameters correspond to some weighted physical value. Using the adjoint flux as weighting function, $w(\mathbf{r}, E) = \phi(\mathbf{r}, E)^*$, has the benefit of producing ‘‘importance’’ weighted kinetics parameters. These can sometimes be interpreted as ‘‘effective’’ values. Since a source-free adjoint weighting function does not correspond to the actual state of a source-driven system the physical meaning of the point kinetics parameters is not clear. However, according to Becker⁹, a complication also arises in a critical system because the weighting function employed in the point kinetics equations is time-independent, nevertheless the adjoint function might change during a transient. In that case, it might not correspond to the actual physical state.

III. TEST MODEL

The model used in the present study is based on a previous OECD/NEA benchmark model¹⁰ with some minor modifications^{b,c}. The original benchmark was not intended as a transient case study, but adopting this system as the basis for the current tests has the benefit that initial static results could be compared with previous studies.

^bThe r - z geometry specification prescribed in the benchmark was converted to a three-dimensional hexagonal- z representation.

^cTo avoid computational artefacts due to the treatment of void regions with a diffusion theory approach, the current model assumes that the coolant fills the full extent of the target and the beam duct region.

The model pertains to an accelerator-driven, lead-bismuth cooled, and minor-actinide loaded transmuter core. The core consists of a central lead-bismuth target region and a homogenized fuel region surrounded by radial and axial reflectors (70% steel and 30% coolant). 114 fuel assemblies are included in the hexagonal-z representation; Fig 1 contains a plan view of a one-sixth symmetry section of the core. The height of the active core is 100 cm. The fuel consists of 2/3 minor actinides and 1/3 plutonium with a ZrN diluent; $(\text{Pu}_{0.1}, \text{MA}_{0.2}, \text{Zr}_{0.7})\text{N}$, where MA represents minor actinides such as Np, Am, and Cm. Fuel compositions correspond to plutonium discharge from UOX-fueled LWRs mixed with MA from a “double strata” strategy¹¹. Start-up core loading is used in the simulations. The fuel is further diluted with 71% ZrN. Core material compositions are summarized in TABLE I. Additional lattice parameters are included in TABLE II.

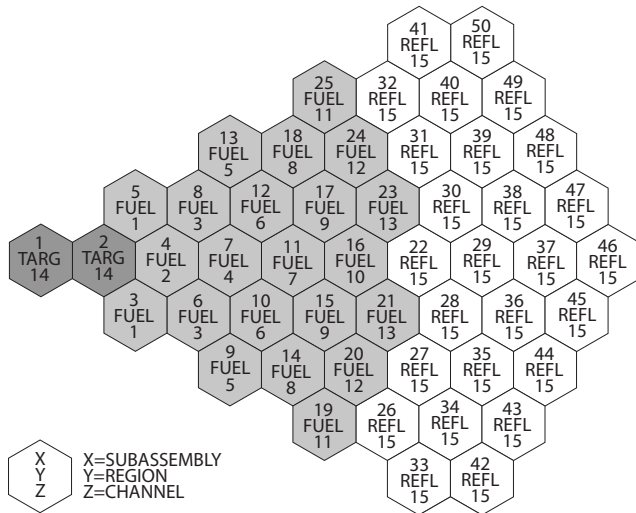


Fig 1. One-Sixth Core Subassembly and Channel Assignment.

TABLE I
Material Specification of the Reference Core Configuration

Core Volume Fractions:	
30 vol%	Fuel
48 vol%	Coolant (Pb/Bi eutectic)
22 vol%	Clad + Structure (stainless steel)
Reflector Volume Fractions:	
30 vol%	Coolant
70 vol%	Stainless Steel
Fuel:	
Fuel Material: $(\text{Pu}_{0.1}, \text{MA}_{0.2}, \text{Zr}_{0.7})\text{N}$	
Theoretical density (300°C): 9.19 g/cm ³	
Fuel smear density: 84 % of theoretical	
68% MA/TRU ratio	
71% molar fraction ZrN	

TABLE II
Lattice parameters

Number of pins per assembly	217
Pitch/diameter ratio	1.6
Pin diameter [mm]	7.366
Cladding thickness [mm]	0.787
Ducts flat-to-flat distance [cm]	15.956

IV. COMPUTATIONAL MODELING TECHNIQUES

Numerical testing was performed with coupled core dynamics calculations using the SAS4A/DIF3D-K¹² code. The “exact” results are obtained from a direct numerical solution of the time-, space-, and energy-dependent multigroup diffusion equation. The direct solution is used as a standard of comparison for the point kinetics solution. One advantage of using the SAS4A/DIF3D-K program for the current task is that the direct solution method and the point kinetics procedure are implemented within the same code. This makes it straightforward to compare the underlying methods without worrying about consistency among different computational procedures and models. For example, the initial steady-state solutions, cross sections, thermal- and hydraulics treatments, and model specifications are all identical.

Thirty-three energy groups are employed in the multi-group treatment. Composition-, temperature- and region-dependent broad group microscopic cross sections were generated based on JEF2.2 data and further processed using the MC²-2¹³ and TWODANT¹⁴ codes. With MC²-2, a homogeneous, ultra-fine group (2082 groups), zero-dimensional spectrum calculation (infinite medium assumption) is first performed for each composition. Individual material microscopic cross sections are reduced to the fine group level (230 groups) by averaging the ultra-fine-group data over the flux and current spectra. Full-core fine group calculations are then carried out with TWODANT. The spectra obtained from TWODANT are used to spatially collapse the fine-group data to a broad group level (33 groups). The broad-group microscopic cross sections are composition-, region- and temperature dependent, i.e., different sets of cross sections for different regions and temperatures (500 K, 980 K, 1580 K, and 2500 K). Local cross sections used in the transient flux calculations are obtained through interpolation in these sets to fit a particular temperature.

Data for delayed neutrons and their precursors were generated based on the ENDF/B-VI library. Delayed neutron data for fissioned curium isotopes was not available in ENDF/B-VI. The missing curium isotopes adopted the delayed neutron yield of ²³⁹Pu.

An external neutron source distribution was supplied in the specification of the benchmark¹⁰. The neutrons are produced by spallation nuclear reactions induced by high-energy protons impinging on a lead-bismuth target. The target has a height of 100 cm and a radius of 20 cm. The

energy of the incident protons is 1 GeV and the beam has a radius of 10 cm. The fine group source (122 groups) is collapsed to a broad group level (33 groups) and the r-z representation was converted to hexagonal-z geometry. The source neutrons are presumed to enter the system at the target meshes. The temporal dependence of the external source intensity enters the SAS4A/DIF3D-K code as one of the system driving functions. For transients involving alterations of the source strength, it is assumed that the neutron spatial and energy distributions are maintained during the transients; i.e., only the magnitude of the external neutron source is adjusted. This is a reasonable assumption since the spatial and energy distributions of the source neutrons depend on the proton beam energy and the target and core configuration, which are fixed during the transients.

The spatial flux solutions are based on a three-dimensional nodal diffusion theory method¹⁵. The core is partitioned into assembly-sized hexagonal unit cells in the horizontal planar direction and axially subdivided into twenty-one axial nodes, each with a mesh spacing of 4.76 cm. In reflector regions, axial mesh sizes of 12.5 cm are employed. The radial distance between the assembly vertical centerlines is 16 cm. The solution takes advantage of one-sixth core symmetry by solving for a single sextant section of the core. Uniform nuclear cross sections are used within each node. In the direct method, the time-dependent component is solved using a fully implicit finite-difference approximation (the DIF3D-K¹⁶ code uses a specified θ -method¹⁷ of time differencing). The theta ($\theta=1$) method consists of representing the time differential operators with their implicit finite-difference formulation. Thermal- and hydraulic calculations are performed for 13 channels, each representative of an average pin within individual subassemblies (See Fig 1 for channel to subassembly assignments). Feedback effects (due to Doppler and coolant density variations) are included as necessary to reproduce the physical situation as closely as possible. Both the direct solution and the point kinetics method account for thermal feedbacks through node-dependent microscopic and macroscopic cross sections. The cross sections are updated with time as local temperatures and densities changes. In the point kinetics solution, the initial flux shape is used throughout the entire transient calculation. Time-dependent point kinetics parameters are computed by means of first-order perturbation theory. The initial flux shape, determined with a given external source distribution, and the initial λ -mode adjoint flux are used along with macroscopic cross sections to compute time-dependent point kinetics parameters, especially the reactivity parameter which reflects the thermal feedbacks. The reactivity is found by summing contributions from local changes in temperature and material densities (as opposed to the use of core-average reactivity coefficients). The adjoint flux is required in the evaluation of the scalar products used in the calculation of the time-dependent kinetics parameters. It corresponds to the initial source-free mathematical nodal adjoint solution¹⁸. The direct solution technique does not

require the formulation of kinetics parameters and adjoint fluxes. The great advantage of the direct solution is that an unambiguous and “exact” solution of the inhomogeneous time-dependent group diffusion equation is obtained, in that sense that no approximations is introduced other than space nodalization and time differencing.

Transient solutions are obtained using a fixed time step size^d of $\Delta t=10$ ms (results for test problems employing smaller time steps suggested that a time increment of 10 ms is adequate for the current set of problems). At the end of each time step, new cross sections are calculated. Heat-transfer and hydraulics time-steps are on separate sub-steps.

V. NUMERICAL RESULTS

Numerical solutions for three different categories of transients were analyzed. The test problems pertain to accident-type events in ADS’s. The first category concerns alterations of the proton beam intensity, i.e., changes in the magnitude of the external neutron source. Secondly, localized reactivity insertions are examined. Finally, a flow reduction event is analyzed. The total power is extracted as a function of time, i.e., fission power plus decay power, as obtained in the direct solution and in the point kinetics solution. The transients are followed for 20.0 seconds.

We further perform calculations at different subcritical levels, i.e., k_{eff} values, to reveal any trends concerning performance characteristics. It will provide information on the numerical accuracy of the point kinetics solution as function of the level of subcriticality. The multiplication constant is altered by changing the concentration of fuel diluents (ZrN), everything else is unchanged, initial k_{eff} values are given in TABLE III. Unless the source strength is adjusted, an increase in k_{eff} would lead to a higher power output. Thus, the intensity of the external source is adjusted to maintain the initial power at 377 MWth. Results from the calculation of the initial effective multiplication constant, shown in TABLE III, proved to be in good agreement with previous results¹⁰.

TABLE III
Initial effective multiplication constant (hot condition)

Case	Fraction ZrN	k_{eff}
Case 1 (ref.)	70.7%	0.9594
Case 2	69.4%	0.9798
Case 3	68.2%	0.9987

^dIt ought to be clarified that the time-dependent flux solution in DIF3D-K employs an automatic time-step selection algorithm, which monitors the rate of change of the fission source and constrains the time-step based on a user-specified value. However, the specified time step was sufficiently small that it prevailed in all test cases.

V.A. Variations in Source Strength

In an ADS, the traditional reactivity based shutdown system is replaced with a beam regulating system that controls the intensity of the external neutron source. The magnitude of the external neutron source is adjusted by changing the proton beam intensity. It is relevant to consider system disturbances in which the source strength suddenly changes. This could for example happen due to a control system failure, accelerator malfunction, or operator error. The first transient is initiated by ramping the source intensity to double strength while keeping the spatial and energy distribution fixed. The ramp is initiated at $t=1$ second and halted at 1.001 seconds. The source is held constant thereafter. The reactor is initially at full power; so the disturbance causes a strong overpower condition. In a second transient, the external source neutrons are completely removed, i.e., a source trip.

Fig 2 and Fig 3, display the results for the source overpowers and the source trip events, respectively. The power responds with a prompt jump followed by a slower adjustment when the delayed neutrons establish a balance with the new flux level. In the source removal transient, the power is reduced to a level determined by fissions induced by delayed neutrons plus the release of decay heat. The fission power dies away faster in cores with larger subcriticality because the multiplication of delayed neutrons is lower. The decay power is given by the fission product inventory and its change requires longer time intervals. The effective delayed neutron fraction is 0.186%. The delayed neutrons typically have a small effect in subcritical reactors²⁰. Note that case 3 ($k_{eff}=0.9987$) is very close to criticality (less than β). Consequently the delayed neutrons are much more influential in that case.

It is seen that the point kinetics method, employing no flux shape recalculations, yields extremely accurate solutions for both the source overpower transient and the source trip transient and at all k_{eff} -levels. In fact, the results are indistinguishable as illustrated in Fig 2 and Fig 3. Numerical performance results are presented in TABLE IV and TABLE V. The maximal deviations are 0.2% and 0.9% for the source overpowers and source trip transients, respectively. Maximum deviation occurs shortly after the source has been fully inserted/removed, followed by better agreement from that point and forward. Deviation from the point kinetics solution is an indication of flux shape changes. The good agreement suggests that spatial effects are less important. Since the only source for spatial distortion is due to reactivity feedbacks, the good agreement implies that these are small and/or distributed such that no noticeable flux deformation develops. The effect of neglecting the system feedbacks is shown in Fig 4. Evidently, the current ADS features inherent positive reactivity feedbacks. This is attributed to a positive coolant density feedback component, characteristic of a minor-actinide loaded reactor operating on a fast neutron spectrum, whereas the Doppler effect is negligible. As a comparison, it is seen that the error of the point kinetics method is much smaller than the error due to the neglect of

thermal feedbacks, even in the deeply subcritical case 2 ($k_{eff}=0.9798$). In the near-critical reactor, this is not so surprising since the feedbacks have a much stronger effect.

The flux shape that develops following a change in the source strength in a subcritical system without feedback is identical to the initial steady-state distribution (except in the case of complete source removal). The adjustment will occur almost instantaneously (within a few tens of prompt periods). A prompt adjustment of the flux shape prevails since the delayed neutrons are less influential; in a critical reactor the delayed neutrons tend to retard the shape transition. Since an external source perturbation, by itself (feedbacks excluded), does not affect the reactivity²¹ the point kinetics results typically become quite accurate. In case strong feedbacks occur, the point kinetics approach may not necessarily provide correct results.

In the source trip transient the feedbacks cause the reactivity to decrease. As shown in TABLE V, the point kinetics method has a tendency to overpredict the negative reactivity insertion in the source trip transient. It also appears as if the numerical performance of the point method is improving slightly as the subcriticality decreases. However, it is difficult to draw any firm conclusions on that behavior; all results are very close together. It could be related to the nature and the interplay of the feedbacks in this particular problem. The source overpower transient does not seem to exhibit the same behavior.

Test calculations confirmed that a time step of 10 ms was adequate suggested by the fact that employing time increments of 1 ms and 0.1 ms provided essentially identical results (not shown).

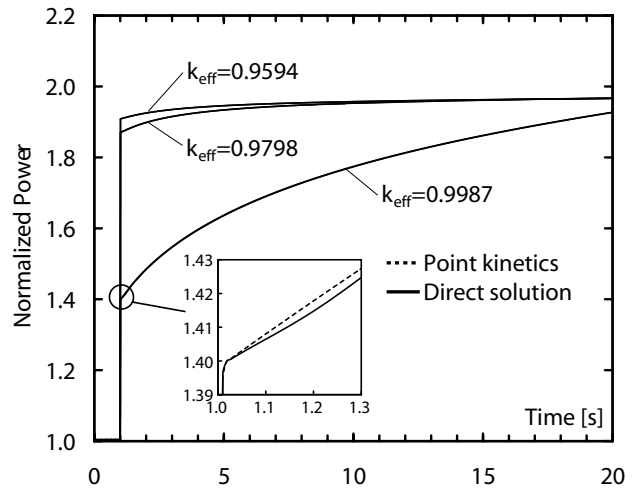


Fig 2. Source overpower transient problem.

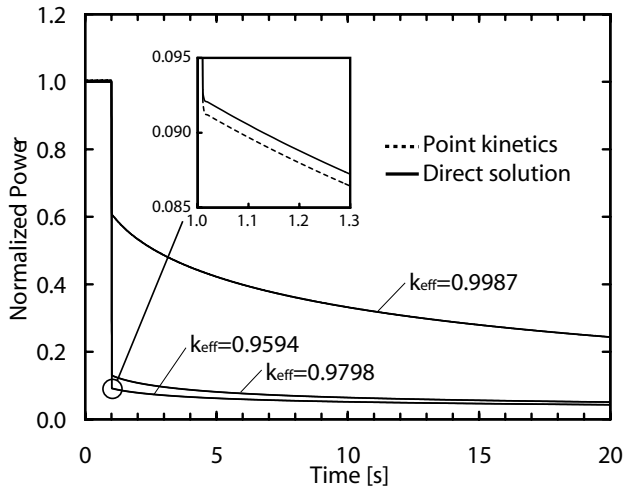


Fig 3. Source trip transient problem.

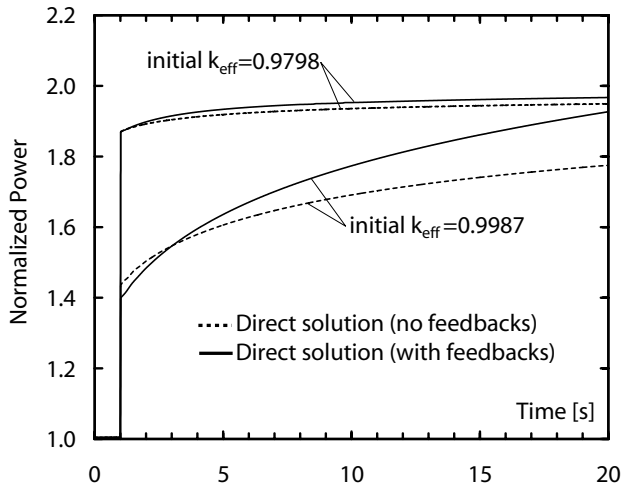


Fig 4. Source overpower transient with and without reactivity feedbacks.

TABLE IV

Comparison of results for the source overpower transient problem^e

Time [s]	Initial $k_{eff}=0.9594$			Initial $k_{eff}=0.9798$			Initial $k_{eff}=0.9987$		
	Direct	PK	ϵ (%)	Direct	PK	ϵ (%)	Direct	PK	ϵ (%)
2.0	1.9245	1.9251	0.03	1.8981	1.8988	0.04	1.4837	1.4853	0.10
5.0	1.9454	1.9458	0.02	1.9336	1.9339	0.01	1.6357	1.6372	0.10
10.0	1.9570	1.9572	0.01	1.9528	1.9530	0.01	1.7734	1.7746	0.06
15.0	1.9626	1.9626	0.00	1.9613	1.9617	0.02	1.8612	1.8620	0.05
20.0	1.9663	1.9662	0.00	1.9671	1.9673	0.01	1.9268	1.9274	0.03
Max deviation (%)		0.05		0.08		0.22			

^eDirect numerical solution (Direct), point kinetics solution (PK), ϵ (%) is relative error in calculated power: $(P_{PK}-P_{direct})/P_{direct}$, max deviation is maximum relative error over a 20 sec. time period.

TABLE V

Comparison of results for the source trip transient problem.

Time [s]	Initial $k_{eff}=0.9594$			Initial $k_{eff}=0.9798$			Initial $k_{eff}=0.9987$		
	Direct	PK	ϵ (%)	Direct	PK	ϵ (%)	Direct	PK	ϵ (%)
2.0	0.0791	0.0784	-0.84	0.1084	0.1077	-0.64	0.5342	0.5337	-0.09
5.0	0.0626	0.0622	-0.68	0.0816	0.0811	-0.60	0.4228	0.4223	-0.11
10.0	0.0521	0.0518	-0.54	0.0647	0.0644	-0.50	0.3323	0.3319	-0.09
15.0	0.0468	0.0466	-0.45	0.0565	0.0562	-0.43	0.2797	0.2797	-0.01
20.0	0.0433	0.0432	-0.40	0.0512	0.0510	-0.39	0.2439	0.2436	-0.11
Max deviation (%)			-0.94			-0.73			-0.36

V.B. Localized Reactivity Insertion

In this section, we consider the effect of local reactivity insertions. It is assumed that a fuel subassembly is fully withdrawn at initial conditions and subsequently drops into the core during operation. Despite the hypothetical nature of this scenario, it is useful for evaluating the performance of the underlying kinetics methods. An idealized model of the subassembly movement is employed, in which the volume fraction of materials representing the control subassembly increases uniformly over its axial distance with time. It is further assumed that the subassembly is inserted in a ramp fashion over a time interval of 1 second. The transient is initiated during operation at full power (the external source strength is initially adjusted so that the steady-state reactor power corresponds to the nominal power).

We investigate the effect of reactivity insertion at two different positions; in one instant we move a subassembly close to core-center (subassembly no. 4 in accordance with Fig 1) and in a second study it is inserted close to the core boundary (subassembly no. 16 in accordance with Fig 1). It is assumed that the region representing the absent subassembly is occupied with coolant at initial conditions. In TABLE VI, the initial k_{eff} -values of the various configurations are shown. The Δk_{eff} given in TABLE VI corresponds to the increase in effective multiplication constant when the subassembly is completely inserted, when thermal feedback effects are not included, i.e. it is the numerical difference in the initial k_{eff} when the core is fully loaded (values tabulated in TABLE III) and for the case when one subassembly is absent from start. It is seen that the reactivity worth of the fuel subassembly near the core-center is approximately 13\$ and 4\$ for the subassembly at the core boundary. It should be noted, however, that starting from normal power and temperature the coolant expansion reactivity coefficient will contribute with some additional reactivity insertion.

TABLE VI

Calculations of the core configurations aimed at studying subassembly movement. Δk_{eff} is the corresponding change in k_{eff} when the subassembly is inserted into the core. The value given in parenthesis is the reactivity insertion quoted in dollars ($1\$\equiv 0.00186$).

Core configuration	Insertion close to core-center		Insertion close to core boundary	
	Initial k_{eff}	Δk_{eff}^f	Initial k_{eff}	Δk_{eff}^f
Case 1	0.9356	+0.0238 (+12.8)	0.9519	+0.0075 (+4.0)
Case 2	0.9558	+0.0240 (+12.9)	0.9722	+0.0076 (+4.1)
Case 3	0.9746	+0.0241 (+13.0)	0.9910	+0.0077 (+4.1)

^fChange in k_{eff} when feedbacks are not taken into account. The amount of reactivity inserted in cases 2 and 3 is slightly higher because of a higher reactivity worth of individual fuel subassemblies.

It is well known, from critical system analysis that for local reactivity insertion events, using the point kinetics technique to calculate the response can lead to significant errors. This is because the basic assumption is that the flux shape remains constant. Comparison with the exact results shows that this is indeed the case. The point approximation severely underestimates the excursion for the case that is closest to the critical state (initial $k_{eff}=0.9746$), shown in Fig 5. However, it is seen that point kinetics is a much better approximation for the deeply subcritical cores, illustrated in Fig 6. In TABLE VII, the relative root-mean-square (*RelRMS*) deviation of the local peak-to-average flux (for all three-dimensional spatial nodes) with respect to the initial distribution is shown. Comparing the *RelRMS* values for the various subcritical test cases provide an indication of the flux spatial distortion sensitivity as function reactor k_{eff} . While the amount of reactivity insertion is essentially the same for all test configurations, the *RelRMS* variation of the flux shape decreases, as the core multiplication constant decreases. Thus, it appears that for a fixed reactivity change the flux spatial distortion decreases when the system is more subcritical. This behavior seems reasonable considering the reduced sensitivity to reactivity inputs in the subcritical state. As the subcritical margin increases, the total (negative) reactivity of the system increases and a given reactivity change will constitute a smaller fraction of the overall reactivity. The net effect is lower reactivity sensitivity as the subcriticality increases. When the fuel subassembly falls into the reactor, the neutron flux increases near this location due to a local increase in the fission rate. In the near-critical reactor, the neutrons are strongly multiplied, and the increase in the fission source produces a local deformation of the flux shape. In a deeply subcritical core, the neutrons are weakly multiplied therefore; the insertion of the subassembly has an overall smaller effect. Due to this lower sensitivity, flux distortions following a reactivity disturbance diminish as the k_{eff} decreases.

In the second problem, the subassembly is inserted at the outer end of the core (subassembly no. 16 according to Fig. 1). Given the lower importance in the outer core regions, the magnitude of the reactivity disturbance is lower. The spatial location of the initiating perturbation is

expected to influence the resulting flux deformation. The point method showed a slight improvement, however, the basic trends were the same, producing better results at lower subcriticality levels. The *RelRMS* deviation in the flux spatial distribution is summarized in TABLE VIII.

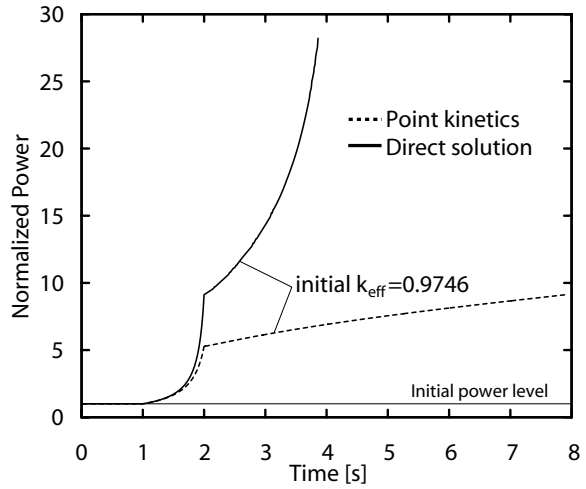


Fig 5. Reactivity insertion near core-center (initial $k_{eff}=0.9746$).

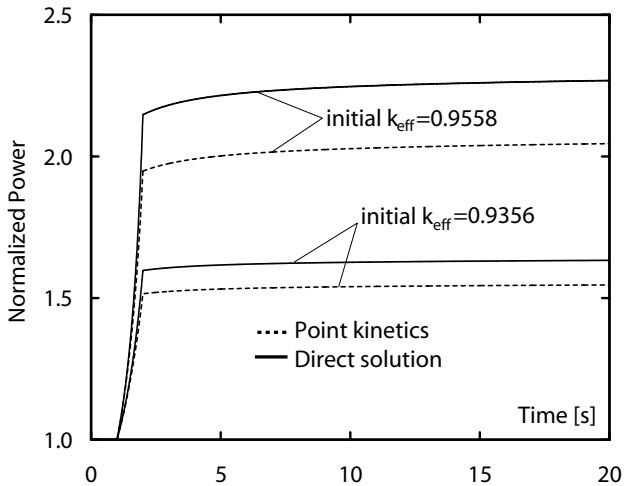


Fig 6. Reactivity insertion near core-center (initial $k_{eff}=0.9356$ and $k_{eff}=0.9558$).

TABLE VII

Relative root-mean-square (*RelRMS*) difference of the peak-to-average flux distribution with respect to the initial flux distribution following insertion of the subassembly near the core-center.

Time [s]	RelRMS ^g peak-to-average flux		
	Initial	Initial	Initial
	$k_{\text{eff}}=0.9356$	$k_{\text{eff}}=0.9558$	$k_{\text{eff}}=0.9746$
1.2	0.9%	1.0%	1.2%
1.4	1.8%	2.2%	2.6%
1.6	2.8%	3.4%	4.1%
1.8	4.0%	4.7%	5.7%
2.0	5.2%	6.2%	7.4%
3.0	5.2%	6.3%	7.8%
20.0	5.4%	6.6%	-

$$^g \text{RelRMS} = \sqrt{\frac{1}{N} \sum_{i=1}^N \left(\frac{p_i - p_0}{p_0} \right)^2}$$

where N is the number of hex-Z nodes

in the three-dimensional space and p is the local peak-to-average flux in each node. The subscript 0 denotes the initial state.

TABLE VIII

Relative root-mean-square (*RelRMS*) difference of the peak-to-average flux distribution with respect to the initial flux distribution following insertion of the subassembly near the core boundary.

Time [s]	RelRMS peak-to-average flux		
	Initial	Initial	Initial
	$k_{\text{eff}}=0.9519$	$k_{\text{eff}}=0.9722$	$k_{\text{eff}}=0.9910$
1.2	0.7%	0.8%	0.9%
1.4	1.4%	1.6%	1.8%
1.6	2.2%	2.6%	2.9%
1.8	3.0%	3.6%	4.0%
2.0	4.0%	4.7%	5.3%
3.0	4.0%	4.7%	5.5%
20.0	4.1%	4.8%	-

Numerical performance data are summarized in TABLE IX for the case when the subassembly is inserted close to core-center and in TABLE X for the case when the subassembly is inserted at the core boundary. Ideally (stripped of reactivity feedbacks), all cases should remain in the subcritical state even after the subassembly has been fully inserted. However, due to positive thermal feedbacks additional reactivity is inserted, which for the case with initial $k_{\text{eff}}=0.9746$ (subassembly inserted close to core-center) leads to an excursion in the range above critical (but below prompt critical). The direct space-time solution predicts that the reactor in that case becomes supercritical at $t=3.3$ seconds and the calculation is subsequently terminated at $t=3.9$ seconds due to reaching excessive temperatures. The point solution, on the other hand, underpredicts the reactivity insertion and the reactor remains in the subcritical range, which leads to considerable discrepancies since it is in the supercritical range where most of the power rise occurs. The cases $k_{\text{eff}}=0.9356$ and $k_{\text{eff}}=0.9558$ are predicted to stay in the subcritical state, therefore the power approaches a stationary level and the error is essentially bounded at the value already accumulated. It is seen that the point kinetics

calculations underestimate the exact space-time solution in all cases. The same non-conservative behavior is observed in critical systems.

The fuel is calculated to reach the melting point at approximately 2.6 sec. into the transient. In reality, the nature of the accident might change significantly from that point. Fuel dispersal may act to terminate the accident prior to reaching supercritical conditions, however, reactivity could also be added due to fuel relocation and expulsion of lead-bismuth. Therefore, current predictions beyond core damaging levels are highly uncertain from a physical point of view, but nonetheless it permits comparison of the basic methods under extreme conditions.

TABLE IX

Comparison of results for the insertion of a fuel subassembly near the core-center (subassembly no. 9 according to the core map in Fig. 1).

Time [s]	Initial $k_{\text{eff}}=0.9356$			Initial $k_{\text{eff}}=0.9558$			Initial $k_{\text{eff}}=0.9746$		
	Direct	PK	ϵ (%)	Direct	PK	ϵ (%)	Direct	PK	ϵ (%)
1.2	1.073	1.072	-0.1	1.108	1.106	-0.2	1.191	1.187	-0.3
1.4	1.163	1.156	-0.6	1.250	1.238	-0.9	1.493	1.464	-1.9
1.6	1.274	1.255	-1.5	1.442	1.408	-2.4	2.034	1.920	-5.6
1.8	1.415	1.372	-3.0	1.719	1.633	-5.0	3.282	2.807	-14.5
2.0	1.598	1.515	-5.2	2.148	1.948	-9.3	9.112	5.270	-42.2
3.0	1.607	1.523	-5.2	2.182	1.975	-9.5	14.314	6.157	-57.0
20.0	1.633	1.546	-5.3	2.268	2.045	-9.8	-	-	-
Max deviation (%)			-5.3			-9.8			-75.9

TABLE X

Comparison of results for the insertion of a fuel subassembly near the core-boundary (subassembly no. 16 according to the core map in Fig. 1).

Time [s]	Initial $k_{\text{eff}}=0.9519$			Initial $k_{\text{eff}}=0.9722$			Initial $k_{\text{eff}}=0.9910$		
	Direct	PK	ϵ (%)	Direct	PK	ϵ (%)	Direct	PK	ϵ (%)
2.0	1.136	1.106	-2.63	1.290	1.223	-5.18	3.382	2.380	-29.6
4.0	1.138	1.108	-2.66	1.302	1.232	-5.44	4.687	2.734	-41.7
6.0	1.140	1.109	-2.71	1.307	1.235	-5.50	6.058	2.941	-51.5
8.0	1.141	1.110	-2.72	1.311	1.237	-5.58	7.980	3.082	-61.4
10.0	1.141	1.110	-2.72	1.312	1.239	-5.56	12.815	3.188	-75.1
20.0	1.143	1.111	-2.75	1.317	1.243	-5.65	-	-	-
Max deviation (%)			-2.77			-5.65			-78.2

V.C. Flow Reduction

Finally, kinetics performance characteristics were compared for a flow coastdown event. Complete loss of forced flow in the primary system is assumed. The analysis further assumes that the shutdown system is inoperable, which in an accelerator-driven system corresponds to a “beam-on” situation. Constant coolant inlet temperature is specified.

The power traces for the cases with initial $k_{\text{eff}}=0.9594$ and $k_{\text{eff}}=0.9798$ are presented in Fig 7 and for $k_{\text{eff}}=0.9987$ in Fig 8; the scale on the left is for the normalized power, and the scale on the right is for the normalized flow. The accident is initiated by gradually reducing the inlet driving

pressure, starting at $t=1$ sec. The pump driving pressure approaches zero at 10 sec. The transient is dictated by coolant reactivity feedback. Coolant heat-up occurs at a rate determined by the flow coastdown. The resulting density reduction of the coolant has a positive effect. For the deeply subcritical cores, i.e. cases $k_{eff}=0.9594$ and $k_{eff}=0.9798$, the power peaks (with some delay) as the flow drops to a minimum. Eventually, the coolant flow balances at a flowrate sustained by natural circulation alone. Given the small reactivity effects, the power settles at a level slightly above the initial state. For the near-critical core, shown in Fig 8, the power trace is different. The feedback-induced reactivity has a much stronger effect in this case. This is because the response is more sensitive near the critical state. At approximately 13.8 seconds into the transient, the reactor becomes supercritical. Continued coolant heat-up causes gradual insertions of reactivity, leading to an essentially unbounded power excursion. The calculation was terminated when the cladding in the hottest channel exceeded the melting point.

In TABLE XI, the numerical error versus time is presented. The point kinetics results were found to be in excellent agreement with the exact solution for the deeply subcritical cases (initial $k_{eff}=0.9594$ and $k_{eff}=0.9798$), indicating that coolant feedbacks did not alter the initial flux shape. For the near-critical reactor (initial $k_{eff}=0.9987$), the direct solution predicts a somewhat higher power than does the point approximation.

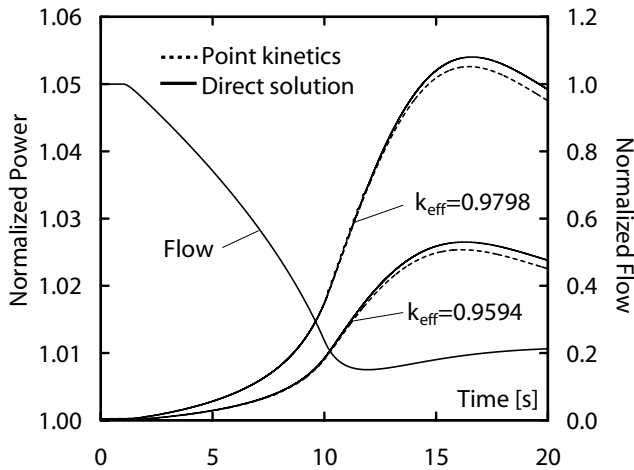


Fig 7. Unprotected Loss-of-flow transient (initial $k_{eff}=0.9594$ and $k_{eff}=0.9798$).

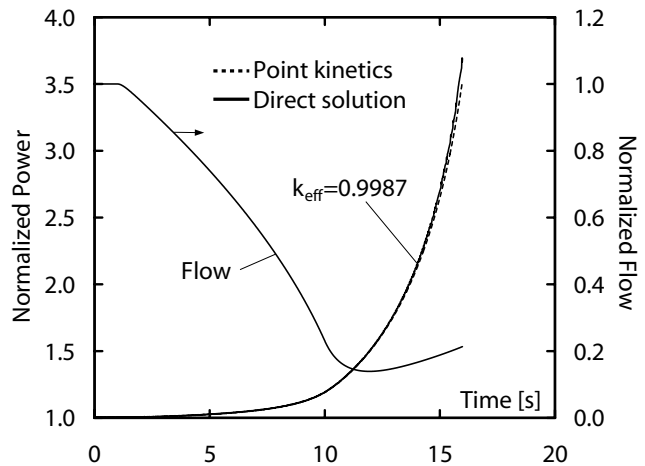


Fig 8. Unprotected Loss-of-flow transient (initial $k_{eff}=0.9987$).

TABLE IX

Comparison of results for the Unprotected Loss-of-Flow transient.

Time [s]	Initial $k_{eff}=0.9594$			Initial $k_{eff}=0.9798$			Initial $k_{eff}=0.9987$		
	Direct	PK	ϵ (%)	Direct	PK	ϵ (%)	Direct	PK	ϵ (%)
2.0	1.0002	1.0002	0.00	1.0004	1.0005	0.01	1.0036	1.0058	0.22
5.0	1.0014	1.0014	0.01	1.0030	1.0028	-0.01	1.0244	1.0267	0.23
10.0	1.0093	1.0090	-0.03	1.0176	1.0175	-0.02	1.1908	1.1915	0.06
15.0	1.0259	1.0249	-0.10	1.0521	1.0509	-0.11	2.6999	2.6493	-1.87
20.0	1.0238	1.0225	-0.12	1.0492	1.0475	-0.16	-	-	-
Max deviation (%)			-0.14			-0.19			-4.56

VI. CONCLUSIONS

The purpose of this paper was to investigate the ability of point kinetics to predict the transient behavior in accelerator-driven systems (ADS) under accident conditions. Numerical experiments were carried out in a minor-actinide loaded and lead-bismuth cooled ADS. The precision of the point approximation was compared in the subcritical range from $k_{eff}=0.9594$ to 0.9987. A full three-dimensional nodal energy-space-time solution, coupled with feedback effects, was provided and used as a standard of comparison. The numerical tests suggest that point kinetics is capable of producing very good predictions of certain types of accidents in ADS's. For transients involving external source perturbations the point method provided extremely accurate results. Such changes are associated with spatially uniform reactivity feedbacks that produce little flux deformation. This may not be the case in severe source disturbances, involving strong reactivity feedbacks, but for most practical situations, it is expected that source disturbances be rather well described by point kinetics. When applied to the analysis of localized reactivity perturbations - a condition when the point treatment is expected to be a poor approximation - the results indicated better precision at lower k_{eff} -levels. This behavior appears to be due to the lower reactivity sensitiveness in the subcritical operating state, which effectively weakens the response and mitigates any spatial distortions. If a subcritical reactor is subject to a change in

the strength of the external source, or a change in reactivity within the subcritical range, the neutron population will adjust to a new stationary level. Therefore, within the normal range of operation, the power predicted by the point kinetics method and the associated error in comparison with the exact solution tends to approach an essentially bounded value. This is quite the contrary of critical reactors, in the absence of reactivity feedbacks the response will either diverge exponentially or decay to zero depending on the sign of the reactivity disturbance. In general, the flux shape in a fast neutron spectrum shows strong space-time coupling, i.e., local spatial disturbances are rapidly distributed to the remaining parts of the core, which softens spatial variations in a transient. This is usually attributed to the relatively large mean free path of fast neutrons and to the comparatively compact core size of a fast reactor. Due to the overall smaller influence of delayed neutrons in the subcritical operating state a prompt adjustment of the flux shape prevails. For a critical reactor, the delayed neutrons tend to retard the shape transition for certain transients. All together these characteristics are favorable from a point kinetics view of application to fast spectrum ADS systems. A non-favorable feature is that proposed ADS designs have large reactivity potential vested in the core²². Changes in lattice geometry or coolant density²³ may contribute with significant reactivity values. Such feedbacks are potential sources of spatial effects, and therefore, possible deviation from the point kinetics model. The essential requirements for an accurate point kinetics treatment are the same in subcritical reactors, i.e., symmetric reactivity insertion, small and tightly coupled core. Thus, favorable point kinetics performance in an ADS appears to be possible as long as the transient does not involve significant shape distortions. Similar conclusions have been drawn by other authors²⁴. While the current study suggests that subcritical operation may provide for improved point kinetics performance and enhanced tolerance to system reactivity perturbations, the results showed that it is not feasible for local reactivity perturbation studies and it should still be used with care in situations involving strong feedback phenomena.

The situation in a loss-of-flow scenario was also studied. Here again, the point method was capable of very accurate calculations. The reasons are similar to those previously discussed. It was also found that the point kinetics model has a tendency to underestimate the severity of reactivity insertion accidents. The same nonconservative behavior is observed in critical systems, but it ought to be recognized for subcritical systems as well because of its overriding importance in reactor safety considerations.

VII. ACKNOWLEDGMENTS

This research was supported by the Swedish Nuclear Fuel and Waste Management Co. (SKB). The calculations reported here were performed on the ANL-NE computer network.

REFERENCES

1. A. RINEISKI and W. MASCHKEK, "On Application of Quasistatic and Point-Kinetics Schemes for Subcritical Systems With External Neutron Source," *Nuclear Mathematical and Computational Sciences: A Century in Review - A Century Anew*, M&C 2003, Gatlinburg, Tennessee, USA, April 6-11 (2003).
2. D. G. CACUCI, "On Perturbation Theory and Reactor Kinetics: From Wigner's Pile Period to Accelerator Driven Systems," *PHYSOR 2002*, Seoul, Korea, October 7-10 (2002).
3. A. F. HENRY, "The Application of Reactor Kinetics to the Analysis of Experiments," *Nuclear Science and Engineering*, **3**, 52-70 (1958).
4. E. P. GYFTOPOULOS, Chapter on "General Reactor Dynamics," in *The Technology of Nuclear Reactor Safety*, Vol. 1, p. 175-204, T. J. THOMPSON and J. G. BECKERLY, Eds., The MIT Press, Cambridge, Massachusetts, USA (1964).
5. J. B. YASINSKY and A. F. HENRY, "Some Numerical Experiments Concerning Space-Time Reactor Kinetics Behavior," *Nuclear Science and Engineering*, **22**, 171-181 (1965).
6. K. O. OTT and D. A. MENELEY, "Accuracy of the Quasistatic Treatment of Spatial Reactor Kinetics," *Nuclear Science and Engineering*, **36**, 402-411 (1969).
7. A. F. HENRY, *Nuclear-Reactor Analysis*, p. 300-329, The MIT Press, Cambridge, Massachusetts, USA (1975).
8. K. O. OTT and R. J. NEUHOLD, *Introductory Nuclear Reactor Dynamics*, p. 69, American Nuclear Society, LaGrange Park, Illinois, USA (1985).
9. M. BECKER, "A Generalized Formulation of Point Nuclear Reactor Kinetics Equations," *Nuclear Science and Engineering*, **31**, 458-464 (1968).
10. "Comparison Calculations for an Accelerator-driven Minor Actinide Burner," OECD/NEA Nuclear Science Committee, NEA/NSC/DOC(2001)13, OECD (2002). Benchmark prepared by P. WYDLER and H. TAKANO, NEA/NSC/DOC(99)13, Revised 27 Aug. 1999.
11. M. SALVATORES, et al., "Long-lived radioactive waste transmutation and the role of accelerator driven (hybrid) systems," *Nucl. Instrum. Methods Phys. Res., Sect. A*, **414**, 5-20 (1998).
12. J. E. CAHALAN, T. AMA, G. PALMIOTTI, T. A. TAIWO, and W. S. YANG, "Development of a Coupled Dynamics Code with Transport Theory Capability," *PHYSOR 2000*, Pittsburgh, USA, 7-11 May (2000).
13. H. HENRYSON II, B. J. TOPPEL, and C. G. STENBERG, "MC²-2: A Code to Calculate Fast Neutron Spectra and Multigroup Cross Sections," ANL-8144, Argonne National Laboratory (1976).

14. R. E. ALCOUFFE, F. W. BRINKLEY, D. R. MARR, and R. D. O'DELL, "User's Guide for TWODANT: A Code Package for Two-Dimensional, Diffusion-Accelerated, Neutral-Particle Transport," LA-10049-M, Los Alamos National Laboratory (1990).
15. R. D. LAWRENCE, "The DIF3D Nodal Neutronics Option for Two- and Three-Dimensional Diffusion Theory Calculations in Hexagonal Geometry," ANL-83-1, Argonne National Laboratory (1983).
16. T. A. TAIWO, "DIF3D-K: A Nodal Kinetics Code for Solving the Time-Dependent Diffusion Equation in Hexagonal-Z Geometry," ANL/NPR-92/17, Argonne National Laboratory (1992).
17. W. M. STACEY, Jr., *Space-Time Nuclear Reactor Kinetics*, p. 43-46, Academic Press, New York, USA (1969).
18. R. D. LAWRENCE, "Perturbation Theory Within the Framework of a Higher-Order Nodal Method," *Trans. Am. Nucl. Soc.*, **46**, 402 (1984).
19. T. A. TAIWO, H. S. KHALIL, J. E. CAHALAN, and E. E. MORRIS, "Time-Step Selection Considerations in the Analysis of Reactor Transients with DIF3D-K," *Trans. Am. Nucl. Soc.*, **68**, 429-430 (1993).
20. R. A. RYDIN and M. L. WOOSLEY, JR., "Evidence of Source Dominance in the Dynamic Behavior of Accelerator-Driven Systems," *Nuclear Science and Engineering*, **126**, 341-344 (1997).
21. Y. KIM, W. S. YANG, T. A. TAIWO, and R. N. HILL, "Reactivity Estimation for Source-Driven Systems Using First-Order Perturbation Theory," PHYSOR 2002, Seoul, Korea, October 7-10 (2002).
22. W. MASCHEK, A. RINEISKI, K. MORITA, M. FLAD, "Inherent and Passive Safety Measures in Accelerator Driven Systems: A Safety Strategy for ADS," GLOBAL 2001, Paris, France, Sep 9-13 (2001).
23. M. ERIKSSON, J. WALLENIUS, J. E. CAHALAN, K. TUCEK, and W. GUDOWSKI, "Safety analysis of Na and Pb-Bi coolants in response to beam instabilities," Proc. 3rd International Workshop on Utilisation and Reliability of High Power Proton Accelerators, Santa Fe, USA, May (2002).
24. A. AMIONE, et al., "Dynamics of Accelerator-Driven Systems by the Quasi-static Method," 6th International Meeting on Nuclear Applications of Accelerator Technology (AccApp'03), June 1-5, San Diego (2003).

Paper IV

Safety Analysis of Na and Pb-Bi Coolants in Response to Beam Instabilities

M. Eriksson, J. Wallenius, J. E. Cahalan, K. Tucek, and W. Gudowski*

Royal Institute of Technology, Dep. Nuclear & Reactor Physics
10691 Stockholm, Sweden.

*Argonne National Laboratory, Reactor Analysis & Engineering Division
9700 South Cass Ave., IL 60439, USA.

Presented at the Third International Workshop on Utilisation and Reliability of High Power
Proton Accelerators, Santa Fe, New Mexico, USA, May 12-16, 2002.

Abstract

A comparative safety study has been performed on sodium vs. lead/bismuth as coolant for accelerator-driven systems. Transient studies are performed for a beam overpower event. We examine a fuel type of recent interest in the research on minor actinide burners, i.e. uranium-free oxide fuel. A strong positive void coefficient is calculated for both sodium and lead/bismuth. This is attributed to the high fraction of americium in the fuel. It is shown that the lead/bismuth-cooled reactor features twice the grace time with respect to fuel or cladding damage compared to the sodium-cooled reactor of comparable core size and power rating. This accounts to the difference in void reactivity contribution and to the low boiling point of sodium. For improved safety features the general objective is to reduce the coolant void reactivity effect. An important safety issue is the high void worth that could possibly drive the system to prompt criticality.

Introduction

Both sodium and lead/bismuth are considered as coolant candidates in accelerator-driven systems. At RIT a global safety study of accelerator driven systems is performed to investigate neutronic and transient characteristics of lead/bismuth vs. sodium as primary coolant and the performance of oxide, nitride, and metallic fuels for various accident initiators and core sizes. In the present analysis we benchmark the two coolants for oxide fuel in the response to a sudden beam excursion. This type of accident initiator is unique to accelerator-driven systems and is open to considerable question. One of the most questionable items is the nature of the initiating circumstances; for example; what is the maximum beam load change that could possibly occur and at what speed can this transition materialize? The outcome will depend strongly on the details of these conditions as well as on the time over which the beam remains on. In the following paper, the beam is presumed to double in strength in an instant and remain on for an unspecified time. The extreme nature of this assumption is subject to debate. However, the analysis of accidents that appear incredible is an important part of the design of a safe reactor. Much can be learned from simulated severe accidents. The purpose of the present paper is to measure the strengths and weaknesses of two particular coolants, independent of probability, or even possibility, of occurrence.

Model and assumptions

The benchmark is performed using a common design, set of assumptions, and computational methods. The continuous energy MCNP simulation code is applied to the neutronics analysis. A three-dimensional pin-by-pin model is defined. Oxide fuel is adopted being diluted with zirconium dioxide. In order to flatten the power distribution, the core is subdivided into two regions with varying content of ZrO_2 . We have adopted a Pu to TRU ratio of 40% at BOL since this composition minimizes reactivity losses over a large number burnup cycles [1]. The Pu/TRU ratio is kept constant. The plutonium isotopic vector corresponds to the discharge from spent MOX fuel (5% ^{238}Pu , 38% ^{239}Pu , 30% ^{240}Pu , 13% ^{241}Pu , and 14% ^{242}Pu). The americium composition consists of two thirds ^{241}Am and one third of ^{243}Am . The analysis aimed at increasing the core diameter through an increase in pin pitch while holding the pin diameter and core height constant. Pitch-to-diameter ratios are varied in the range from $P/D=1.25$ to 2.25 (constant $D=8$ mm). To compensate the reactivity loss when P/D is increased the fraction of ZrO_2 is adjusted (from core average of 30% at $P/D=2.25$ to 70% at $P/D=1.25$) in order to preserve $k_{\text{eff}}=0.97$. A summary of design parameters is presented in Table 1.

Transient analysis is performed with the aid of the SAS4A safety code [2]. A primary heat transport system is defined and represented by the core, primary pumps, the shell side of the heat exchangers, connecting piping, and compressible pool volumes with cover-gas surfaces. Coolant passage through the core is modelled by a single thermal and hydraulics channel. The feedwater system is assumed to remove heat at 100% for all time. Thus, when the power increases above nominal, there will be a mismatch in heat production and heat removal and the net effect is core inlet temperature rising with time. The point kinetics approximation is used for calculating transient power. A value of β_{eff} equal to 0.20% is assumed, a representative value for a minor actinide burner. The coolant flow rate in a lead/bismuth-cooled reactor is limited by erosion/corrosion damage of structural material. At present the flow rate of lead/bismuth is taken to be 2.5 m/s. No such limitation exists for the sodium-cooled reactor where the main concern in the past has been to limit pumping power requirement. For that reason a sodium flow rate of 5 m/s is adopted. Transient response is calculated assuming intact core geometry; i.e., fuel pins and coolant channels are well defined, precluding the possibility for insertion of large reactivity values by core compaction. Temporal and spatial void distributions are calculated. Reactivity feedbacks are modelled by coolant density changes and an assumed Doppler constant of $T_{\text{dk}}/dT=-38$ pcm. As will be seen, the Doppler coefficient has negligible influence on the operational behavior. The void reactivity coefficient and the prompt neutron lifetime are determined from static neutronic analysis, as discussed in the next section. In a preliminary study, a uniform void coefficient is used. Structural reactivity feedback phenomena (e.g. radial and axial core expansion) have been excluded considering the low responsiveness of a source-driven system to reactivity changes [3]. Under the present conditions, structural expansion introduces reactivity changes that are small with respect to the void effect. It is recognized, however, that such reactivity feedback effects may affect the calculated performance values.

Table 1. Design parameters

Characteristic	Value
Core power	800 MWth
Average linear power	16 kW/m
Core coolant inlet temperature	573 K (Pb/Bi and Na)
Coolant flow rate	2.5 m/s (Pb/Bi) and 5.0 m/s (Na)
Fuel composition	(Pu _{0.6} Am _{0.4})O ₂ + ZrO ₂
Fuel porosity	10 %
Core height	1.0 m
Fission gas plenum height	1.50 m
Outer fuel radius	3.45 mm
Inner cladding radius	3.50 mm
Outer cladding radius	4.00 mm
P/D	Varied from 1.25 to 2.25
Doppler constant (Tdk/dT)	-38 pcm
k_eff (eigenvalue)	0.97
β_eff	0.20 %

Neutronics analysis

Following coolant voiding there is hardening of the spectrum caused by a decrease in neutron scattering. Removal of coolant also results in higher neutron leakage. Hardening of the neutron spectrum and increased neutron leakage are the two dominating physical phenomena contributing to the void reactivity effect. In general, hardening of the spectrum leads to a positive reactivity component due to an increase in the number of neutrons released per neutron absorbed in the fuel while increased leakage gives rise to a reactivity loss since more neutrons may escape the core. The void reactivity effect has been calculated for the present system and is illustrated in Figure 1. The void coefficient is expressed as a function of pitch-to-diameter ratio. The void coefficient is obtained by calculating the k-eigenvalue at a given density and then performing a second calculation but with a density corresponding to a temperature increase of 200 degrees Celsius. The density is changed uniformly over the core and the upper plenum. Figure 1 indicates that the negative reactivity effect associated with increased neutron leakage is not sufficient to offset the positive reactivity contribution of a harder spectrum. The spectrum effect becomes more positive as P/D increases. As a result, the void reactivity coefficient becomes increasingly positive at higher P/D. It is observed that both coolants possess a significant positive void reactivity coefficient. However, the void coefficient tends to be more positive for sodium because of higher moderating power and an influential scattering resonance in ²³Na at 3 keV. In the energy region above 100 keV, the fission-to-capture ratio for ²⁴¹Am rises more rapidly than for ²³⁹Pu. For that reason, the void coefficient becomes more positive if the fraction of americium is increased and the fraction of plutonium is correspondingly decreased.

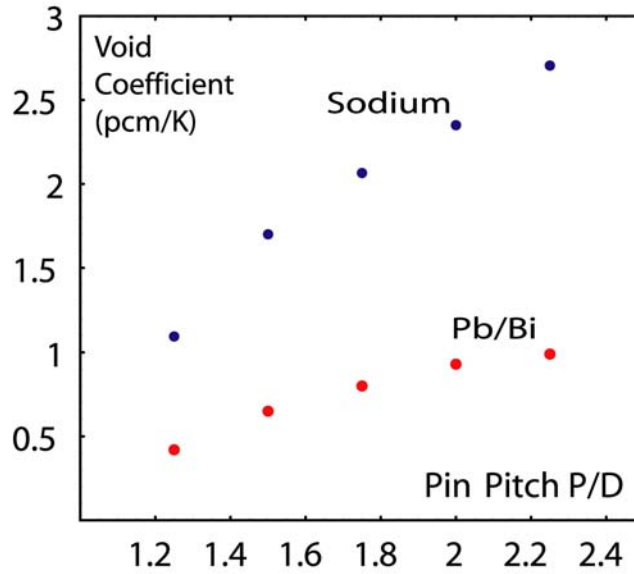


Figure 1. Void reactivity coefficient [pcm/K]

The prompt neutron lifetime was calculated using MCNP. As expected, the prompt neutron lifetime increases with increasing P/D, corresponding to a softer spectrum and longer distance travelled by neutrons up to their point of absorption. Note that the average neutron lifetime in the lead/bismuth-cooled core exceeds $1\mu\text{s}$ for high pin pitches ($P/D > 2.0$).

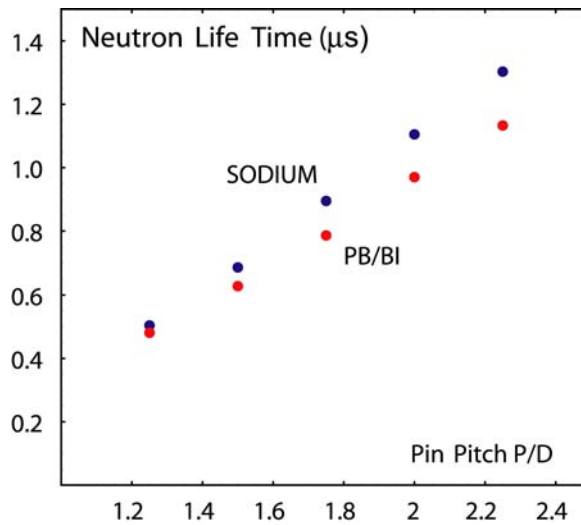


Figure 2. Prompt neutron lifetimes

Failure criteria

In order to predict core damage a set of failure criteria has been postulated, those are listed in Table 2. Several difficulties exist in attempting to provide failure criteria for the existing system. The principal difficulty is the uncertainty in the operating performance of the fuel and structural materials. Chemical and mechanical interactions between the fuel, cladding, and coolant, as well as irradiation performance, etc. are not well known. Validation of failure criteria will require the availability of experimental test data. Nonetheless, preliminary safety margins can be established as a first estimate to envelop worst-case conditions. The fuel is assumed to be stable up to the melting point, which is a reasonable assumption for sub-

stoichiometric oxide fuel. The fuel melting point as well as thermophysical properties vary with the stoichiometry. Present fuel properties correspond to an oxygen-to-metal ratio of 1.93. The failure temperature is based on the melting point of PuO₂ [4] and AmO₂ [5] together with the melting point of diluent ZrO₂, applying Vegard's law. The maximum cladding temperature is constrained by mechanical considerations. The primary cladding loading is the internal gas pressure; fuel-cladding mechanical interaction is neglected. We have assumed a maximum internal pin pressure of 10 MPa in steady-state as a result of pressure build-up by the continuous release of fission gases. Under transient conditions the pressure may increase even further causing an increase in the loading of the cladding. Simultaneously, the cladding loses its strength at elevated temperatures. The cladding failure temperature is determined from correlations based on the calculated hoop stress and the failure temperature measured in cladding burst tests (20% cold-worked type 316 austenitic stainless steel) [6]. The transient burst temperature is representative for fast transients where the temperature is rapidly increasing until the cladding fails, providing less time for creep-type deformation.

Table 2. List of failure temperatures

Failure mechanism	Failure temperature	Comment
Melting of oxide fuel	2886 K	0.11(Pu _{0.6} Am _{0.4})O ₂ + 0.89ZrO ₂
Cladding burst temperature	1333 K	20% CW SS316, 5.56 °C/sec, hoop stress 100 MPa.

Transient analysis

Transient response has been examined for an unprotected transient overpower (UTOP) event. It is assumed that the intensity of the external neutron source is *promptly increased by twice the initial value*. Reactor shutdown is disregarded. It is possible to imagine that a control system failure or simply inadvertent operation of the accelerator could lead to an accidental increase of beam power. However, it is important to acknowledge the highly hypothetical nature of the accident under discussion.

Transient power is displayed in Figure 3. For the case displayed the pitch-to-diameter ratio is 1.50. The magnitude of the initial burst is the same, independent of the coolant. The steady-state power will multiply by a factor of S/S_0 if the source strength is stepped from S_0 to S . The speed of the transition is determined by the prompt period. Delayed neutrons do not appreciably slow the response. Following the prompt jump, the power changes as a result of reactivity feedbacks. Coolant void reactivity feedbacks contribute to the course of the accident by adding reactivity. The small negative reactivity feedback associated with the Doppler effect does not influence the course of the accident. Differences in transient behaviour between lead/bismuth and sodium result primarily from the difference in boiling point and void reactivity effect. Coolant density changes provide modest changes in reactivity compared to the full void reactivity effect, which may introduce significant positive reactivity values. This causes the reactivity insertion rate to be considerable larger in the sodium-cooled core. Void generation, and thus positive reactivity insertion, is abrupt in the vicinity when boiling starts. Sodium boiling begins at the core outlet and develops axially downward. In the sodium-cooled core, the void effect adds enough reactivity to bring the reactor to a prompt critical state, with possible severe safety consequences. Prompt critical conditions are established about 400 seconds after accident initiation. Large positive reactivity insertions are potentially possible due to lead/bismuth voiding as well. However, it is seen that the high boiling temperature for lead/bismuth (1943 K) compared to sodium (1154 K) makes voiding less probable even though

there are other ways of voiding the coolant besides boiling, i.e. large scale steam generator failure or possibly sudden gas release from ruptured pins. Voiding could possibly occur in severe loss of coolant accidents, such as tank rupture, however this must be regarded as extremely unlikely. It should be recognized that structural damage most likely occurs before boiling is encountered in a lead/bismuth-cooled reactor.

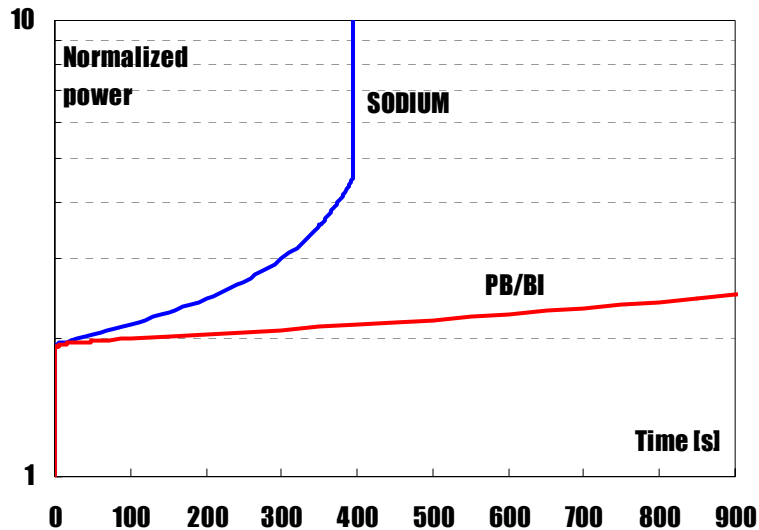


Figure 3. Normalized reactor power. $P/D=1.50$.

In Figure 4 peak fuel and cladding temperatures are shown for the case $P/D=1.50$. Since no time is required for heat transport, the fuel suffers a rapid temperature rise. The amount of beam input determines whether there is immediate fuel damage or not. Subsequent heat-up occurs as a result of positive feedback from voiding and insufficient heat removal capability. The steam generators are assumed to remove heat at a rate of nominal power, resulting in increasing core inlet temperature as the transient proceeds. Sharp fuel temperature increase is calculated in the sodium case, as a result of a significant void reactivity insertion. The failure criterion for the fuel is exceeded in 200 seconds and the cladding is expected to reach its burst temperature in 350 seconds. The fuel fails prior to the initiation of sodium boiling (~350 sec) and this might disable the reactor before boiling and prompt criticality occurs. However, it is difficult to determine the consequences of fuel melting. In the sodium case, cladding failure is predicted to occur by burnout. Cladding failure occurs simultaneously with sodium boiling. It is recognized that a substantial change in the nature of the accident may occur at the onset of fuel or cladding damage. Therefore, extrapolation beyond the actual failure points is subject to considerable uncertainty.

The assumption of constant heat rejection rate is conservative. In an overpower accident it is likely there will be some increase in the heat removal above 100%. Taking this into account would yield less pessimistic results. In reality, the feedwater system would try to maintain the correct coolant temperature returning to the core, and if it is not able to do so, the feedwater system would trip and issue reactor shutdown. It should be recognized that for both coolants considered the grace period is in the order of several minutes, which, in principle, provides considerable time for a well-designed safety system to act.

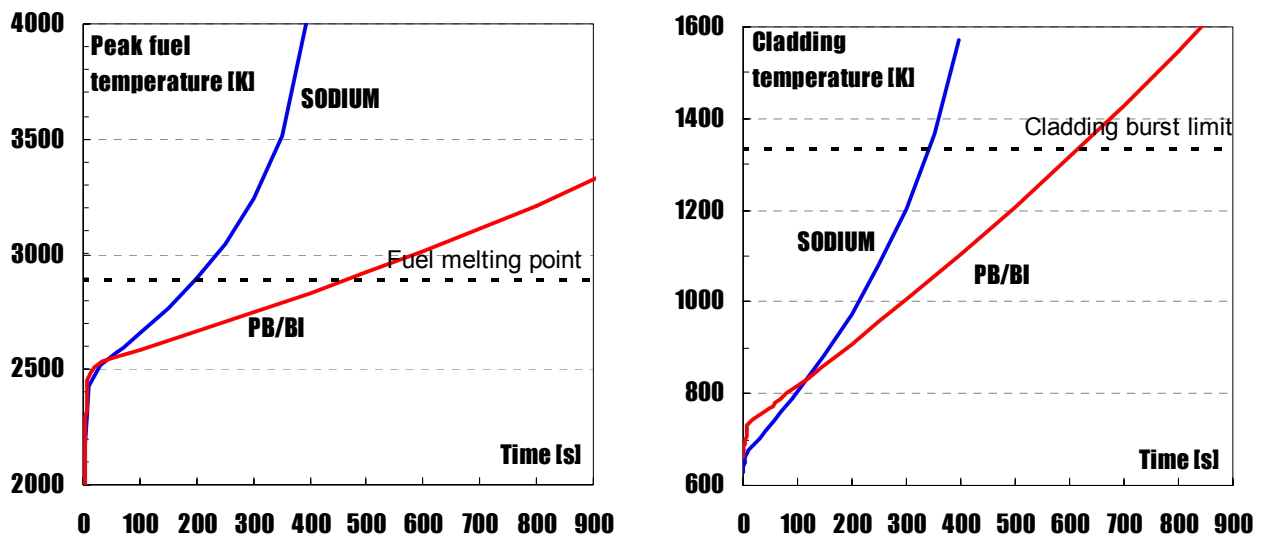


Figure 4. Peak fuel temperature (left) and peak cladding temperature (right). P/D=1.50.

The calculation is repeated for a range of pitch-to-diameter ratios. In Figure 5, the grace period is calculated for different P/D's. The grace period is measured in seconds. The grace time decreases somewhat at large pitches, a consequence of higher void coefficient for larger P/D. From the very basis of the assumptions, the choice of coolant does not change the inevitability of reaching a failure point; the timing of failure is different, however. The Pb/Bi cooled core features twice the grace time compared to the sodium-cooled core with the same P/D and power rating. The calculation revealed a small margin to prompt criticality at large pitches (sodium case). It was found that rapid sodium vaporization and expulsion occurred at the onset of boiling. Prompt criticality could possibly occur in less than 1 sec ($P/D > 1.50$) once sodium boiling is initiated.

Oxide fuel temperatures are sensitive to linear power ratings. The allowable linear power is limited by the melting point. The low thermal conductivity of oxide fuel is compensated somewhat by a high melting point. Figure 6 illustrates the sensitivity of grace time on linear power. The calculation was performed for $P/D=1.50$. It should be recognized that different power ratings correspond to different core total powers in Figure 6. The number of fuel pins is fixed while the steady-state linear power is varied. In the reference case the linear power is 16 kW/m corresponding to a total reactor power of 800 MWth. The mode of failure differs; fuel failure dominates at high linear powers while cladding failure supersedes as the mode of failure at low linear power (< 14 kW/m). The grace period provides an indication of the time available for a safety system to act. It was found that the safety performance of oxide fuel deteriorates rapidly with increasing pin power rating. At high linear power immediate fuel damage may occur, providing little time for a protection system to respond. It is possible to extend the grace period by derating the oxide fuel, but it has some obvious penalties.

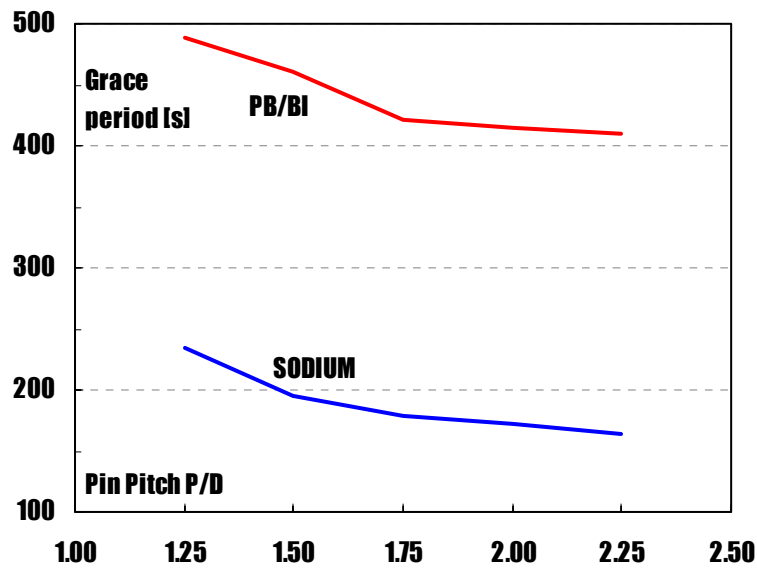


Figure 5. Grace period as a function of pin pitch. Linear power=16 kW/m.

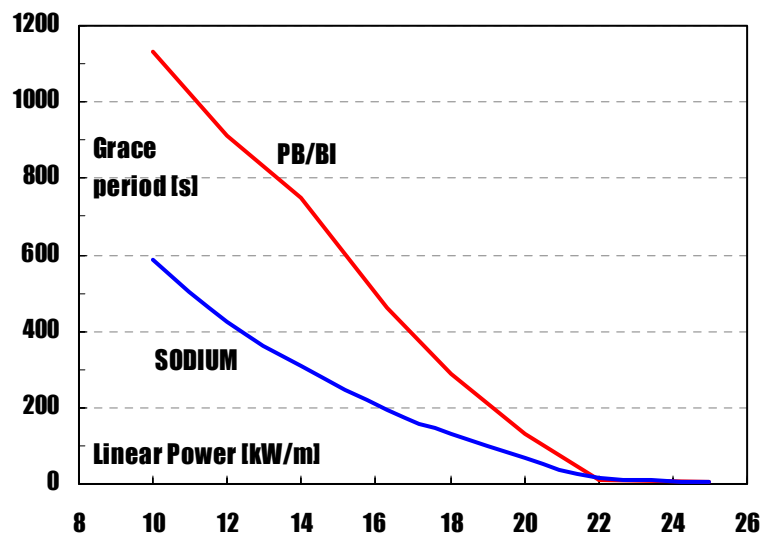


Figure 6. Grace period as a function of linear power rating. P/D=1.50.

The characteristics that have the greatest effect in the present analysis are the differences in boiling point and void coefficient. While the boiling temperature is fixed, the void coefficient can change significantly with design parameters. The void reactivity effect is the result of several physical phenomena and various methods have been proposed for reducing the void worth by design [7]. One possible way of void worth reduction is to reduce the pin size. The net result is shown in Figure 7, where the void worth of lead/bismuth and sodium, respectively, is calculated as a function of P/D. The coolant void worth is determined by removing all coolant from the core and the upper plenum. The results suggest that a significant reduction in the void worth is achievable using smaller pin diameter. Reducing the void worth is an essential design objective. Large values of the void worth may present a difficulty in the licensing of minor actinide burners because of the risk for severe damage to the plant and public safety.

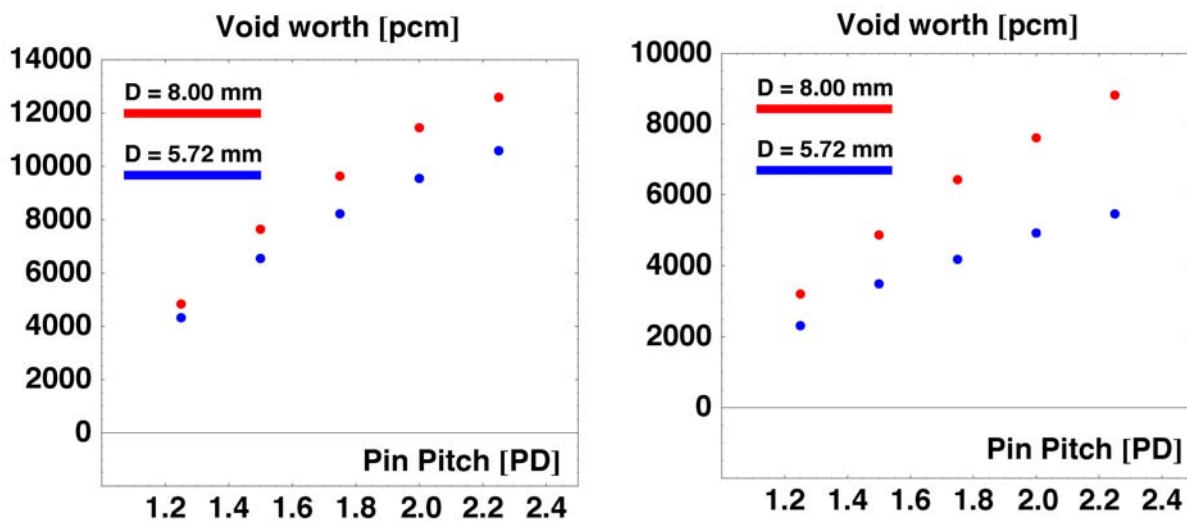


Figure 7. Sodium (left) and lead/bismuth (right) void worth as a function of P/D. Pin diameter is a parameter.

Summary

Comparison was made of the safety performance of sodium vs. lead/bismuth as primary coolant in a minor actinide burner reactor. The systems were benchmarked for oxide fuel. Neutronic investigations were made on the void reactivity effect for a range of pitch-to-diameter ratios. Transient behavior for a beam overpower event and the time-to-failure were compared.

A strong positive void coefficient was found for both sodium and lead/bismuth. The considerable void effect is attributed to a high fraction of americium (60%) in the fuel. It was found that void reactivity insertion rates increases with P/D. In response to the particular accident under discussion, the Pb/Bi-cooled core featured twice the grace time compared to the sodium-cooled core. The essential difference is attributed to the difference in boiling point and void reactivity contribution. An important safety issue is the high void worth that could possibly drive the system to prompt criticality. The problem is the result of the present fuel composition and it exists in both the sodium-cooled reactor and the lead/bismuth-cooled reactor. To some degree, this may be counter-balanced with proper core design, e.g. smaller pitch and pin diameter. For improved safety features, the general objective is to reduce the coolant void reactivity effect. The sodium-cooled core was found to have a smaller safety margin to prompt criticality. The high boiling temperature of lead/bismuth makes voiding less probable. The low effective thermal conductivity of oxide fuel results in high fuel temperatures and imposes constraints on the allowable linear power. Derating the oxide fuel could enhance the safety performance, but it has some obvious penalties.

References

- [1] T. Takizuka et al., Studies on accelerator-driven transmutation systems, Proc. 5th information exchange meeting on actinide and fission product partitioning and transmutation, EUR 18898 EN, OECD/NEA 1998.
- [2] J. E. Cahalan, A. M. Tentner, and E. E. Morris, "Advanced LMR Safety Analysis Capabilities in the SASSYS-1 and SAS4A Computer Codes," Proc. of the International Topical Meeting on Advanced Reactors Safety, Pittsburgh, April 17-21, 1994.
- [3] M. Eriksson and J. E. Cahalan, "Inherent shutdown capabilities in accelerator-driven systems," *Annals of Nuclear Energy*, vol 29/14 pp 1689-1706, (2002).

- [4] E. H. P. Cordfunke, R. J. M. Konings, G. Prins, P. E. Potter, and M. H. Rand, "Thermochemical Data for Reactor Materials and Fission Products," Elsevier Science, Amsterdam, 1990.
- [5] J. J. Katz, G. T. Seaborg, L. R. Morss, The Chemistry of actinide elements, 2nd Ed., Vol. 1 and 2, Chapman and Hall, London, 1986.
- [6] Hunter, C. W., Fish, R. L., Holmes, J. J., 1975. Mechanical properties of unirradiated fast reactor cladding during simulated overpower transients. *Nucl. Technol.* 27(3), pp. 376-388 (Nov 1975).
- [7] H. S. Khalil and R. N. Hill, "Evaluation of Liquid-Metal Reactor Design Options for Reduction of Sodium Void Worth," *Nucl. Sci. Eng.*, 109, 221-266 (1991).

Paper V



PERGAMON

Annals of Nuclear Energy 29 (2002) 1689–1706

annals of
NUCLEAR ENERGY

www.elsevier.com/locate/anucene

Inherent shutdown capabilities in accelerator-driven systems

M. Eriksson^{a,*}, J.E. Cahalan^b

^aRoyal Institute of Technology, Stockholm Center for Physics, Astronomy and Biotechnology,
Department of Nuclear and Reactor Physics, S-106 91 Stockholm, Sweden

^bArgonne National Laboratory, Reactor Analysis and Engineering Division, 9700 South Cass Avenue,
IL 60439, USA

Received 16 October 2001; accepted 3 December 2001

Abstract

The applicability for inherent shutdown mechanisms in accelerator-driven systems (ADS) has been investigated. We study the role of reactivity feedbacks. The benefits, in terms of dynamics performance, for enhancing the Doppler effect are examined. Given the performance characteristics of source-driven systems, it is necessary to manage the neutron source in order to achieve inherent shutdown. The shutdown system must be capable of halting the external source before excessive temperatures are obtained. We evaluate methods, based on the analysis of unprotected accidents, to accomplish such means. Pre-concepted designs for self-actuated shutdown of the external source suggested. We investigate time responses and evaluate methods to improve the performance of the safety system. It is shown that maximum beam output must be limited by fundamental means in order to protect against accident initiators that appear to be achievable in source driven systems. Utilizing an appropriate burnup control strategy plays a key role in that effort. © 2002 Elsevier Science Ltd. All rights reserved.

1. Introduction

In the design process of a nuclear reactor, important consideration is given to the utilization of passive safety systems and inherent safety features. There is a consensus among reactor designers, supporting the value of passive safety designs. Passive safety systems rely on natural physical phenomena, such as thermal expansion, fundamental nuclear properties, gravity, and heat-transfer by natural convection, to perform essential safety functions. The laws of physics dictate such properties and their effectiveness is not influenced by human action. In the ideal case, passive safety

* Corresponding author. Tel.: +46-8-5537-8197; fax: +46-8-5537-8465.

E-mail address: marcus@neutron.kth.se (M. Eriksson).

design does not require the action of any mechanical or electrical device, making safety functions less dependent on active components. The incentives for employing such designs are improved reliability and simplified operation, both resulting in better safety performance. Inherent features are valuable means for minimizing public concern and gaining public perception on new reactor concepts.

Most work on passive safety in the past has been related to the study of the innovative use of natural convection, decay heat removal, and inherent negative reactivity feedbacks. Such schemes have been successfully implemented in many reactor designs, including water-cooled reactors, gas-cooled reactors, and liquid metal-cooled reactors.

In this paper, we explore the use of passive safety mechanisms to accelerator-driven systems (ADS). While an intrinsic heat-transport path and sufficient natural convection are necessary to achieve passive safety in any reactor system, those requirements are of a general character and are treated elsewhere e.g. (Karlsson and Wider, 2000). Our attention is focused on inherent shutdown capabilities. We evaluate the applicability for such schemes and we suggest some concepts for that purpose.

2. Reference design and modelling

In the assessment, we employ a reference design of an ADS to obtain operating performance data. Accident analysis is performed with the aid of the SAS4A safety code (Cahalan et al., 1994).

The reference design is a model of an ADS that has evolved at the Royal Institute of Technology, Sweden (Wallenius et al., 2001a,b). The core has a nominal power of 800 MWth. It is cooled by liquid lead-bismuth eutectic (LBE) and the fuel is based on a nitride matrix. Fuel pins are configured in an open pin lattice with core average volume fractions of 8/12/80% (fuel/structure/coolant). The fuel consists of (core average): 58% plutonium, 12% minor actinides, 14% boron carbide, 10% uranium-238, and 6% zirconium nitride. Uranium-238 is used in the inner zones to compensate for burnup and poisoning effects (Tucek et al., 2001). Boron carbide is utilized to increase fission-to-absorption probabilities in even neutron number americium isotopes. Radial zoning is applied with an optimized distribution of minor actinides, plutonium, burnable absorbers, and diluents to mitigate power peaking factors and reduce long-term reactivity swing. Taking advantage of a multi-batch fuel loading strategy (Yang and Khalil, 2000), where some fuel sub-assemblies are added to the perimeter of the core on an intermediate time schedule (150 days), the required beam insertion capacity can be reduced. In the present design, it is necessary to ramp the beam by a factor of 1.8 to maintain constant power through an irradiation period of 510 days. Basic design parameters are listed in Table 1.

The primary circuit is illustrated in Fig. 1. The core, heat exchangers, and primary pumps are immersed in a single pool containing LBE. Coolant temperatures, in steady state, range from 573 K at inlet to 702 K at the outlet. In the present design, the inlet flow velocity is set to 2.5 m/s. Deterioration of the protective oxide film

Table 1
Reference ADS design parameters

Core power, MWth	800
Coolant	LBE
Core inlet temperature, K	573
Core outlet temperature, K	702
Flow velocity, m/s	2.50
Volume hot pool, m ³	435
Volume cold pool, m ³	197
Volume inlet plenum, m ³	20
Fuel composition (core average)	Nitrides: 12%MA/73%Pu/15%U238
Inner radius, mm	1.00
Outer radius, mm	2.40
Cladding	HT-9
Inner radius, mm	2.49
Outer radius, mm	2.94
P/D	1.83 and 2.33
k_{eff} eigenvalue, BOL, steady-state	0.954
β_{eff} , %	0.160
Doppler constant, $T_f dk/dT_f$	$-3.87 \cdot 10^{-4}$
Coolant density reactivity feedback, dk/dT_c	$-2.28 \cdot 10^{-6}$

layer on structural material imposes an upper limit on the flow velocity. The actual limit depends on the temperature and is not well known, however, it is estimated to be in the range of 2–3 m/s (Novikova et al., 1999). The reactor vessel is filled with LBE to a prescribed level, with the remainder of the vessel being occupied by an inert cover gas. The steam generators are elevated well above the core to promote natural convection.

A primary system model is set-up in SAS4A, including a detailed multi-channel model of the core, heat exchangers, pumps, compressible pool volumes, etc. Point kinetics is used for calculating transient power. The neutronic response between core regions is strongly coupled and space-time effects may be neglected for our purposes.

3. Applicability of reactivity feedbacks in ADS

Intelligent use of inherent reactivity feedbacks (e.g. Doppler effect, coolant density effect, structural expansion, etc.) has provided excellent safety characteristics to advanced, critical, reactor. In the design process of a new reactor, it is simply good engineering practice to utilize the inherent nuclear properties of the reactor to ensure optimal safety performance. In particular, operating experience and experiments on liquid metal reactors have demonstrated that better use of the inherent nuclear properties may provide a high level of safety even in severe accidents where the shutdown system fails completely (Lucoff et al., 1992). Nowadays, because of design efforts and increased understanding, the safety characteristics of critical, liquid metal

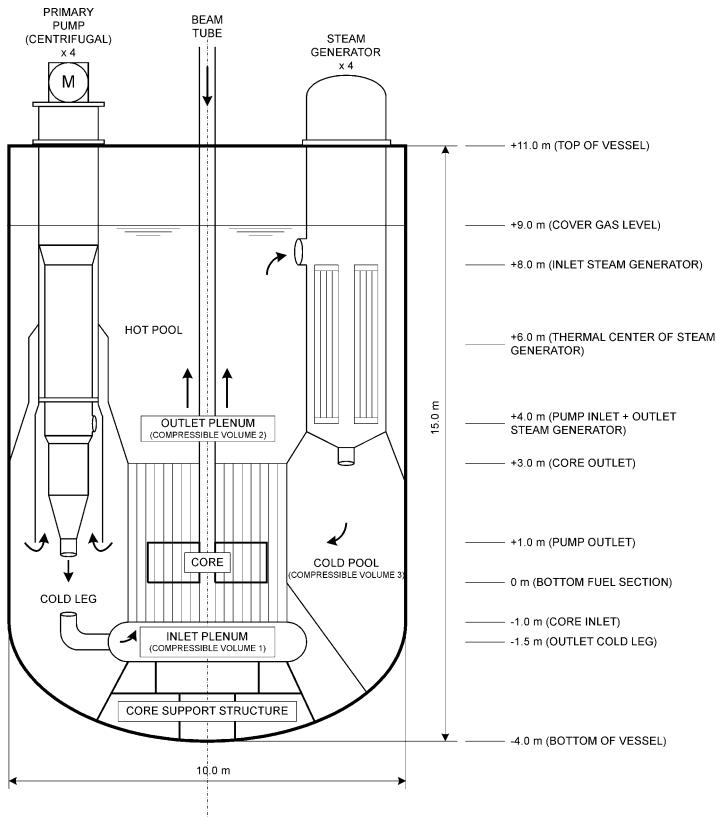


Fig. 1. Primary circuit of reference ADS design.

reactors, are considered as a principal advantage. In that context, it may seem natural to use a similar strategy for ADS's. However, an ADS does not respond to reactivity feedbacks like a critical reactor. While the critical reactor is sensitive to reactivity feedbacks, the ADS is not. The ADS is largely offset from criticality. The net effect is a substantially reduced sensitivity to reactivity changes. This feature diminishes the practical use of reactivity feedbacks as a means for natural safety mechanisms in accelerator-driven systems.

To study these features we exposed the reference design to an unprotected transient overpower (UTOP) event. The initiator for the accident is a sudden increase in source intensity. The intensity of the external neutron source is promptly increased by a factor of 1.8, corresponding to the insertion of maximum beam power at begin-of-life. It represents a strong transient, integral power increases by a factor of 1.8 within a few hundred prompt periods. In Fig. 2, the impact of subcriticality on the combined reactivity effect from Doppler feedback ($Tdk/dT = -3.87 \times 10^{-4}$) and coolant density feedback ($dk/dT = -2.28 \times 10^{-6}$) is illustrated. The unconstrained response, when no feedbacks are accounted for, is also shown to facilitate comparison.

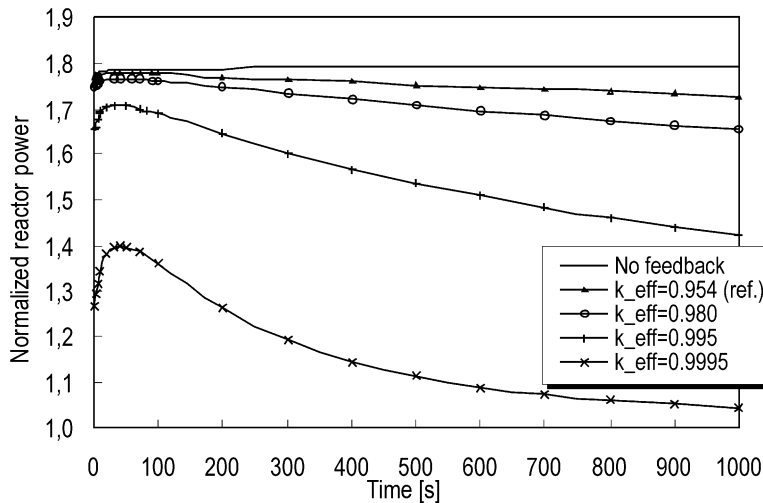


Fig. 2. Impact of reactivity feedbacks in a source-driven system. Accident initiator by sudden increase in source intensity ($S = 1.8 \cdot S_0$). Subcriticality is a parameter.

The response is calculated for a varying degree of subcriticality, $k_{\text{eff}} = 0.954$ (reference design), $k_{\text{eff}} = 0.98$, $k_{\text{eff}} = 0.995$, and $k_{\text{eff}} = 0.9995$. Structural reactivity feedback phenomena (e.g. radial and axial core expansion) are not incorporated into the model. Nevertheless Fig. 2 is instructive in the sense that it demonstrates the general characteristics of a source-driven system subject to reactivity feedbacks.

The reference ADS ($k_{\text{eff}} = 0.954$) experiences minor influence from Doppler and coolant density feedback whereas the close-to-critical system ($k_{\text{eff}} = 0.9995$) exhibits strong feedback effects. Approaching criticality, at the expense of reducing the margin to prompt criticality, results in a stronger reactivity feedback coupling. Thus the significance of reactivity feedback depends on the specific design and in particular the choice of the subcritical level. Taking advantage of reactivity feedbacks calls for a careful balance between the desired feedback performance and the subcritical margin. It is clear, however, that reactivity feedbacks will not be as effective a means in source-driven systems as they are in critical systems. Much stronger reactivity effects, from what is experienced in critical reactors, are necessary to impact on the source driven system. Therefore, it is not practical to implement reactivity feedbacks, by physics or engineering design, as the sole means to bring an ADS to safe shutdown condition. Inherent shutdown must be reinforced by other means.

3.1. Doppler effect

There has been considerable interest in the use of so-called “dedicated” fuels as to achieve maximum transmutation rate in accelerator-driven systems. The dedicated fuels contain large amounts of minor actinides (Np, Am, and Cm) and plutonium, but lack the classical fertile isotopes (i.e. ^{238}U and ^{232}Th). Subsequent deterioration

of safety parameters, when using such fuels, is well known (Maschek et al., 2000). While Doppler broadening of capture resonances is the most important inherent shutdown mechanism in a liquid–metal reactor, the effect is vanishing in accelerator-driven systems using dedicated fuels. The reduction of the fertile inventory and the spectrum hardness are the main reasons for this impairment (Maschek et al., 1999, 2000). It has been argued that a typical ADS core, based on dedicated fuels, contains several critical masses, which in principle provides the potential for criticality if the fuel is rearranged in a more dense configuration. In the absence of the Doppler effect, such accidents may occur without any restraining prompt negative reactivity feedback. Provisions for increasing the Doppler effect in dedicated cores have been proposed (Tommasi and Massara, 1999). In Table 2, values of the Doppler constant are listed for various heavy-metal cooled reactors. The Doppler constant for a sodium-cooled reactor is also included.

The Doppler constant for the dedicated cores (cases 1 and 2) are an order of magnitude lower than those of the mixed U–Pu fuels (cases 4 and 5) with their large Doppler constant. Tommasi and Massara (1999) enhanced the Doppler effect in a fertile-free core by adding some amount of hydrogenated moderator. The Doppler effect obtained in the sodium design (case 6), by Hill et al. (1999), surpasses the Doppler values in the lead-based designs by a factor of two. The argument is that the softer spectrum of the sodium design allows more neutrons to appear in the resonance region. Practically all the Doppler effect occurs below about 25 keV, where cross section variations with temperature are large (Hummel and Okrent, 1978).

We have investigated the merits; in terms of safety performance of the core, of increasing the Doppler effect in an ADS. By explicitly taking into account the Doppler feedback, we studied the response following a sudden “source jump” (same as previous transient). The source transient was chosen because it results in high fuel temperatures, which is the driver for reactivity input by the Doppler effect. Different values for the Doppler constant were modelled, $Tdk/dT = -3.87 \times 10^{-4}$ and $Tdk/dT = -2.71 \times 10^{-3}$, representing a core containing dedicated fuels and a core containing large amounts of fertile material, respectively. The results are presented in Fig. 3.

The dynamics response, including Doppler reactivity feedback in the reference ADS ($k_{\text{eff}} = 0.954$) with dedicated fuel is tiny. Even if the Doppler constant is increased by a

Table 2
List of Doppler constants in various LMR designs

Case	Tdk/dT	Fuel composition	Coolant	Comment	Reference
1	$-3.87 \cdot 10^{-4}$	(U _{0.1} Pu _{0.7} MA _{0.2})	PbBi	Mostly MA and Pu	Present design
2	$-1.50 \cdot 10^{-4}$	(Pu _{0.5} MA _{0.5})	Pb	Very hard spectrum	Tommasi and Massara (1999)
3	$-2.03 \cdot 10^{-4}$	(Pu _{0.5} MA _{0.5})	Pb	Added moderator	Tommasi and Massara (1999)
4	$-1.63 \cdot 10^{-3}$	(U _{0.8} Pu _{0.2})	PbBi	Compact design	Hill et al. (1999)
5	$-2.71 \cdot 10^{-3}$	(U _{0.9} Pu _{0.1})	PbBi	Derated design	Hill et al. (1999)
6	$-4.89 \cdot 10^{-3}$	(U _{0.9} Pu _{0.1})	Na	Derated design	Hill et al. (1999)

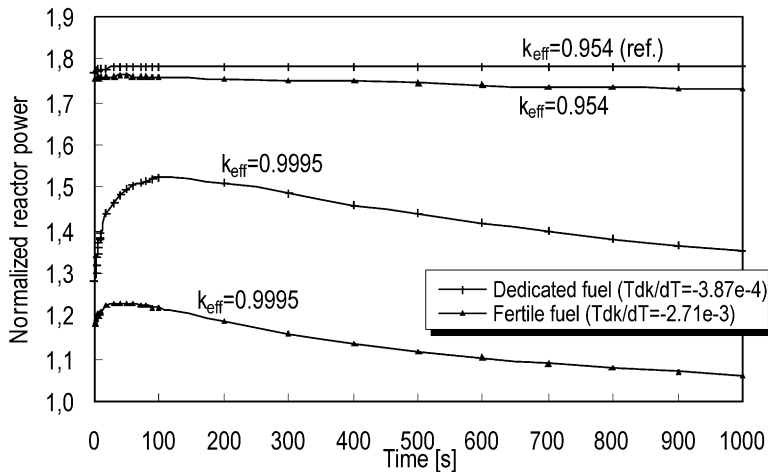


Fig. 3. Issue of enhancing the Doppler effect in ADS's. Lower Doppler value representing a dedicated core, higher Doppler value representing a core containing a large fraction of ^{238}U . Two different subcritical levels are considered. Accident initiator by sudden increase in source intensity ($S = 1.8 \cdot S_0$).

factor of seven, by introducing massive amounts of fertile material, the gain in feedback effect is small. There seems to be little benefit for increasing the Doppler effect in an effort to obtain a more benign response to accidents that remain in the subcritical state. In general, the importance of the Doppler effect in an ADS is strongly related to the level of subcriticality. In a close-to-critical system an equivalent increase of the Doppler effect would result in a significant improvement (see Fig. 3) ($k_{\text{eff}} = 0.9995$). The role of Doppler feedback in hypothetical accidents exceeding the critical margin must be further evaluated.

4. Time response

The thermal response of core constituents and the time to reach failure in various accidents influences the requirements on the shutdown device. Knowledge of the grace period, as defined by IAEA (1991), is essential in the evaluation of such devices. The plant must survive long enough for a passive safety action to be initiated in time to prevent core damage.

The numerical value of the grace period is necessarily specific to the particular design and is of less interest, but the time responses of accidents. Our intention is to study the response in order to assess the requirements on the safety system and to evaluate possible safety actions to enhance the performance. We may express response times defined by time constants rather than by absolute values, which has a broader range of applicability.

We subjected the reference design to three representative sequences of unprotected (i.e. no shutdown or plant protection system action) accidents, namely:

- (a) *Unprotected transient overpower (UTOP)* by a prompt insertion of maximum beam current. It is assumed that the steam generators remove heat at a rate of nominal power (constant temperature drop in steam generators).
- (b) *Unprotected loss-of-flow (ULOF)* by a loss of primary pump power. Feed-water flow is assumed to remain at its initial value and coolant inlet temperature is constant (constant outlet temperature in steam generator).
- (c) *Unprotected loss-of-heat-sink (ULOHS)* by a sudden inability of the steam generators to remove heat (zero temperature drop in steam generators).

Constant steam generator boundary conditions are assumed. The actual boundary condition depends on the particular accident (see above). Safety margins that are applicable to the reference design are indicated in the figures. These are based on postulated transient failure temperatures (listed in Table 3).

The dissociation temperature of minor actinide nitride fuel (NpN, AmN, CmN) is not well known (Suzuki and Arai, 1998). However, it is known that stable AmN has been fabricated at 1573 K (Takano et al., 1999). Mechanical failure limits, used to evaluate cladding failure, are those for 20% cold-worked 316 stainless steel due to lack of reliable data on HT-9. Mechanical strength properties are based on transient burst tests conducted on unirradiated and internally pressurized cladding specimens (Hunter et al., 1975).

In Figs. 4 and 5, peak fuel temperatures and peak cladding temperatures, respectively, are displayed as a function of time.

In the source transient (UTOP), the power “jumps” by a factor of 1.8, see Fig. 2. Since no time is required for heat flow, the fuel suffers a rapid, almost adiabatic thermal excursion, Fig. 4. Coolant and structure are heated at a rate determined by the characteristic time constant of the fuel element. The fuel itself, has the shortest time response and is most sensitive to source transients. After a few seconds, the fuel pins have adjusted to the new power level and temperatures temporarily settle in a quasi-equilibrium (not visible in the figure). For an extended period, mainly determined by the primary loop circulation time and the coolant heat capacity, the coolant inlet temperature remains at its initial value. The steam generators are assumed to remove heat at a rate of nominal power, resulting in a mismatch in the heat production and heat removal. The net effect is increasing inlet temperature, which causes the reactor core, coolant, and other components to overheat, inevitably leading to core damage unless the reactor is shut down.

Table 3
List of failure temperatures for the reference design

Failure mechanism	Failure temperature	Comment
Dissociation of AmN	1573 K	Conservative assumption (Takano et al., 1999)
Cladding burst temperature	1333 K	20% CW SS316, 5.56 °C/s, hoop stress 100 MPa (Hunter et al., 1975)
Cladding/coolant corrosion	946 K	Extended operation (Novikova et al., 1999)

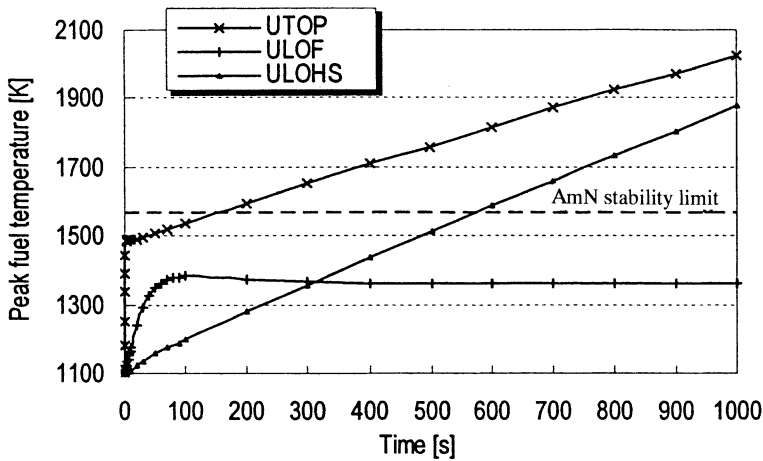


Fig. 4. Peak fuel temperatures in unprotected TOP, LOF, and LOHS.

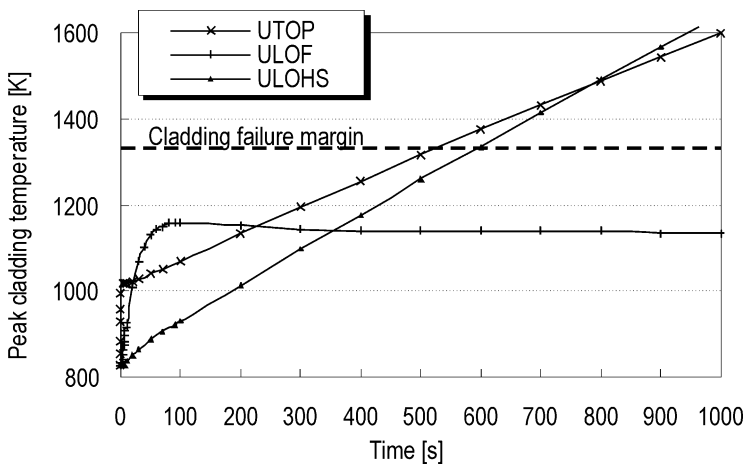


Fig. 5. Peak cladding temperature in unprotected TOP, LOF, and LOHS.

In the loss-of-flow (ULOF) accident, core heat-up occurs at a rate determined by the flow coast-down. Inertial forces help to push the coolant through the primary system for an extended period. Peak temperatures occur as the pump impeller comes to a complete rest. Core temperatures and buoyancy forces eventually balance. In the asymptotic state, flow is sustained by natural convection alone. Reactivity feedbacks have negligible effect on the transient. For this particular system, an unprotected loss-of-flow accident should result in little or no damage. The integrity of the fuel and the cladding is not compromised. The protective oxide film layer on the cladding may suffer some damage that potentially could harm the cladding in the long run.

The loss-of-heat-sink (ULOHS) accident tends to be a more slowly evolving accident than the source transient and the loss-of-flow accident. The accident manifests as rising inlet temperature, which accompanies loss of primary heat sink. Response time is determined by the primary loop circulation time and coolant heat capacity. The prolonged grace period in a ULOHS accident facilitates successful performance of the safety system. Core damage is inevitable unless safety measures are taken to shut down the reactor.

In the unprotected LOHS accident shown in Fig. 4, we assumed that the primary pumps continued to operate. We also studied the response to a combination of loss-of-heat-sink and malfunctioning primary pumps. The temperature increased much more rapidly as the initial response, in that case, is mainly determined by the flow coast-down. It turned out that the grace period in a combined ULOHS and ULOF accident for this specific system was reduced by 50% compared to an isolated ULOHS. It should be taken into account, however, that it is likely that a loss-of-heat-sink accident will be in the form of impairment rather than a sudden and complete loss of heat rejection capability.

In Fig. 6, the thermal response of the coolant in the hot pool is displayed. The coolant temperature is an important safety system parameter since it is related to the heat production in the core. It can be used to sense power excursions and reduction in coolant flow rate. The coolant temperature may be used as an actuator in a passive safety device.

The thermal response of the coolant in the hot pool following a change in power or flow is delayed by the heat capacity of the coolant and transport lags. Therefore, it must be ascertained whether the time response of the coolant is sufficient to serve as an accident indicator and protect against the fastest transients conceivable in an ADS. Rapid coolant response is advantageous since it promotes prompt action of the safety system. In general, UTOP caused by insertion of maximum beam power, is likely to exert the fastest transient. The absence of any moveable control rods, that may rather quickly add or remove large amounts of reactivity, diminishes the

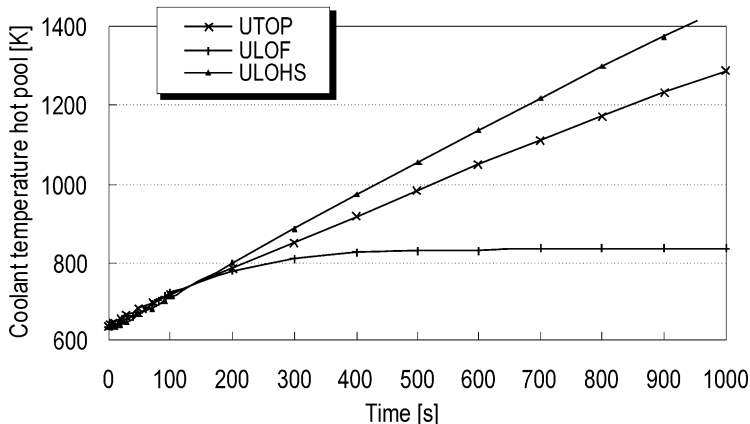


Fig. 6. Coolant temperature in the hot pool.

potential for fast transients caused by reactivity insertion. Significant reactivity is potentially available in core compaction or voiding phenomenon, but such sequences stretch over a longer period. It is noticeable in Fig. 6, that the initial response (<200 s) is more or less the same for all transients. However, source transients introduce the shortest grace period (with respect to fuel damage), while the temperature rise in the coolant is modest. In that sense, source transients impose the highest demands on a passive device that relies on the thermal response of the coolant.

5. An approach to inherent shutdown

Compared to reactivity changes, variations in source strength or source importance have a strong influence on the ADS. The power is linearly proportional to the source, 10% reduction in source strength yields 10% reduction of power, and so on. Shutdown of the external source effectively halts the fission process in the entire core.

Our approach is to design a passive system for the primary purpose to shut down the source in an emergency. The passive device would be comprised in an overall plant control system strategy similar to (Table 4): (a) use an active, regulating system that adjusts the source during normal operation. The regulating system function is to meet the power demand rather than to shut the reactor down if an accident occurs. (b) Use an active plant protection system (PPS) as a first level of protection to shut off the beam in an accident. The PPS would signal on excess temperature levels, low coolant flows, high neutron flux levels, etc. (c) Use the passive, self-actuated, shutdown system providing the second line of protection whenever the PPS function is not properly carried out. The passive system must be inherently independent of the normal beam control system.

It should be recognized that system redundancy makes the assumption of PPS failure highly unlikely. In fact, actual activation of the passive shutdown system must be regarded as hypothetical. Indeed, it affects the requirements on the device.

The shutdown system must be capable of halting the external source before excessive temperatures are obtained. This may be accomplished by reducing the time required for the shutdown system to act and by limiting the thermal response by design considerations. As mentioned previously, the fastest credible transient in an ADS is a source insertion transient. Worst conditions occur when the maximum

Table 4
Plant control system strategy

Control system	Classification	Action
Regulating system	Active	Source regulation. Online usage during normal operation
Plant protection system (PPS)	Active	Beam/source shutdown. Actuated in an off-normal event
Passive shutdown system	Passive	Source shutdown. Actuated when PPS malfunctions

beam power is inserted in a step fashion at the begin-of-life. Source transients result in a rapid, but bounded power excursion. Consequently, it is unsafe to rely on a safety system to assure protection in the early phase of a source transient. Instead, protection must be accomplished through safety-by-design principles, e.g. minimizing the beam output capability by utilizing an appropriate burnup control strategy. While the speed of the beam controller may be limited by fundamental means, the capacity of the accelerator (beam power) is dictated by reactivity losses governed by fuel burnup. Various options exist, for example, shorter irradiation-cycle time and multi-batch fuel loading strategy (Yang and Khalil, 2000), lower power density and higher transuranic inventory (Hill and Khalil, 2000), optimal distribution of plutonium and minor actinides (Gonzalez et al., 2000), use of burnable absorbers (Wallenius et al., 2001a, b). Safety-by-design relaxes the requirements on the shutdown system.

In UTOP and ULOHS accidents, the grace period may be prolonged by the primary loop circulation time and the coolant heat capacity. Typical accidents where the coolant inventory has an appreciable effect on the thermal response involve situations when there is a net change in internal energy (primary system). Loss-of-flow accidents do not necessarily involve any accumulation of internal energy in the primary system, as the heat-removal rate may be unaffected. For loss-of-flow transients, the initial response is determined by the flow coast-down. It may be influenced by changing the moment of inertia of the pump and by increasing natural convection.

Taking these circumstances in consideration, our approach is to prolong grace periods, increase safety margins, and utilize safety-by-design principles, all easing the demands on the safety system. Prolonged grace periods do not only improve our chances for successful safety performance but reduces the probability for false actuation and interference of the passive system during normal operation. The second objective, in order to achieve high reliability, is to design simple, redundant and diverse shutdown systems, and to use components of proven high reliability. Greater complexity generally means reduced reliability.

6. Inherent shutdown mechanisms

In this section, we suggest some concepts for inherent beam shutdown. The intention is to demonstrate the basic working principle. Appropriate references are included for strategies suggested by separate authors.

6.1. Flooding of the beam tube

Shutdown of the external source can be accomplished by flooding the beamtube with coolant. The main purpose for filling the beamtube is to shift the axial position of beam impact, which in principle reduces the importance of source neutrons. Actuation may be based on thermal expansion of coolant or use of bursting disk devices. Several authors have proposed designs that utilize such principles.

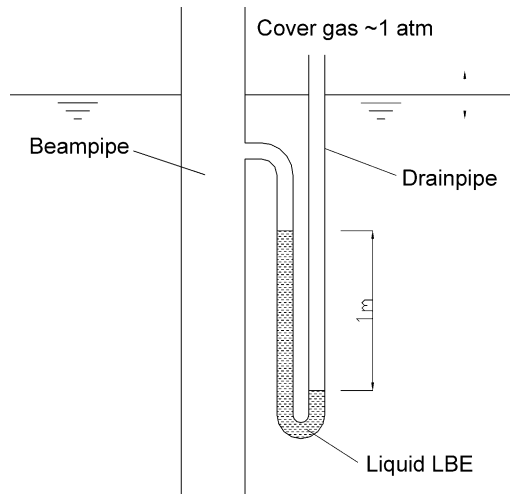


Fig. 7. Basic scheme for filling the beamtube with coolant through a U tube. Concept relies on a working moving fluid (class B device).

Rubbia et al. (1995) proposed a technique for the “energy amplifier” in which coolant rising above a prescribed level activates an overflow path and floods the cavity in the beam tube.

To fill the beamtube, we suggest installing a drainpipe in the shape of a U tube, shown in Fig. 7.

One side of the U tube is open to the cover gas region while the other side is connected to the beamtube. A portion of the coolant is retained in the U bend, forming a liquid seal that separates the beamtube from the cover gas region. A liquid column is supported by the pressure difference. A pressure difference of 1 atm is equivalent to a column height of LBE of 1 m (11 m for sodium). The inlet is located at a certain height above the surface. As the coolant expands, it would rise to the inlet, flood the drainpipe, and subsequently spill into the beamtube. The intake to the drainpipe must be elevated high enough to reduce the risk for false actuation. Difficulties may exist if the surface is seriously disturbed by turbulence and vapor bubbles.

In our reference design, the coolant level rises at a rate of 10 cm/100 K. In Fig. 8, the coolant surface elevation is calculated for unprotected TOP, LOF, and LOHS accidents. Zero level is the surface elevation at steady-state. The points at which the fuel and the cladding exceed their safety margins are also indicated. For the source transient (UTOP), the surface rises approximately 10 cm before fuel failure, corresponding to the smallest level change yet leading to core damage. In a loss-of-flow accident there is a gradual loss of pressure head why the coolant level actually drops during pump coast-down. The rate at which the coolant rises can be affected by the geometry of the vessel.

The basic design only relies on the integrity of the components and a moving working fluid. It does not require signals, external power, moving mechanical parts.

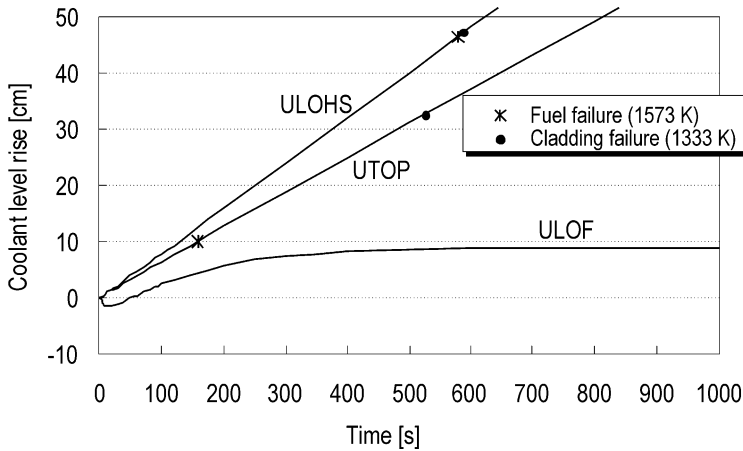


Fig. 8. Rise of coolant level in hot pool in unprotected accidents.

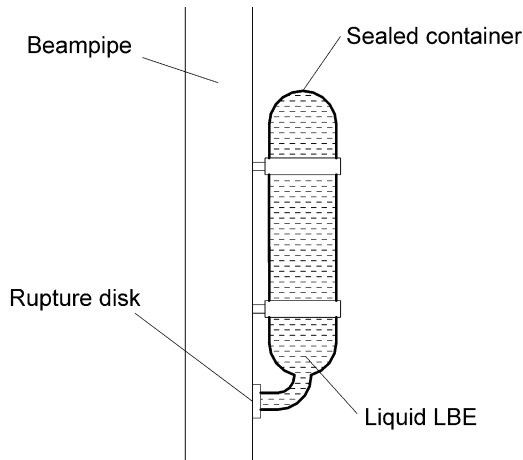


Fig. 9. Scheme for filling the beamtube using a pressurized container. Concept relies on a bursting disk device (class C device).

In that case, it is classified as a passive device in category B, in compliance with IAEA's categorization of passive systems (IAEA, 1991).

A straightforward method was proposed by Wider et al. (1999), in which a melt-rupture disk is installed in the side-wall of the beam tube. The membrane is in contact with the coolant. Source shutdown is actuated as the disk fails and the vacuum tube is flooded with coolant.

Another option is to have a liquid, e.g. LBE, completely fill a sealed container of fixed volume, see Fig. 9. The container is placed in thermal contact with the coolant and it is sealed off to the beamtube by a rupture disk. When excessive pressures occur then the rupture disk fractures releasing the liquid to the beamtube.

In general, bursting disk devices tend to be less accurate. The burst pressure or temperature is unpredictable. The problem is accentuated due to ageing and when used in a hostile environment. A drawback is that the disk is destroyed in the action, thus eliminating the possibility of testing the device prior to its installation or when it is in service. In order to attain a short time response, the disk must be operated close to its bursting point, which increases the possibility for false actuation. Passive safety based on bursting disk devices is classified in category C, in accordance with IAEA regulation.

Beam chambers typically require high vacuums and chemically clean surfaces to prevent proton interaction with trapped gas. Filling the beamtube with coolant may cause serious contamination of the accelerator tunnel. One option is to install a second beam window at the top of the tube to separate the beamtube from the accelerator tunnel. If the passive system provokes a shutdown, it may require replacing the beamtube, however, it is likely the plant needs correction anyhow, to assure its integrity and to reinstate the original safety function. In that perspective, filling of the beam tube could possibly serve as a last resort. False actuation, however, must be eliminated.

6.2. *Alternative methods*

In most pre-conceptual ADS designs, the beam is subject to some bending action before entering the vessel. Bending of a charged particle beam is normally carried out by magnets. In principle, a bending magnet could serve as an on/off switch for the external source. If the magnet is de-energized, the beam would safely end-up in a beamstop, otherwise the beam is diverted to the target.

For such a device switching is necessary, e.g. an electrical circuit must open/close, which limits the safety level achievable by this principle. Preferably, the passive switch is of a fail-safe type, i.e. unless connection is established the magnet is off. Possible agencies for actuating such a switch include:

- A ferromagnetic Curie-point-operated device. Above the Curie temperature, the magnetization of a permanent magnet vanishes. Such a device could either be used for switching or in a lock-release function acting on safety rods. Similar devices showed considerable promise for application in self-actuated shutdown systems in liquid-metal fast breeder reactors (Sowa et al., 1976). The Curie temperature of carbon steel is 1043 K.
- Elongation of a metal rod that is submerged in the coolant or bending of a bi-metallic component could be used as a temperature-sensitive switch.
- Rising coolant levels could elevate a float device that is connected to an electrical circuit. Alternatively, the medium itself could act as a conductor and establish connection.
- Pressure build-up in the cover gas region (or some other compartment), due to thermal expansion of the medium could actuate a switch that operates at a predetermined pressure. A weighted lever or a spring could set the limiting pressure. Alternatively, thermal expansion of a fixed mass of a fluid (LBE) in a confined space could perform a similar task.

- A generator that is connected to the coolant flow may supply power to the bending magnet. The generator may be driven by mechanical forces or as a reversed electromagnetic pump. However, the drawbacks include, obstruction of flow in a free-convection mode, need for significant pumping power, and lack of temperature feedback.
- Liquid metal coolants feature temperature-dependent resistivity. Increasing the temperature will increase the resistivity. Resistivity rising above a limiting value could trigger an electrical or magnetic switch.

7. Conclusions

The applicability for passive safety to accelerator-driven systems was studied. The current study focused on means for inherent shutdown. The usefulness for reactivity feedbacks was evaluated and some schemes for inherent source shutdown were suggested.

It seems that inherent shutdown based solely on reactivity feedbacks is fruitless in accelerator-driven systems. Inherent shutdown must be reinforced by other means. It was shown that increasing the Doppler effect, by introducing massive amounts of fertile material, have limited effect on transients that remain in the subcritical state. Doppler feedback may be important for accidents exceeding criticality. The significance of reactivity feedbacks, in general, depends on the specific design and in particular on the choice of the subcritical level. Taking advantage of reactivity feedbacks calls for a careful balance between the desired feedback performance and the subcritical margin.

Safety analysis indicated that transient overpower accidents, caused by insertion of the maximum beam power, is likely to exert the fastest transients conceivable in an ADS. In that perspective, source transients have profound impact on the requirements for a shutdown device. Safety-by-design principles must be utilized to assure protection to source transients.

Some concepts to accomplish passive source shutdown were presented. Two methods that seek to block the beam by filling the beamtube with coolant were proposed. Actuation is caused by thermal expansion of coolant. Other options include shutdown of beam bending magnets or insertion of shutdown rods by passive means.

Shutdown of the beam by passive means can provide an important additional safety feature for accelerator-driven systems. Such systems may contribute significantly to the reliability of the overall plant protection system. At this point, however, considering the premature nature and the lack of experimental validation, further work is necessary in order to determine the practicability of the present design concepts.

Acknowledgements

Sincere appreciation is expressed to the SKB AB and The Swedish Center for Nuclear Technology who financially supported the project.

References

- Cahalan, J.E., Tentner, A.M., Morris, E.E., 1994. Advanced LMR safety analysis capabilities in the SASSYS-1 and SAS4A computer codes. Proceedings of the International Topical Meeting on Advanced Reactors Safety, Pittsburgh.
- Gonzalez, E., et al. 2000. Transuranics on fertile and inert matrix lead-bismuth cooled ADS. 6th Information Meeting on Actinide and Fission Product Partitioning and Transmutation, Madrid.
- Hill, R.N., Cahalan, J.E., Khalil, H.S., Wade, D.C., 1999. Development of small, fast reactor core designs using lead-based coolant. Proceedings of the International Conference On Future Nuclear Energy Systems, GLOBAL'99, Jackson Hole.
- Hill, R., Khalil, H., 2000. Physics studies for a Na-cooled ATW design. IAEA Technical Committee Meeting on Core Physics and Engineering Aspects of Emerging Nuclear Energy Systems for Energy Generation and Transmutation, Argonne.
- Hummel, H.H., Okrent, D., 1978. Reactivity coefficients in large fast power reactors. American Nuclear Society, Illinois, pp. 133.
- Hunter, C.W., Fish, R.L., Holmes, J.J., 1975. Mechanical properties of unirradiated fast reactor cladding during simulated overpower transients. *Nucl. Technol* 27 (3), 376–388.
- IAEA, 1991. Safety Related Terms for Advanced Nuclear Power Plants. TECDOC-626.
- Karlsson, J., Wider, H., 2000. New aspects of emergency decay heat removal from a Pb/Bi-cooled ADS by auxiliary cooling. Proceedings of the ICONE 8, 8th International Conference on Nuclear Engineering, Baltimore.
- Lucoff, D.M., Waltar, A.E., Sackett, J.I., Aizawa, K., 1992. Experimental and design experience with passive safety features of liquid metal reactors. International Conference on Design and Safety of Advanced Nuclear Power Plants, Tokyo.
- Maschek, W., Rineiski, A., Morita, K., Muhling, G., Flad, M., 2000. Safety analysis for ADS cores with dedicated fuel and proposals for safety improvements. Proceedings of the IAEA Technical Committee Meeting on Core Physics and Engineering Aspects of Emerging Nuclear Energy Systems for Energy Generation and Transmutation, Argonne.
- Maschek, W., Thiem, D., Heusener, G., 1999. Safety features of a reactor core with minor actinide transmutation and burning capabilities. Proceedings of the International Conference On Future Nuclear Energy Systems, GLOBAL'99, Jackson Hole.
- Novikova, N., Pashkin, Y., Chekunov, V., 1999. Some features of sub-critical blankets cooled with lead-Bismuth. Proceedings of the International Conference on Accelerator-driven Technologies and Applications, ADTTA'99, Praha.
- Sowa, E.S., et al., 1976. LMFBR Self-actuated Shutdown Systems, Vol. II. Proceedings of the International Meeting of fast Reactor Safety and Related Physics, Chicago.
- Rubbia, C., et al., 1995. Conceptual Design of a Fast Neutron Operated Energy Amplifier. Cern publication, CERN/AT/95-44.
- Suzuki, Y., Arai, Y., 1998. Thermophysical and thermodynamic properties of actinide mononitrides and their solid solutions. *J. Alloys Comp.* 271–273, 577–582.
- Takano, M., et al., 1999. Synthesis of americium mononitride by carbothermic reduction method. Proceedings of the International Conference on Future Nuclear Energy Systems, GLOBAL'99, ANS, Jackson Hole.
- Tommasi, J., Massara, S., 1999. L.M.F.R dedicated cored for transmutation critical vs. subcritical systems comparison. Proc. International Conf. On Future Nuclear Energy Systems, GLOBAL'99, Jackson Hole.
- Tucek, K., Wallenius, J., Gudowski, W., 2001. Source efficiency in an accelerator-driven system with burnable absorbers. GLOBAL 2001, International conference on the Back-end of the Fuel Cycle: from Research to Solutions, Paris.
- Wallenius, J., Tucek, K., Carlsson, J., Gudowski, W., 2001a. Application of burnable absorbers in an accelerator-driven system. *Nucl. Sci. Eng.* 137, 96–106.
- Wallenius, J., Tucek, K., Eriksson, M., Gudowski, W., 2001. The Sing Sing core: a sub-critical TRU burner with low reactivity losses. Proceedings of the International Conference on Accelerator

Applications/Accelerator Driven Transmutation Technology and Applications '01. AccApp/ADTTA '01, Reno.

Wider, H., Karlsson, J., Jones, A. V., 1999. Safety considerations of heavy metal-cooled accelerator-driven systems. Proceedings of the International Conference on Future Nuclear Energy Systems, GLOBAL'99, Jackson Hole.

Yang, W. S., Khalil, H. S., 2000. Reduction in burnup reactivity loss in accelerator driven transmutation systems. Proceedings of the 4th Topical Meeting on Nuclear Applications of Accelerator Technology, Washington.

Paper VI

RELIABILITY ASSESSMENT OF THE LANSCE ACCELERATOR SYSTEM

Marcus Eriksson

Royal Institute of Technology, Sweden

Christopher Piasczyk

Northrop Grumman Corporation, USA

Abstract

This paper describes the reliability analysis of the accelerator facility at Los Alamos Neutron Science Center (LANSCE)[1]. The goal of the analysis is to present beam failure statistics of LANSCE and identify the root cause of a beam failure. Beam trips and failure causes are assembled using operational data records, accelerator logbook and beam monitor data. Mean Time Between Failure and Mean Down Time estimates are obtained for typical accelerator components. The results are useful in accelerator reliability modelling and identifying development issues in high power accelerators.

Introduction

The reliability and availability of the accelerator in an accelerator driven system is an important issue. New applications for high power proton accelerators such as the production and destruction of radioactive elements demand high availability, reliability and maintainability. Persistent beam power fluctuations have a negative influence on a hybrid system. In order to estimate and improve the availability and reliability of future accelerator designs, data from existing accelerators are being analyzed. The accelerator facility at Los Alamos Neutron Science Center (LANSCE) is the most powerful linear proton accelerator in the world. The accelerator offers enough operating history to supply meaningful reliability data.

The objective of the present data collection and analysis effort is to understand the behavior of existing operating accelerator facilities so that better, more reliable systems can be designed and built in the future. Previous work has identified the current state of the art lacking in the area of reliability database information for components typically used in rf accelerator systems, such as rf stations, rf drives, rf transport, cooling, vacuum systems, magnets, and magnet power supplies. Thus, while it is possible to use the reliability theory to model accelerator systems, the input data currently available for such analyses lacks credibility. This led to the initiation of an effort of data collection and analysis of which this study is one of the tasks. The present work examines the data set of failure events for the LANSCE 800 MeV accelerator facility.

The LANSCE Accelerator Facility

The LANSCE accelerator delivers two proton beams at 800 MeV: the H⁺ and the H⁻ beam. The H⁺ beam may deliver 1.25 mA current (routine operation is at 1 mA) and the H⁻ beam delivers 70 μ A. Each injector system includes a 750 keV Cockcroft-Walton type generator. Both ions are accelerated simultaneously in one and the same structure. After acceleration the H⁺ and H⁻ beams are separated. The H⁻ beam is injected into a Proton Storage Ring for accumulation and delivery to the neutron scattering center or weapons neutron research.

Beamline	Energy	Current	Injector (High Voltage Generator)	Proton Storage Ring
H+ beam	800 MeV	1.25 mA	Cockcroft-Walton	No
H- beam	800 MeV	70 μ A	Cockcroft-Walton	Yes

Table 1. The LANSCE accelerator delivers two ion beams

The low energy section of the accelerator is an Alvarez Drift Tube Linac (DTL). The drift tube linac accelerate the protons from 750 keV to 100 MeV. The high energy section is a Side Coupled Linac (SCL). The SCL may accelerate protons up to 800 MeV. Different rf systems are used for the drift tube linac and for the side coupled linac. In the DTL, triode power tubes are used for the generation of rf power while in the side coupled linac klystrons are used. The rf system for the DTL is sometimes referred to as the 201 system since the rf frequency in the drift tube linac is 201.25 MHz. The rf system for the SCL is called the 805 rf system since the rf frequency is 805 MHz.

Linac Section	Energy region	RF Power	RF Frequency
Drift Tube Linac	750 keV-100 MeV	Triode power tubes	201.25 MHz
Side Coupled Linac	100 MeV-800 MeV	Klystrons	805 MHz

Table 2. Different rf systems are used in the DTL and the SCL

Ahead of time a beam schedule has been organized with respect to time-sharing between experiments, beam intensity, and beam energy. An overall schedule of commissioned beam time for each beamline is set out. Scheduled operation at LANSCE is divided into run cycles. During scheduled operation, the accelerator is operated almost 24 hours per day for an entire run cycle with only a few scheduled breaks. A run cycle is maintained for approximately 5-6 weeks (800-1000 hours). A large fraction of the year the accelerator is not scheduled due to maintenance activities. Scheduled operation is usually in the region of 2000-3000 hours per year, which is about 30 % of the year. In reliability assessment of LANSCE the total scheduled beam time is an important factor **-beam trips are only analyzed if they occur within scheduled accelerator operation.**

Input Data

Beam delivery is measured by current monitors near the targets. If the beam current for some reason is below half the scheduled current the beam is considered as interrupted. This event/trip generates loss of scheduled beam time, commonly called down time. The operator assigns a failure cause, or down time assignment, to each trip. The down time assignment is recorded in the logbook. The failures and down time assignments are also entered into operational data records. Separate data records are maintained for each beam line or target area. In this investigation beam trips associated with the H+ beam and the H- beam are analyzed. The records obtained cover run cycles 71 through 76, over the period 1996-97.

The first, and most time intensive task of this effort was collecting the input data. Thanks to the cooperation of the LANSCE Operations Group, a large amount of data was collected. This included the:

- 1) Operational data records
- 2) Central Control Room Logbook
- 3) Operations Shift Supervisor's Summary Reports
- 4) Beam Monitor data for 1997

Overall LANSCE Reliability

In this section, the distribution of beam trips and down time for the entire LANSCE accelerator facility is presented. The analysis considers scheduled accelerator operation of the H+ beam for 1997 and of the H- beam for 1996 and 1997. The H+ and the H- beams are investigated separately. All

calculations are based on operational data records or indirectly accelerator logbook data. A histogram of beam trips that occur in the H+ and the H- beam is presented in figure 1.

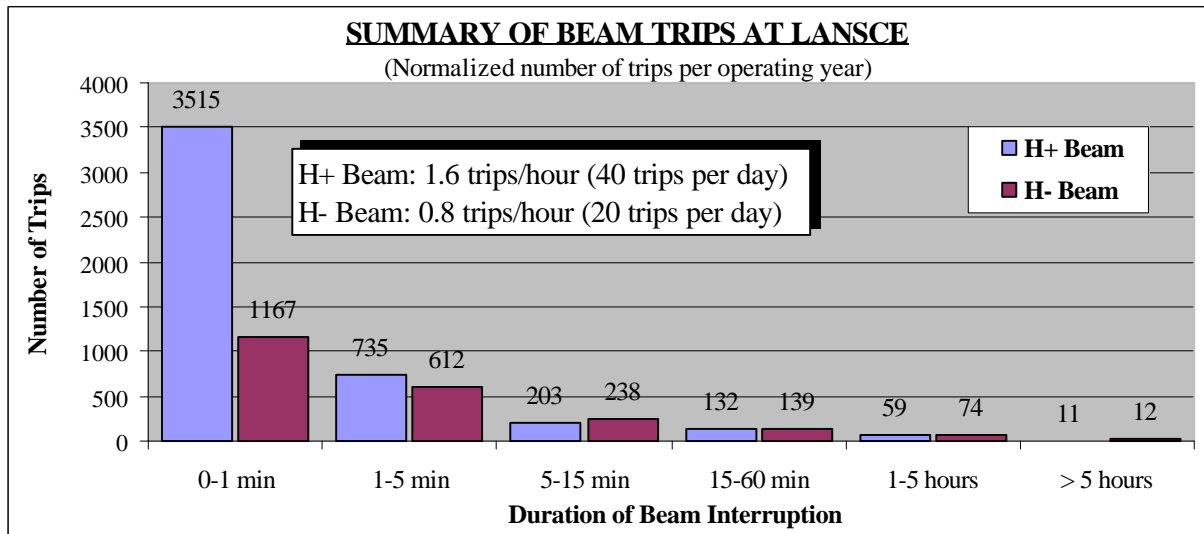


Figure 1. Beam failure statistics of the LANSCE accelerator facility

From figure 1 it is obvious that the H+ beam is exposed to many beam trips with short duration. 76% of all trips in the H+ beam are 0-1 minute long. When comparing the total number of trips in the H+ and H- beams, the conclusion is that twice as many trips occur in H+ beam. When operating, the H+ beam is exposed to 1.6 trips/hour and the H- beam 0.8 trips/hour. The main reason is the larger number of short trips in the H+ beam. For long down times (> 5 minutes), almost the same number of trips occur in the H+ and the H- beams. This makes sense since both beamlines utilize, for most of their length, the same accelerating structure. At a closer look, a slightly larger number of long trips occur in the H- beam. The reason is that the H- beamline is more complex. It includes the Proton Storage Ring and hence more components are subject to failure.

In figure 2, the most frequent causes for beam failure and beam downtime in the H+ beam are presented. Two columns are displayed for each individual system. The leftmost column in each system shows the fraction of total number of H+ trips the system is responsible for. The rightmost column shows the equivalent fraction of total downtime. It is a good thing to separate trips and downtime. Trips affect beam stability and produce power fluctuations. Downtime has a negative influence on the overall beam availability.

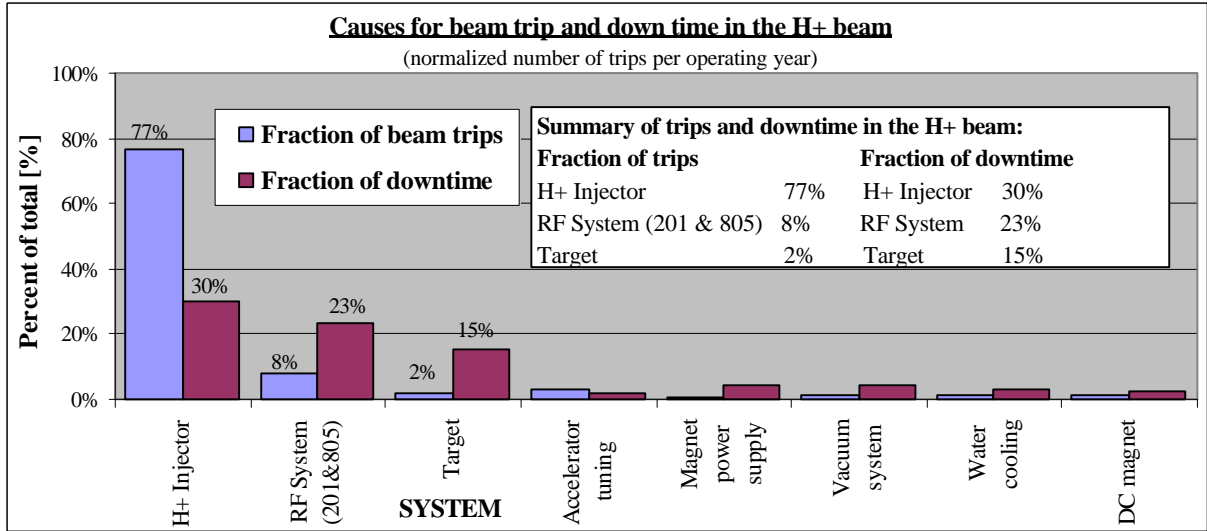


Figure 2. Systems responsible for trips and downtime in the H+ beam

From figure 2, it is obvious that an injector failure is the most frequent cause for beam trip. In the H+ beam 77% of all trips are caused by a failure in the H+ injector. The characteristic of the injector failure is the interruption length. It is usually shorter than 1 minute, often in the order of 15-20 seconds, the time it takes to reset the trip and re-energize the Cockcroft-Walton generator. An injector failure is usually caused by electric breakdown in the high voltage column. Since a typical injector failure is short, the injector is not as dominating when it comes to the generation of downtime. While the H+ injector is responsible for 77% of the trips it is "only" responsible for 30% of the downtime. In other words, the injector is the main reason for beam current fluctuations but it has a significantly smaller influence on the overall beam availability. The rf system, including the rf system for the DTL and the SCL, is generating 8% of the trips but is accountable for 23% of the downtime. Hence, a failure in the rf system usually results in a long downtime (> 5 minutes).

In figure 3, historical data on overall beam availability and beam schedule for the years 1979-97 is presented [2]. The line graph represents beam availability and the column bars represent the scheduled beamtime. It is important to remember that the availability only measures the availability of the accelerator during scheduled operation. A common misunderstanding is that the availability of the machine gives the year round availability.

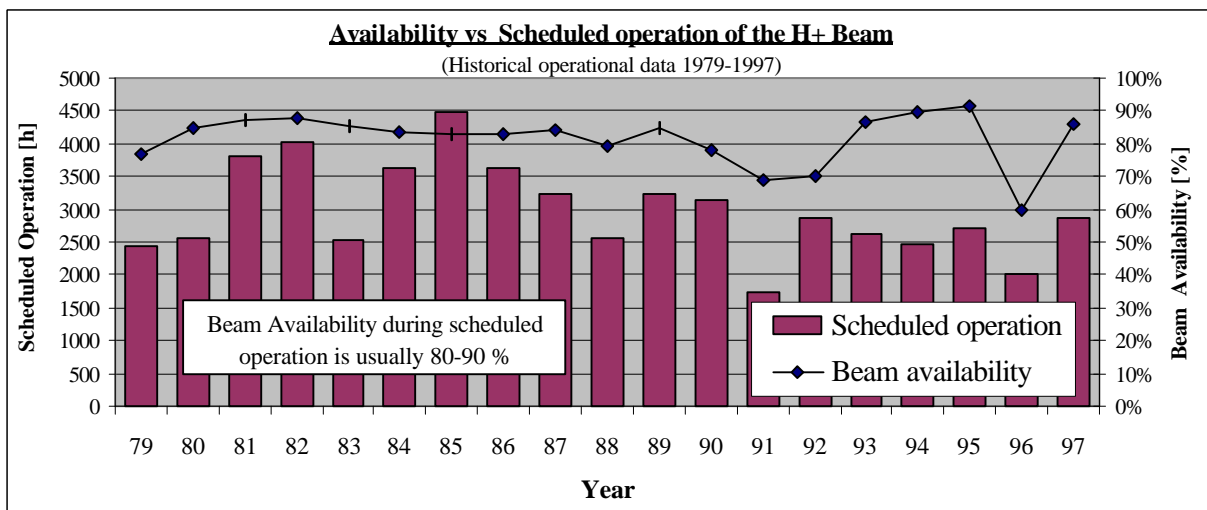


Figure 3. Historical availability and scheduled beamtime of the H+ beam [2]

Figure 3 is interesting in that sense it shows the relation between beam availability and the length of the operating period. Since a short scheduling period is usually followed by a longer maintenance period figure 3 also gives information on the affect of accelerator maintenance on overall availability. When examining figure 3, the conclusion is that **the scheduled beamtime seems to have little influence on the availability**. It means that a long schedule does not have to imply lower beam availability. This is not all true but one obvious example occurred in 1985. In 1985, the longest schedule ever was practiced. The accelerator was commissioned for 4500 hours (50% of the year) and it operated with normal availability (83%). In some years the availability actually drops when the accelerator is operated for less time! In 1996, the availability experienced a decline due to a single water leak in one of the targets, otherwise the standard availability of LANSCE is in the region of 80-90%. This level of availability is similar to the availability experienced in other accelerator facilities.

Analysis of beam current

Previous calculations and diagrams presented in this paper were all based on data originating from the accelerator logbook. Similar beam reliability analysis is performed for data originating from beam current monitors. The H+ beam current has been analyzed during scheduled operation of 1997. The beam current at the end of the H+ beamline is inspected and interruptions are registered. A total of 163,000 beam current recordings are included in the analysis. The current analysis will verify previous results and it will present the "true" beam performance. When analyzing beam current data it is not possible to investigate the failure cause. Results of the beam current analysis are presented in figure 4. The histogram includes the total number of beam trips detected in the beam current and the corresponding down time. For comparison, the total number of trips registered in the logbook during the same time period are also included in the histogram.

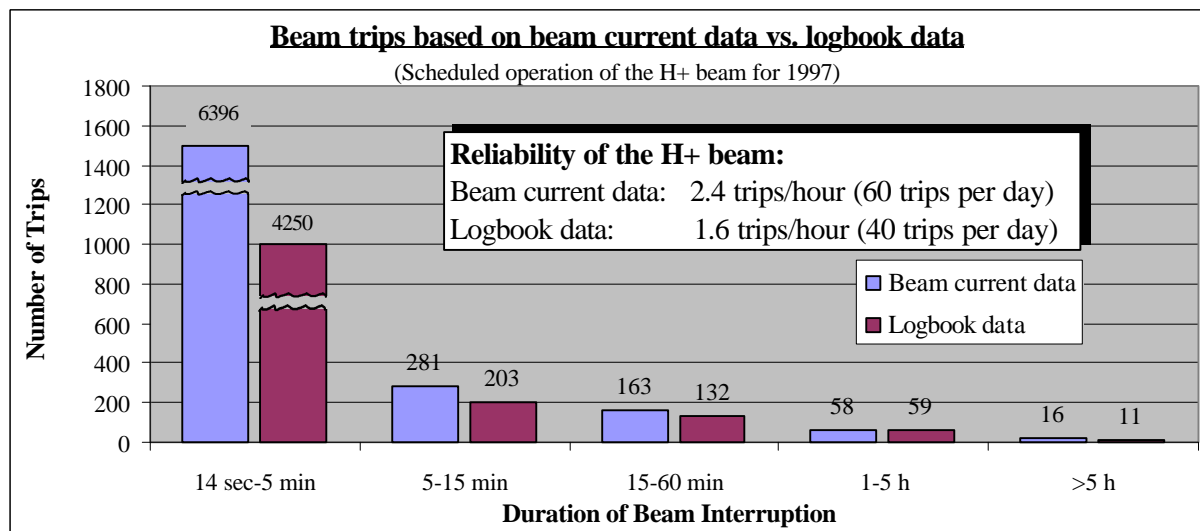


Figure 4. Reliability of the H+ beam at LANSCE

The trips occurred during scheduled operation of the H+ beam for 1997. When analyzing the beam current a total of 6914 beam trips are detected. This number is larger than the number of trips recorded in the logbook (4655 trips) under the same period of time. From figure 4 it is clear that the main reason is that a large number of short interruptions (15-20 seconds) are detected in the beam current which are not included in the logbook. This is also confirmed by operating personnel. For example, in difficult periods when the injector is tripping frequently all short beam trips are not recorded in the logbook, instead comments like "continuous arcing in the injector column" are used.

For trips with long downtime (>5 minutes) it is remarkable how well the results agree even though the underlying data origins from two completely different sources. That is a strong evidence for the correctness of the results from both analyses. When analyzing the beam current it is also evident that practically no interruptions with downtime shorter than 10 seconds occur. In other words, if an interruption occurs it is likely it will last for at least 10 seconds.

Reliability of subsystems & components

In this section the reliability of major LANSCE subsystems and components are investigated. A first cut analysis of the available LANSCE data is performed. Mean Time Between Failure (MTBF) and Mean Down Time (MDT) for individual subsystems are studied to obtain input data for accelerator reliability modelling (RAMI). Individual failures are thoroughly investigated with the help of logbooks, operational reports, operators, maintenance personnel. In case the cause of a trips is uncertain, experts in particular field are consulted to correctly classify the event. The aim is to detect the root cause, down to components level, of each failure. For this purpose, the raw data is divided into categories corresponding to individual subsystems and subsequently estimates of failure and repair rates are obtained. These categories are listed in table 2.

MAIN SYSTEM	SUBSYSTEMS		
805 RF	Klystron assembly	Phase and Amplitude Control	Other
	High Voltage system	Resonance Control	Unknown
	805 Tank	Module Control	
DC Magnets	Magnet Hardware	Water cooling	Vacuum
	Interlocks		
Magnet Power Supplies	Electronics	Transformers	Interlocks
	Capacitors	Water cooling	Unknown
Pulsed Power	Harmonic Buncher	Chopper	Kicker
	Deflector		
Water System	Water Pump	Piping	Unknown
	Other		
Vacuum System	Ion Pump	Piping	Unknown

Table 2. Classification of subsystems

Failures corresponding to each subsystem are merged and classified into individual databases. In table 3, an illustration of the database format for failures in the Klystron Assembly of the 805 RF System is presented. Similar databases are compiled for each subsystem. The database contain trips that affect both the H+ and the H- beams. Failures are only recorded if they occur within scheduled operation.

DURATION OF BEAM INTERRUPTION			LOCATION OF FAILURE			CAUSE OF FAILURE	
Date & Time of Outage	Date & Time of restoration	Down Time [h:min]	Area	System	Subsystem	Component failure or other reason	Comment
Klystron Assembly							
11/01/96 02:09	11/01/96 02:29	0:20	LINAC	805	Klystron	Flow switch	Module 21 Klystron water not okay. Mechanically agitated flow switch and it made up.
11/23/96 09:43	11/23/96 09:56	0:13	LINAC	805	Klystron	Water flow	Sector D off. Module 21 klystron water flow trip. The klystron magnet supply valve has been opened 1/8 of a turn.
11/23/96 23:17	11/23/96 23:32	0:15	LINAC	805	Klystron	Water flow	Module 21 klystron water flow trip
03/17/97 07:25	03/17/97 07:40	0:15	LINAC	805	Klystron	Ion Pump	Module 46 (Sector H) Klystron ion pump supply failed. It was replaced.
05/24/97 07:24	05/24/97 13:14	5:50	LINAC	805	Klystron	Klystron	Module 36 Main Amplitude crowbar. Sector F tripped a second time and the fire alarm went off. Acrid smell from the capacitor room. Module 36 klystron was replaced.

Table 3. Illustration of final database format

The database is for practical reasons divided into three major sections: One section deals with the Duration of the Interruption. It contains the date and time of the beam outage and restoration. It also includes the Down Time of each interruption. The second section considers the Location of the Failure. The Area defines the geographical location of the failure [3]. The System and Subsystem columns specify in what System and Subsystem the failure is located. The third section gives detailed information on the Cause of the Failure. The cause may be a component failure that needs replacement, a bad condition such as a water flow problem or an adjustment failure that needs to be tuned. In the comment column, extra text has been added to explain the failure.

The main objective of the analyses is to obtain estimates for the MTBF and MDT for typical accelerator components, such as RF amplifiers, HV power supplies, magnets, magnet power supplies, vacuum system components, or water cooling components. For illustration the mean down time estimate as a function of time for the magnet power supplies is presented in figure 5. Each dot marks a failure in the magnet power supply. Spaces in between dots is the time between failure. The diagram shows the Mean Down Time estimate at a certain number of failures. The final Mean Down Time estimate for the magnet power supplies is obtained at the last failure in the diagram.

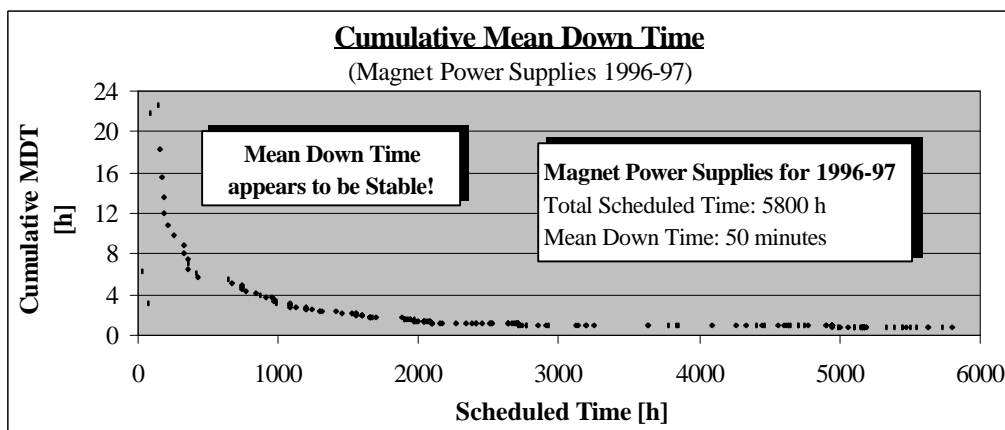


Figure 5. Cumulative Mean Down Time for Magnet Power Supplies

One indication of sufficient number of entries in the data set is the asymptotic behavior of the statistical estimators for the desired quantities, such as the Cumulative Mean Downtime which is calculated as the ratio of the cumulative downtime to the cumulative number of events as shown in figure 5. The conclusion in this case is that further data collection is not necessary, Mean Down Time estimate appears to be stable at approximately 50 minutes. A similar plot is made for the cumulative Mean Time Between Failure in figure 6.

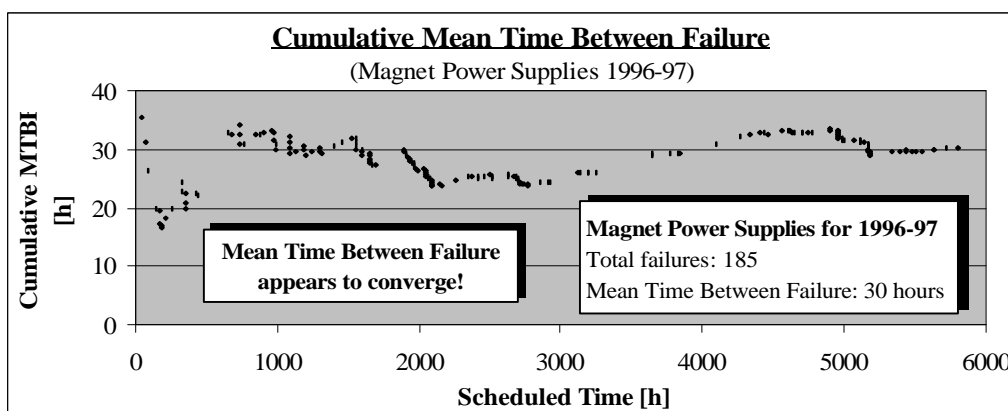


Figure 6. Cumulative Mean Time Between Failure for a single Magnet Power Supply

Cumulative Mean Time Between Failure is calculated as the ratio of the cumulative number of failures to the cumulative up time (scheduled time - downtime). As illustrated in figure 6, the MTBF behavior for the magnet power supplies is not as smooth as for the cumulative downtime but it appears to converge somewhere in the region of 30 h. With 278 magnet power supplies total in the system, the MTBF estimate for an individual magnet power supply is 8445 hours, assuming that all supplies have the same failure rate and can be treated as a series system of independent power supplies.

The results obtained via similar analyses for the other subsystems at LANSCE are summarized in table 4.

RESULTS OF RELIABILITY STUDY AT LANSCE				
Main System	Subsystem	MDT [h:mm]	MTBF for all devices [h]	MTBF for a single device [h]
805 RF	Klystron Assembly	0:44	262	11560
	High Voltage System	0:18	137	960
DC Magnets		0:53	290	232280
Magnet Power Supplies		0:50	30	8445
Pulsed Power	Harmonic Buncher	0:09	44	44
	Chopper magnet	0:08	291	291
	Deflector magnet	0:10	342	684
	Kicker magnet	1:58	185	557
Water System		1:20	120	
	Water pump	0:29	245	29506
Vacuum System		0:48	77	
	Ion pump	0:29	101	25308

Table 4. Some results of the reliability investigation of subsystems and components

The MTBF for the klystron assembly calculated from the raw data corresponds to the entire 805 RF system consisting of 44 klystron assemblies. An estimate of the MTBF for an individual klystron assembly was obtained by multiplying this value by 44 as 11560 hours. This value is not unreasonable when compared with the 20-50,000 hours commonly quoted for the typical klystron tube by itself. A total of 800 dc magnets exist in the LANSCE facility. MTBF for a single magnet is 232280 hours (≈ 26 years). The dc magnets at LANSCE are very reliable. This is also confirmed by maintenance personnel at LANSCE. 50% of the magnet failures are water cooling problems inside the magnet. The most frequent failure cause in a magnet power supply is malfunctioning electronic equipment. Most of the power supplies at LANSCE are controlled by manual electronics. Modern power supplies are computer controlled and proves to be much more reliable. MDT for a water pump is 29 minutes and MTBF is 29500 hours (≈ 3 years). MDT for an ion pump is 29 minutes and MTBF is 25300 hours (≈ 3 years).

Failure analysis

Analysis of failure causes is performed for all major systems. In this section the failure analysis of the rf system is illustrated. In figure 7, the distribution of trips in the rf system is presented. In figure 8, on a deeper level, the distribution of trips in the klystron assembly is presented.

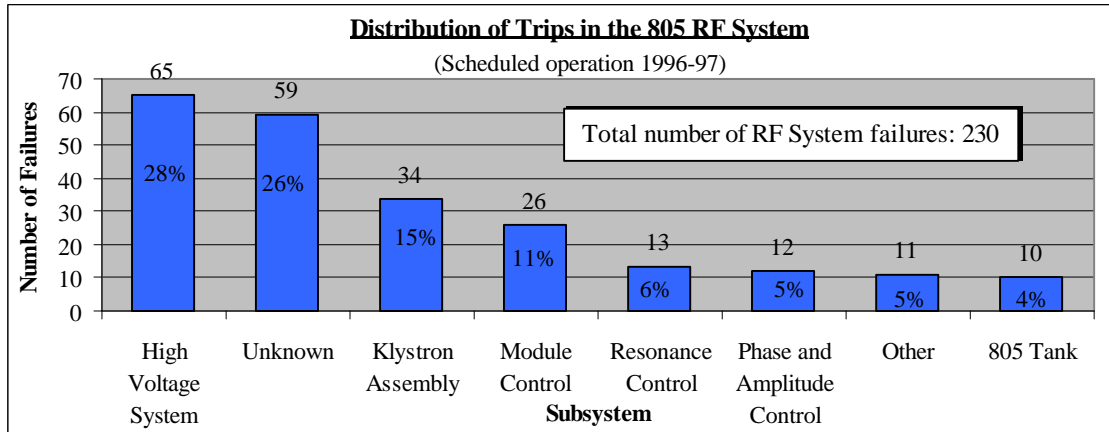


Figure 7. Distribution of trips in the 805 rf system

All subsystems of the 805 rf system are represented in figure 7. The High Voltage System causes many short interruptions. Usually the High Voltage system causes phase or amplitude disturbances to the beam. 26% of the failures in the rf system are unknown. Sometimes when a failure occurs in the rf system it is not possible to point out any specific subsystem (but it is known that the failure occurred in the rf system!). 15% of the failures in the rf system are caused by the klystron assembly. In figure 8, typical failure causes in the klystron assembly are presented.

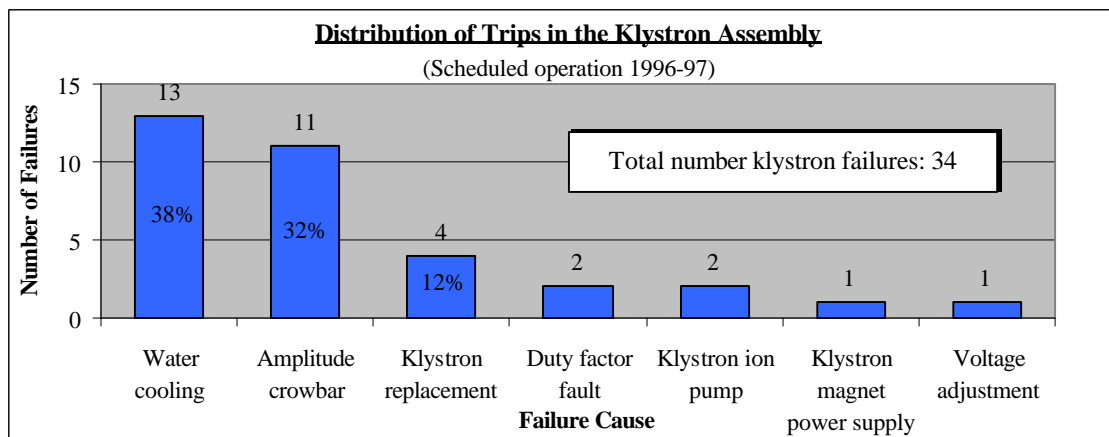


Figure 8. Failure causes in the Klystron Assembly

The klystron assembly includes some other components beside the klystron tube, for example an ion pump, a klystron magnet etc. 38% of all failures in the klystron assembly are water cooling problems and 32% are amplitude crowbars. Amplitude crowbars are usually electric sparking in the klystron tube or switchtube (and this may be due to an old switchtube). Most of the downtime occurs when klystron replacement is necessary. During scheduled operation of 1996-97, four klystron replacements occurred.

Conclusions

Operational statistics of the powerful 1.25 mA H⁺ beam at LANSCE has been obtained using the accelerator logbook and beam monitor data. When the beam current is inspected over a long period of time (2800 hours), on average 2.4 trips/hour or 60 trips per day are registered. Approximately 75% of all trips are 0-1 minute long. The typical down time of a beam trip is 15-20 seconds.

In the overall reliability balance of the entire LANSCE accelerator, the injector is responsible for most of the trip events. The injector is accountable for 77 % of all trips in the H⁺ beam. The injector is primarily generating short trips. For long down times (>5 min) the rf system is the largest producer of trips. Upgrading the injector will result in a more stable beam with less interruptions, especially short ones. Upgrading the rf system will result in a better beam availability.

In summary, as a result of the investigation of individual systems, estimates for both MTBF and MDT were obtained for several typical accelerator components: DC magnet power supplies, DC magnets, klystron assemblies, HV power supplies, vacuum system, and water system. The results will be useful in developing preliminary estimates for reliability, availability, and maintainability of high power accelerator systems planned in the future. However, before we can fully trust them, they have to be corroborated through comparison with statistics obtained from other facilities. The impact of maintenance activities outside of the scheduled production time needs to be tracked down and included in the estimates as well.

Acknowledgement

The generous assistance of many LANSCE Operations Personnel in performing this work is greatly appreciated. Special thanks are due to Michael Oothoudt and Tim Callaway of LANSCE-6. Also, special thanks are due to Stan Cohen of LANSCE-6 for valuable help with magnet power supplies and John Lyles of LANSCE-5 for help with RF Technology.

References

- [1] Marcus Eriksson, "Reliability Assessment of the LANSCE Accelerator System", M.Sc. thesis at the Royal Institute of Technology, Stockholm, 1998.
- [2] Olin van Dyck, "LAMPF Reliability History and Program", International Conference on Accelerator-driven Transmutation Technologies and Applications, Las Vegas, 1994.
- [3] Michael Oothoudt, "Availability for cycle 75", LANSCE-6 Technical Report LANSCE-6-97-51-TR, 1997